

**ANALYSIS OF BIOMARKERS IN CRUDE OILS, PROCESSED OILS, AND
SPILLED OILS**

Pornpetch Hattakijvilai

A Thesis Submitted in Partial Fulfillment of the Requirements
for the Degree of Master of Science
The Petroleum and Petrochemical College, Chulalongkorn University
in Academic Partnership with
The University of Michigan, The University of Oklahoma,
Case Western Reserve University, and Institut Français du Pétrole
2017

บทคัดย่อและแฟ้มข้อมูลฉบับเต็มของวิทยานิพนธ์ตั้งแต่ปีการศึกษา 2554 ที่ให้บริการในคลังปัญญาจุฬาฯ (CUIR)
เป็นแฟ้มข้อมูลของนิสิตเจ้าของวิทยานิพนธ์ที่ส่งผ่านทางบัณฑิตวิทยาลัย

The abstract and full text of theses from the academic year 2011 in Chulalongkorn University Intellectual Repository (CUIR)
are the thesis authors' files submitted through the Graduate School.

Thesis Title: Analysis of Biomarkers in Crude Oils, Processed Oils, and Spilled Oils
By: Pornpetch Hattakijvilai
Program: Petroleum Technology
Thesis Advisor: Assoc. Prof. Siriporn Jongpatiwut

Accepted by The Petroleum and Petrochemical College, Chulalongkorn University, in partial fulfillment of the requirements for the Degree of Master of Science.

..... College Dean
(Prof. Suwabun Chirachanchai)

Thesis Committee:

.....
(Assoc. Prof. Siriporn Jongpatiwut)

.....
(Dr. Ampira Charoensaeng)

.....
(Dr. Pornsri Mingkwan)

ABSTRACT

5873013063: Petroleum Technology Program
Pornpetch Hattakijvilai: Analysis of Biomarkers in Crude Oils,
Processed Oils, and Spilled Oils
Thesis Advisor: Assoc. Prof. Siriporn Jongpatiwut 173 pp.
Keywords: Chemical fingerprinting/Biomarkers/PAHs/Crude oil/Processed
oil/Fuel oil/Lube oil

Oil spills in marine are commonly come from crude oils, fuel oils and lubricating oils by accidental leakages or purposeful discharges to the surroundings. As crude oil and fuel oil which refined from the heavy fraction of crude oil have similar physical properties especially if they were weathering, it is difficult to differentiate that the spill has the origin from crude oil or fuel oil. In this study, five crude oils, two fuel oils, one fresh and one used lube oil that are typically used in Thailand were investigated. All crude oils, fuel oils, and used lube oil were weathered in the sea water. All samples were characterized using GC-FID and GCxGC TOFMS. The attention of this work is focused on the distribution pattern of polycyclic aromatic hydrocarbons (PAHs) such as phenanthrenes (P), anthracenes (A), dibenzothiophenes (D) and their alkylation, and biomarkers in hopanes group. The statistic method was applied to distinguish crude oils, fuel oils and lube oil. The results from GC-FID showed a useful basis information of hydrocarbon in oils which could distinguish lube oil from other oil type due to the huge unresolved complex mixture (UCM). The distribution patterns of methyl-phenanthrenes (MP) and methyl-anthracenes (MA) were different in most crude oils and processed oils. The double ratio plots of MP and MA showed the most positive method to differentiate two refined products and crude oils. The results from weathering simulation showed that biomarkers were high degradation-resistant, however, hopanes distribution patterns were different between fuel oils and their crude oil feedstocks. In addition, the distribution pattern of hopanes biomarker in fresh or unused lube oil and used lube oil were dissimilar as they were generated or degraded during the combustion in the engine.

บทคัดย่อ

พรเพชร หัตถกิจวิไล : การวิเคราะห์ไบโอมาร์คเกอร์ในน้ำมันดิบ ผลิตภัณฑ์จากกระบวนการกลั่นน้ำมันดิบ และน้ำมันที่รั่วไหล (Analysis of Biomarkers in Crude Oils, Processed Oils, and Spilled Oils) อ. ที่ปรึกษา : รศ. ดร. ศิริพร จงผาคูวุฒิ 173 หน้า

การรั่วไหลของน้ำมันในทะเลเกิดได้จากหลายสาเหตุ เช่น อุบัติเหตุจากท่อขนส่งหรือเรืออัปปาง และการลักลอบทิ้งน้ำมันลงสู่ทะเล โดยส่วนใหญ่ประเภทของน้ำมันที่รั่วไหลมักเป็นประเภทน้ำมันดิบ น้ำมันเตา หรือน้ำมันหล่อลื่น ลักษณะโดยทั่วไปของน้ำมันดิบและน้ำมันเตานั้นมีคุณสมบัติที่คล้ายคลึงกันมากทำให้ไม่สามารถระบุประเภทของน้ำมันได้ว่าน้ำมันที่รั่วนั้นมาจากน้ำมันชนิดใด ในงานวิจัยนี้ได้ศึกษาตัวอย่างน้ำมันดิบ 5 ชนิด ตัวอย่างน้ำมันเตา 2 ชนิด รวมถึงน้ำมันหล่อลื่นทั้งที่ยังไม่ได้ใช้งานและที่ผ่านการใช้งานในเรือเดินสมุทร 1 ชนิด โดยน้ำมันดิบและน้ำมันเตาทุกชนิด รวมถึงน้ำมันหล่อลื่นที่ผ่านการใช้งานแล้วถูกจำลองเหตุการณ์น้ำมันรั่วในน้ำทะเลเพื่อศึกษาการเปลี่ยนแปลงที่เกิดจากกระบวนการเปลี่ยนแปลงทางสภาพอากาศ ตัวอย่างน้ำมันทั้งหมดถูกวิเคราะห์แยกสารด้วยเครื่องมือทางวิทยาศาสตร์เพื่อหาตัวบ่งชี้เอกลักษณ์ งานวิจัยนี้ศึกษาหาลักษณะการกระจายตัวของตัวบ่งชี้เอกลักษณ์เฉพาะในกลุ่มพอลิไซคลิกอะโรมาติก และไบโอมาร์คเกอร์กลุ่มโฮปเพน ประยุกต์รวมกับการใช้วิธีทางสถิติ และการหาค่าดัชนีของตัวบ่งชี้เอกลักษณ์เฉพาะเหล่านี้เพื่อจำแนกประเภทน้ำมัน น้ำมันหล่อลื่นสามารถจำแนกแยกจากน้ำมันชนิดอื่น ๆ ได้จากผลของเครื่องมือแยกองค์ประกอบอย่างง่ายเนื่องจากกราฟที่ได้มีลักษณะยกตัวขึ้นสูงเหมือนภูเขา ลักษณะการกระจายตัวของตัวบ่งชี้เอกลักษณ์เฉพาะในกลุ่มพอลิไซคลิกอะโรมาติกมีความแตกต่างระหว่างน้ำมันดิบโดยส่วนใหญ่และผลิตภัณฑ์จากกระบวนการกลั่น รวมไปถึงผลจากการเปรียบเทียบค่าดัชนีของตัวบ่งชี้เอกลักษณ์เฉพาะในกลุ่มพอลิไซคลิกอะโรมาติกมีความเป็นไปได้ที่จะใช้ในการแยกประเภทชนิดน้ำมัน ผลจากการจำลองน้ำมันรั่วพบว่าไบโอมาร์คเกอร์กลุ่มโฮปเพนมีความต้านทานต่อการเปลี่ยนแปลงสภาพอากาศสูง แต่ลักษณะการกระจายตัวของไบโอมาร์คเกอร์กลุ่มโฮปเพนนี้แตกต่างกันในน้ำมันเตาและน้ำมันดิบที่เป็นวัตถุดิบในการกลั่น นอกจากนี้ลักษณะการกระจายตัวของโฮปเพนในน้ำมันหล่อลื่นที่ยังไม่ผ่านการใช้งานก็มีความแตกต่างกันกับน้ำมันหล่อลื่นที่ผ่านการใช้งานแล้ว เนื่องจากน้ำมันหล่อลื่นผ่านการใช้งานในเครื่องยนต์ที่มีการเผาไหม้ทำให้มีไบโอมาร์คเกอร์ชนิดใหม่เกิดขึ้นมาและมีบางตัวสลายไป

ACKNOWLEDGEMENTS

I am grateful for the partial scholarship and partial funding of the thesis work provided by the Petroleum and Petrochemical College.

I would like to extend my sincere thanks to PTT Global Chemical Public Company Limited, Star Petroleum Refining Public Company Limited, and Inter Marine Lube Company Limited, Thailand for providing all samples, supports and helpful suggestions.

In particular, I would like to express my gratitude to my advisor, Assoc. Prof. Siriporn Jongpatiwut for her advice, supervision and support in various ways from the very stage of this research.

I also gratefully thank to Asst. Prof. Penjai Sompongchaiyakul and Asst. Prof. Kornrawee Aiemsomboon from Department of Marine Science, Faculty of Science, Chulalongkorn University for their suggestion and important support. Dr. Ampira Charoensaeng and Dr. Pornsri Mingkwan for their kindness to be committees and important comments on this research.

I am deeply grateful to my family and friends for their encouragement and greatest support.

Finally, I would like to thank all PPC staffs and those whose names are not mentioned here who made valuable contributions to this research.

TABLE OF CONTENTS

| | PAGE |
|--|-------------|
| Title Page | i |
| Abstract (in English) | iii |
| Abstract (in Thai) | iv |
| Acknowledgements | v |
| Table of Contents | vi |
| List of Tables | x |
| List of Figures | xi |
| Abbreviations | xxvi |
| | |
| CHAPTER | |
| I INTRODUCTION | 1 |
| | |
| II THEORETICAL BACKGROUND AND LITERATURE REVIEW | 3 |
| 2.1 Crude Oil and Refined Product | 3 |
| 2.2 Petroleum Chemical Fingerprintings | 8 |
| 2.2.1 Oil Chemical Composition | 8 |
| 2.2.2 PAHs | 9 |
| 2.2.2.1 Characterization PAHs in Heavy Oil | 10 |
| 2.2.3 Biomarkers | 13 |
| 2.2.3.1 Biomarker Distribution in Heavy Oil | 13 |
| 2.2.4 Weathering Process | 17 |
| 2.2.4.1 Spreading | 18 |
| 2.2.4.2 Evaporation | 18 |
| 2.2.4.3 Dispersion | 19 |
| 2.2.4.4 Emulsification | 19 |
| 2.2.4.5 Dissolution | 19 |
| 2.2.4.6 Photo-oxidation | 19 |
| 2.2.4.7 Sedimentation and Sinking | 20 |

| CHAPTER | PAGE |
|--|-------------|
| 2.2.4.8 Biodegradation | 20 |
| 2.2.5 Effect of Weathering on Chemical Fingerprintings | 20 |
| 2.3 Oil Spill Characterization and Identification Methodology | 21 |
| 2.3.1 Chemical Fingerprinting Techniques | 22 |
| 2.3.2 NORDTEST Methodology for Oil Spill Identification | 22 |
| 2.3.3 Example of Oil Spill in Thailand | 29 |
| III EXPERIMENTAL | 31 |
| 3.1 Materials and Equipment | 31 |
| 3.1.1 Source of Oil Samples | 31 |
| 3.1.2 Gases | 32 |
| 3.1.3 Chemicals | 32 |
| 3.1.4 Equipment | 32 |
| 3.2 Methodology | 33 |
| 3.2.1 Oil Spill Simulation in Natural Weathering Process | 33 |
| 3.2.2 Oil Testing | 33 |
| 3.2.2.1 Extraction of Oil Samples | 33 |
| 3.2.2.2 Analysis of Oil Samples Using GC-FID | 34 |
| 3.2.2.3 Analysis of Oil Samples Using GCxGC-TOFMS | 34 |
| 3.3 Software | 35 |
| 3.3.1 ChromaTOF Software | 35 |
| 3.3.4 Microsoft Excel | 36 |

| CHAPTER | PAGE |
|---|-------------|
| IV RESULTS AND DISCUSSION | 37 |
| 4.1 Standard Analysis | 37 |
| 4.2 Effect of Weathering Process | 37 |
| 4.2.1 Physical Effect of Studied Spilled Oils | 37 |
| 4.2.2 Characterization of Aliphatic Hydrocarbons | 39 |
| 4.3 The Differentiation of Crude Oils and Processed Oil by PAHs | 46 |
| 4.3.1 The Distribution of Polycyclic Aromatic Hydrocarbons | 47 |
| 4.3.2 Diagnostic Ratio of 4-MD/1-MD | 50 |
| 4.3.3 Diagnostic Ratio of 2-MP/1-MP | 52 |
| 4.3.4 Cross Plot of C2D/C2P vs C3D/C3P | 53 |
| 4.3.5 Cross Plot of MA/MP Isomers | 55 |
| 4.4 The Differentiation of Crude Oils and Processed Oil by Biomarkers | 61 |
| 4.5 The Difference Between Fresh Lube Oil and Used Lube Oil | 70 |
| 4.5.1 Characterization of Aliphatic Hydrocarbons | 70 |
| 4.5.2 PAHs Characterization | 70 |
| 4.5.3 Biomarkers Characterization | 72 |
| 4.6 The Summarized Protocol for the Differentiation of Crude Oils and Processed Oils | 73 |
| V CONCLUSIONS AND RECOMMENDATIONS | 76 |
| REFERENCES | 78 |
| APPENDICES | 83 |
| Appendix A GCxGC-TOFMS Total Ion Surface Plot Result | 83 |

| CHAPTER | PAGE |
|---|-------------|
| Appendix B GCxGC-TOFMS Target Ion (m/z 178) Surface Plot Result | 92 |
| Appendix C GCxGC-TOFMS Target Ion (m/z 192) Surface Plot Result | 101 |
| Appendix D GCxGC-TOFMS Target Ion (m/z 206) Surface Plot Result | 110 |
| Appendix E GCxGC-TOFMS Target Ion (m/z 220) Surface Plot Result | 119 |
| Appendix F GCxGC-TOFMS Target Ion (m/z 184) Surface Plot Result | 128 |
| Appendix G GCxGC-TOFMS Target Ion (m/z 198) Surface Plot Result | 137 |
| Appendix H GCxGC-TOFMS Target Ion (m/z 212) Surface Plot Result | 146 |
| Appendix I GCxGC-TOFMS Target Ion (m/z 226) Surface Plot Result | 155 |
| Appendix J GCxGC-TOFMS Target Ion (m/z 191) Surface Plot Result | 164 |
| CURRICULUM VITAE | 173 |

LIST OF TABLES

| TABLE | | PAGE |
|-------|--|------|
| 2.1 | Classification of marine fuel (Wallace, 2016, Bunker Oil-Marine Fuel Oil, 2016) | 6 |
| 2.2 | Typical composition of crude oil and petroleum products (Wang <i>et al.</i> , 2006) | 9 |
| 2.3 | A part of physics and chemical properties of some PAHs (Nagpal, 1993) | 16 |
| 2.4 | Values of Student's t (Harris, 1995) | 24 |
| 2.5 | Recommended criteria for correlation studies of diagnostic ratios (LivGuri Faksness <i>et al.</i> , 2002) | 26 |
| 3.1 | Information of five crude oils and three refined products samples | 33 |
| 4.1 | Biodegradation ratios of all oil samples | 45 |
| 4.2 | The detection of alkyl-phenanthrenes (MP) and alkyl-anthracenes (MA) presented in all fresh and weathered samples | 50 |
| 4.3 | Diagnostic ratio value of 4-MD/1-MD of all fresh and weathered sample in day 3, day 45 and day 90 | 51 |
| 4.4 | Diagnostic ratio value of 2-MP/1-MP of all fresh and weathered samples in day 3, day 45 and day 90 | 52 |
| 4.5 | Diagnostic ratio value of C2D/C2P of all fresh and weathered sample in day 3, day 45 and day 90 | 53 |
| 4.6 | Diagnostic ratio value of C3D/C3P of all fresh and weathered sample in day 3, day 45 and day 90 | 54 |
| 4.7 | Diagnostic ratio value of MA and MP isomer in all fresh (D0) and weathered samples in day 3, day 45 and day 90 (a) 2-MA/2-MP (b) 2-MA/3-MP | 56 |
| 4.8 | Diagnostic ratios value in used lube oil and fresh lube oil | 71 |

LIST OF FIGURES

| FIGURE | PAGE |
|---|------|
| 2.1 Crude oil formation diagram (History of Oil, 2014). | 3 |
| 2.2 Scheme flowchart of oil refining process (Oil Refining Process, 2014). | 4 |
| 2.3 (a) Simple straight run refinery block diagram (Chevron, 2012). | 5 |
| 2.4 (b) Complex refinery with FCC and visbreaking block diagram (Chevron, 2012). | 5 |
| 2.5 The structures of naphthalene anthracene and phenanthrene (Reusch, 2013). | 10 |
| 2.6 Phe, Ant, MP and MA mass-chromatograms of HFO and crude oil (Zhang <i>et al.</i> , 2016). | 11 |
| 2.7 Double ratio plots of Phe, Ant and their alkylation of HFOs and crude oils (Zhang <i>et al.</i> , 2016). | 12 |
| 2.8 Carbon number range of common cyclic biomarkers present in crude oils and refined products (Wang <i>et al.</i> , 2004). | 14 |
| 2.9 Distribution of biomarker terpane compounds (at m/z 191) in different oils (Wang <i>et al.</i> , 2004). | 15 |
| 2.10 Chromatogram of biomarker terpane (m/z 191) in different lube oils (Yang <i>et al.</i> , 2016). | 16 |
| 2.11 Weathering processes (ITOPF, 2011). | 18 |
| 2.12 Diagram of gas chromatograph (Helmenstine, 2016). | 22 |
| 2.13 Protocol/decision chart for oil spill identification (Liv-Guri Faksness <i>et al.</i> , 2002). | 25 |
| 2.14 Correlation between spill 1 and source A, using a 95 % confidence limit (Positive match) (Liv-Guri Faksness <i>et al.</i> , 2002). | 27 |

| FIGURE | PAGE |
|--|-------------|
| 2.15 Correlation between spill 1 and source D, using a 95 % confidence limit (Non match) (Liv-Guri Faksness <i>et al.</i> , 2002). | 27 |
| 2.16 Correlation between spill 1 and source C, using a 95 % confidence limit (Non match) (Liv-Guri Faksness <i>et al.</i> , 2002). | 28 |
| 2.17 Correlation between spill 1 and source C, using a 98 % confidence limit (Non match) (Liv-Guri Faksness <i>et al.</i> , 2002). | 28 |
| 2.18 Correlation between spill 1 and source C, using a 99 % confidence limit (Non match) (Liv-Guri Faksness <i>et al.</i> , 2002). | 29 |
| 2.19 A satellite image of oil spill in Rayong, 2013 (Chomchuen, 2013). | 30 |
| 2.20 Oil slick mapping area of the 2015 oil spill in Thailand (Mokkhasen, 2015). | 30 |
| 4.1 The surface chromatogram of IS 17 β (H), 21 β (H)-hopane solution. | 37 |
| 4.2 Physical appearance of all fresh samples (D0) comparing with their spills in day 3 (D3), and day 90 (D90). | 38 |
| 4.3 GC-FID overlay chromatograms of all fresh samples and their weathered samples in D3, D45 and D90. | 41 |
| 4.4 GC-FID chromatogram at R.T 44.17 min of ULO spilled on sea water and DI water. | 43 |
| 4.5 Fuel oil and lube oil processing block flow diagram. | 46 |
| 4.6 The total ion and target ion m/z 192 surface plot of all samples in day 0. | 48 |
| 4.7 The plot of diagnostic ratio of 4-MD/1-MD of all fresh (D0) and weathered samples in day 3, day 45 and day 90. | 51 |

| FIGURE | | PAGE |
|---------------|--|-------------|
| 4.8 | The plot of diagnostic ratio of 2-MP/1-MP of all fresh (D0) and weathered samples in day 3, day 45 and day 90. | 52 |
| 4.9 | The cross plot of C2D/C2P vs C3D/C3P of all fresh and weathered samples in day 3, day 45 and day 90. | 54 |
| 4.10 | The cross plot of (a) 2-MA/2-MP vs 2-MA/3-MP, (b) 2-MA/1-MP vs 2MA/9-MP, (c) 2-MA/(3+2)-MP vs 2MA/(9+1)-MP, (d) (3+2)-MP/(9+1)-MP vs 2-MA/ Σ MP of all fresh and weathered samples in day 3, day 45 and day 90. | 59 |
| 4.11 | The surface plots of hopanes (m/z191) for all samples in D0 and D90. | 61 |
| 4.12 | The correlation plot of diagnostic ratios of hopane biomarkers between all fresh oils and their weathered samples in day 90 using 95% confidence limit. | 64 |
| 4.13 | Comparing of hopane biomarkers in fresh fuel oil (FO1 and FO2) and their crude oil feedstocks (COF1 and COF2). | 67 |
| 4.14 | The correlation plot of diagnostic ratios of hopane biomarkers between fuel oils (FO1 and FO2) and their crude oil feedstocks using 95% confidence limit. | 68 |
| 4.15 | GC-FID overlay chromatogram of fresh lube oil and used lube oil. | 70 |
| 4.16 | The plot of diagnostic ratio of 4-MD/1-MD of used lube oil and fresh lube oil. | 71 |
| 4.17 | The plot of diagnostic ratio of 2-MP/1-MP of used lube oil and fresh lube oil. | 71 |
| 4.18 | The cross plot of C2D/C2P vs C3D/C3P of used lube oil and fresh lube oil. | 72 |

| FIGURE | PAGE |
|--|-------------|
| 4.19 The cross plot of (3+2)-MP/(9+1)-MP vs 2-MA/ Σ MP of used lube oil and fresh lube oil. | 72 |
| 4.20 The correlation plot of hopanes biomarkers between ULO and FLO using a 95% confidence limit. | 73 |
| 4.21 Protocol chart for differentiation of crude oil, fuel oil and used lube oil. | 75 |
| A1 Total ion surface plot of CO1. | 83 |
| A2 Total ion surface plot of WCO1-D3. | 83 |
| A3 Total ion surface plot of WCO1-D45. | 83 |
| A4 Total ion surface plot of WCO1-D90. | 84 |
| A5 Total ion surface plot of CO2. | 84 |
| A6 Total ion surface plot of WCO2-D3. | 84 |
| A7 Total ion surface plot of WCO2-D45. | 84 |
| A8 Total ion surface plot of WCO2-D90. | 85 |
| A9 Total ion surface plot of CO3. | 85 |
| A10 Total ion surface plot of WCO3-D3. | 85 |
| A11 Total ion surface plot of WCO3-D45. | 85 |
| A12 Total ion surface plot of WCO3-D90. | 86 |
| A13 Total ion surface plot of CO4. | 86 |
| A14 Total ion surface plot of WCO4-D3. | 86 |
| A15 Total ion surface plot of WCO4-D45. | 86 |
| A16 Total ion surface plot of WCO4-D90. | 87 |
| A17 Total ion surface plot of CO5. | 87 |
| A18 Total ion surface plot of WCO5-D3. | 87 |
| A19 Total ion surface plot of WCO5-D45. | 87 |
| A20 Total ion surface plot of WCO5-D90. | 88 |
| A21 Total ion surface plot of FO1. | 88 |
| A22 Total ion surface plot of WFO1-D3. | 88 |
| A23 Total ion surface plot of WFO1-D45. | 88 |

| FIGURE | PAGE |
|---|-------------|
| A24 Total ion surface plot of WFO1-D90. | 89 |
| A25 Total ion surface plot of FO2. | 89 |
| A26 Total ion surface plot of WFO2-D3. | 89 |
| A27 Total ion surface plot of WFO2-D45. | 89 |
| A28 Total ion surface plot of WFO2-D90. | 90 |
| A29 Total ion surface plot of ULO. | 90 |
| A30 Total ion surface plot of WULO-D3. | 90 |
| A31 Total ion surface plot of WULO-D45. | 90 |
| A32 Total ion surface plot of WULO-D90. | 91 |
| A33 Total ion surface plot of FLO. | 91 |
| B1 Target ion (m/z 178) surface plot of CO1. | 92 |
| B2 Target ion (m/z 178) surface plot of WCO1-D3. | 92 |
| B3 Target ion (m/z 178) surface plot of WCO1-D45. | 92 |
| B4 Target ion (m/z 178) surface plot of WCO1-D90. | 93 |
| B5 Target ion (m/z 178) surface plot of CO2. | 93 |
| B6 Target ion (m/z 178) surface plot of WCO2-D3. | 93 |
| B7 Target ion (m/z 178) surface plot of WCO2-D45. | 93 |
| B8 Target ion (m/z 178) surface plot of WCO2-D90. | 94 |
| B9 Target ion (m/z 178) surface plot of CO3. | 94 |
| B10 Target ion (m/z 178) surface plot of WCO3-D3. | 94 |
| B11 Target ion (m/z 178) surface plot of WCO3-D45. | 94 |
| B12 Target ion (m/z 178) surface plot of WCO3-D490. | 95 |
| B13 Target ion (m/z 178) surface plot of CO4. | 95 |
| B14 Target ion (m/z 178) surface plot of WCO4-D3. | 95 |
| B15 Target ion (m/z 178) surface plot of WCO4-D45. | 95 |
| B16 Target ion (m/z 178) surface plot of WCO4-D90. | 96 |
| B17 Target ion (m/z 178) surface plot of CO5. | 96 |
| B18 Target ion (m/z 178) surface plot of WCO5-D3. | 96 |
| B19 Target ion (m/z 178) surface plot of WCO5-D45. | 96 |

| FIGURE | | PAGE |
|---------------|--|-------------|
| B20 | Target ion (m/z 178) surface plot of WCO5-D90. | 97 |
| B21 | Target ion (m/z 178) surface plot of FO1. | 97 |
| B22 | Target ion (m/z 178) surface plot of WFO1-D3. | 97 |
| B23 | Target ion (m/z 178) surface plot of WFO1-D45. | 97 |
| B24 | Target ion (m/z 178) surface plot of WFO1-D90. | 98 |
| B25 | Target ion (m/z 178) surface plot of FO2. | 98 |
| B26 | Target ion (m/z 178) surface plot of WFO2-D3. | 98 |
| B27 | Target ion (m/z 178) surface plot of WFO2-D45. | 98 |
| B28 | Target ion (m/z 178) surface plot of WFO2-D90. | 99 |
| B29 | Target ion (m/z 178) surface plot of ULO. | 99 |
| B30 | Target ion (m/z 178) surface plot of WULO-D3. | 99 |
| B31 | Target ion (m/z 178) surface plot of WULO-D45. | 99 |
| B32 | Target ion (m/z 178) surface plot of WULO-D90. | 100 |
| B33 | Target ion (m/z 178) surface plot of FLO. | 100 |
| C1 | Target ion (m/z 192) surface plot of CO1. | 101 |
| C2 | Target ion (m/z 192) surface plot of WCO1-D3. | 101 |
| C3 | Target ion (m/z 192) surface plot of WCO1-D45. | 101 |
| C4 | Target ion (m/z 192) surface plot of WCO1-D90. | 102 |
| C5 | Target ion (m/z 192) surface plot of CO2. | 102 |
| C6 | Target ion (m/z 192) surface plot of WCO2-D3. | 102 |
| C7 | Target ion (m/z 192) surface plot of WCO2-D45. | 102 |
| C8 | Target ion (m/z 192) surface plot of WCO2-D90. | 103 |
| C9 | Target ion (m/z 192) surface plot of CO3. | 103 |
| C10 | Target ion (m/z 192) surface plot of WCO3-D3. | 103 |
| C11 | Target ion (m/z 192) surface plot of WCO3-D45. | 103 |
| C12 | Target ion (m/z 192) surface plot of WCO3-D90. | 104 |
| C13 | Target ion (m/z 192) surface plot of CO4. | 104 |
| C14 | Target ion (m/z 192) surface plot of WCO4-D3. | 104 |
| C15 | Target ion (m/z 192) surface plot of WCO4-D45. | 104 |

| FIGURE | | PAGE |
|---------------|--|-------------|
| C16 | Target ion (m/z 192) surface plot of WCO4-D90. | 105 |
| C17 | Target ion (m/z 192) surface plot of CO5. | 105 |
| C18 | Target ion (m/z 192) surface plot of WCO5-D3. | 105 |
| C19 | Target ion (m/z 192) surface plot of WCO5-D45. | 105 |
| C20 | Target ion (m/z 192) surface plot of WCO5-D90. | 106 |
| C21 | Target ion (m/z 192) surface plot of FO1. | 106 |
| C22 | Target ion (m/z 192) surface plot of WFO1-D3. | 106 |
| C23 | Target ion (m/z 192) surface plot of WFO1-D45. | 106 |
| C24 | Target ion (m/z 192) surface plot of WFO1-D90. | 107 |
| C25 | Target ion (m/z 192) surface plot of FO2. | 107 |
| C26 | Target ion (m/z 192) surface plot of WFO2-D3. | 107 |
| C27 | Target ion (m/z 192) surface plot of WFO2-D45. | 107 |
| C28 | Target ion (m/z 192) surface plot of WFO2-D90. | 108 |
| C29 | Target ion (m/z 192) surface plot of ULO. | 108 |
| C30 | Target ion (m/z 192) surface plot of WULO-D3. | 108 |
| C31 | Target ion (m/z 192) surface plot of WULO-D45. | 108 |
| C32 | Target ion (m/z 192) surface plot of WULO-D90. | 109 |
| C33 | Target ion (m/z 192) surface plot of FLO. | 109 |
| D1 | Target ion (m/z 206) surface plot of CO1. | 110 |
| D2 | Target ion (m/z 206) surface plot of WCO1-D3. | 110 |
| D3 | Target ion (m/z 206) surface plot of WCO1-D45. | 110 |
| D4 | Target ion (m/z 206) surface plot of WCO1-D90. | 111 |
| D5 | Target ion (m/z 206) surface plot of CO2. | 111 |
| D6 | Target ion (m/z 206) surface plot of WCO2-D3. | 111 |
| D7 | Target ion (m/z 206) surface plot of WCO2-D45. | 111 |
| D8 | Target ion (m/z 206) surface plot of WCO2-D90. | 112 |
| D9 | Target ion (m/z 206) surface plot of CO3. | 112 |
| D10 | Target ion (m/z 206) surface plot of WCO3-D3. | 112 |
| D11 | Target ion (m/z 206) surface plot of WCO3-D45. | 112 |

| FIGURE | | PAGE |
|---------------|--|-------------|
| D12 | Target ion (m/z 206) surface plot of WCO3-D90. | 113 |
| D13 | Target ion (m/z 206) surface plot of CO4. | 113 |
| D14 | Target ion (m/z 206) surface plot of WCO4-D3. | 113 |
| D15 | Target ion (m/z 206) surface plot of WCO4-D45. | 113 |
| D16 | Target ion (m/z 206) surface plot of WCO4-D90. | 114 |
| D17 | Target ion (m/z 206) surface plot of CO5. | 114 |
| D18 | Target ion (m/z 206) surface plot of WCO5-D3. | 114 |
| D19 | Target ion (m/z 206) surface plot of WCO5-D45. | 114 |
| D20 | Target ion (m/z 206) surface plot of WCO5-D90. | 115 |
| D21 | Target ion (m/z 206) surface plot of FO1. | 115 |
| D22 | Target ion (m/z 206) surface plot of WFO1-D3. | 115 |
| D23 | Target ion (m/z 206) surface plot of WFO1-D45. | 115 |
| D24 | Target ion (m/z 206) surface plot of WFO1-D90. | 116 |
| D25 | Target ion (m/z 206) surface plot of FO2. | 116 |
| D26 | Target ion (m/z 206) surface plot of WFO2-D3. | 116 |
| D27 | Target ion (m/z 206) surface plot of WFO2-D45. | 116 |
| D28 | Target ion (m/z 206) surface plot of WFO2-D90. | 117 |
| D29 | Target ion (m/z 206) surface plot of ULO. | 117 |
| D30 | Target ion (m/z 206) surface plot of WULO-D3. | 117 |
| D31 | Target ion (m/z 206) surface plot of WULO-D45. | 117 |
| D32 | Target ion (m/z 206) surface plot of WULO-90. | 118 |
| D33 | Target ion (m/z 206) surface plot of FLO. | 118 |
| E1 | Target ion (m/z 220) surface plot of CO1. | 119 |
| E2 | Target ion (m/z 220) surface plot of WCO1-D3. | 119 |
| E3 | Target ion (m/z 220) surface plot of WCO1-D45. | 119 |
| E4 | Target ion (m/z 220) surface plot of WCO1-D90. | 120 |
| E5 | Target ion (m/z 220) surface plot of CO2. | 120 |
| E6 | Target ion (m/z 220) surface plot of WCO2-D3. | 120 |
| E7 | Target ion (m/z 220) surface plot of WCO2-D45. | 120 |

| FIGURE | | PAGE |
|---------------|--|-------------|
| E8 | Target ion (m/z 220) surface plot of WCO2-D90. | 121 |
| E9 | Target ion (m/z 220) surface plot of CO3. | 121 |
| E10 | Target ion (m/z 220) surface plot of WCO3-D3. | 121 |
| E11 | Target ion (m/z 220) surface plot of WCO3-D45. | 121 |
| E12 | Target ion (m/z 220) surface plot of WCO3-D90. | 122 |
| E13 | Target ion (m/z 220) surface plot of CO4. | 122 |
| E14 | Target ion (m/z 220) surface plot of WCO4-D3. | 122 |
| E15 | Target ion (m/z 220) surface plot of WCO4-D45. | 122 |
| E16 | Target ion (m/z 220) surface plot of WCO4-D90. | 123 |
| E17 | Target ion (m/z 220) surface plot of CO5. | 123 |
| E18 | Target ion (m/z 220) surface plot of WCO5-D3. | 123 |
| E19 | Target ion (m/z 220) surface plot of WCO5-D45. | 123 |
| E20 | Target ion (m/z 220) surface plot of WCO5-D90. | 124 |
| E21 | Target ion (m/z 220) surface plot of FO1. | 124 |
| E22 | Target ion (m/z 220) surface plot of WFO1-D3. | 124 |
| E23 | Target ion (m/z 220) surface plot of WFO1-D45. | 124 |
| E24 | Target ion (m/z 220) surface plot of WFO1-D90. | 125 |
| E25 | Target ion (m/z 220) surface plot of FO2. | 125 |
| E26 | Target ion (m/z 220) surface plot of WFO2-D3. | 125 |
| E27 | Target ion (m/z 220) surface plot of WFO2-D45. | 125 |
| E28 | Target ion (m/z 220) surface plot of WFO2-D90. | 126 |
| E29 | Target ion (m/z 220) surface plot of ULO. | 126 |
| E30 | Target ion (m/z 220) surface plot of ULO-D3. | 126 |
| E31 | Target ion (m/z 220) surface plot of ULO-D45. | 126 |
| E32 | Target ion (m/z 220) surface plot of ULO-D90. | 127 |
| E33 | Target ion (m/z 220) surface plot of FLO. | 127 |
| F1 | Target ion (m/z 184) surface plot of CO1. | 128 |
| F2 | Target ion (m/z 184) surface plot of WCO1-D3. | 128 |
| F3 | Target ion (m/z 184) surface plot of WCO1-D45. | 128 |

| FIGURE | | PAGE |
|---------------|--|-------------|
| F4 | Target ion (m/z 184) surface plot of WCO1-90. | 129 |
| F5 | Target ion (m/z 184) surface plot of CO2. | 129 |
| F6 | Target ion (m/z 184) surface plot of WCO2-D3. | 129 |
| F7 | Target ion (m/z 184) surface plot of WCO2-D45. | 129 |
| F8 | Target ion (m/z 184) surface plot of WCO2-90. | 130 |
| F9 | Target ion (m/z 184) surface plot of CO3. | 130 |
| F10 | Target ion (m/z 184) surface plot of WCO3-D3. | 130 |
| F11 | Target ion (m/z 184) surface plot of WCO3-D45. | 130 |
| F12 | Target ion (m/z 184) surface plot of WCO3-90. | 131 |
| F13 | Target ion (m/z 184) surface plot of CO4. | 131 |
| F14 | Target ion (m/z 184) surface plot of WCO4-D3. | 131 |
| F15 | Target ion (m/z 184) surface plot of WCO4-D45. | 131 |
| F16 | Target ion (m/z 184) surface plot of WCO4-90. | 132 |
| F17 | Target ion (m/z 184) surface plot of CO5. | 132 |
| F18 | Target ion (m/z 184) surface plot of WCO5-D3. | 132 |
| F19 | Target ion (m/z 184) surface plot of WCO5-D45. | 132 |
| F20 | Target ion (m/z 184) surface plot of WCO5-90. | 133 |
| F21 | Target ion (m/z 184) surface plot of FO1. | 133 |
| F22 | Target ion (m/z 184) surface plot of WFO1-D3. | 133 |
| F23 | Target ion (m/z 184) surface plot of WFO1-D45. | 133 |
| F24 | Target ion (m/z 184) surface plot of WFO1-90. | 134 |
| F25 | Target ion (m/z 184) surface plot of FO2. | 134 |
| F26 | Target ion (m/z 184) surface plot of WFO2-D3. | 134 |
| F27 | Target ion (m/z 184) surface plot of WFO2-D45. | 134 |
| F28 | Target ion (m/z 184) surface plot of WFO2-90. | 135 |
| F29 | Target ion (m/z 184) surface plot of ULO. | 135 |
| F30 | Target ion (m/z 184) surface plot of WULO-D3. | 135 |
| F31 | Target ion (m/z 184) surface plot of WULO-D45. | 135 |
| F32 | Target ion (m/z 184) surface plot of WULO-D90. | 136 |

| FIGURE | | PAGE |
|---------------|--|-------------|
| F33 | Target ion (m/z 184) surface plot of FLO. | 136 |
| G1 | Target ion (m/z 198) surface plot of CO1. | 137 |
| G2 | Target ion (m/z 198) surface plot of WCO1-D3. | 137 |
| G3 | Target ion (m/z 198) surface plot of WCO1-D45. | 137 |
| G4 | Target ion (m/z 198) surface plot of WCO1-D90. | 138 |
| G5 | Target ion (m/z 198) surface plot of CO2. | 138 |
| G6 | Target ion (m/z 198) surface plot of WCO2-D3. | 138 |
| G7 | Target ion (m/z 198) surface plot of WCO2-D45. | 138 |
| G8 | Target ion (m/z 198) surface plot of WCO2-D90. | 139 |
| G9 | Target ion (m/z 198) surface plot of CO3. | 139 |
| G10 | Target ion (m/z 198) surface plot of WCO3-D3. | 139 |
| G11 | Target ion (m/z 198) surface plot of WCO3-D45. | 139 |
| G12 | Target ion (m/z 198) surface plot of WCO3-D90. | 140 |
| G13 | Target ion (m/z 198) surface plot of CO4. | 140 |
| G14 | Target ion (m/z 198) surface plot of WCO4-D3. | 140 |
| G15 | Target ion (m/z 198) surface plot of WCO4-D45. | 140 |
| G16 | Target ion (m/z 198) surface plot of WCO4-D90. | 141 |
| G17 | Target ion (m/z 198) surface plot of CO5. | 141 |
| G18 | Target ion (m/z 198) surface plot of WCO5-D3. | 141 |
| G19 | Target ion (m/z 198) surface plot of WCO5-D45. | 141 |
| G20 | Target ion (m/z 198) surface plot of WCO5-D90. | 142 |
| G21 | Target ion (m/z 198) surface plot of FO1. | 142 |
| G22 | Target ion (m/z 198) surface plot of WFO1-D3. | 142 |
| G23 | Target ion (m/z 198) surface plot of WFO1-D45. | 142 |
| G24 | Target ion (m/z 198) surface plot of WFO1-D90. | 143 |
| G25 | Target ion (m/z 198) surface plot of FO2. | 143 |
| G26 | Target ion (m/z 198) surface plot of WFO2-D3. | 143 |
| G27 | Target ion (m/z 198) surface plot of WFO2-D45. | 143 |
| G28 | Target ion (m/z 198) surface plot of WFO2-D90. | 144 |

| FIGURE | | PAGE |
|---------------|--|-------------|
| G29 | Target ion (m/z 198) surface plot of ULO. | 144 |
| G30 | Target ion (m/z 198) surface plot of WULO-D3. | 144 |
| G31 | Target ion (m/z 198) surface plot of WULO-D45. | 144 |
| G32 | Target ion (m/z 198) surface plot of WULO-D90. | 145 |
| G33 | Target ion (m/z 198) surface plot of FLO. | 145 |
| H1 | Target ion (m/z 212) surface plot of CO1. | 146 |
| H2 | Target ion (m/z 212) surface plot of WCO1-D3. | 146 |
| H3 | Target ion (m/z 212) surface plot of WCO1-D45. | 146 |
| H4 | Target ion (m/z 212) surface plot of WCO1-D90. | 147 |
| H5 | Target ion (m/z 212) surface plot of CO2. | 147 |
| H6 | Target ion (m/z 212) surface plot of WCO2-D3. | 147 |
| H7 | Target ion (m/z 212) surface plot of WCO2-D45. | 147 |
| H8 | Target ion (m/z 212) surface plot of WCO2-D90. | 148 |
| H9 | Target ion (m/z 212) surface plot of CO3. | 148 |
| H10 | Target ion (m/z 212) surface plot of WCO3-D3. | 148 |
| H11 | Target ion (m/z 212) surface plot of WCO3-D45. | 148 |
| H12 | Target ion (m/z 212) surface plot of WCO3-D90. | 149 |
| H13 | Target ion (m/z 212) surface plot of CO4. | 149 |
| H14 | Target ion (m/z 212) surface plot of WCO4-D3. | 149 |
| H15 | Target ion (m/z 212) surface plot of WCO4-D45. | 149 |
| H16 | Target ion (m/z 212) surface plot of WCO4-D90. | 150 |
| H17 | Target ion (m/z 212) surface plot of CO5. | 150 |
| H18 | Target ion (m/z 212) surface plot of WCO5-D3. | 150 |
| H19 | Target ion (m/z 212) surface plot of WCO5-D45. | 150 |
| H20 | Target ion (m/z 212) surface plot of WCO5-D90. | 151 |
| H21 | Target ion (m/z 212) surface plot of FO1. | 151 |
| H22 | Target ion (m/z 212) surface plot of WFO1-D3. | 151 |
| H23 | Target ion (m/z 212) surface plot of WFO1-D45. | 151 |
| H24 | Target ion (m/z 212) surface plot of WFO1-D90. | 152 |

| FIGURE | | PAGE |
|---------------|--|-------------|
| H25 | Target ion (m/z 212) surface plot of FO2. | 152 |
| H26 | Target ion (m/z 212) surface plot of WFO2-D3. | 152 |
| H27 | Target ion (m/z 212) surface plot of WFO2-D45. | 152 |
| H28 | Target ion (m/z 212) surface plot of WFO2-D90. | 153 |
| H29 | Target ion (m/z 212) surface plot of ULO. | 153 |
| H30 | Target ion (m/z 212) surface plot of WULO-D3. | 153 |
| H31 | Target ion (m/z 212) surface plot of WULO-D45. | 153 |
| H32 | Target ion (m/z 212) surface plot of WULO-D90. | 154 |
| H33 | Target ion (m/z 212) surface plot of FLO. | 154 |
| I1 | Target ion (m/z 226) surface plot of CO1. | 155 |
| I2 | Target ion (m/z 226) surface plot of WCO1-D3. | 155 |
| I3 | Target ion (m/z 226) surface plot of WCO1-D45. | 155 |
| I4 | Target ion (m/z 226) surface plot of WCO1-D90. | 156 |
| I5 | Target ion (m/z 226) surface plot of CO2. | 156 |
| I6 | Target ion (m/z 226) surface plot of WCO2-D3. | 156 |
| I7 | Target ion (m/z 226) surface plot of WCO2-D45. | 156 |
| I8 | Target ion (m/z 226) surface plot of WCO2-D90. | 157 |
| I9 | Target ion (m/z 226) surface plot of CO3. | 157 |
| I10 | Target ion (m/z 226) surface plot of WCO3-D3. | 157 |
| I11 | Target ion (m/z 226) surface plot of WCO3-D45. | 157 |
| I12 | Target ion (m/z 226) surface plot of WCO3-D90. | 158 |
| I13 | Target ion (m/z 226) surface plot of CO4. | 158 |
| I14 | Target ion (m/z 226) surface plot of WCO4-D3. | 158 |
| I15 | Target ion (m/z 226) surface plot of WCO4-D45. | 158 |
| I16 | Target ion (m/z 226) surface plot of WCO4-D90. | 159 |
| I17 | Target ion (m/z 226) surface plot of CO5. | 159 |
| I18 | Target ion (m/z 226) surface plot of WCO5-D3. | 159 |
| I19 | Target ion (m/z 226) surface plot of WCO5-D45. | 159 |
| I20 | Target ion (m/z 226) surface plot of WCO5-D90. | 160 |

| FIGURE | | PAGE |
|---------------|--|-------------|
| I21 | Target ion (m/z 226) surface plot of FO1. | 160 |
| I22 | Target ion (m/z 226) surface plot of WFO1-D3. | 160 |
| I23 | Target ion (m/z 226) surface plot of WFO1-D45. | 160 |
| I24 | Target ion (m/z 226) surface plot of WFO1-D90. | 161 |
| I25 | Target ion (m/z 226) surface plot of FO2. | 161 |
| I26 | Target ion (m/z 226) surface plot of WFO2-D3. | 161 |
| I27 | Target ion (m/z 226) surface plot of WFO2-D45. | 161 |
| I28 | Target ion (m/z 226) surface plot of WFO2-D90. | 162 |
| I29 | Target ion (m/z 226) surface plot of ULO. | 162 |
| I30 | Target ion (m/z 226) surface plot of WULO-D3. | 162 |
| I31 | Target ion (m/z 226) surface plot of WULO-D45. | 162 |
| I32 | Target ion (m/z 226) surface plot of WULO-D90. | 163 |
| I33 | Target ion (m/z 226) surface plot of FLO. | 163 |
| J1 | Target ion (m/z 191) surface plot of CO1. | 164 |
| J2 | Target ion (m/z 191) surface plot of WCO1-D3. | 164 |
| J3 | Target ion (m/z 191) surface plot of WCO1-D45. | 164 |
| J4 | Target ion (m/z 191) surface plot of WCO1-D90. | 165 |
| J5 | Target ion (m/z 191) surface plot of CO2. | 165 |
| J6 | Target ion (m/z 191) surface plot of WCO2-D3. | 165 |
| J7 | Target ion (m/z 191) surface plot of WCO2-D45. | 165 |
| J8 | Target ion (m/z 191) surface plot of WCO2-D90. | 166 |
| J9 | Target ion (m/z 191) surface plot of CO3. | 166 |
| J10 | Target ion (m/z 191) surface plot of WCO3-D3. | 166 |
| J11 | Target ion (m/z 191) surface plot of WCO3-D45. | 166 |
| J12 | Target ion (m/z 191) surface plot of WCO3-D90. | 167 |
| J13 | Target ion (m/z 191) surface plot of CO4. | 167 |
| J14 | Target ion (m/z 191) surface plot of WCO4-D3. | 167 |
| J15 | Target ion (m/z 191) surface plot of WCO4-D45. | 167 |
| J16 | Target ion (m/z 191) surface plot of WCO4-D90. | 168 |

| FIGURE | | PAGE |
|---------------|--|-------------|
| J17 | Target ion (m/z 191) surface plot of CO5. | 168 |
| J18 | Target ion (m/z 191) surface plot of WCO5-D3. | 168 |
| J19 | Target ion (m/z 191) surface plot of WCO5-D45. | 168 |
| J20 | Target ion (m/z 191) surface plot of WCO5-D90. | 169 |
| J21 | Target ion (m/z 191) surface plot of FO1. | 169 |
| J22 | Target ion (m/z 191) surface plot of WFO1-D3. | 169 |
| J23 | Target ion (m/z 191) surface plot of WFO1-D45. | 169 |
| J24 | Target ion (m/z 191) surface plot of WFO1-D90. | 170 |
| J25 | Target ion (m/z 191) surface plot of FO2. | 170 |
| J26 | Target ion (m/z 191) surface plot of WFO2-D3. | 170 |
| J27 | Target ion (m/z 191) surface plot of WFO2-D45. | 170 |
| J28 | Target ion (m/z 191) surface plot of WFO2-D90. | 171 |
| J29 | Target ion (m/z 191) surface plot of ULO. | 171 |
| J30 | Target ion (m/z 191) surface plot of WULO-D3. | 171 |
| J31 | Target ion (m/z 191) surface plot of WULO-D45. | 171 |
| J32 | Target ion (m/z 191) surface plot of WULO-D90. | 172 |
| J33 | Target ion (m/z 191) surface plot of FLO. | 172 |

ABBREVIATION

| | |
|-----|-------------------------|
| A | Anthracene |
| CO | crude oil |
| COF | crude oil feedstock |
| CL | confident limit |
| D | Dibenzothiophene |
| FLO | fresh lube oil |
| FO | fuel oil |
| P | Phenanthrene |
| MA | methethyl-anthracene |
| MD | methyl-dibenzothiophene |
| MP | methyl-phenanthrene |
| m/z | mass to charge ratio |
| ULO | used lube oil |

CHAPTER I

INTRODUCTION

Oil spill in marine is an important environmental issue. Once oil is released into marine environment, it subjects to an expanded damage to marine lives, human and coastal environments for example, in Thailand, the largest oil spill from a leaked pipeline that operated by PTT Global Chemical in Rayong in 2013 and more recently spilled in Hua-Hin district which remained unknown sources in 2015. Investigation and identification of oil type is indeed important for finding response in order to take effective clean up and rehabilitate the ecosystem (Wang and Fingas, 2003). The spilled oil in marine, could happened from both accidents and unauthorized drainage, is commonly come from crude oil, marine fuel which refers to fuel oil (FO), used and wasted lubricating oil. After oil is discharged into the sea, the chemical composition is changed as it undergoes with a variety of weathering processes, for example, evaporation, emulsification, dissolution and biodegradation. In addition, weathering time and oil type are also related to the change of the oil fingerprint (ITOPF, 2011).

Nowadays, the common method to characterize and identify of spilled oils are followed the NORDTEST methodology which focuses on molecular characterization of oil and relies on analyses by gas chromatography (GC) and gas chromatography – mass spectrometry (GC-MS) (Liv-Guri Faksness *et al.*, 2002). The complexity of crude oil and/or bottom products like fuel oil may not be resolved some isomer structures clearly by using GC-MS. Then GCxGC-TOFMS or comprehensive two-dimensional gas chromatography time-of-flight mass spectrometry could resolve this problem as GCxGC-TOFMS uses two columns of different selectivities with thermal modulation to create two dimensions of separation (Misselwitz *et al.*, 2013).

Crude oil and FO are extremely difficult to identify especially after weathering as FO is refined from the heaviest fraction of crude oils. FO provides similar physical properties and some chromatographic characteristics with crude oil. Crude oil and refined products from different sources often give different polycyclic aromatic hydrocarbon (PAH) and biomarker distributions (Zhang *et al.*, 2016). However, lower molecular weight PAHs are lost during the weathering, higher

molecular weight PAHs and biomarkers are more resistant to weathering and be a valuable fingerprinting for oil identification (Stout *et al.*, 2005).

This study is focused on the distributions of PAHs, such as anthracene (A), phenanthrene (P), dibenzothiophenes (D) and their alkyl-isomers and biomarkers, especially pristane, phytane and hopane in fresh crude oils, fuel oils and used lubricating oil comparing with weathering of these type of oils. The change of these chemical fingerprintings due to the weathering time also investigated.

CHAPTER II

THEORETICAL BACKGROUND AND LITERATURE REVIEW

2.1 Crude Oil and Refined Product

Crude oil is liquid petroleum that can be found beneath the earth's crust. It is classified as a fossil fuel which originated from decayed sea plants and animals matter in source rocks under temperature and pressure condition as illustrated in Figure 2.1. Crude oil contains primarily carbon and hydrogen called hydrocarbon, organic compounds like nitrogen, oxygen and sulfur together with small amount of metal such as nickel vanadium and iron (Freudenrich, 2016).

Several sources and conditions of oil forming leads to a variety of types and a difference in oil component. Crude oil is usually black, dark brown or it can also be yellowish and greenish, depending on its hydrocarbon composition. The variety of crude oil types are generally described in the terms of light or heavy according to API gravity of crude oil, and sweet or sour according to its sulfur content. The different composition results in a unique chemical that can be fingerprinting of each oil (Chevron, 2012).

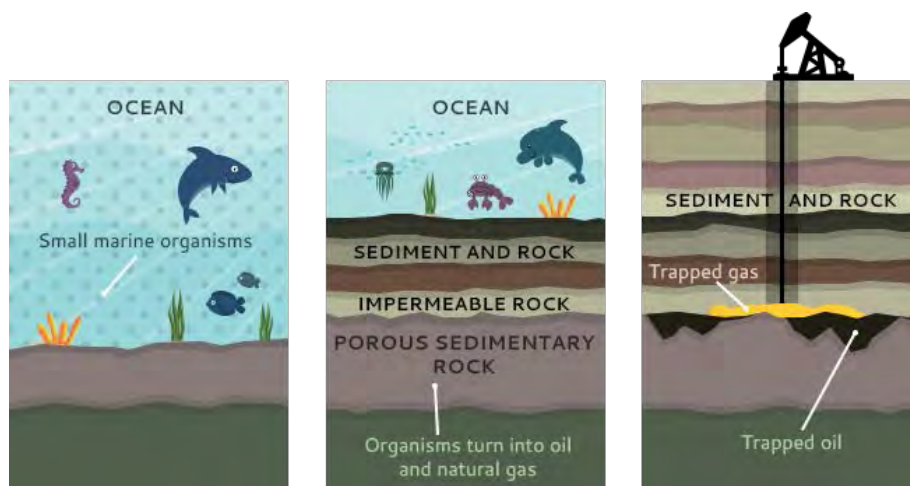


Figure 2.1 Crude oil formation diagram (History of Oil, 2014).

Crude oil will be refined and processed to produce useable refined products such as gasoline, jet fuel, diesel, lube oil and various forms of petrochemicals.

Distillation is the first stage to heat and fractionate crude oil. In this study will focus on only fuel oil and lubricating oil.

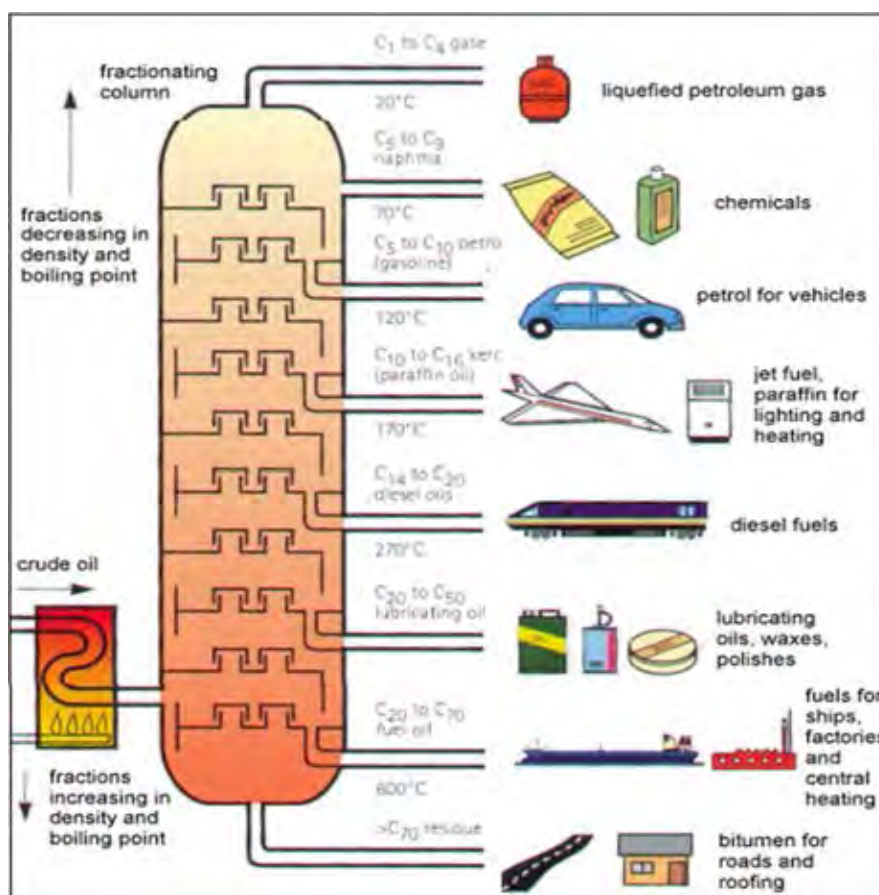


Figure 2.2 Scheme flowchart of oil refining process (Oil Refining Process, 2014).

Fuel oils (FOs) are produced from residuals in the oil refining process (Leffler, 2000). As light products demand are increasing, the additional steps, for example thermal cracking and catalytic cracking are added to refining process for producing more light products from the residuals. This result in lower quality especially in terms of higher concentration of sulfur, metals, ash or even related to catalyst fine and higher viscosity of cracked FO feedstocks than the feedstocks from straight run atmospheric and/or vacuum distilled residues (Uhler *et al.*, 2016). Due to low quality of FO feedstocks, blending with other lower boiling point and/or lighter residuals such as cracked gas oil and other refinery intermediates, is required in order

to achieve the FO performance specifications (Winkler, 2003). Each refinery operates individually therefore FO blending is particular to each refinery depends on its current operating and economic at that moment. While it may be complicated to complete FOs process, this will be an advantage in identification and tracking spilled residual fuels in the sea (Uhler *et al.*, 2016).

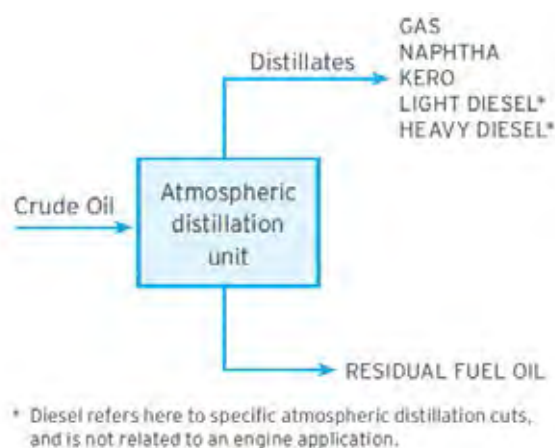


Figure 2.3 Simple straight run refinery block diagram (Chevron, 2012).

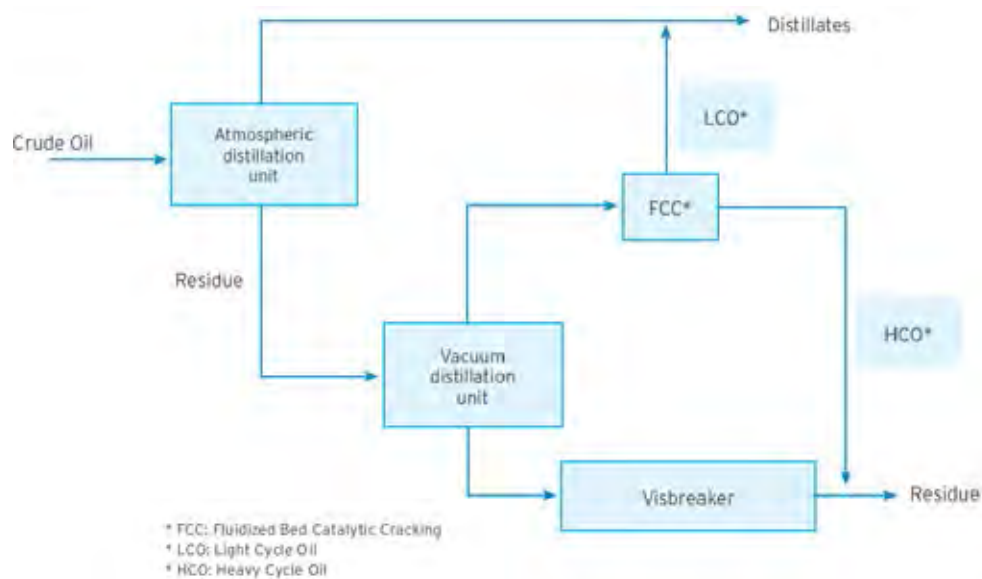


Figure 2.4 Complex refinery with FCC and visbreaking block diagram (Chevron, 2012).

Fuel oil is typically used as an energy fuel to generate heat in furnace and boiler or generate power in an engine. In the early twentieth century, a ship propulsion used diesel engines and there were a series of developments to make them possible to use heavy fuel oil (Chevron, 2012). Technically, fuel oils are labelled into 6 classes, numbering from 1 to 6, according to their boiling point, composition and purpose. In maritime, the ship or marine fuels are commonly called bunker fuels which is a generally referred to any type of fuel oil used on aboard vessel. Bunker fuels, typically, are classified into 3 types which is bunker A, B and C. Bunker A corresponds to distilled fuel No. 2 fuel oil, bunker B is synonymous with No. 4 or residual fuel oil No. 5 – also called navy special, and bunker C is generally used as a synonym for residual fuel oil No. 6 which is the most commonly used bunker oil. There are some conventional ways to classify the marine fuels, namely as the following (Bunker Oil-Marine Fuel Oil, 2016),

- Marine gas oil (MGO) which is similar to bunker A
- Marine diesel oil (MDO) is a blend of MGO and HFO
- Intermediate fuel oil (IFO) is a blend of MGO and HFO, with less gas oil than MDO
- Medium fuel oil (MFO) is a blend of MGO and HFO, with less gas oil than IFO
- Heavy fuel oil (HFO) is a residual fuel oil that similarly to No. 5 and 6

Table 2.1 Classification of marine fuel (Wallace, 2016, Bunker Oil-Marine Fuel Oil, 2016)

| Name | Alias | Type | Chain Length | Note |
|---------------|------------------------|----------------------|--------------|--------------------------|
| No.1 fuel oil | - | Distillated | 9-16 | Similar to Kerosene |
| No.2 fuel oil | Bunker A, MGO | Distillated | 10-20 | - |
| No.3 fuel oil | - | Distillated | 10-20 | Rarely used |
| No.4 fuel oil | Bunker B | Distillated/Residual | 12-70 | Blending with No.2 and 6 |
| No.5 fuel oil | Bunker B, navy special | Residual | 12-70 | Heavy fuel oil |
| No.6 fuel oil | Bunker C | Residual | 20-70 | or residual oil |

Lubricating oils or lubricants are substance to reduce friction and heat between the metal surfaces contact during their operation. Lubricating oils also improve performance, extend the operational life and also ensure the maximum output efficiency of the engine and equipments – gearboxes, compressors, motors, etc. Lube oil can be manufactured from petroleum and/or synthetic to meet specifications including of high boiling points, high viscosity indices, thermal stability, corrosion resistance and low freezing point (Uhler *et al.*, 2016). Lubricants compose of largely base oils and a small amount of chemical additives. Base oils or basic oils are usually referred to petroleum fractions called mineral oils and synthetic oils. The mineral-based lube oils are commonly used.

Mineral-based oil are obtained from a series of processing covered by (Stipanovic, 2003):

- (1) Basic distillation – To separate the fraction of crude oil proper for the mineral oil's end user.
- (2) Deasphalting – To expel undesirable heavy fraction of oil which could lead to gumming and other undesirable characteristics.
- (3) Extraction or solvent refining – To remove or reduce aromatic and related heteroaromatic compounds.
- (4) Dewaxing – To eliminate undesirable paraffins and other alkanes that could crystallize at low temperature.
- (5) Hydrotreating – To remove olefins and other unstable compounds which may cause smoking at high temperature

Base oils that are manufactured by mineral oils are typically classified into 2 types (1) naphthenic in nature or (2) paraffinic in nature, which mean (1) enriched with cyclic aliphatic hydrocarbon, in order words, small amount of aromatic or (2) containing mostly branched paraffins and only minimally normal paraffins, respectively. Synthetic base oils such as polyalphaolefins (PAO), esters, and polyglycols, are created by the chemicals reaction of several ingredients (Wang *et al.*, 2006). Additives are added into the lube oils in order to achieve desired properties – viscosity, thermal stability, foaming, compressibility, oxidation resistance, corrosivity, pour point, flash point, etc. The common additives using to blend with base oil are

emulsifiers, detergent, corrosion inhibitors, extreme pressure, alkaline (mostly added in marine oil to neutralize the engine) and along with others (Kopeliovich, 2012).

2.2 Petroleum Chemical Fingerprintings

2.2.1 Oil Chemical Composition

Petroleum composition, generally, can be characterized by their structures into groups of saturates, olefins, aromatics, resin and asphaltenes which might be known as SARA analysis.

- Saturates are an influential hydrocarbon with only carbon-carbon bonds groups of oil for example, paraffins (straight and branched HC chain), naphthenes (alkanes ring structure or cycloalkanes) and also including biomarkers.
- Olefines or alkenes are unsaturated hydrocarbons that consist of at least one double carbon-carbon bonds. These components are particularly found in some refined products, but rarely to find in crude oil as they are formed from larger molecules in cracking processes.
- Aromatic hydrocarbons are cyclic and planar compound. Aromatics in petroleum are consist of mono-aromatic hydrocarbons – benzene, toluene, ethylbenzene and xylene (BTEX), other alkyl-substituted benzene compounds and condensed aromatic benzene rings called polycyclic aromatic hydrocarbons (PAHs).
- Resins and Asphaltenes, which are typically concentrated in heaviest fraction of oils, are polar compounds or heteroatom constituents which bearing nitrogen, sulfur and oxygen atoms (also called NSO compounds) (Lundegard and Knott, 2014). In petroleum industry, resins are called for groups of small polar compounds such as NOS compounds containing in PAHs, phenols, acids, alcohol and monoaromatic steroids.

- Asphaltenes are large heteroatomic compounds which not dissolve in oil, but are dispersed as colloids. The quantity of asphaltenes has a significant effect on oil behavior. Table 2.2 shows that heavy oils comprise more aromatics and heteroatomic compound such as N-, O-, S- and metal containing (Wang *et al.*, 2006; Speight, 2007; Lundegard and Knott, 2001).

Table 2.2 Typical composition of crude oil and petroleum products (Wang *et al.*, 2006)

| Group | Compound Class | Gasoline | Diesel | Light crude | Heavy crude | IFO | Bunker C |
|------------------------|----------------|----------|--------|-------------|-------------|----------|----------|
| Saturates | | 50-60 | 65-95 | 55-90 | 25-80 | 25-45 | 20-40 |
| | alkanes | 45-55 | 35-45 | | | | |
| | cyclo-alkanes | ~5 | 30-50 | | | | |
| | waxes | | 0-1 | 0-20 | 0-10 | 2-10 | 5-15 |
| Olefins | | 5-10 | 0-10 | - | - | - | - |
| Aromatics | | 25-40 | 5-25 | 10-35 | 15-40 | 40-60 | 30-50 |
| | BTEX | 15-35 | 0.5-2 | 0.1-2.5 | 0.01-2 | 0.05-1 | 0-1 |
| | PAHs | | 0.5-5 | 0.5-3 | 1-4 | 1-10 | 1-10 |
| Polar compounds | | - | 0-2 | 1-15 | 5-40 | 15-25 | 10-30 |
| | resins | - | 0-2 | 0-10 | 2-25 | 10-15 | 10-20 |
| | asphaltenes | - | - | 0-10 | 0-20 | 5-10 | 5-20 |
| Sulphur | | <0.05 | 0.05 | 0-2 | 0-5 | 0.5-2 | 2-4 |
| Metals (ppm) | | | | 30-50 | 100-500 | 100-1000 | 100-2000 |

BTEX = benzene, toluene, ethylbenzene, and xylenes; PAHs = polycyclic aromatic hydrocarbons.

2.2.2 PAHs

Polycyclic aromatic hydrocarbons or polynuclear aromatic hydrocarbons (PAHs) are consisted of two or more benzene rings which are condensed together. Commonly, PAHs are the molecules contain two to seven benzene rings. Table 2.3 shows a part of physical and chemical properties of some PAHs which vary with molecular weight. PAHs resistance to oxidation, reduction and vaporization are

increased with increasing molecular weight. From these reasons, PAHs are different in distribution in environment, their behavior and effect on biological system (Nagpal, 1993). PAHs may cause a health hazard as most of these class of chemicals are toxic, carcinogenic and relatively persistent in the environment. Naphthalene, anthracene and phenanthrene are three simple compound in this class. Naphthalenes are the smallest and lowest molecular weight of all PAHs that structured by condensing two benzene rings together also called as bicyclic. Anthracene and phenanthrene are tricyclic aromatic hydrocarbon which contained of 3 benzene rings. PAHs are an important fingerprinting for the characterization and identification of spilled oil.

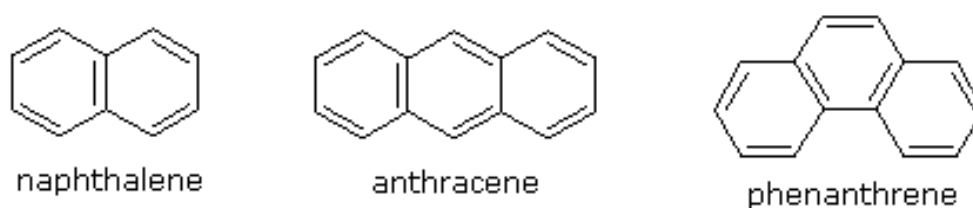


Figure 2.5 The structures of naphthalene anthracene and phenanthrene (Reusch, 2013).

2.2.2.1 Characterization PAHs in Heavy Oil

The concentration and distribution of PAHs present and differentiate the composition of original crude oil feedstock from its intermediates or residuals refined products. Phenanthrenes are dominant aromatic hydrocarbon presenting in the most of oils and typically used to distinguish between combustion and petroleum source (Yunker *et al.*, 2002). Comparing crude oil with heavy fuel oil (HFO) using the relative of phenanthrene (Phe), anthracene (Ant), methyl-phenanthrene (MP) and methyl-anthracene (MA). As shown in Figure 2.6, the relative of 2-methyl-anthracene in crude oil is much less abundant than HFO. Methyl-anthracenes, particular 2-MA, are pyrolytic organic materials which may be produced under pyrolytic condition e.g. thermal cracking (Zhang *et al.*, 2016). The alkylated phenanthrene indices are interesting measures for maturity of sedimentary organic matter and there are several related ratios used in petroleum geochemistry field. Zhang *et al.* (2016) also studied on double ratio plots of diagnostic indices based on

phenanthrene, anthracene and their alkylation for distinguish HFOs and crude oils as shown in Figure 2.7.

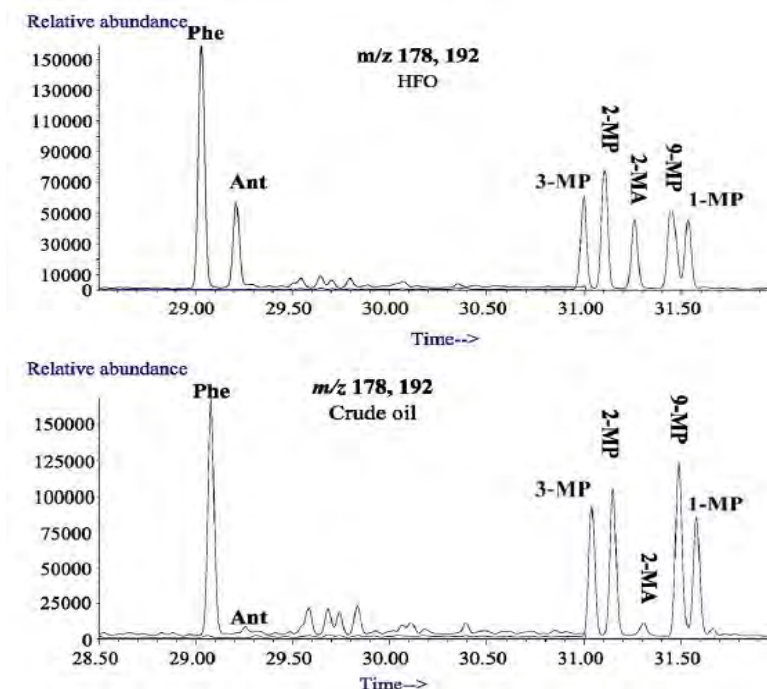


Figure 2.6 Phe, Ant, MP and MA mass-chromatograms of HFO and crude oil (Zhang *et al.*, 2016).

Four- to six- ring PAHs, for example, fluoranthenes, pyrenes and benzofluoranthenes are usually exist at only low concentration or not detectable in most crude oil and distillate fuels, but these compounds are found and detectable in HFOs as they are concentrated within distilled residual and/or produced during the process (Uhler *et al.*, 2016). Moreover, 4, 5- and 6- ring PAHs are the most PAH compound environmentally stable and their relative ratios are potential use in source identification (Emsbo-Mattingly *et al.*, 2006).

For lubricating oil, most of aromatic hydrocarbons including PAHs are removed during refining base oil process in order to improve the performance characteristics of lube oil. Consequently, PAHs in fresh lube oil is presented in very little concentration. However, PAHs concentration in used lube oil (ULO) are usually higher than fresh lube oil due to the formation of pyrogenic high

molecular weight PAHs (4- to 6- rings) during heating while in use and contaminating by low molecular weight PAHs (dominant 3- rings alkylated phenanthrenes) from unburned fuel oil and combustion residue. Uhler *et al.*(2016) suggested that as the common use of diesel fuel in marine industry, some unburnt fuels from middle distillate, specifically diesel fuel may be mixed with lubricating oil (Uhler *et al.*, 2016 and Yang *et al*, 2016).

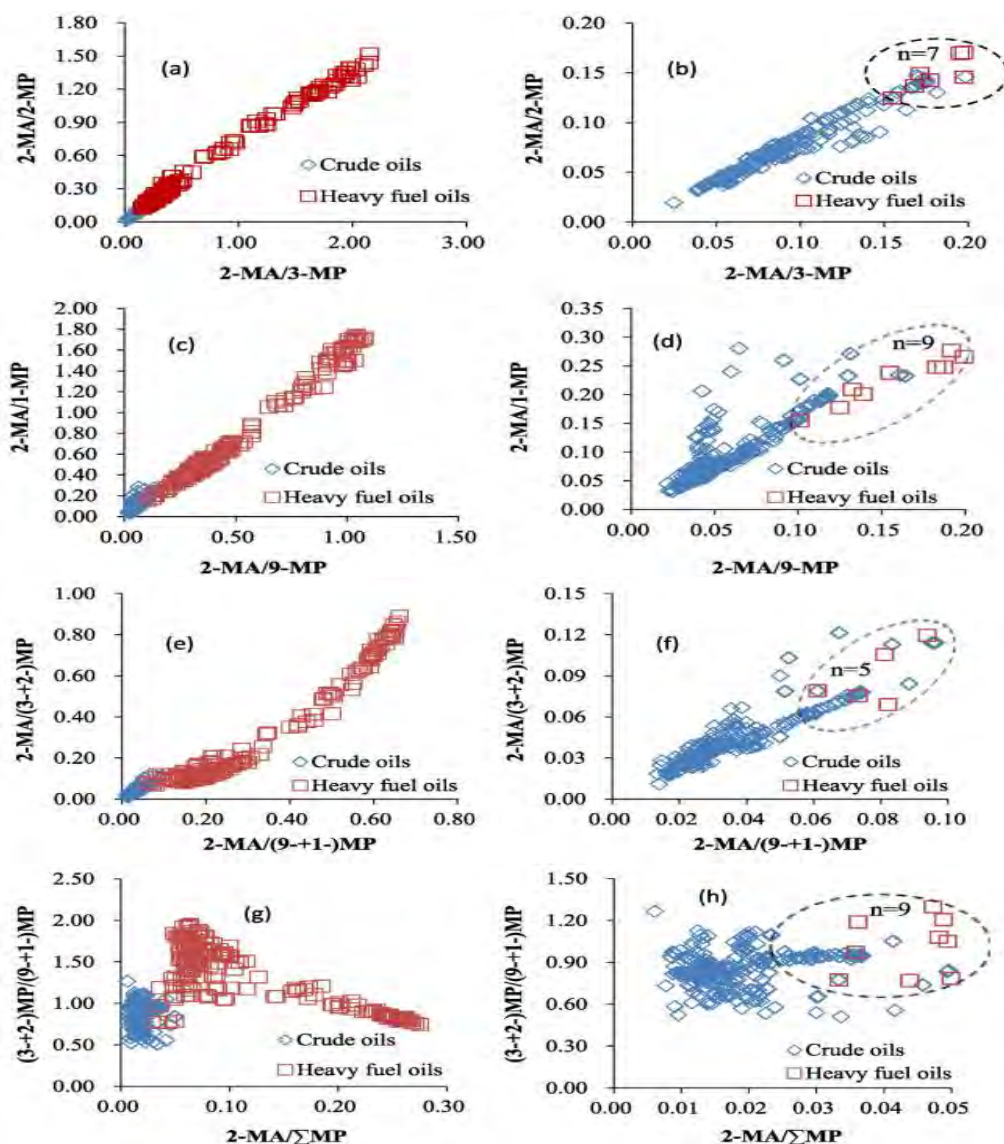


Figure 2.7 Double ratio plots of Phe, Ant and their alkylation of HFOs and crude oils (Zhang *et al.*, 2016).

2.2.3 Biomarkers

Biomarkers or biological markers are complex organic hydrocarbon molecules or known as molecule fossils which derived from living organisms in the source rock (Misselwitz *et al.*, 2013). Biomarkers are one of the most useful and important hydrocarbon groups in petroleum for oil characterization and identification as they preserve all or most prominent structure of original natural product and their similarly structure. Biomarkers are also more resistant to weathering and degradation than other hydrocarbon groups. Furthermore, biomarkers are formed under varieties of geological condition and ages which may exhibit a unique biomarker fingerprint in every crude oil. Chemical analysis of biomarkers is an essential information of forensic investigation included of tracing the source of spilled oil, differentiating oils, monitoring the degradation process and weathering state of oils (Wang *et al.*, 2004).

Pristane (2,6,10,14- tetramethyl pentadecane) and phytane (2,6,10,14-tetramethyl hexadecane) are the common aliphatic biomarker that became dominant highly weathered compounds in crude oils until they are degraded. The pristane/phytane (Pr/Ph) ratio is one of the most commonly used correlation parameters which have been used as an indicator of biodegradation (Moustafa *et al.*, 2012 and Liv-Guri Faksness *et al.*, 2002)

2.2.3.1 *Biomarker Distribution in Heavy Oil* (Wang *et al.*, 2004)

Various biomarkers can be detected in different carbon ranger of crude oil as illustrated in Figure 2.8. Hopanes (pentacyclic terpanes) and steranes are the most common biomarkers observed in crude oil (Mulabagal, 2013). Finished or refined petroleum products, which are obtained from crude oil, can have wide variety in chemical compositions depending on their parent crude oil feed stocks and the variety of refining approach and conditions, applications, economic requirements.

Some cases, two oils are given similarly or comparably *n*-alkane and isoprenoid distributions which observed from GC-FID whereas their biomarkers distribution may give differently. The biomarker distribution patterns are generally different from crude oil to refined products. The differences in the relative distribution of terpanes in crude oil and refined products are presented in Figure 2.9. The concentration and variety distribution of terpane in finished products are lower

than crude oils since refining process have removed or concentrated high molecular mass biomarkers from their parent crude oil feedstock.

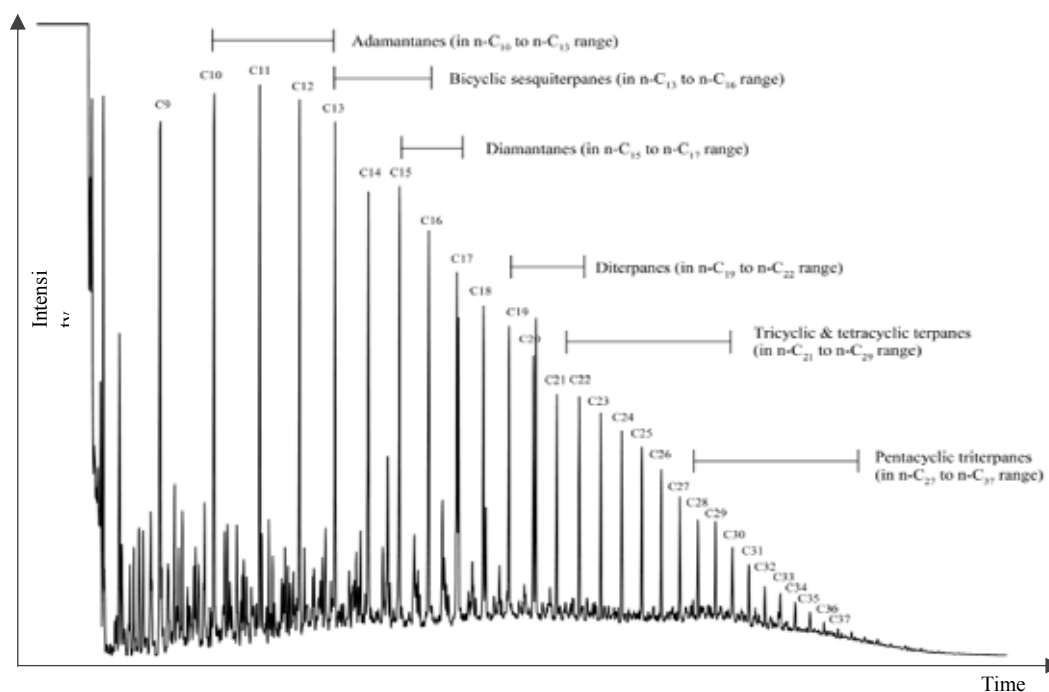


Figure 2.8 Carbon number range of common cyclic biomarkers present in crude oils and refined products (Wang *et al.*, 2004).

Some cases, two oils are given similarly or comparably *n*-alkane and isoprenoid distributions which observed from GC-FID whereas their biomarkers distribution may give differently. The biomarker distribution patterns are generally different from crude oil to refined products. The differences in the relative distribution of terpanes in crude oil and refined products are presented in Figure 2.9. The concentration and variety distribution of terpane in finished products are lower than crude oils since refining process have removed or concentrated high molecular mass biomarkers from their parent crude oil feedstock.

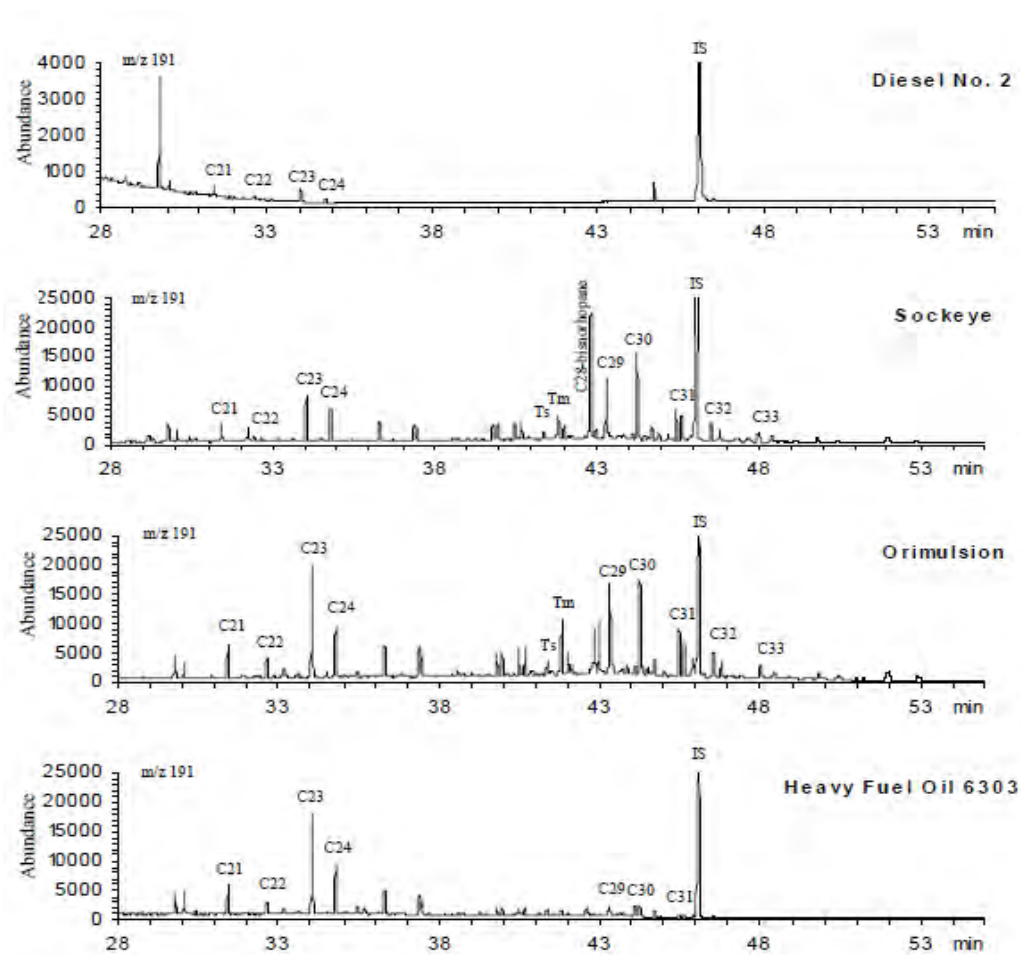


Figure 2.9 Distribution of biomarker terpane compounds (at m/z 191) in different oils (Wang *et al.*, 2004).

For lubricate oil, biomarkers are usually located in the high carbon range, contained in high level when compared with other petroleum products and can be detected in equivalent or higher concentrations in comparison with their crude oils feedstock as these compounds remain in the residual fraction during the distillation (Uhler *et al.*, 2016) as shown in Figure 2.10. Lubricants are refined from middle to heavy fraction base oil, thus they are rich in high carbon range of terpane and steranes but contain relatively low lighter tricyclic terpanes (C₂₁-C₂₄). Furthermore, smaller biomarkers including bicyclic sesquiterpanes (C₁₄-C₁₆) and diamondoid hydrocarbon (adamantanes, C₁₀-C₁₄ and adamantanes, C₁₄-C₁₆) are rarely detected in virgin (fresh)

lubricants, but they are detectable in used and waste lube oil due to the diesel contamination (Yang *et al.*, 2016).

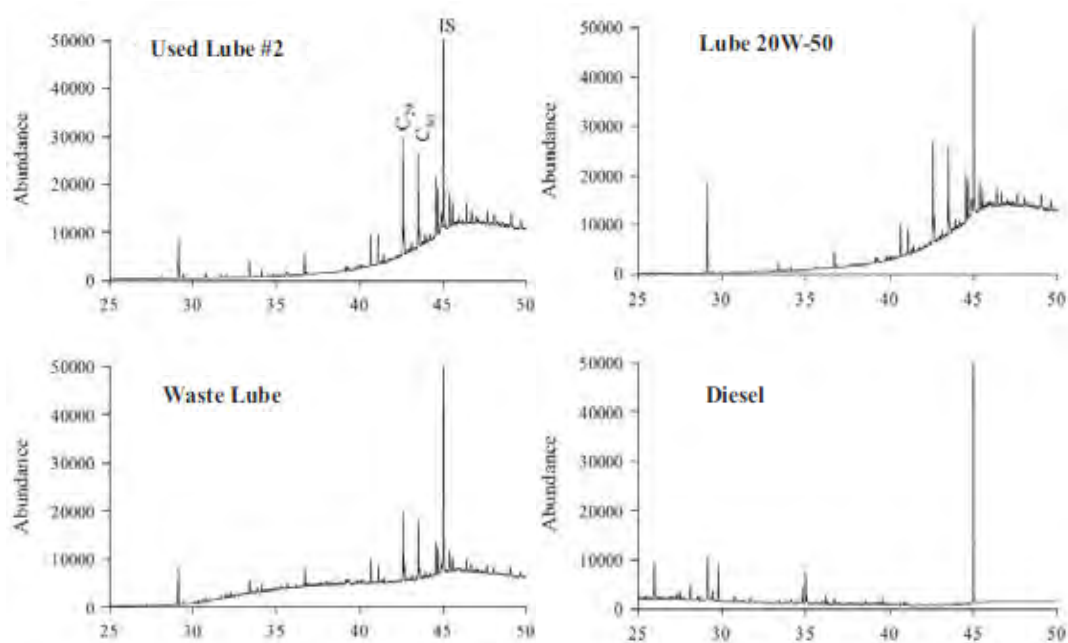


Figure 2.10 Chromatogram of biomarker terpane (m/z 191) in different lube oils (Yang *et al.*, 2016).

Table 2.3 A part of physics and chemical properties of some PAHs (Nagpal, 1993)

| PAH | MW (g) | Benzene (total) rings | Solubility at 25 °C ($\mu\text{g/L}$) | Vap. Pressure at 25 °C (mm Hg) | Carcino- genicity |
|----------------------|-----------|-----------------------------|---|--------------------------------------|----------------------|
| Naphthalene | 128.2 | 2 | 12500 -34000 | 1.8×10^{-2} | NC |
| Acenaphthylene | 152.2 | 2 | 3420 | $10^{-3} - 10^{-4}$ | NC |
| Acenaphthene | 154.2 | 2 | | | NC |
| Fluorene | 166.2 | 2 (3) | 800 | | NC |
| Anthracene | 178.2 | 3 | 59 | 2.4×10^{-4} | NC |
| Phenanthrene | 178.2 | 3 | 435 | 6.8×10^{-4} | NC |
| Acridine | 179.2 | 3 | | | NC |
| 2-Methylanthracene | 192.3 | 3 | 21.3 | | NC |
| 9-Methylphenanthrene | 192.3 | 3 | 261 | | NC |
| 1-Methylphenanthrene | 192.3 | 3 | 269 | | NC |
| Fluoranthene | 202.3 | 3 (4) | 260 | | NC |

Table 2.3 (cont.) A part of physics and chemical properties of some PAHs (Nagpal, 1993)

| PAH | MW (g) | Benzene (total) rings | Solubility at 25 °C (µg/L) | Vap. Pressure at 25 °C (mm Hg) | Carcino- genicity |
|--------------------------------|-----------|-----------------------------|----------------------------------|--------------------------------------|----------------------|
| 9,10-Dimethylanthracene | 206.3 | 3 | 56 | | NC |
| Benzo[a]fluorene | 216.3 | 3 (4) | 45 | | NC |
| Benzo[b]fluorene | 216.3 | 3 (4) | 29.6 | | NC |
| Pyrene | 202.1 | 4 | 133 | 6.9×10^{-7} | NC |
| Benz[a]anthracene | 228.3 | 4 | 11.0 | 1.1×10^{-7} | C |
| Naphthacene | 228.3 | 4 | 1.0 | | NC |
| Chrysene | 228.3 | 4 | 1.9 | | WC |
| Triphenylene | 228.3 | 4 | 43 | | |
| Benzo[b]fluoranthene | 252.3 | 4 (5) | 2.4 | | C |
| Benzo[j]fluoranthene | 252.3 | 4 (5) | 2.4 | | C |
| Cholanthrene | 254.3 | 4 (5) | 2.0 | | C |
| 7,12-Dimethylbenz[a]anthracene | 256.3 | 4 | 1.5 | | SC |
| Dibenzo[a,h]fluorene | 266.3 | 4 (5) | 0.8 | | WC |
| Dibenzo[a,g]fluorene | 266.3 | 4 (5) | 0.8 | | C |
| Dibenzo[a,c]fluorene | 266.3 | 4 (5) | 0.8 | | WC |
| 3-Methylcholanthrene | 267.3 | 4 (5) | 0.7 | | SC |
| Benzo[ghi]fluoranthene | 214.2 | 4 (5) | 0.5 | | NC |
| Benzo[a]pyrene | 252.3 | 5 | 3.8 | 5.5×10^{-9} | SC |
| Benzo[e]pyrene | 252.3 | 5 | 2.4 | 5.5×10^{-9} | NC |
| Perylene | 252.3 | 5 | 2.4 | | NC |
| Indeno(1,2,3-cd)pyrene | 276.3 | 5(6) | - | | C |
| Dibenz[a,h]anthracene | 278.3 | 5 | 0.4 | | C |
| Benzo[ghi]perylene | 276.4 | 6 | 0.3 | 1.0×10^{-10} | NC |
| Coronene | 300.3 | 7 | 0.14 | 1.5×10^{-11} | NC |

Note: NC = Non-carcinogenic, WC = Weakly carcinogenic, C = Carcinogenic, SC = Strongly carcinogen

2.2.4 Weathering Process (ITOPF, 2011)

Once oil spill into the sea, it is subject to a number of physical and chemical changes because of various natural processes namely weathering include of spreading, evaporation, dispersion, emulsification, dissolution, photo-oxidation, sedimentation and sinking, biodegradation. The natural weathering processes are complicated and have many important factors for example, duration time of

weathering, quantity and type of spilled oil, prevailing weather and sea condition. (Wang *et al.*, 2013).

2.2.4.1 Spreading

Spreading of the oil occurs immediately after oil is discharged into the sea. The rate of spreading depends on winds, turbulence, waves, tidal stream and current and the most directly influential factors are viscosity and volume of spilled oil. The less viscosity fluid, the faster it will spread and increase the sea surface area covered by oil slick.

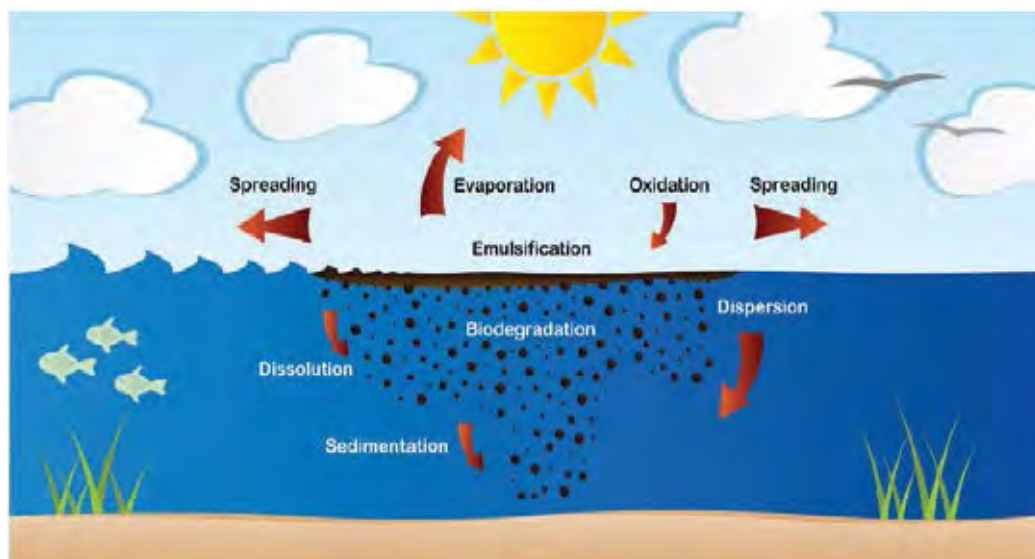


Figure 2.11 Weathering processes (ITOPF, 2011).

2.2.4.2 Evaporation

Evaporation involves with losing low components. Generally, oil components with having boiling point below 200°C will evaporate to the atmosphere within 24 hours. The evaporating rate depends on ambient temperature, wind speed and the rate of spreading. Because the increasing surface area of the spill allows more light component evaporated. Additionally rough seas, high wind speeds and warm temperatures also increase evaporation rates.

2.2.4.3 Dispersion

Dispersion is the action of wave and turbulence at the sea surface break all or part of oil slick into droplets. The oil droplets can be either remain in suspension if they are in very small size, or float back to the surface if they are fairly large. The large droplets that rise back to the sea surface may rebuild a slick by coalesced with other droplets or spread themselves out to very thin film. The rate of dispersion is mainly rely on the viscosity of spilled oil and the sea condition. Lower viscosity oils disperse faster and easier within only a few days. The result of dispersion, slick thin film and small droplet suspension, also support other procedures such as dissolution, biodegradation and sedimentation.

2.2.4.4 Emulsification

This process is an incorporation of oil and water droplet forming water in oil. Emulsification changes volume of oil, thickness of the oil slick and causes clean up more difficult. Wave and wind cause emulsification. Viscosity and composition of oil is influenced in emulsification process. Oils which contain grater metals (Ni/V) or asphaltenes are easier to emulsify than lower metals or asphaltenes concentration oils. However, more viscous oils like heavy fuel oil will emulsify at slower rates than less viscous oils. Increasing amount of water that integrate oil and water, emulsions become more viscous and stable (70%-80% water). Once they are stay in the stable state, they are highly persistent and may remain emulsions continually. On the other hand, less stable emulsions are heated in the sun and may isolate into water and oil.

2.2.4.5 Dissolution

Dissolution rate is built upon oil compositions, spreading, water temperature, turbulence and degree of dispersion. Typically, the dissolve hydrocarbons concentration in the sea after oil spill is rarely exceed 1 ppm and has no significant in cleaning procedure since the heavy fractions are indissoluble in the sea while lighter components are slightly dissolve, but they are rapidly loss during evaporation process.

2.2.4.6 Photo-oxidation

As hydrocarbon can react with oxygen, photo-oxidation is leaded to form tars or soluble compounds. Despite photo-oxidation occurs during the

entire spilled period, it causes only in long-term duration process and a minor effect compared to other weathering processes such as evaporation, dispersion and spreading.

2.2.4.7 *Sedimentation and Sinking*

Generally, most oils have low specific gravities that make them float on the surface. Sedimentation, is a long terms process, occurs from dispersed oil droplets interact with sediment particle or organic matter suspended and become substantial and dense enough to sink to the seabed. Heavy oil including heavy crude oil, most heavy fuel oil and water in oil emulsion have specific gravity equivalent to or greater than the sea, even they have less interaction with water they can be sufficient to cause sinking. However, sinking is only observed in shallow water or the area nearby shore.

2.2.4.8 *Biodegradation*

Biodegradation is one of long term weathering process. This process is a metabolism of oil compounds by the microorganisms such as bacteria, fungi, yeast, moulds and protozoa. Different microorganisms degrade specific hydrocarbons, thus multiple species of microorganisms must be involved for biodegradation. Biodegradation is influenced by oil properties, temperature, amount of oxygen and nutrients. Microorganism populations increase during a spill due to the availability of nutrients increasing. Once nutrients and oxygen become limiting, populations return to their natural state. Larger and more complex molecules are more difficult to biodegrade.

2.2.5 Effect of Weathering on Chemical Fingerprintings (Zhang *et al.*, 2015)

Zhang *et al.* (2015) studied on weathering process under 95-day natural weathering condition of Dalian crude oil using GC-MS. Aliphatic hydrocarbons including normal alkanes and isoalkanes are undergone with weathering process. Prominent aliphatic compounds like pristane (Pr) and phytane (Ph) are stronger degradation from weathering effects than n-alkanes. The commonly used diagnostic ratios for n-alkanes (e.g. C17/Pr, C18/Ph, Pr/Ph) changed seriously. Furthermore, Ph shows more resistant degradation compared to Pr. For polycyclic aromatic hydrocarbon and alkylated homologues, lower molecular weight of these compound are influenced during the weathering process. They observed five families of PAHs

composed of naphthalenes (N), phenanthrenes (P), dibenzothiophenes (D), fluorens (F), chrysenes (C) and their alkylated homologues. The result showed that naphthalene and its isomers weathered first followed by P and its methyl isomers. On the other hand, biomarkers showed good stability with nearly constant of diagnostic ratio during the weathering period.

2.3 Oil Spill Characterization and Identification Methodology

2.3.1 Chemical Fingerprinting Techniques

Analyzing hydrocarbons in oil either use instrumental and non-instrumental techniques such as gas chromatography (GC), gas chromatography-mass spectrometry (GC-MS), high-performance liquid chromatography (HPLC), size-exclusion HPLC, infrared spectroscopy (IR), supercritical fluid chromatography (SFC), thin-layer chromatography (TLC), ultraviolet (UV) and fluorescence spectroscopy, isotope ratio mass spectrometry, and gravimetric methods (Wang *et al.*, 1999). However GC techniques are the most commonly used to identify biomarkers and other chemical fingerprinting. GC-MS can be considered as the most normally used while GC provides significant advantage of the separation of different structures of biomarkers and MS can detect and identify these structures (Moustafa *et al.*, 2012).

Gas chromatography has three main parts which are injector, column and detector. The sample solution is injected into the instrument by injector and immediately vaporized into a vapor phase. The sample steam is carried to column in order to separate various components using carrier gas such as helium and nitrogen. The separated components are detected and measured quantities by detector.

The GC column is the heart of the separation system; the structure of the stationary phase and the packed material greatly influence the separation of the compounds and affect the time of separation (retention time). Generally, two type of column which are packed and capillary columns have been used. The capillary columns give better fine structured chromatographic fingerprints and it widely used in environmental forensic than the packed columns. The column is placed in an oven where temperature can be controlled accurately over a wide range of temperatures (Moustafa *et al.*, 2012).

There are many different types of detectors which can choose based on the compounds to be analyzed, application, sensitivity and required data (quantitative and qualitative data). The mass spectrometer is widely used for a gas chromatograph due to its high sensitivity and specificity and its capability to elucidate compound structure. Therefore GC-MS have become the well-known principal and techniques in the oil spill identification work (Barakat *et al.*, 1997; Pavlova A. *et al.*, 2003; Sun, 2009; Kamalia, 2011; Mulabagal *et al.*, 2013). However, the result from GC-MS will be complex with peaks that coelute due to a lot of information (Christensen *et al.*, 2005), GCxGC-TOFMS is used instead of GC-MS which easier to identify because it offers continuous full range non-skewed mass spectral information and fast acquisition rates ideal (Misselwitz *et la.*, 2013).

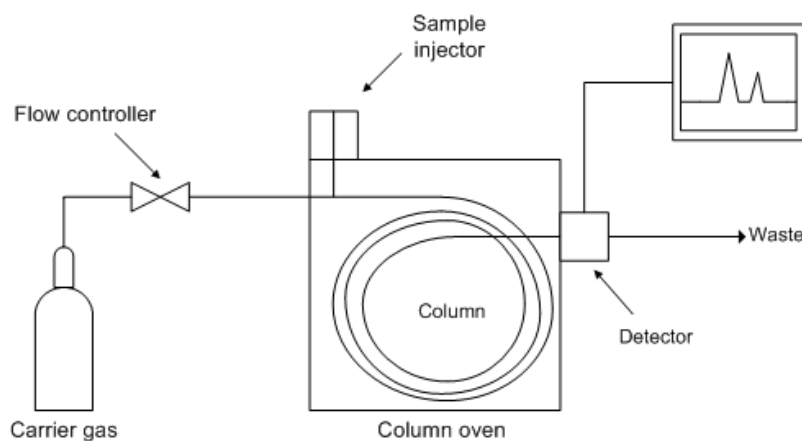


Figure 12 Diagram of gas chromatograph (Helmenstine, 2016).

2.3.2 NORDTEST Methodology for Oil Spill Identification (Liv-Guri Faksness *et al.*, 2002)

NORDTEST is recommended the new methodology to identify oil spill which is based on a reversion of the NORDTEST method NT CHEM 001 “Oil spill identification” (1991) and has been tested and verify in a Round Robin test. The Round Robid test demonstrated the potential of this method as a strong technically defensible tool in oil spill identification. The procedure chart of the recommended methodology

is illustrated in Figure 2.13 and tiered “levels” of analyses and data treatment are concluded.

Level 1: After sample preparation, the chemical fingerprint analysis in laboratory starts with GC-FID. This level gives a basic hydrocarbon information such as overall boiling (carbon) range of the oil (valuable for deciding which biomarkers are most relevant for the spill) and acyclic isoprenoid indices. At this level, the spill sample can be qualitatively and quantitatively compared to the suspected source, and obviously “non-match” samples can be eliminated from additional levels of analysis.

Level 2: This next analytical level uses GC-MS in the selected ion monitoring mode (SIM mode). This analysis is useful for determining the content and distributions of suite of petroleum biomarkers and polycyclic aromatic hydrocarbons (PAHs) target. Diagnostic ratios of PAH and selected biomarkers are calculated in the step.

Level 3: This level assess the results from level 1 and level 2 to evaluating the diagnostic ratios and eliminating any of those that have variability. The diagnostic ratios which more robust are used for correlation analysis using student’s t statistic tool. The results can be shown as a correlation, simple x-y, plot which benefit in identify a positive match of spilled oil and suspected sources.

Observation’s diagnostic ratio can be calculated by equation (2.1)

$$\text{Diagnostic ratio} = \frac{100 \times A}{(A + B)} \quad (2.1)$$

A and B are concentrations generated from a multi-point calibration curve for biomarker compound with standard.

For biomarkers with no corresponding standard, the values for A and B were (area of analyte) / (area of internal standard).

Correlation analysis of Diagnostic ratio (2.2)

$$\mu = x \pm \frac{t \times s}{\sqrt{N}} \quad (2.2)$$

Where, \bar{x} is mean value, the center of the distribution.
 s is standard deviation.
 t is student's t distribution.
 N is number of observations.

T value is a relation between degree of freedom (N-1) and confident level which can be found in Table 2.4

Table 2.4 Values of Student's t (Harris, 1995)

| Degree of freedom (N-1) | Confidence level (%) | | |
|----------------------------|----------------------|--------|--------|
| | 95 | 98 | 99 |
| 1 | 12.706 | 31.821 | 63.657 |
| 2 | 4.303 | 6.965 | 9.925 |
| 3 | 3.182 | 4.541 | 5.841 |
| 4 | 2.776 | 3.747 | 4.604 |
| 5 | 2.571 | 3.365 | 4.032 |
| ∞ | 1.960 | 2.236 | 2.576 |

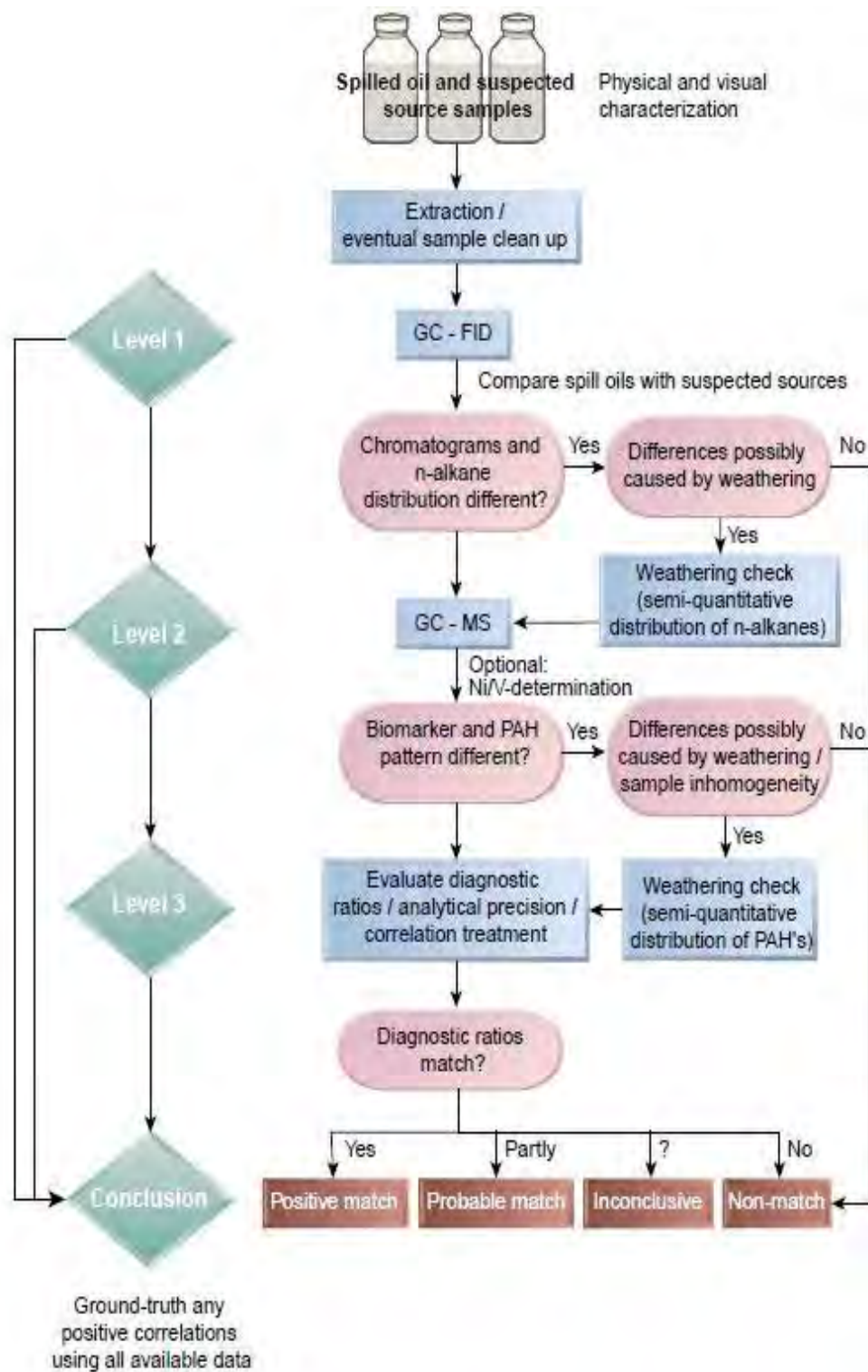


Figure 2.13 Protocol/decision chart for oil spill identification (Liv-Guri Faksness *et al.*, 2002).

Based on the example from the Round Robin study which shown in Figure 2.14-2.18, it is suggested a definition of positive match at a 95 % confidence interval and other correlation analysis of the diagnostic ratios are used to classify the sample as described in Table 2.5.

Table 2.5 Recommended criteria for correlation studies of diagnostic ratios (Liv-Guri Faksness *et al.*, 2002)

| Classification | Definition |
|-----------------------|--------------------------------|
| Positive match | All DRs within the CL 95 % |
| Possible match | All DRs within the CL 98 % CL |
| No match | Any key DRs outside of CL 98 % |

Note DRs = Diagnostic ratios, CL = Confidence limit

The comparing result of the spill sample and suspected source(s) are presented in x-y plots, linear regressions are performed, and conclusion based on the “fit” between spill and source samples for the selected suite of robust diagnostic ratios can be made.

The straight line ($x=y$) is presented the perfect match which is all DRs of the spill samples are exactly the same as the suspected source oil. If the error bars of all DRs are overlapping the straight line, the spill sample shows positive match to the source oil as shown in Figure 2.14. Unless one of the DRs is overlapping the line $x=y$, it could be concluded no match to the source oil as illustrated in Figure 2.15.

The use of different confidence intervals such as 95 %, 98 %, and 99 % CL is shown in Figures 2.16, 2.17, and 2.18, respectively. It showed that some of the ratios are still outside the straight line although it was increased to 98 % or 99 % which gave the same conclusion “No match”.

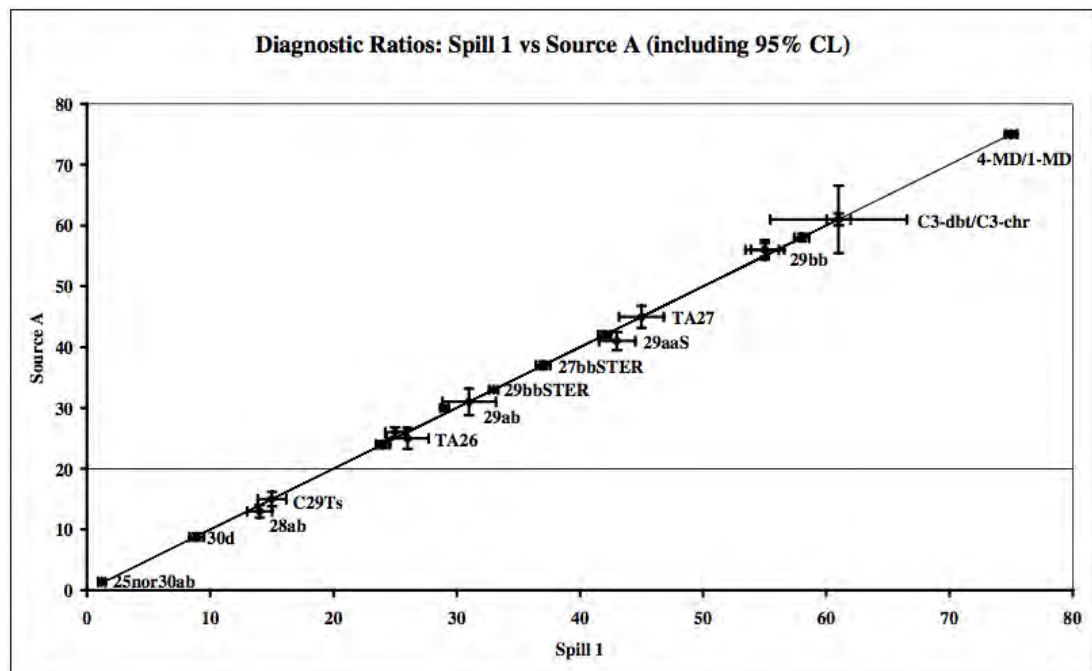


Figure 2.14 Correlation between spill 1 and source A, using a 95 % confidence limit (Positive match) (Liv-Guri Faksness *et al.*, 2002).

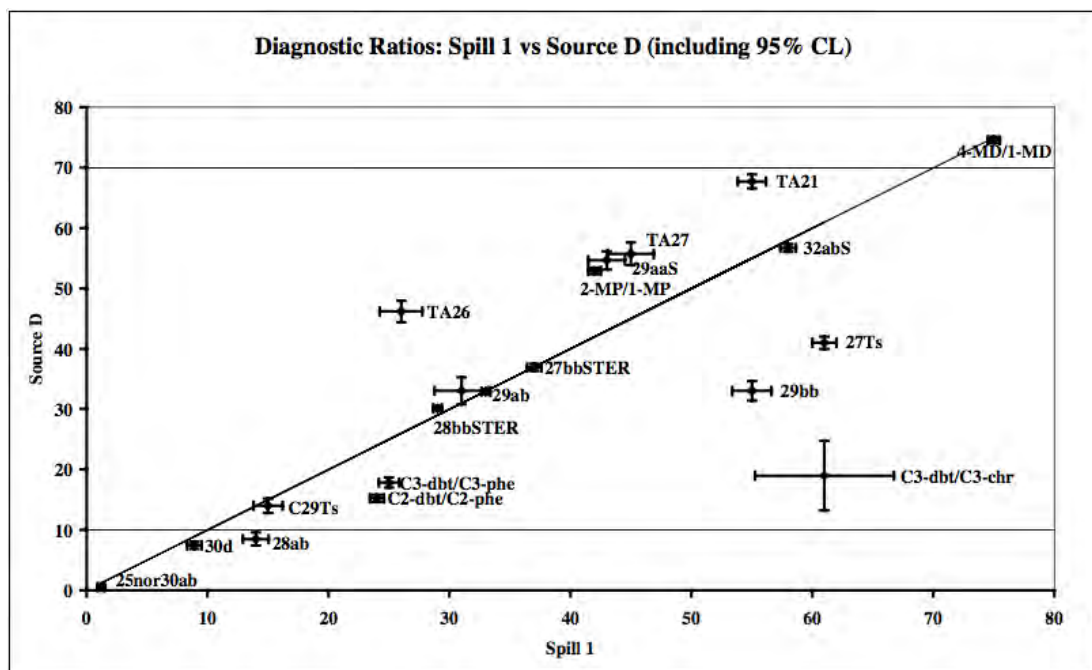


Figure 2.15 Correlation between spill 1 and source D, using a 95 % confidence limit (Non match) (Liv-Guri Faksness *et al.*, 2002).

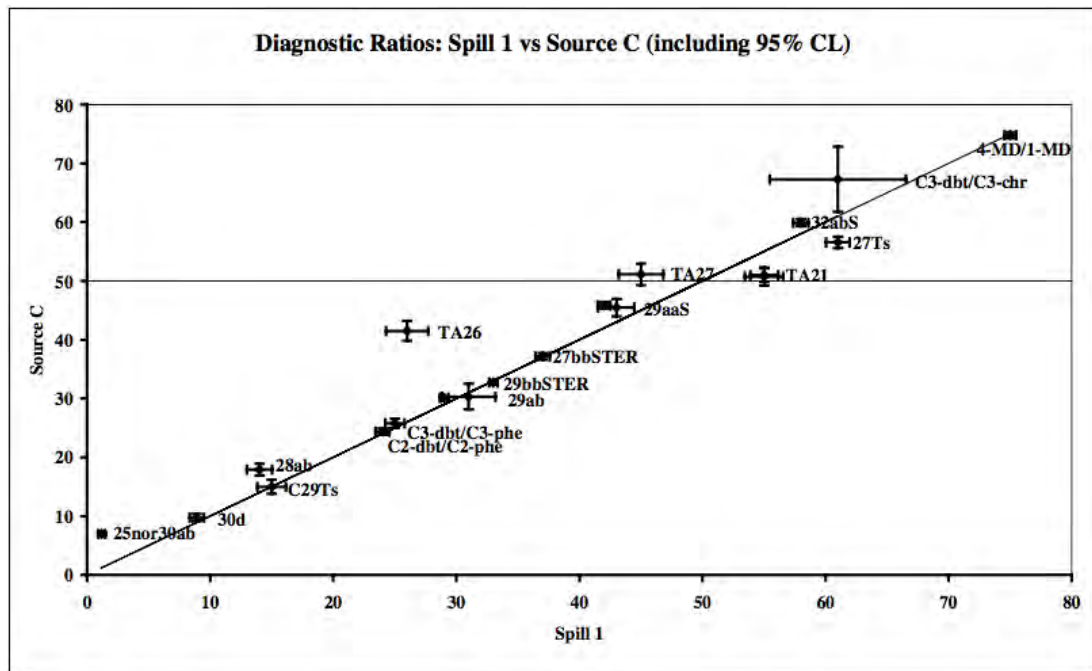


Figure 2.16 Correlation between spill 1 and source C, using a 95 % confidence limit (Non match) (Liv-Guri Faksness *et al.*, 2002).

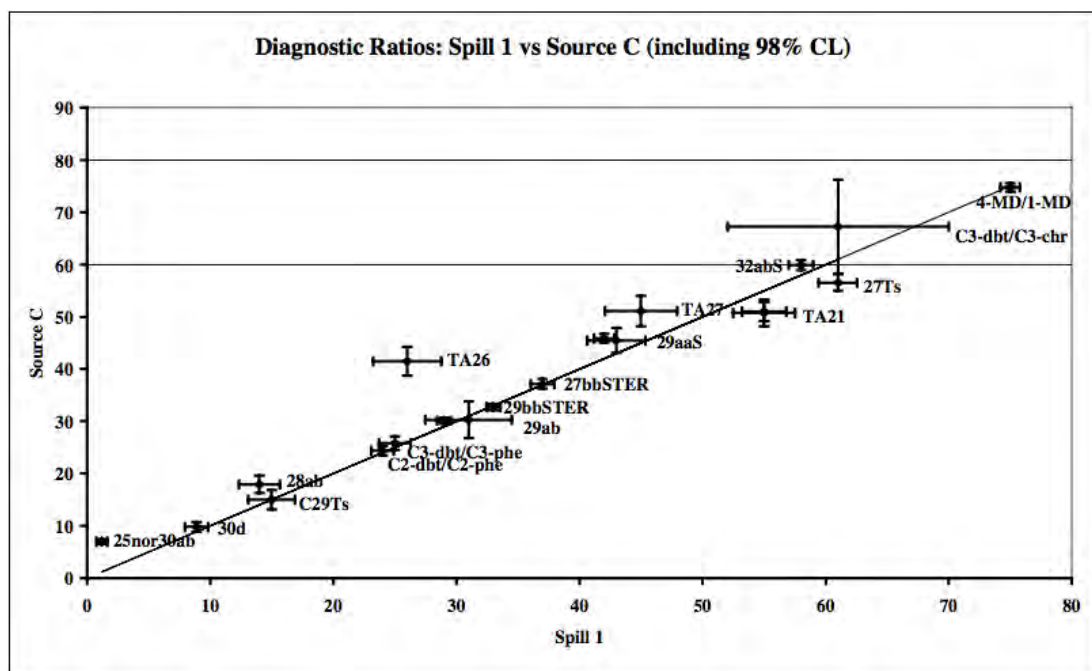


Figure 2.17 Correlation between spill 1 and source C, using a 98 % confidence limit (Non match) (Liv-Guri Faksness *et al.*, 2002).

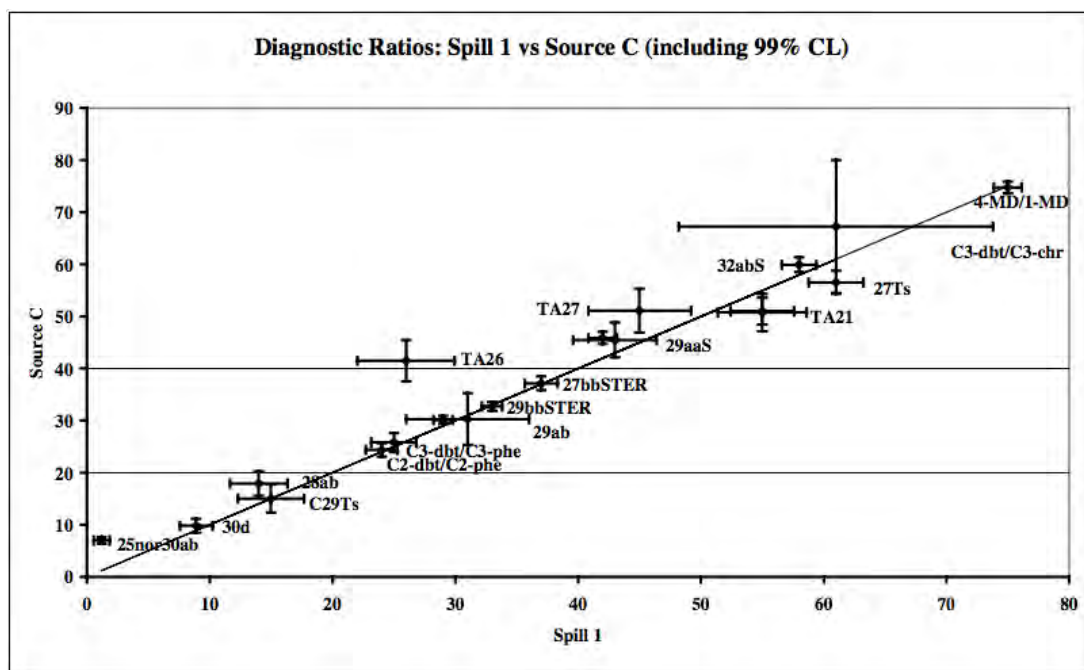


Figure 2.18 Correlation between spill 1 and source C, using a 99 % confidence limit (Non match) (Liv-Guri Faksness *et al.*, 2002).

2.3.3 Example of Oil Spill in Thailand

In July 2013, a large spill was happened in the Gulf of Thailand in Rayong Province. A 16-inch diameter pipeline owned by Petroleum Authority of Thailand, Global Chemical Plc. (PTTGC) leaked while discharging crude oil from a vessel to refinery, 20 kilometers far from Map Ta Phut, Rayong Province. The leakage resulted in oil spill of approximately 50,000 liters or equivalent to 316 barrels or 50 tons (Beans, 2013). The oil slick eventually flooded ashore in Prao bay, Samet Island where damaged marine ecology, tourism and the livelihood of local residents (Thailand's Civil Society statement, 2013). Figure 2.19 illustrates a satellite image of the extended area of the spill.

In October 2015, there was an oil spill in Hua-hin district, Prachuap-
khirikhan and nearby areas which had affected a larger area than the spill in Rayong as shown in Figure 2.20. The total amount of spilled oil was smaller than the accidental spill in Rayong, but the oil spread faster due to the wind and currents which covering

about 11 square kilometers of oil slick (Rujivanarom, 2013). However, there was no conclusion about who caused this oil spill (Charuvastra, 2015).

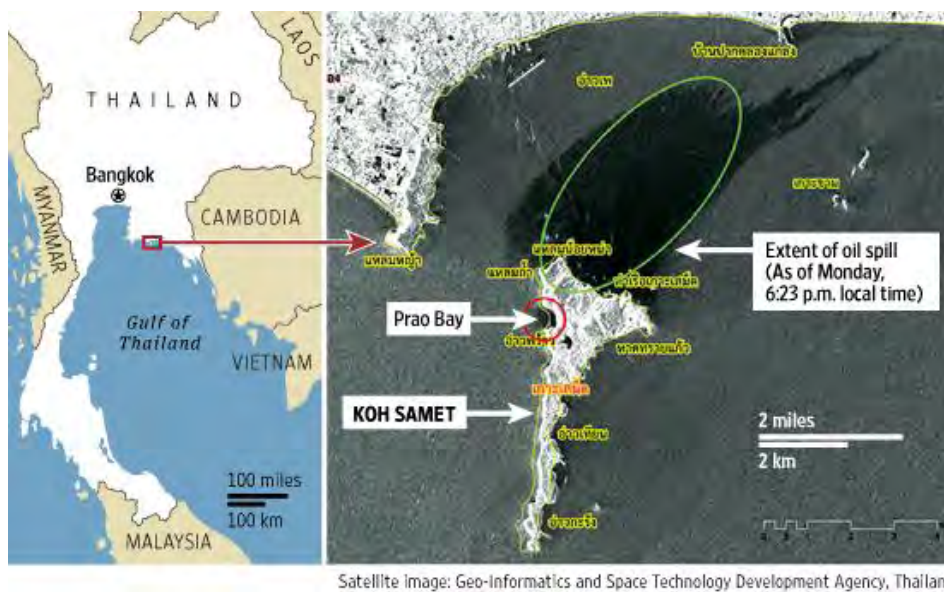


Figure 2.19 A satellite image of oil spill in Rayong, 2013 (Chomchuen, 2013).

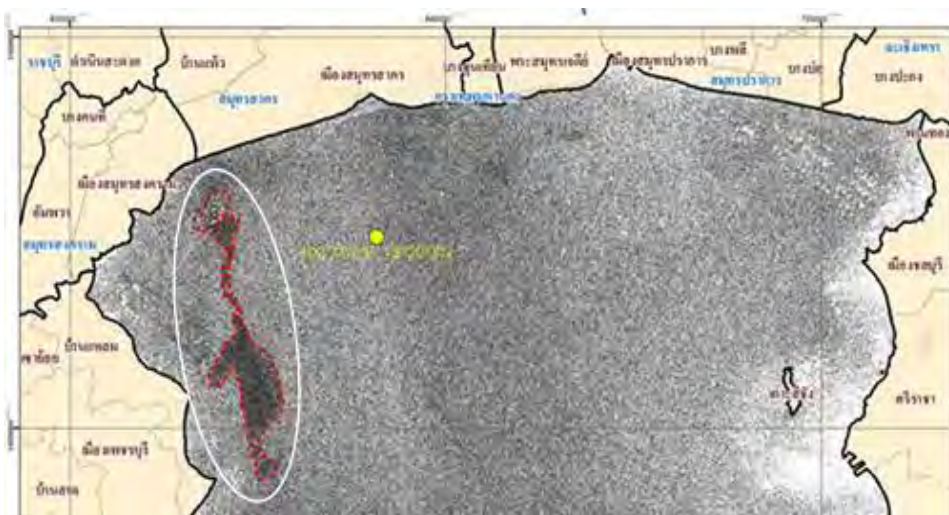


Figure 2.20 Oil slick mapping area of the 2015 oil spill in Thailand (Mokkhasen, 2015).

CHAPTER III EXPERIMENTAL

Part 1 Extraction and Analyses of Oils

3.1 Materials and Equipment

3.1.1 Sources of Oil Samples

In this work, five crude oils, two fuel oils and lubricating oil were investigated as the list shown in Table 3.1. Four crude oils (CO1-CO4) and fuel oil (FO2) samples were obtained from PTTGC. Other crude oil (CO5) and fuel oil (FO1) samples were obtained from Star Petroleum Refining Company Limited. Both fresh and used lubricating oils were obtained from Inter Marine Lube Company Limited.

Table 3.1 Information of five crude oils and three refined products samples

| No | Code | Sample Name | Description |
|----|------|-----------------------|---------------|
| 1 | CO1 | Murban Crude | Crude Oil |
| 2 | CO2 | Banang Crude | Crude Oil |
| 3 | CO3 | Qatar Marine Crude | Crude Oil |
| 4 | CO4 | Upper Zakum Crude | Crude Oil |
| 5 | CO5 | Al Shaheen Crude | Crude Oil |
| 6 | FO1 | Residue Fuel Oil | Processed Oil |
| 7 | FO2 | Visbreaking Fuel Oil | Processed Oil |
| 8 | ULO | Used Lubricating Oil | Processed Oil |
| 9 | FLO | Fresh lubricating Oil | Processed Oil |

Murban crude (CO1) and Al Shaheen crude (CO4) are main crude oils feedstock for producing fuel oil 1 (FO1). While fuel oil 2 (FO2) is produced from the main proportion crude oils feedstock of Murban crude (CO1), Banang crude (CO2), Qatar Marine crude (CO3), and Upper Zakum (CO4). Fuel oil 1 (FO1) is produced from the vacuum residue diluted with cutter from FCC unit while Fuel oil 2 (FO2) is

produced from visbreaking unit and diluted with kerosene and/or gas oil. Fresh lube oil and used lube oil are SAE Marine 40 which are produced from the same process while used lube oil is used with an engine system in the marine ship for 500 hours.

3.1.2 Gases

- Ultra-high purity (UHP) nitrogen is used for GCxGC-TOFMS.
- Ultra-high purity (UHP) helium 99.999% is used for GCxGC-TOFMS.
- High purity (HP) helium 99.995% is used for GC-FID.
- Ultra-high purity (UHP) hydrogen is used for FID detector.
- Zero grade air is used for FID detector.

3.1.3 Chemicals

- *n*-Hexane AR grade from RCI Labscan, Thailand.
- Dichloromethane from Burdick Jackson, South Korea.
- Silica gel is obtained from Merck, Germany.
- Anhydrous sodium is obtained from Merck, Germany.
- Sodium carbonate sulfate is obtained from Asia Pacific Specially Chemicals Limited, Australia.
- 17 β (H), 21 β (H)-hopane solution is obtained from Fluka.

3.1.4 Equipment

- 20" fish tank (dimension in cm.): 25x50x32) for oil spill simulation.
- Nylon syringe filter 0.45 μ m and 0.2 μ m.
- Varian[®] CP-3800 stimulated distillation gas chromatography (SIMDIST-GC) with flame ionization detector (FID).
- Agilent[®] 7890 comprehensive two dimensional gas chromatography time-of-flight mass spectrometry (GCxGC-TOFMS).

3.2 Methodology

3.2.1 Oil Spill Simulation in Natural Weathering Process

15 L of seawater were filled into each clear container. Then approximately 10 mL of all crude oils, fuel oils and used lube oil were spilled on the seawater surface. All the containers were left in the sun for 90 days and were sampled at day 0, day 3, day 45, and day 90.

3.2.2 Oil Testing

3.2.2.1 *Extraction of Oil Samples*

The extraction of oil samples method was combined from two published articles which are Mulabagal *et al.* (2013) and Zhang *et al.* (2016)

- 1) Approximately 0.15 g of oil samples were placed into clear vials.
- 2) Add 10 mL of high purity *n*-hexane/dichloromethane (1:1, v/v) to extract the oil samples.
- 3) Add 0.5 g of sodium carbonate sulfate to remove water.
- 4) The mixture was vortexed for 5 min.
- 5) The solutions were allowed to settle at room temperature for 4 h.
- 6) The supernatants in each vial was filtered through 0.45 μm filter and transferred to a vial containing 0.5 g of clean up mixture containing 0.25 g of silica gel and 0.25 g of anhydrous sodium sulfate.
- 7) The mixture was vortexed for 2 min and allowed to settle for 2 min.
- 8) The final sample was filtered through 0.2 μm filter.

All of extracted samples were added with 1 μL of 17 β (H), 21 β (H)-hopane solution as an internal standard (IS) before analyzed with GCxGC-TOFMS.

3.2.2.2 Analysis of Oil Samples Using GC-FID

Analyzing oil samples using GC-FID technique will give the overall boiling (carbon) range of the oils which is beneficial for deciding which PAHs and biomarkers are most relevant for spill and planning for GC-MS analysis.

The GC-FID conditions were following the NORDTEST oil spill identification (Liv-Guri Faksness *et al.*, 2002)

The prepared samples were analyzed by capillary GC (equipped with Electron pressure control) using the following the GC conditions:

Inlet: Splitless
 Detector: Flame ionization
 Column: 30 m long \times 0.25 mm internal diameter, and 0.25 μ m film thickness, high resolution capillary HP-5 column (5 % diphenyl and 95 % dimethylpolysiloxane stationary phase)
 Gas: Carrier: Hydrogen 2 mL/min (or Helium)
 Make up: Helium 25 mL/min (can be ignored)
 Detector: Air 360 mL/min
 Hydrogen: 30 mL/min
 Temperature: Injection port: 275 °C
 Detector: 325 °C
 Oven program:
 40 °C for 5 min, then 6 °C/min to 310 °C, hold time 10 min.
 The GC oven temperature program may be modified to improve resolution.
 Daily calibration: Alkane standard mixture
 Quantification: Internal standard/calibration standard

3.2.2.3 Analysis of Oil Sample Using GC \times GC-TOFMS

Analysis of oil samples using gas chromatography-mass spectrometry method provides the significant advantage for determining all of biomarkers, polycyclic aromatic hydrocarbons and their alkyl homologues simultaneously. The prepared samples were performed in selected ion monitoring mode (SIM) with target ion (m/z) of 178, 192, 206, 220 which were monitored for anthracene, phenanthrene and their alkylated homologues, 184, 198, 212, 226 were

used for dibenzothiophene and its alkylated isomer and m/z 191 was selected for hopane.

The prepared oil samples were analyzed by a Leco Pegasus 4D GC×GC-TOFMS using the following GC conditions:

Inlet: Splitless

Detector: Mass spectrometry

Column: First column: 60 m long × 0.25 mm internal diameter, and 0.25 μm film thickness, capillary Rxi-PAH column.

Second column: 1m long × 0.25 mm internal diameter, and 0.25 μm film thickness, capillary Rxi-1HT column.

Gas: Carrier: Helium 1 mL/min

Temperature: Injection port: 300 °C

Injection ratio: 10:1 split

Oven program:

The primary oven conditions were: 40 °C for 1 min, ramped at 2.5 °C/min to 340 °C, hold time 5 min. The secondary programming tracked the primary program with a +5 °C offset. The transfer line temperature was 300 °C and the MS source temperature was set to 250 °C.

Part 2 Collect and Analysis Data

3.3 Software

3.3.1 ChromaTOF Software

Data is acquired and processed using Leco ChromaTOF software. Both PAH and hopane groups were set up to resample with a mass range 45 to 550 atomic mass units with an acquisition rate of 200 spectra/sec.

Diagnostic ratios were calculated using equation (2.1)

$$\text{Ratio} = 100 \cdot A / (A+B) \quad (2.1)$$

where the value for A and B were calculated by (area of analyte)/(area of internal standard).

3.3.2 Microsoft Excel

Microsoft Excel was provided for the calculation of diagnostic ratios including the double ratio plots and the correlation plot using the statistical theory that concerns about the confidence interval relatives to the student's constant value which depend on number of the observation.

CHAPTER IV

RESULTS AND DISCUSSION

This Chapter shows and discusses the result of the effect of weathering processes on both physical appearances and distribution of chemical fingerprintings in five crude oils (CO1-CO5), two different pathway process of fuel oils (FO1-FO2) and one used lubricating oil (ULO) using GC-FID and GCxGC-TOFMS. The differentiation of crude oils and processed oils using distribution pattern and diagnostic ratio of PAHs and biomarker are also discussed. In addition, the comparison of fresh lube and used lube oil is also investigated.

4.1 Standard Analysis

All samples analyzing by GCxGC-TOFMS were spiked 1 μ l of internal standard (IS) to confirm retention time. The chromatogram of the internal standard (IS) with selected ion mass 191 (m/z 191) was illustrated in Figure 4.1. The internal standard was detected by GCxGC-TOFMS at retention time around 6365 s.

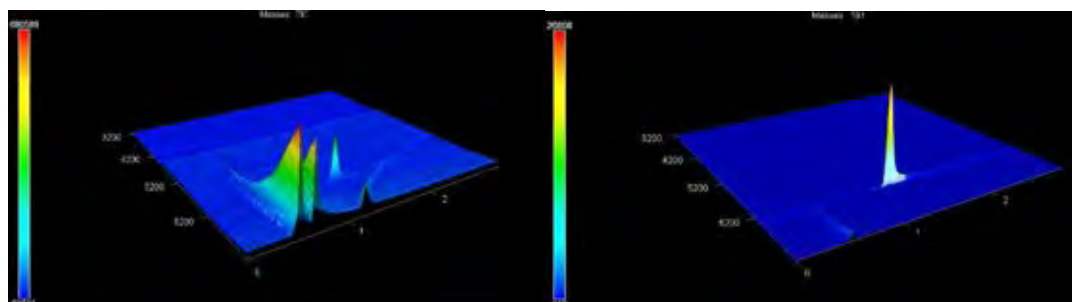


Figure 4.1 The surface chromatogram of IS 17 β (H), 21 β (H)-hopane solution.

4.2 Effect of Weathering Processes

4.2.1 Physical Effect of Studied Spilled Oils

The physical appearances of all fresh samples and their spills are illustrated in Figure 4.2. Crude oils from different sources showed particular spread out. Most of crude oil samples were spread suddenly spilled onto the seawater surface,

excluding Banang crude (CO2) which did not expand to cover the seawater surface. Both fuel oil (FO) samples were spread as a bunch sheet, while used lubricating oil (ULO) was extended over the surface after a few hours of spilling as its property that has low viscosity. During the oil spills simulation between day 3 and day 90, there were moss and algae on the bed of the containers in every tank with various attitudes. For example, in tank CO5, algae grew up to the surface and encompassed the sheet of oil, and made that oil sheet smaller. Thus, it could be concluded that in this simulation, biodegradation also occurred during the weathering processes. Murban crude oil (CO1) was highly weathering and expanded as a very thin film in D45 and D90 which extremely hard to collect the sample.

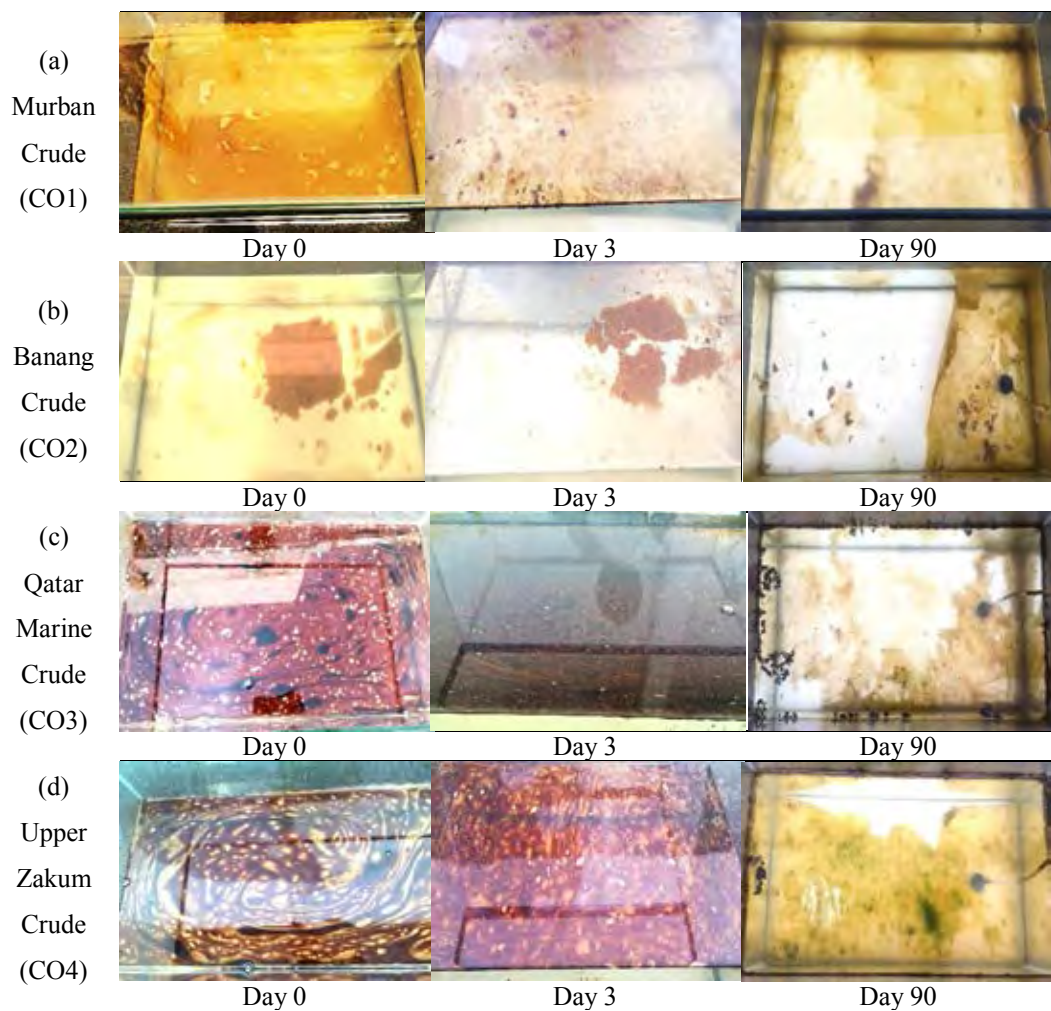


Figure 4.2 Physical appearance of all fresh samples (D0) comparing with their spills in day 3 (D3), and day 90 (D90).

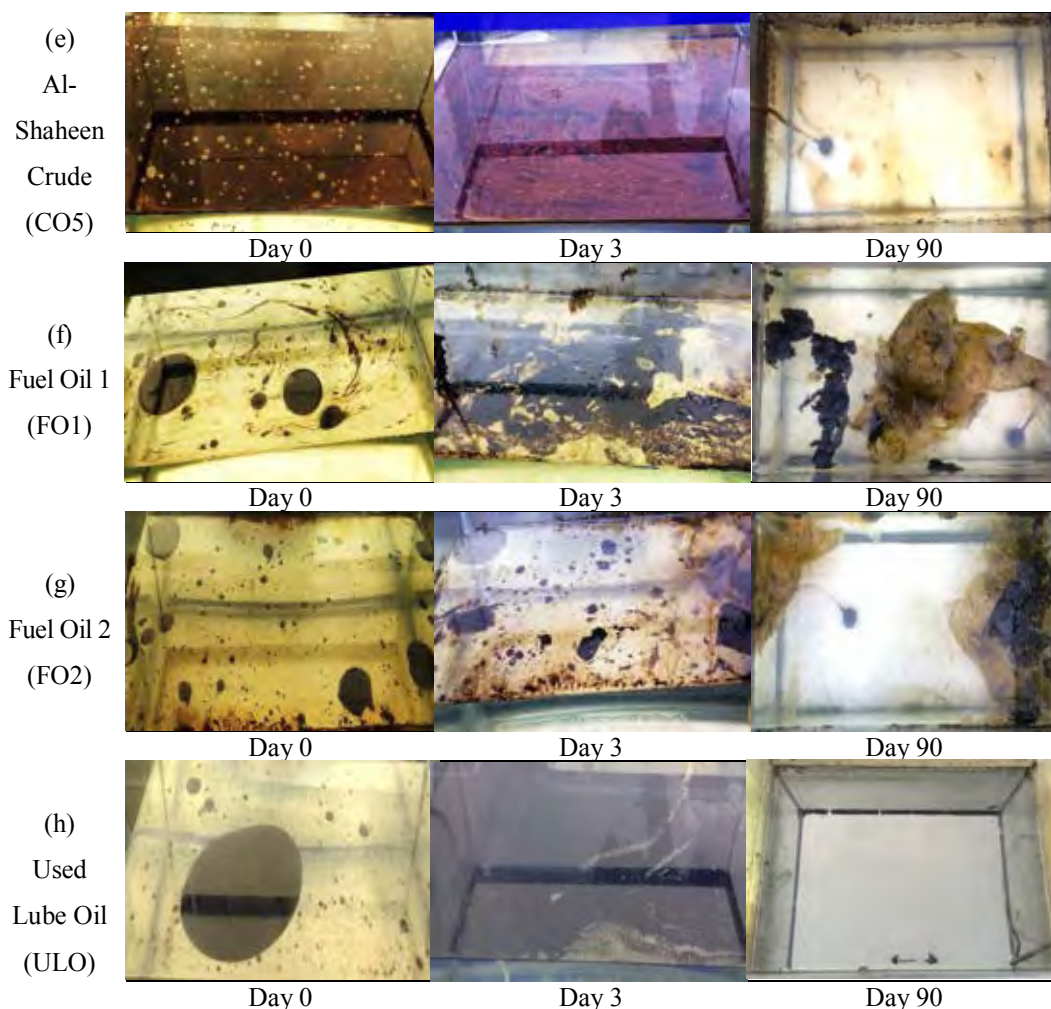


Figure 4.2 (cont.) Physical appearance of all fresh samples (D0) comparing with their spills in day 3 (D3), and day 90 (D90).

It could be said that the main weathering process parameters, which had significant effect on this oil spill simulation, included evaporation, biodegradation, dispersion, sedimentation and sinking. The lighter oil components evaporated during the weathering process and dried the oil sheet and/or film. Microbe or microorganisms in the sea water could decompose the oil compounds. Dispersion broke oil slick into droplets due to a wave imitation by stirring and caused sedimentation and sinking.

4.2.2 Characterization of Aliphatic Hydrocarbons

Once oil is spilled, the weathering processes are affected by the chemical composition in oil. The distribution of *n*-alkanes can provide a basic

information about the weathering of oil samples. Figure 4.3 demonstrates overlay chromatograms of all samples in D0, D3, D45 and D90. In day 0, used lube oil can be distinguished from crude oils and fuel oils obviously by GC-FID chromatograms due to the unresolved complex mixture (UCM) or hump raising from C24. Subsequently, the UCM arised in all samples expect CO2 and FO2 in day 3. The UCM in FO2 appeared after day 45 while CO2 did not give the UCM pattern in any weathering period. In addition, the chromatograms showed that after weathering processes in day 3, light hydrocarbons in range of C8-C11 were completely lost in all samples. After that the middle hydrocarbons (C14-C19) were significantly decreased. In day 90 (D90), *n*-alkane were seriously suffer from weathering processes which could be seen from dramatically decreasing ratio of *n*-C17/*n*-C18 as shown in Table 4.1. It would be noted that, the weights of all spilled samples were collected in day 45 were larger than the other collecting days, therefore it might be seen that the concentration in day 45 was higher, especially, CO2. Moreover, GC-FID could detect a peak at R.T. 44.17 min after the peak of *n*-C25 in every weathered sample after day 3. It was believed that these were occurred by biodegradation. There are some living microorganisms in the sea water that can alter and/or metabolize various classes of compounds presented in oil, which might turn 4- or 5- ring PAHs to simpler aromatic and/or some isomers of carboxylic acids and phenols were generated (Atlas *et al.*, 1991, Weatherford Laboratories, 2017). These could be confirmed by the results of GCxGC-TOFMS chromatogram (Figure Appendix A) where the additional peak at R.T. around 5117 s. could be detected as isomer of phthalic acid or aromatic dicarboxylic acid compounds. In addition, ULO was spilled onto DI water and sea water in order to ensure that they were generated by biodegradation. Figure 4.4 presents the GC-FID chromatogram at R.T. 44.17 min, the result showed only ULO spilled on sea water had the peak at R.T 44.17 min.

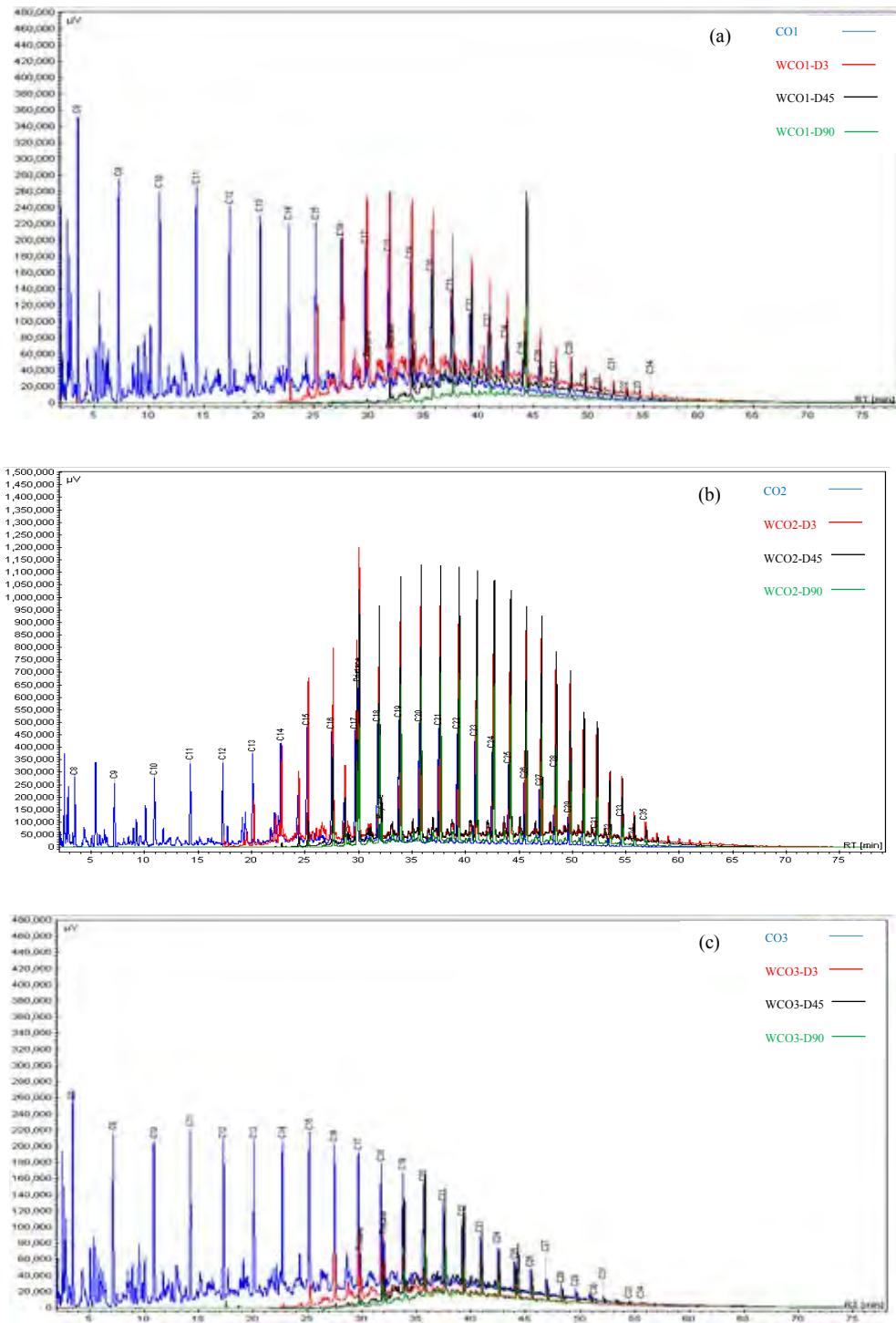


Figure 4.3 GC-FID overlay chromatograms of all fresh samples and their weathered samples in D3, D45 and D90.

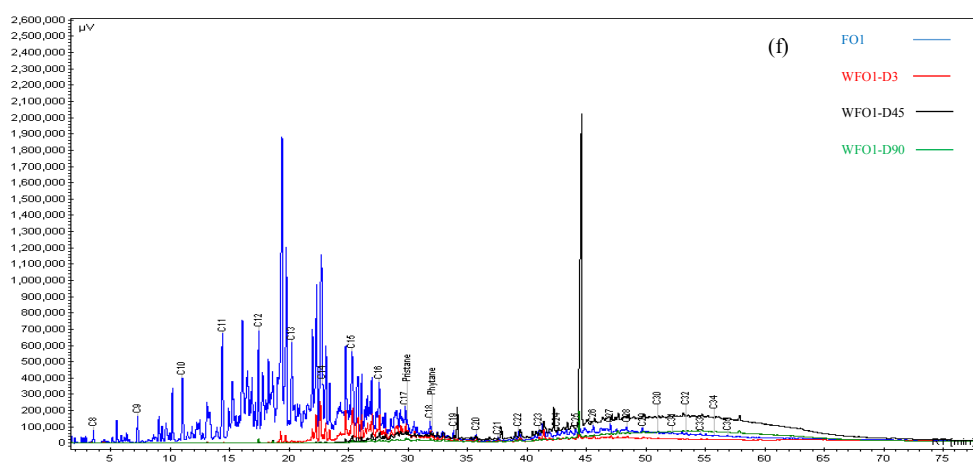
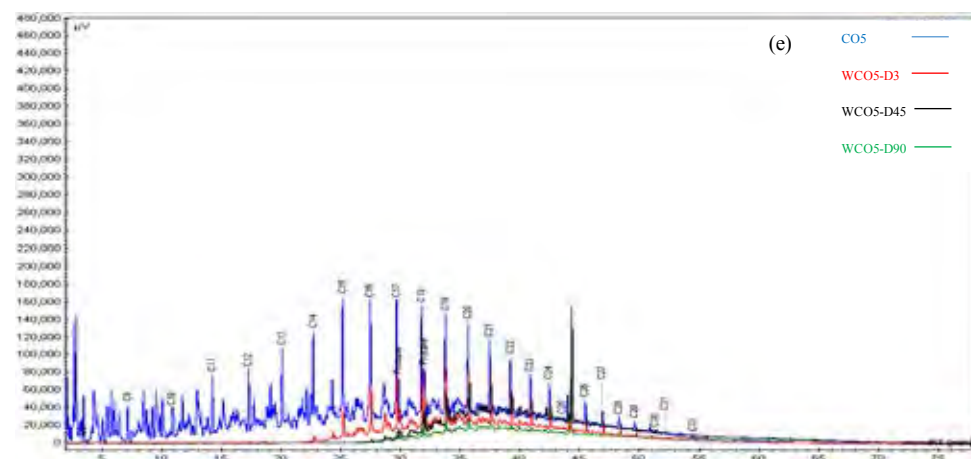
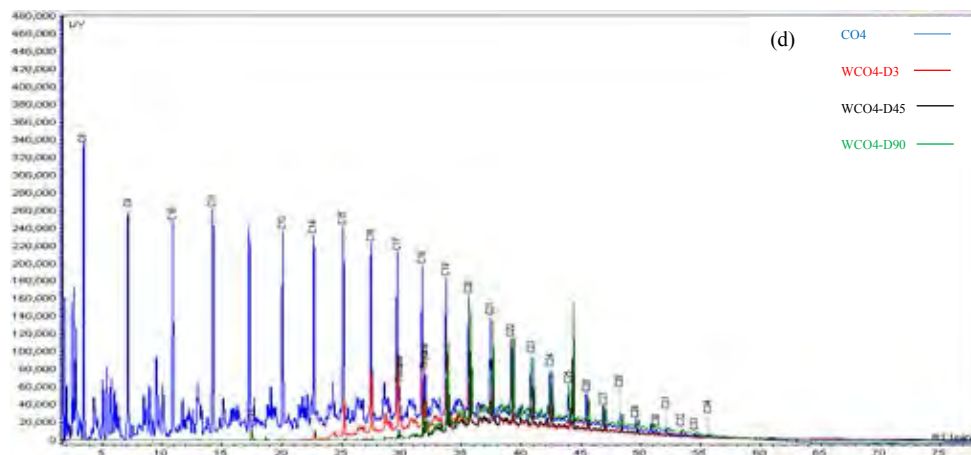


Figure 4.3 (cont.) GC-FID overlay chromatograms of all fresh samples and their weathered samples in D3, D45 and D90.

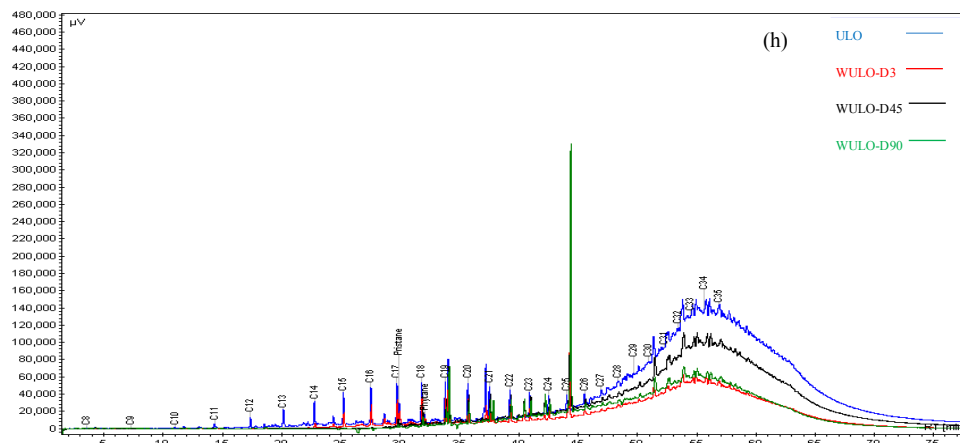
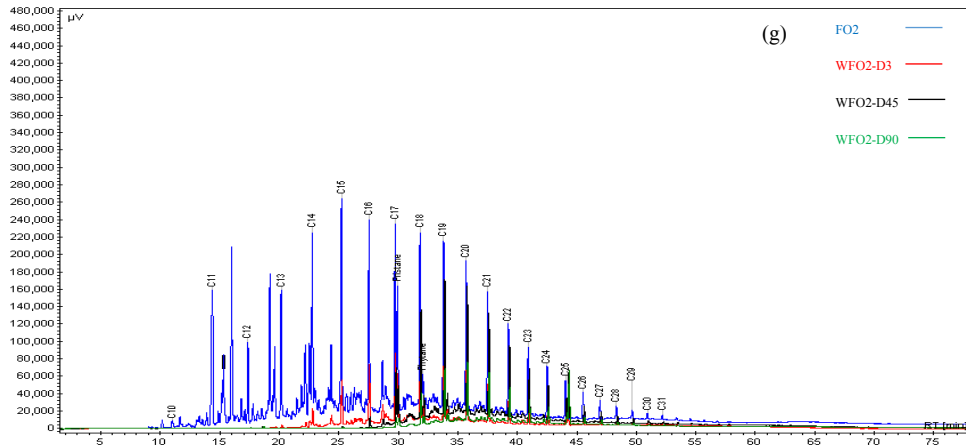


Figure 4.3 (cont.) GC-FID overlay chromatograms of all fresh samples and their weathered samples in D3, D45 and D90.

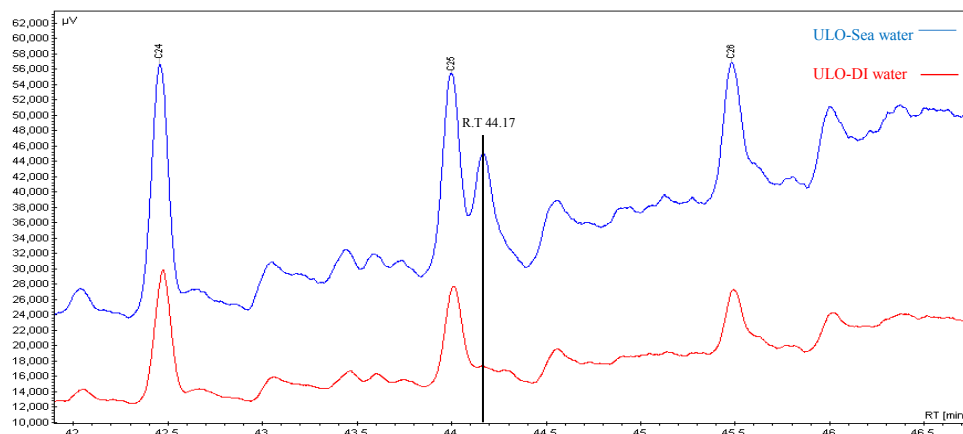


Figure 4.4 GC-FID chromatogram at R.T 44.17 min of ULO spilled on sea water and DI water.

The ratio of n -17/Pr, n -18/Ph, Pr/Ph and n -17/ n -18 have been applied for being as biodegradation indicators of the spilled oil and suspect sources (Liv-Guri Faksness *et al.*, 2002 and Zhang *et al.*, 2015). Table 4.1 tabulates all these ratios in all studied oil samples. For CO1 in day 45 and day 90, it could not collect the spilled samples properly because it might be suffered from weathering and spread out as a very thin film on the sea surface therefore n -C17 and pristane were disappeared in day 45 and n -C18 and phytane were lost in day 90. Generally, isoprenoids (pristane and phytane) are more degradation-resistant than n -C17 and n -C18 thus, the ratios of n -17/Pr, n -18/Ph should be decreased along the weathering period (Zhang *et al.*, 2015). For example in CO2, the values of n -17/Pr for D0, D3, D45 and D90 were 0.72, 0.71, 0.68 and 0.67, respectively; the valves of n -18/Ph were 5.99, 5.82, 5.71, and 5.64 for D0, D3, D45 and D90, respectively. Comparing ability of degradation resistant between pristane and phytane, Pr showed less resistant than Ph as the decreasing result in the ratio of Pr/Ph for example in FO2, in D0, D3, D45 and D90 were 4.18, 2.99, 1.53, and 1.06, respectively. The trend of ratio of n -17/ n -18 also decreased with the increasing weathering periods as in FO1, the ratios of n -17/ n -18 in D0, D3, D45 and D90 were 1.95, 1.65, 1.35 and 1.28, respectively.

Table 4.1 Biodegradation ratios of all oil samples

| Oils | Weathering Period | Biodegradation Ratios | | | |
|------|----------------------|-----------------------|----------|-------|-------------|
| | | n-C17-Pr | n-C18/Ph | Pr/Ph | n-C17/n-C18 |
| CO1 | D0 | 4.32 | 2.93 | 0.75 | 1.08 |
| | D3 | 3.85 | 2.83 | 0.73 | 0.99 |
| | D45 | - | 3.80 | 0 | 0 |
| | D90 | - | 1.83 | 0 | 0 |
| CO2 | D0 | 0.72 | 5.99 | 8.32 | 1.00 |
| | D3 | 0.71 | 5.82 | 7.94 | 0.96 |
| | D45 | 0.68 | 5.71 | 6.24 | 0.75 |
| | D90 | 0.67 | 5.64 | 5.43 | 0.64 |
| CO3 | D0 | 3.21 | 2.00 | 0.76 | 1.22 |
| | D3 | 2.68 | 1.77 | 0.63 | 0.96 |
| | D45 | 2.73 | 1.93 | 0.20 | 0.28 |
| | D90 | 2.21 | 1.92 | 0.23 | 0.26 |
| CO4 | D0 | 4.08 | 2.54 | 0.75 | 1.21 |
| | D3 | 3.30 | 2.21 | 0.66 | 0.99 |
| | D45 | 3.04 | 2.23 | 0.18 | 0.25 |
| | D90 | 2.91 | 2.14 | 0.14 | 0.19 |
| CO5 | D0 | 2.49 | 1.68 | 0.79 | 1.17 |
| | D3 | 2.08 | 1.52 | 0.72 | 0.99 |
| | D45 | 1.06 | 0.76 | 0.18 | 0.25 |
| | D90 | 0.75 | 0.61 | 0.18 | 0.23 |
| FO1 | D0 | 1.94 | 1.45 | 1.46 | 1.95 |
| | D3 | 1.82 | 1.38 | 1.25 | 1.65 |
| | D45 | 1.38 | 0.93 | 0.91 | 1.35 |
| | D90 | 1.31 | 0.92 | 0.90 | 1.28 |
| FO2 | D0 | 1.37 | 5.03 | 4.18 | 1.14 |
| | D3 | 1.23 | 3.73 | 2.99 | 0.99 |
| | D45 | 1.29 | 3.95 | 1.53 | 0.50 |
| | D90 | 0.94 | 3.47 | 1.06 | 0.28 |
| ULO | D0 | 1.61 | 4.09 | 2.56 | 1.01 |
| | D3 | 1.49 | 3.96 | 2.58 | 0.97 |
| | D45 | 1.64 | 3.58 | 1.07 | 0.47 |
| | D90 | 1.51 | 3.57 | 0.70 | 0.29 |

4.3 The Differentiation of Crude Oils and Processed Oils by PAHs

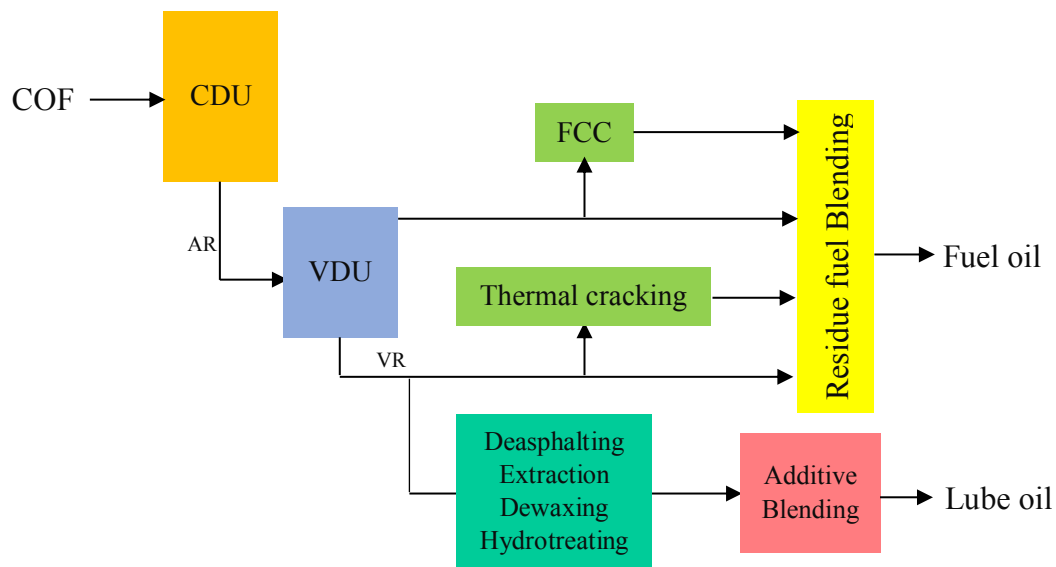


Figure 4.5 Fuel oil and lube oil processing block flow diagram.

In petroleum refinery, fuel oil can be produced from various processes such as straight run from atmospheric distillation (CDU) and vacuum distillation (VDU), thermal cracking unit and fluid catalytic cracking unit as illustrated in Figure 4.5. In this study, FO1 is received from the vacuum residue (VR) and diluted with cutter from FCC unit to reach the fuel oil specification. Another type of fuel oil in this study, FO2, is processed from thermal cracking unit called visbreaking unit and blended with kerosene, gas oil (both light and heavy gas oil) to control the specification. Generally, Lubricating oil can be produced from base oil which is refined from VDU and treated by deasphalting to remove asphaltic and heavy fraction, extraction or solvent refining to reduce or remove aromatics compounds, then dewaxing to remove undesirable paraffins and alkanes and eliminated olefins and other unsaturated compounds by hydrotreating. Finally, base oil is added and blended with additives to achieve the specification and desired application.

4.3.1 The Distribution of Polycyclic Aromatic Hydrocarbons

From GCxGC-TOFMS, the detection of target ion 178, 192, 206, 220 was monitored for anthracene (A), phenanthrene (P) and their alkylated homologues (MP), 184, 198, 212, 226 were used for dibenzothiophene (D) and its alkylated isomer (MD) and m/z 191 was selected for hopane. The total ion and target ion m/z 192 surface plot of all crude oils (CO1-CO5), fuel oils (FO1-FO2), and used lube oil (ULO) in day 0 are shown in Figure 4.6. The total ion surface plots existed the different paraffins, aromatics and PAHs, and hopane distribution pattern between crude oils and refined products. Comparing the distribution pattern in refined products, FO1 existed more aromatics and PAHs group, FO2 showed more paraffins peaks, while ULO presented less in aromatic and PAHs, but more paraffin and hopane. Therefore, the refining and blending processes had the effect on the distribution pattern of chemical fingerprints in oils. From the surface plots of target ion m/z 192 in Figure 4.6, they could be observed that the distribution patterns of methyl-phenanthrene (MP) and methyl-anthracene (MA) were different in most crude oils and fuel oils. The common alkyl-phenanthrenes, 3-, 2-, 9- and 1-MP were appeared in all of fresh oils and almost of their weathered samples while 4- MP and 2-MA could be detected in the fuel oil samples and only one crude oil which is Banang crude (CO2). Due to the less stable in thermodynamic of linear MA (Uhler *et al.*, 2016), 2-MA in CO2 and both fuel oils (FO1 and FO2) were disappeared in day 45. At the same time, all these MPs and MA were completely lost in the weathered CO1 and used lubricant oil. The detection of MP and MA in all samples is shown in Table 4.2. Moreover, the first two peaks of 3-MP and 2- MP was smaller than the last two peaks of 9-MP and 1- MP in most crude oils expect CO2. Whereas in fuel oils, both of FO1 and FO2, the first two peaks of 3-MP and 2-MP were larger than the last two peaks of 9-MP and 1-MP. (Liv-Guri Faksness *et al.*, 2002).

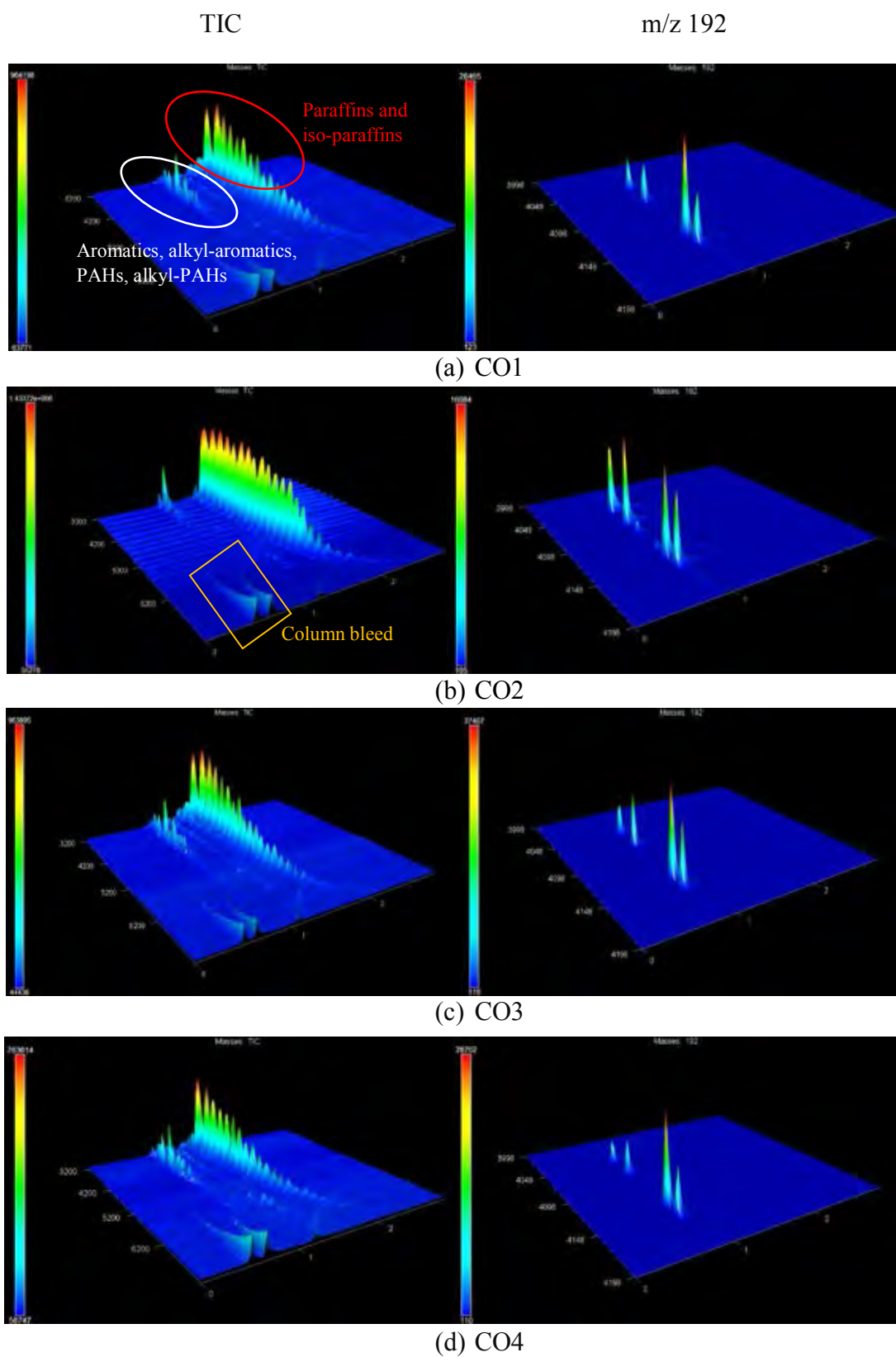


Figure 4.6 The total ion and target ion m/z 192 surface plot of all sample in day 0.

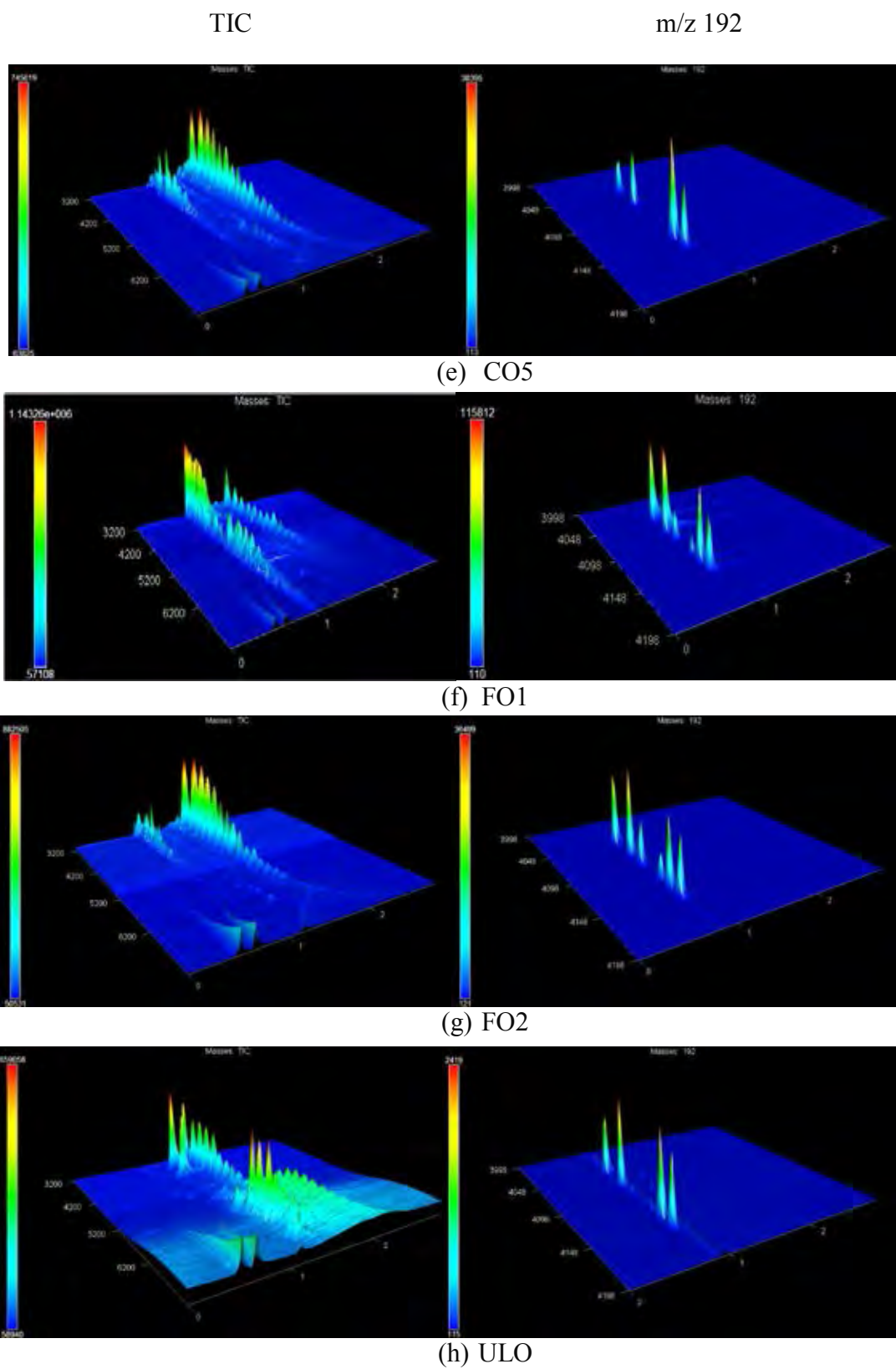


Figure 4.6 (cont.) The total ion and target ion m/z 192 surface plot of all sample in day 0.

Table 4.2 The detection of alkyl-phenanthrenes (MP) and alkyl-anthracenes (MA) presented in all fresh and weathered samples

| PAHs | 3-MP | 2-MP | 2-MA | 4-MP | 9-MP | 1-MP |
|----------|------|------|------|------|------|------|
| CO1 | ✓ | ✓ | | | ✓ | ✓ |
| CO2 | ✓ | ✓ | ✓ | ✓ | ✓ | ✓ |
| CO3 | ✓ | ✓ | | | ✓ | ✓ |
| CO4 | ✓ | ✓ | | | ✓ | ✓ |
| CO5 | ✓ | ✓ | | | ✓ | ✓ |
| FO1 | ✓ | ✓ | ✓ | ✓ | ✓ | ✓ |
| FO2 | ✓ | ✓ | ✓ | ✓ | ✓ | ✓ |
| ULO | ✓ | ✓ | | | ✓ | ✓ |
| WCO1-D3 | ✓ | ✓ | | | ✓ | ✓ |
| WCO2-D3 | ✓ | ✓ | ✓ | | ✓ | ✓ |
| WCO3-D3 | ✓ | ✓ | | | ✓ | ✓ |
| WCO4-D3 | ✓ | ✓ | | | ✓ | ✓ |
| WCO5-D3 | ✓ | ✓ | | | ✓ | ✓ |
| WFO1-D3 | ✓ | ✓ | ✓ | ✓ | ✓ | ✓ |
| WFO2-D3 | ✓ | ✓ | ✓ | ✓ | ✓ | ✓ |
| WULO-D3 | ✓ | ✓ | | | ✓ | |
| WCO1-D45 | | | | | | |
| WCO2-D45 | ✓ | ✓ | | | ✓ | ✓ |
| WCO3-D45 | ✓ | ✓ | | | ✓ | ✓ |
| WCO4-D45 | ✓ | ✓ | | | ✓ | ✓ |
| WCO5-D45 | ✓ | ✓ | | | ✓ | ✓ |
| WFO1-D45 | ✓ | ✓ | | | ✓ | ✓ |
| WFO2-D45 | ✓ | ✓ | ✓ | ✓ | ✓ | ✓ |
| WULO-D45 | | | | | | |
| WCO1-D90 | | | | | | |
| WCO2-D90 | ✓ | ✓ | | | ✓ | ✓ |
| WCO3-D90 | ✓ | ✓ | | | ✓ | ✓ |
| WCO4-D90 | ✓ | ✓ | | | ✓ | ✓ |
| WCO5-D90 | ✓ | ✓ | | | ✓ | ✓ |
| WFO1-D90 | ✓ | ✓ | | | ✓ | ✓ |
| WFO2-D90 | ✓ | ✓ | | | ✓ | ✓ |
| WULO-D90 | | | | | | |

4.3.2 Diagnostic Ratio of 4-MD/1-MD

Table 4.3 and Figure 4.7 show the value of 4-MD/1-MD diagnostic ratio. From this result, it could be claimed that most of crude oils (except CO2) had 4-MD/1-MD ratio less than 0.75 while fuel oil and CO2 were resulted more than 0.75. For used lube oil, 1-MD could not be detected thus the ratio are equivalent. However, this diagnostic

ratio would not be a suitable ratio for differential crude oils from refined product because the weathering processes had an influence on this ratio (Liv-Guri Faksness *et al.*, 2002) which could be seen that the trend of this ratio was significantly dropped in most oils comparing between D0 and D90.

Table 4.3 Diagnostic ratio value of 4-MD/1-MD of all fresh and weathered samples in day 3, day 45 and day 90

| 4MD/1MD | D0 | D3 | D45 | D90 |
|---------|------|------|------|------|
| CO1 | 0.72 | 0.72 | 0.61 | ND |
| CO2 | 0.94 | 0.90 | 0.91 | 1.00 |
| CO3 | 0.58 | 0.58 | 0.51 | 0.49 |
| CO4 | 0.61 | 0.62 | 0.53 | 0.51 |
| CO5 | 0.63 | 0.65 | 0.60 | 0.60 |
| FO1 | 0.83 | 0.82 | 0.82 | 1.00 |
| FO2 | 0.77 | 0.76 | 0.75 | 0.79 |
| ULO | 1.00 | ND | ND | ND |

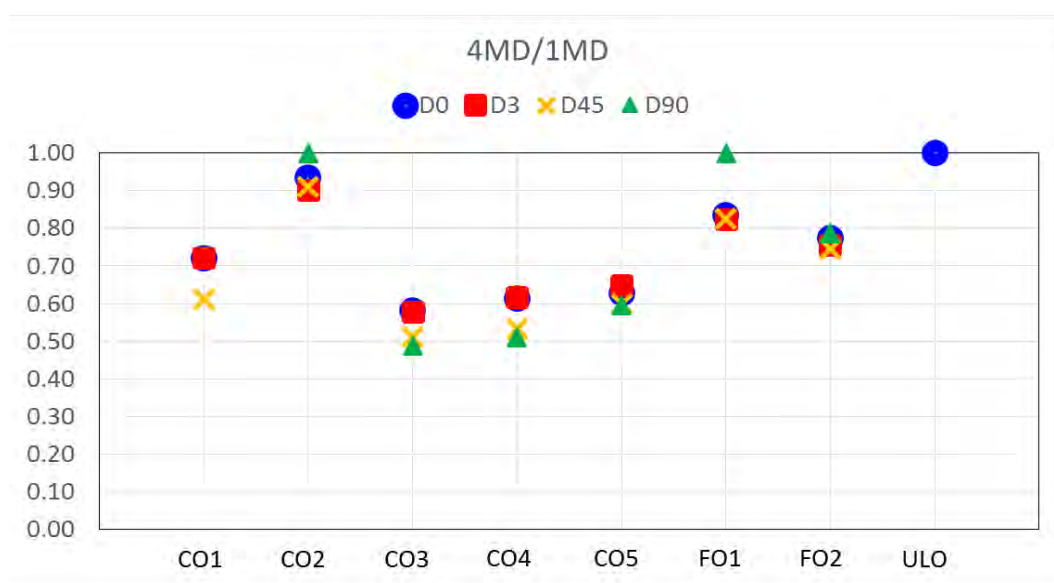


Figure 4.7 The plot of diagnostic ratio of 4-MD/1-MD of all fresh (D0) and weathered samples in day 3, day 45 and day 90.

4.3.3 Diagnostic Ratio of 2-MP/1-MP

The result of 2-MP/1-MP ratio is illustrated in Table 4.4 and Figure 4.8. In crude oil samples, the ratio of 2-MP/1-MP was below 0.5 excluding CO2 which gave the similar ratio to the fuel oils. The refined products gave the ratio higher than 0.5. This diagnostic ratio might be valuable to distinguish crude oil from the refined product especially, fuel oil as it was more resistant to weathering than the ratio of 4-MD/1-MD.

Table 4.4 Diagnostic ratio value of 2-MP/1-MP of all fresh and weathered samples in day 3, day 45 and day 90

| 2MP/1MP | D0 | D3 | D45 | D90 |
|---------|------|------|------|------|
| CO1 | 0.47 | 0.46 | ND | ND |
| CO2 | 0.59 | 0.60 | 0.63 | 0.65 |
| CO3 | 0.46 | 0.46 | 0.44 | 0.46 |
| CO4 | 0.46 | 0.45 | 0.42 | 0.42 |
| CO5 | 0.48 | 0.47 | 0.45 | 0.43 |
| FO1 | 0.73 | 0.74 | 0.74 | 0.74 |
| FO2 | 0.62 | 0.62 | 0.62 | 0.60 |
| ULO | 0.89 | 1.00 | ND | ND |

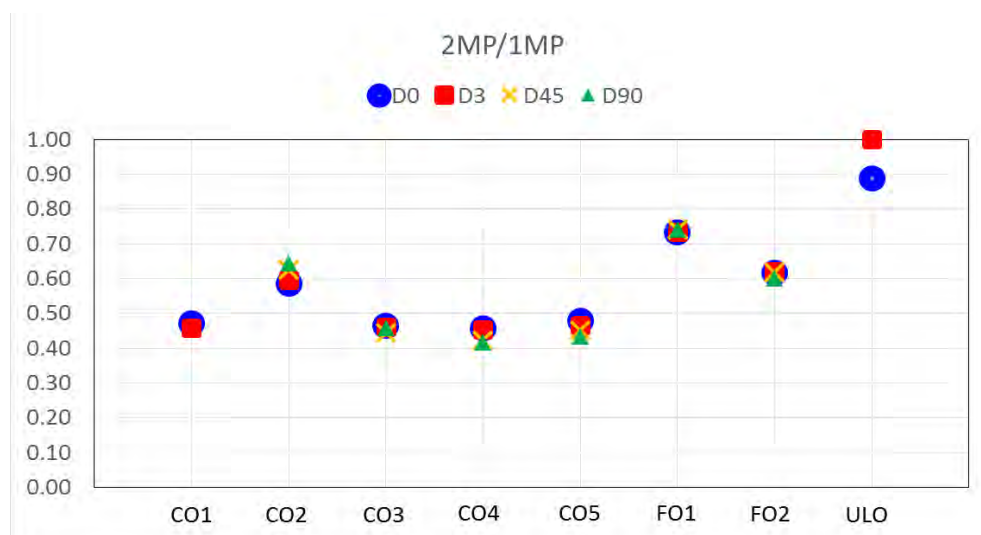


Figure 4.8 The plot of diagnostic ratio of 2-MP/1-MP of all fresh (D0) and weathered samples in day 3, day 45 and day 90.

4.3.4 Cross Plot of C2D/C2P vs C3D/C3P

Figure 4.9 shows the cross plot of C2D/C2P vs C3D/C3P in all fresh and weathering samples. Tables 4.5 and 4.6 show the diagnostic ratios of C2D/C2P and C3D/C3P, respectively. The result of the cross plot showed a possible trend for differentiation crude oils and refined products. The ratio of C2D/C2P and C3D/C3P which was higher than 0.7, was belonged to most crude oils (except CO2). While this ratio in CO2, which contains lowest sulfur percentage, was in range of 0-0.15. The ratio of fuel oils was around 0.2-0.5. ULO could be detected in C2D only at D0 and could not be detected in C3D for any ULO samples. The ratios of C2D/C2P and C3D/C3P were moderately stable even in moderate or advanced weathering stages (Fernandez-Varela *et al.*, 2009), thus this cross plot might be a good indicator to distinguish crude oils and refined products.

Table 4.5 Diagnostic ratio value of C2D/C2P of all fresh and weathered samples in day 3, day 45 and day 90

| C2D/C2P | D0 | D3 | D45 | D90 |
|---------|------|------|------|------|
| CO1 | 0.79 | 0.82 | 1.00 | 1.00 |
| CO2 | 0.11 | 0.12 | 0.06 | 0.02 |
| CO3 | 0.77 | 0.76 | 0.76 | 0.76 |
| CO4 | 0.81 | 0.83 | 0.81 | 0.80 |
| CO5 | 0.78 | 0.79 | 0.81 | 0.81 |
| FO1 | 0.30 | 0.45 | 0.39 | 0.33 |
| FO2 | 0.34 | 0.32 | 0.37 | 0.24 |
| ULO | 0.12 | 0.00 | ND | ND |

Table 4.6 Diagnostic ratio value of C3D/C3P of all fresh and weathered samples in day 3, day 45 and day 90

| C3D/C3P | D0 | D3 | D45 | D90 |
|---------|------|------|------|------|
| CO1 | 0.83 | 0.83 | 1.00 | ND |
| CO2 | 0.03 | 0.03 | 0.00 | 0.00 |
| CO3 | 0.76 | 0.77 | 0.82 | 0.81 |
| CO4 | 0.81 | 0.83 | 0.86 | 0.87 |
| CO5 | 0.76 | 0.80 | 0.93 | 0.85 |
| FO1 | 0.26 | 0.25 | 0.29 | 0.25 |
| FO2 | 0.28 | 0.30 | 0.34 | 0.45 |
| ULO | 0.00 | ND | ND | ND |

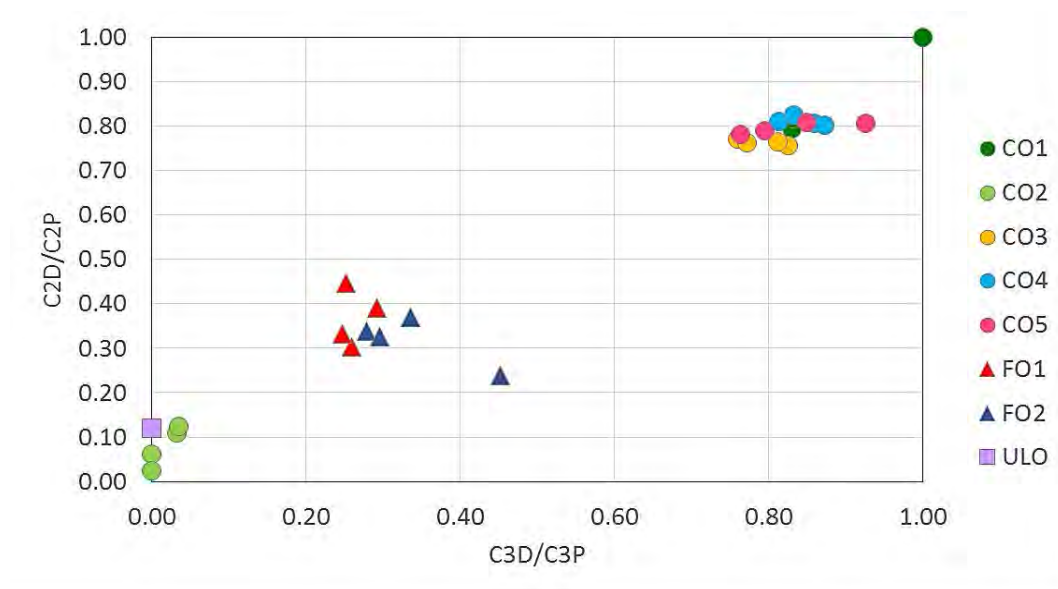


Figure 4.9 The cross plot of C2D/C2P vs C3D/C3P of all fresh and weathered samples in day 3, day 45 and day 90.

4.3.5 Cross Plot of MA and MP Isomers

As the distribution pattern of 2-MA and MP was different in crude oils and refined products, especially fuel oils, it might be useful to use these chemical fingerprints as diagnostic ratios to differential crude oils and fuel oils. Table 4.7 shows the results of eight diagnostic ratios such as 2-MA/2-MP, 2-MA/3-MP, 2-MA/1-MP, 2-MA/9-MP, 2-MA/(3+2)-MP, 2-MA/(9+1)-MP, (3+2)-MP/(9+1)-MP, and 2-MA/ Σ MP. The results showed that most of crude oil samples (CO1, CO3, CO4, and CO5) had no 2-MA thus, the ratios were equal to zero excluding the ratio of (3+2)-MP/(9+1)-MP were in a range of 0.3-0.4. Comparing CO2 and fuel oils which showed the similar distribution pattern of MA and MP, the ratios of CO2 were below 0.15 in 2-MA/2-MP and 2-MA/3-MP and lower than 0.2 in 2-MA/1-MP and 2-MA/9-MP while they were above 0.15 and 0.2 in FO1 and FO2, respectively. For ULO, there was no 2-MA as same as in the most crude oils therefore, all 2-MA/MP ratios are equal zero besides the ratio of (3+2)-MP/(9+1)-MP was above 0.6. In Figure 4.10, the cross plots of 2-MA/2-MP vs 2-MA/3-MP, 2-MA/1-MP vs 2-MA/9-MP, 2-MA/(3+2)-MP vs 2-MA/(9+1)-MP, (3+2)-MP/(9+1)-MP vs 2-MA/ Σ MP are illustrated. They showed positive results to distinguish crude oils and processed oils due to the obviously boundary of the ratio in each oil types. However, it could not detect 2-MA which might be degraded as the weathering processes in CO2, FO1 and FO2 in the last period of weathering in D45 and 90. In addition, comparing the stability of MP isomers, β -type of 3- and 2- MP isomers are more stable than α -type 4-, 9- and 1-MP isomers (Zhang *et al.*, 2016 and Wang *et al.*, 2006), It could be said that the ratio of 2-MA/1-MP, 2-MA/9-MP and 2-MA/(9+1)-MP might not be suitable for highly weathering oil spill identification.

Table 4.7 Diagnostic ratio value of MA and MP isomer in all fresh (D0) and weathered samples in day 3, day 45 and day 90

(a) 2-MA/2-MP

| 2-MA/2-MP | D0 | D3 | D45 | D90 |
|-----------|------|------|------|------|
| CO1 | 0.00 | 0.00 | ND | ND |
| CO2 | 0.13 | 0.04 | 0.00 | 0.00 |
| CO3 | 0.00 | 0.00 | 0.00 | 0.00 |
| CO4 | 0.00 | 0.00 | 0.00 | 0.00 |
| CO5 | 0.00 | 0.00 | 0.00 | 0.00 |
| FO1 | 0.17 | 0.15 | 0.00 | 0.00 |
| FO2 | 0.34 | 0.30 | 0.03 | 0.00 |
| ULO | 0.00 | 0.00 | ND | ND |

(b) 2-MA/3-MP

| 2-MA/3-MP | D0 | D3 | D45 | D90 |
|-----------|------|------|------|------|
| CO1 | 0.00 | 0.00 | ND | ND |
| CO2 | 0.11 | 0.04 | 0.00 | 0.00 |
| CO3 | 0.00 | 0.00 | 0.00 | 0.00 |
| CO4 | 0.00 | 0.00 | 0.00 | 0.00 |
| CO5 | 0.00 | 0.00 | 0.00 | 0.00 |
| FO1 | 0.17 | 0.15 | 0.00 | 0.00 |
| FO2 | 0.33 | 0.29 | 0.03 | 0.00 |
| ULO | 0.00 | 0.00 | ND | ND |

(c) 2-MA/1-MP

| 2-MA/1-MP | D0 | D3 | D45 | D90 |
|-----------|------|------|------|------|
| CO1 | 0.00 | 0.00 | ND | ND |
| CO2 | 0.17 | 0.06 | 0.00 | 0.00 |
| CO3 | 0.00 | 0.00 | 0.00 | 0.00 |
| CO4 | 0.00 | 0.00 | 0.00 | 0.00 |
| CO5 | 0.00 | 0.00 | 0.00 | 0.00 |
| FO1 | 0.36 | 0.33 | 0.00 | 0.00 |
| FO2 | 0.45 | 0.41 | 0.05 | 0.00 |
| ULO | 0.00 | ND | ND | ND |

Table 4.7 (cont.) Diagnostic ratio value of MA and MP isomer in all fresh (D0) and weathered samples in day 3, day 45 and day 90

(d) 2-MA/9-MP

| 2-MA/9-MP | D0 | D3 | D45 | D90 |
|-----------|------|------|------|------|
| CO1 | 0.00 | 0.00 | ND | ND |
| CO2 | 0.13 | 0.04 | 0.00 | 0.00 |
| CO3 | 0.00 | 0.00 | 0.00 | 0.00 |
| CO4 | 0.00 | 0.00 | 0.00 | 0.00 |
| CO5 | 0.00 | 0.00 | 0.00 | 0.00 |
| FO1 | 0.33 | 0.29 | 0.00 | 0.00 |
| FO2 | 0.43 | 0.38 | 0.05 | 0.00 |
| ULO | 0.00 | 0.00 | ND | ND |

(e) 2-MA/(3+2)-MP

| 2-MA/(3+2)-MP | D0 | D3 | D45 | D90 |
|---------------|------|------|------|------|
| CO1 | 0.00 | 0.00 | ND | ND |
| CO2 | 0.06 | 0.02 | 0.00 | 0.00 |
| CO3 | 0.00 | 0.00 | 0.00 | 0.00 |
| CO4 | 0.00 | 0.00 | 0.00 | 0.00 |
| CO5 | 0.00 | 0.00 | 0.00 | 0.00 |
| FO1 | 0.09 | 0.09 | 0.00 | 0.00 |
| FO2 | 0.20 | 0.21 | 0.02 | 0.00 |
| ULO | 0.00 | 0.00 | ND | ND |

(f) 2-MA/(9+1)-MP

| 2-MA/(9+1)-MP | D0 | D3 | D45 | D90 |
|---------------|------|------|------|------|
| CO1 | 0.00 | 0.00 | ND | ND |
| CO2 | 0.08 | 0.03 | 0.00 | 0.00 |
| CO3 | 0.00 | 0.00 | 0.00 | 0.00 |
| CO4 | 0.00 | 0.00 | 0.00 | 0.00 |
| CO5 | 0.00 | 0.00 | 0.00 | 0.00 |
| FO1 | 0.21 | 0.22 | 0.00 | 0.00 |
| FO2 | 0.28 | 0.32 | 0.02 | 0.00 |
| ULO | 0.00 | 0.00 | ND | ND |

Table 4.7 (cont.) Diagnostic ratio value of MA and MP isomer in all fresh (D0) and weathered samples in day 3, day 45 and day 90

(g) $(3+2)\text{-MP}/(9+1)\text{-MP}$

| $(3+2)\text{-MP}/(9+1)\text{-MP}$ | D0 | D3 | D45 | D90 |
|-----------------------------------|------|------|------|------|
| CO1 | 0.38 | 0.37 | ND | ND |
| CO2 | 0.57 | 0.55 | 0.61 | 0.64 |
| CO3 | 0.36 | 0.36 | 0.34 | 0.36 |
| CO4 | 0.33 | 0.31 | 0.30 | 0.30 |
| CO5 | 0.37 | 0.36 | 0.33 | 0.32 |
| FO1 | 0.72 | 0.71 | 0.71 | 0.71 |
| FO2 | 0.61 | 0.61 | 0.60 | 0.57 |
| ULO | 0.62 | 0.67 | ND | ND |

(h) $2\text{-MA}/\Sigma\text{MP}$

| $2\text{-MA}/\Sigma\text{MP}$ | D0 | D3 | D45 | D90 |
|-------------------------------|------|------|------|------|
| CO1 | 0.00 | 0.00 | ND | ND |
| CO2 | 0.04 | 0.01 | 0.00 | 0.00 |
| CO3 | 0.00 | 0.00 | 0.00 | 0.00 |
| CO4 | 0.00 | 0.00 | 0.00 | 0.00 |
| CO5 | 0.00 | 0.00 | 0.00 | 0.00 |
| FO1 | 0.07 | 0.06 | 0.00 | 0.00 |
| FO2 | 0.12 | 0.12 | 0.01 | 0.00 |
| ULO | 0.00 | 0.00 | ND | ND |

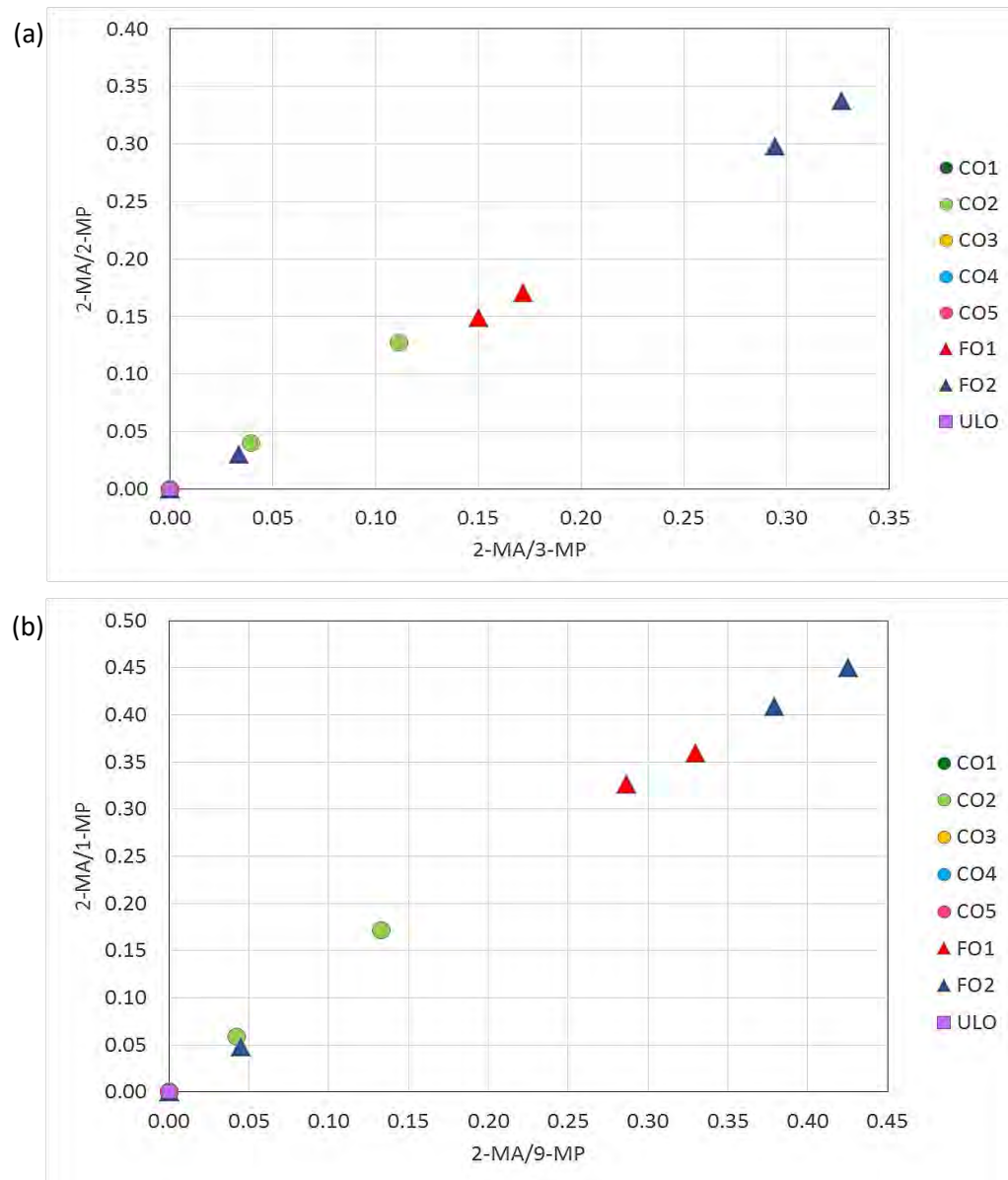


Figure 4.10 The cross plot of (a) 2-MA/2-MP vs 2-MA/3-MP, (b) 2-MA/1-MP vs 2MA/9-MP, (c) 2-MA/(3+2)-MP vs 2MA/(9+1)-MP, (d) (3+2)-MP/(9+1)-MP vs 2-MA/ Σ MP of all fresh and weathered samples in day 3, day 45 and day 90.

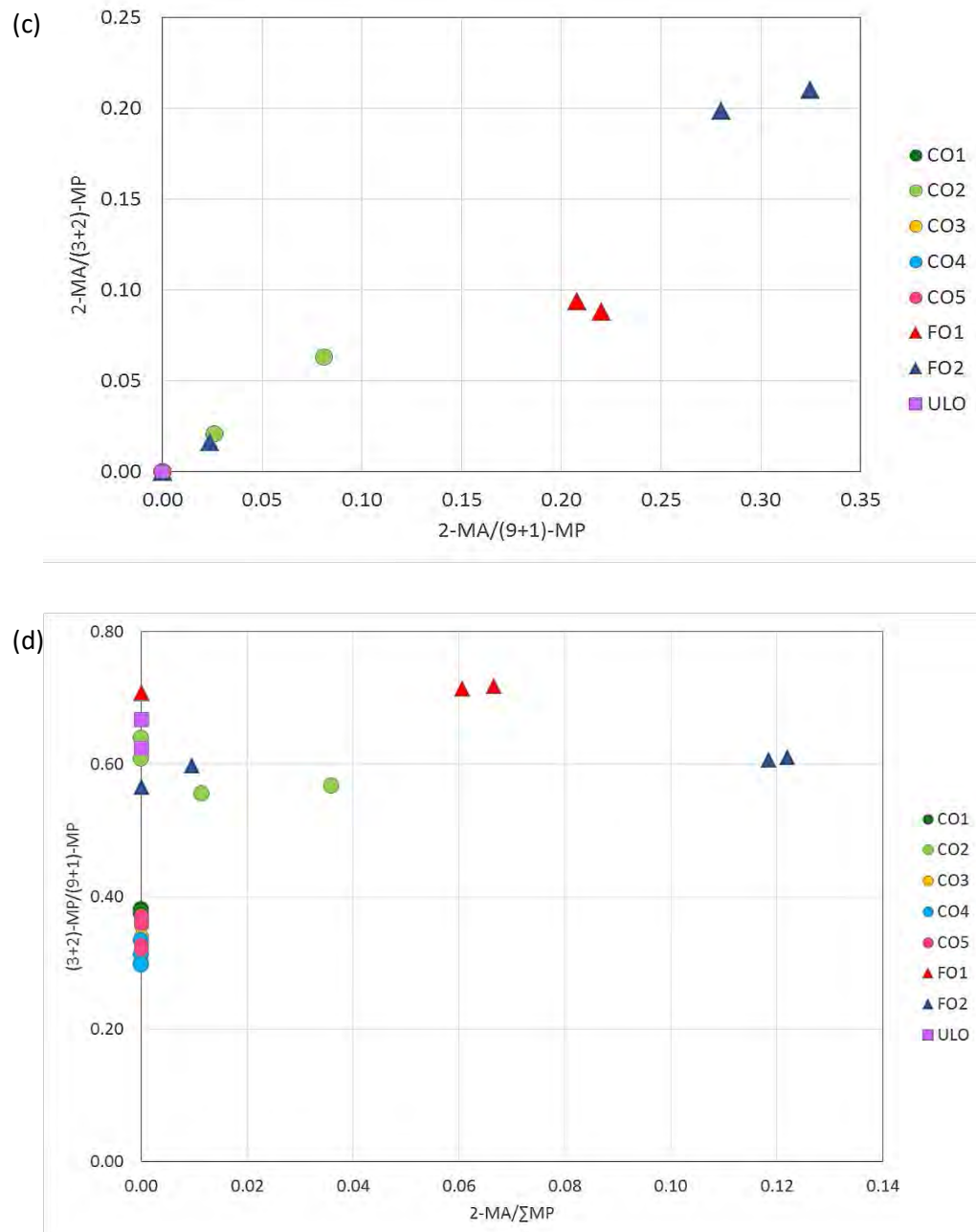


Figure 4.10 (cont.) The cross plot of (a) 2-MA/2-MP vs 2-MA/3-MP, (b) 2-MA/1-MP vs 2MA/9-MP, (c) 2-MA/(3+2)-MP vs 2MA/(9+1)-MP, (d) (3+2)-MP/(9+1)-MP vs 2-MA/ΣMP of all fresh and weathered samples in day 3, day 45 and day 90.

4.4 The Differentiation of Crude Oils and Processed Oils by Biomarkers

The result from GCxGC-TOFMS with target ion 191 (m/z 191) was used to monitor hopanes as illustrated in Figure 4.11. The distribution patterns of hopane were different between crude oils, fuel oils and ULO, but they were not far different between the fresh samples (D0) and their weathered samples as confirmation by the correlation plot of diagnostic ratios of hopanes biomarker between fresh and their weathered sample in day 90 using 95% confidence limit in Figure 4.12 which. All of the error bars of each key were overlapped the straight line $x=y$ indicating a positive match, thus these two oil types came from the same origin. Consequently, the weathering processes had less significant effect on hopane biomarkers.

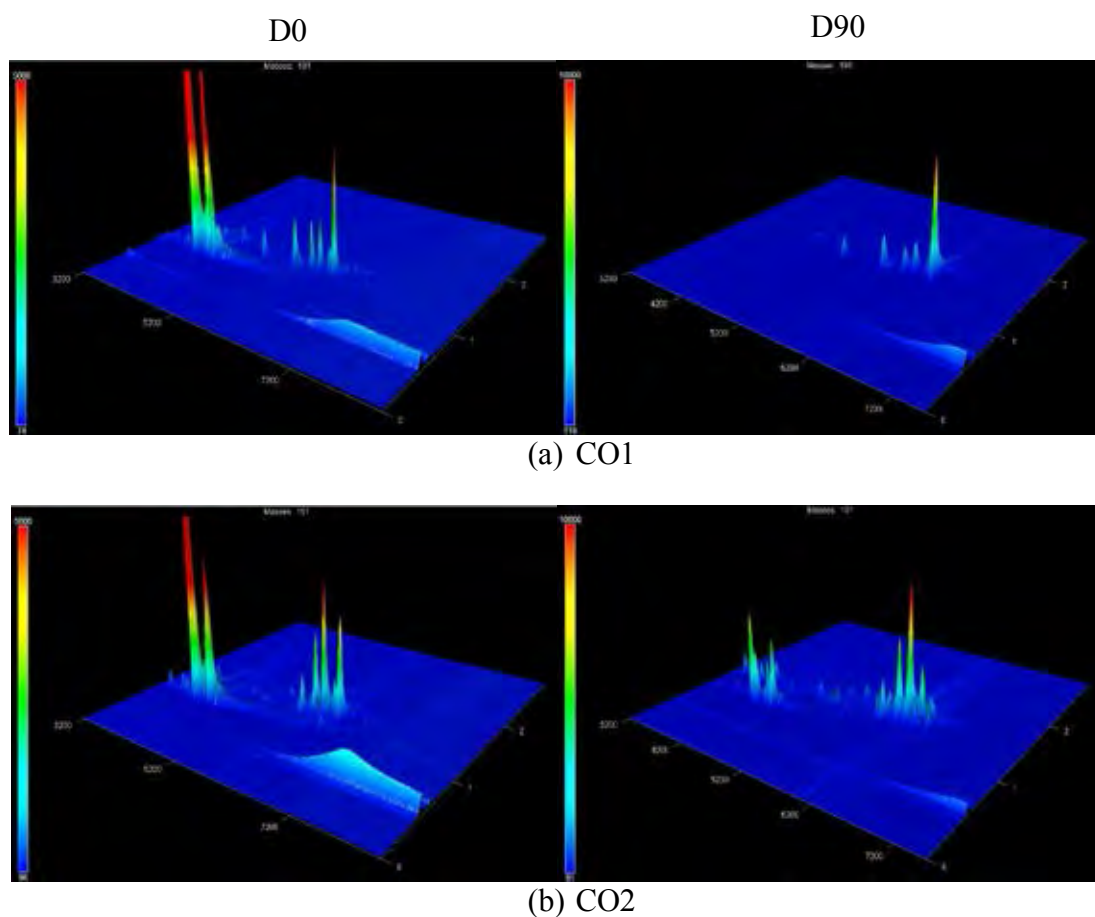
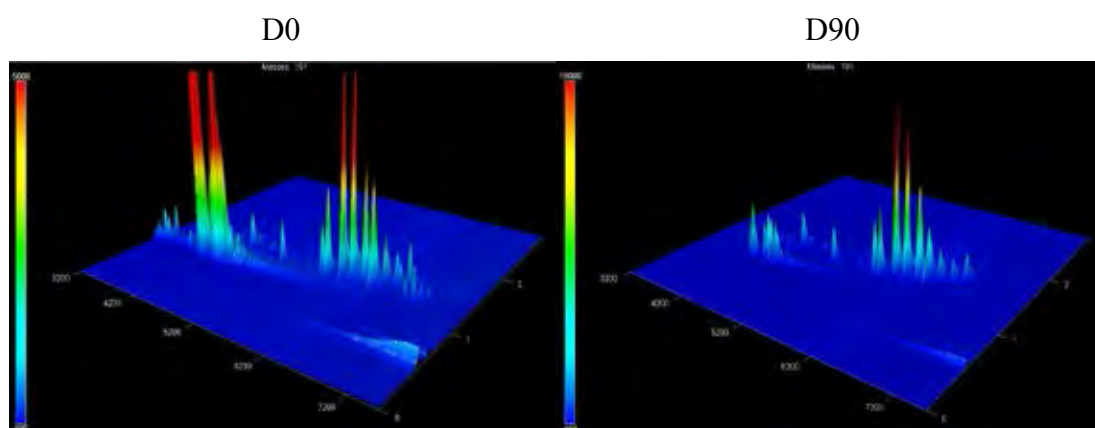
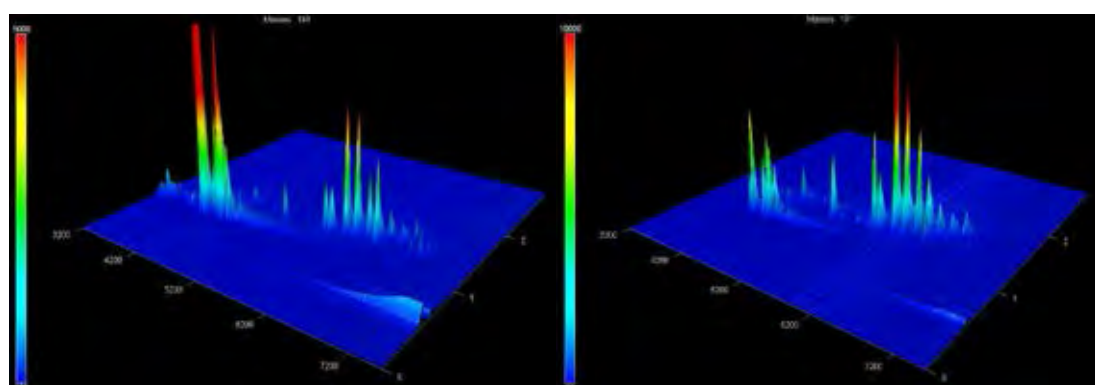


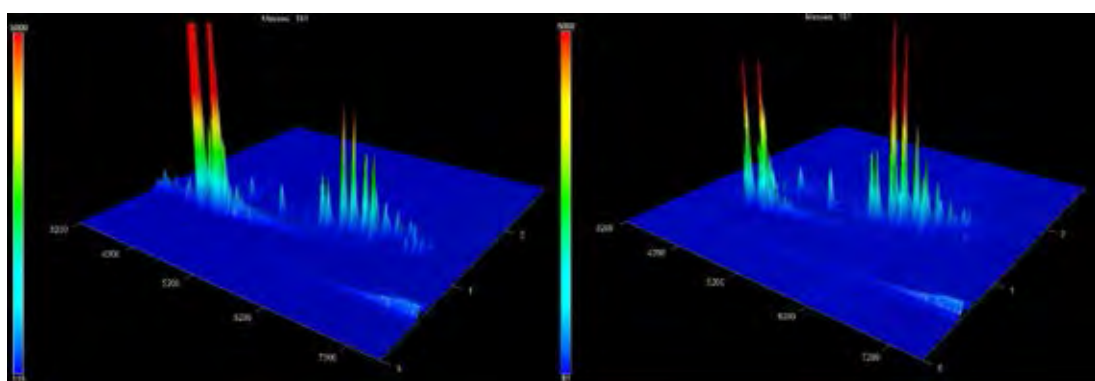
Figure 4.11 The surface plots of hopanes (m/z 191) for all samples in D0 and D90.



(c) CO3

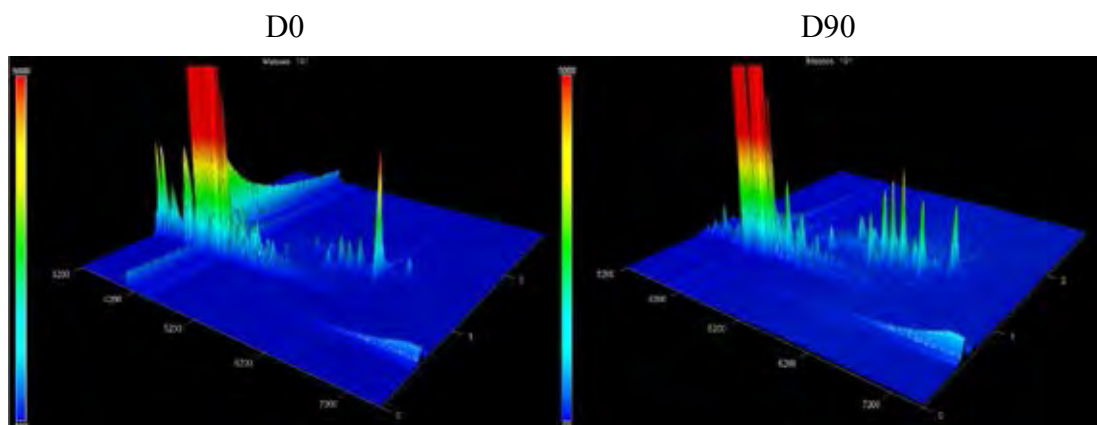


(d) CO4

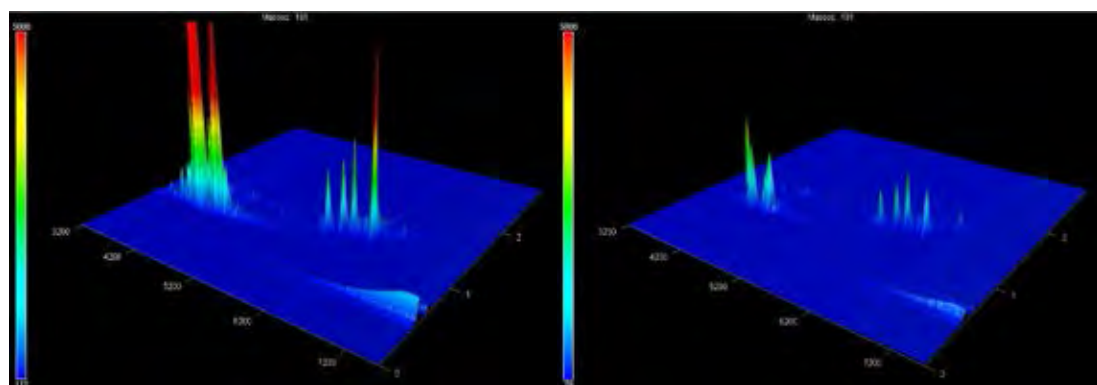


(e) CO5

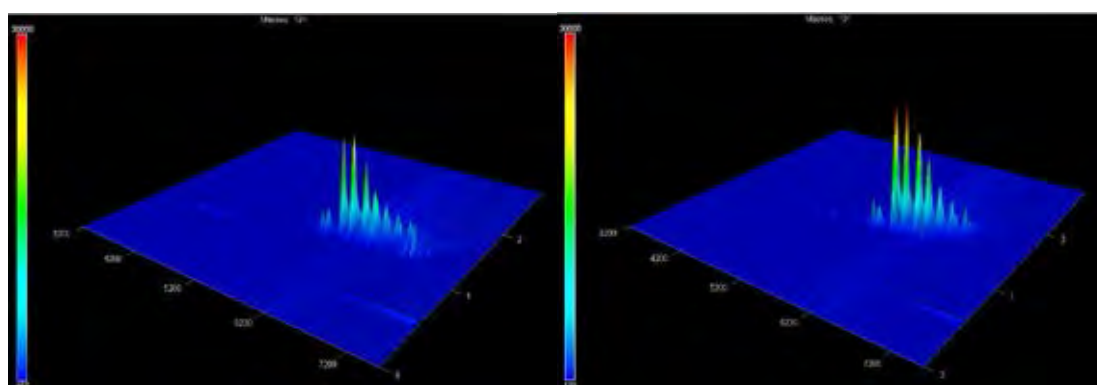
Figure 4.11 (cont.) The surface plots of hopanes ($m/z191$) for all samples in D0 and D90.



(f) FO1



(g) FO2



(h) ULO

Figure 4.11 (cont.) The surface plots of hopanes ($m/z191$) for all samples in D0 and D90.

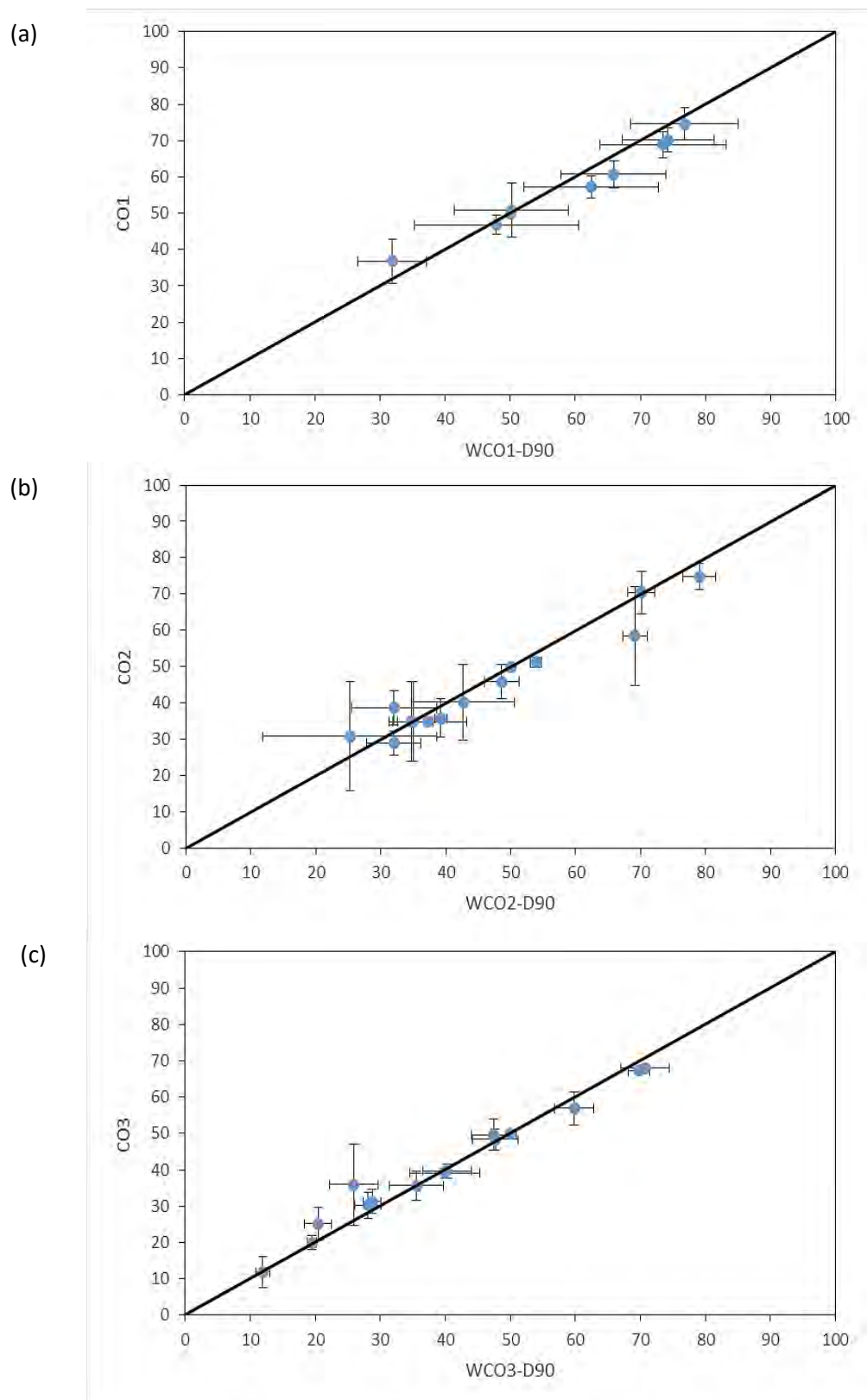


Figure 4.12 The correlation plot of diagnostic ratios of hopane biomarkers between all fresh oils and their weathered samples in day 90 using 95% confidence limit.

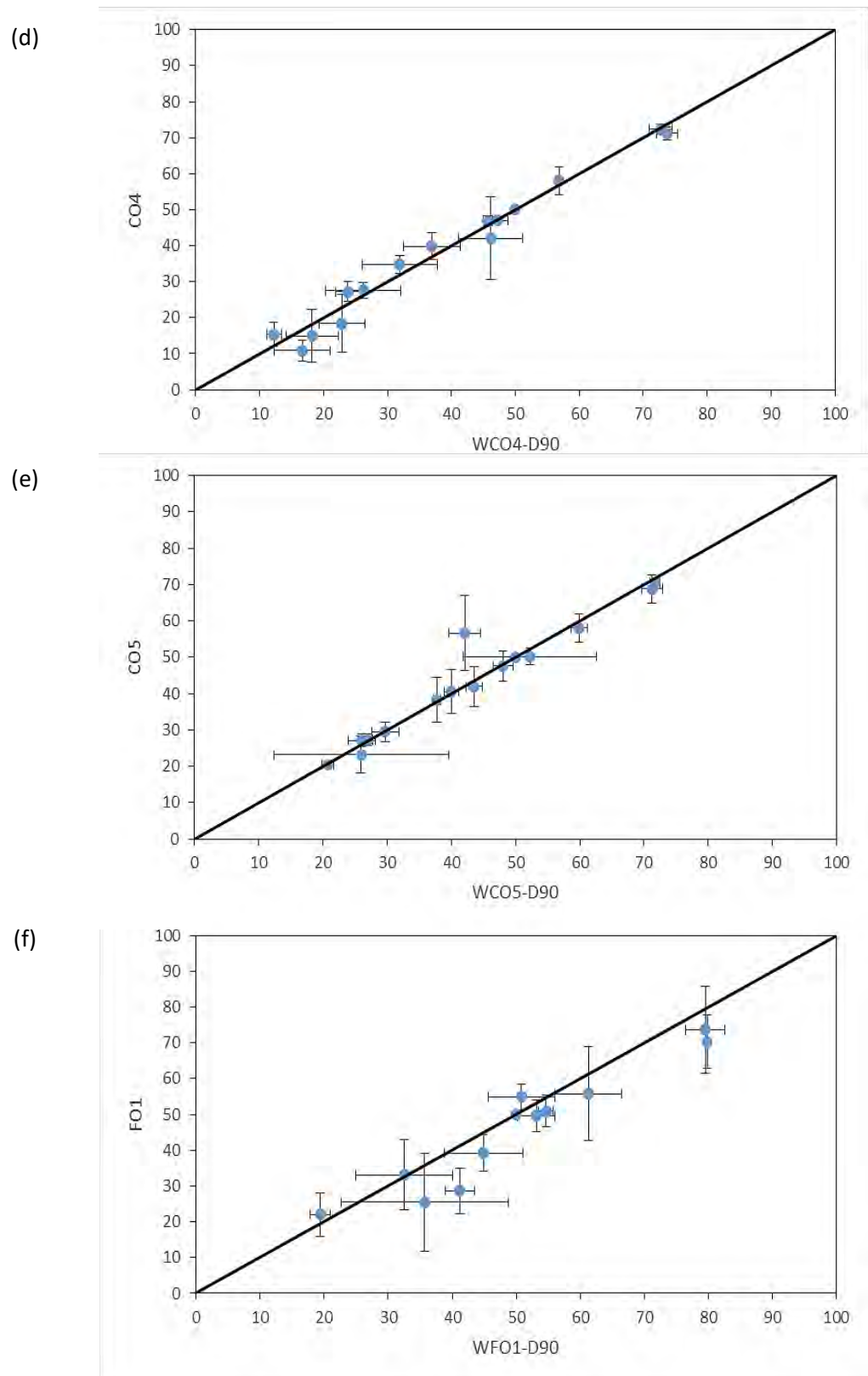


Figure 4.12 (cont.) The correlation plot of diagnostic ratios of hopane biomarkers between all fresh oils and their weathered samples in day 90 using 95% confidence limit.

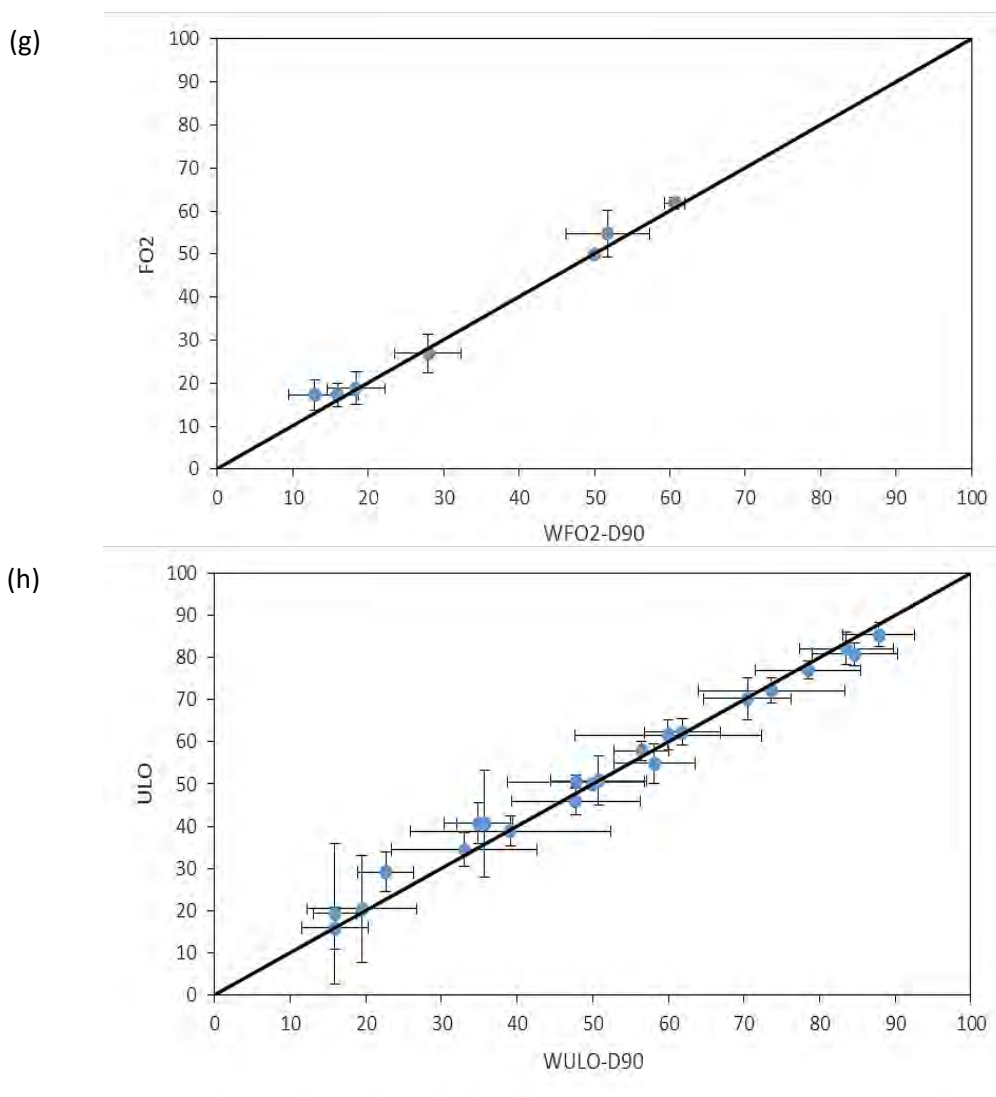


Figure 4.12 (cont.) The correlation plot of diagnostic ratios of hopane biomarkers between all fresh oils and their weathered samples in day 90 using 95% confidence limit.

Comparing fuel oils and their crude oil feedstock as in Figure 4.13, there were concluded that the refinery process had an effect on distribution pattern of hopane biomarkers, some were generated, some were degraded due to pressure and temperature of the refinery units such as vacuum distillation, hydrocracking and visbreaking unit (Russell *et al.*, 2004). From the bar chart, COF1 was combined the list of hopanes that could be detected from CO1 and CO5 which were crude oil feedstock for FO1, whereas COF2 was a crude oil feedstock for FO2 that combined with existing hopanes in CO1, CO2, CO3 and CO4. The amount of detected hopane biomarkers in COF1 was 16 types, 11 types were still existing and 1 hopane type was

generated in FO1 while 20 types of hopanes were detected in COF2, but existed in FO2 only 7 types of hopanes.

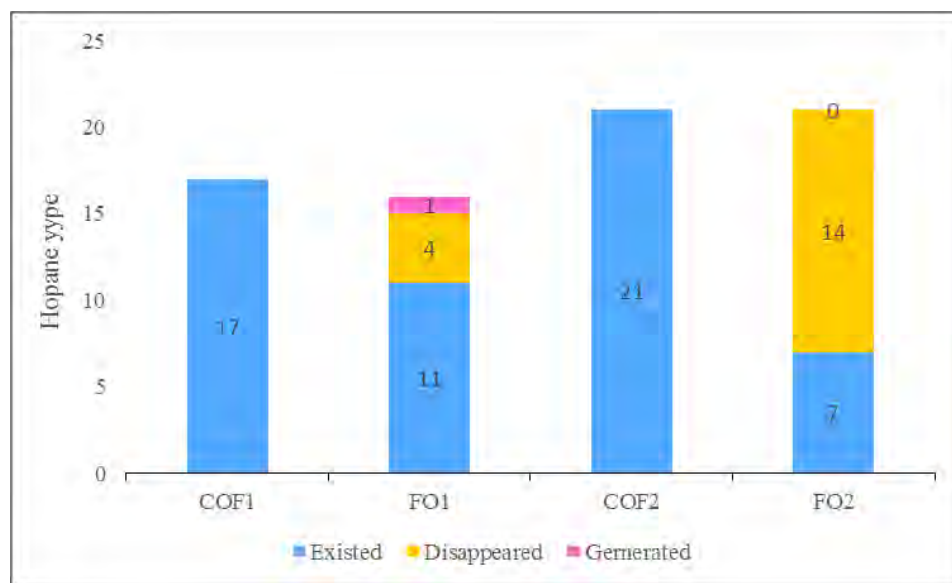


Figure 4.13 Comparing of hopane biomarkers in fresh fuel oils (FO1 and FO2) and their crude oil feedstocks (COF1 and COF2).

As the different hopane distribution between fuel oils and their crude oil feedstocks, the correlation plots of diagnostic ratio of hopane biomarkers between each crude oil feedstock and fuel oil using 95% confidence limit indicated to be non-match since there were several keys not overlapping the straight line $x=y$ as illustrated in Figure 4.14.

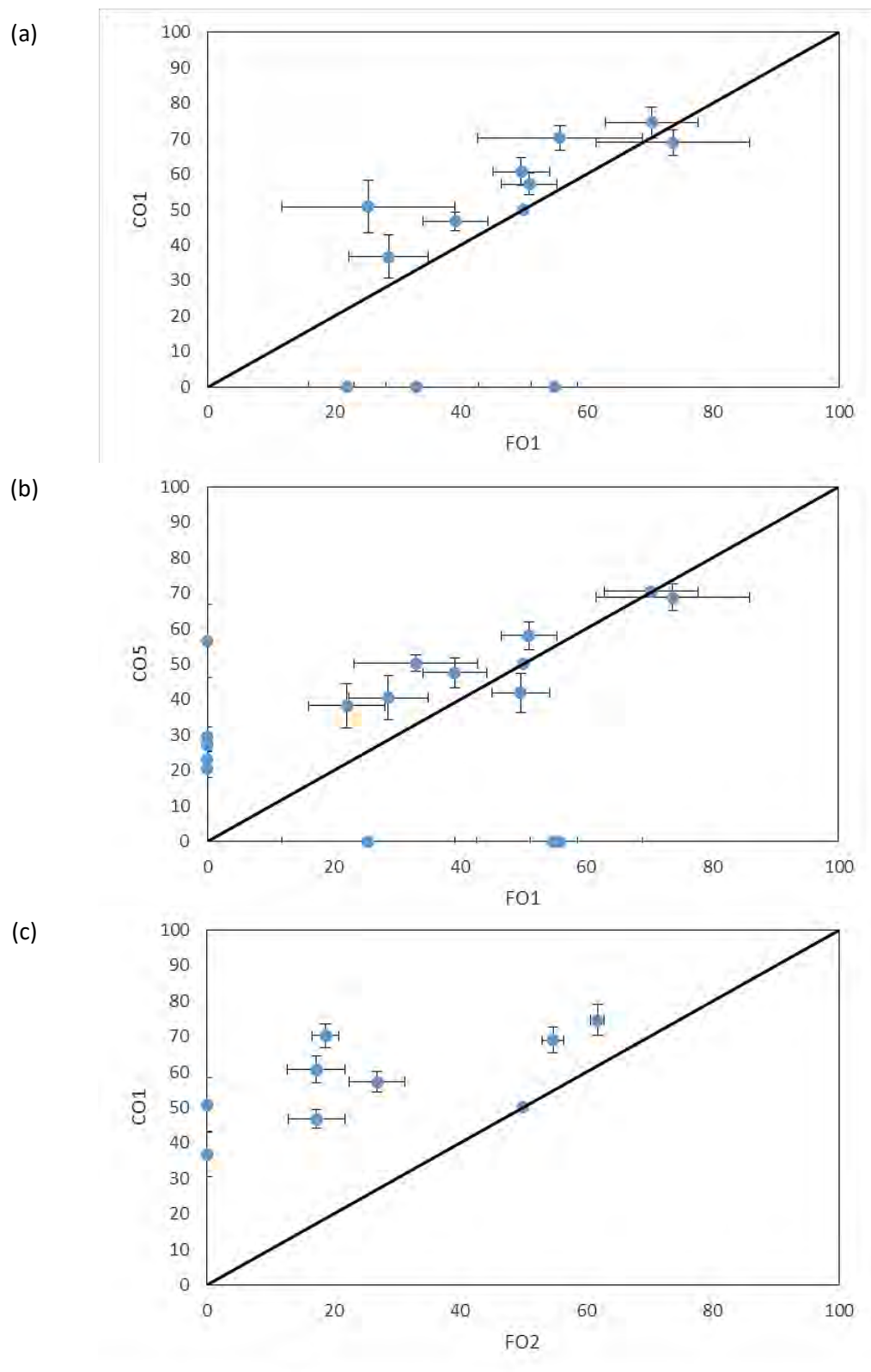


Figure 4.14 The correlation plot of diagnostic ratios of hopane biomarkers between fuel oils (FO1 and FO2) and their crude oil feedstocks using 95% confidence limit.

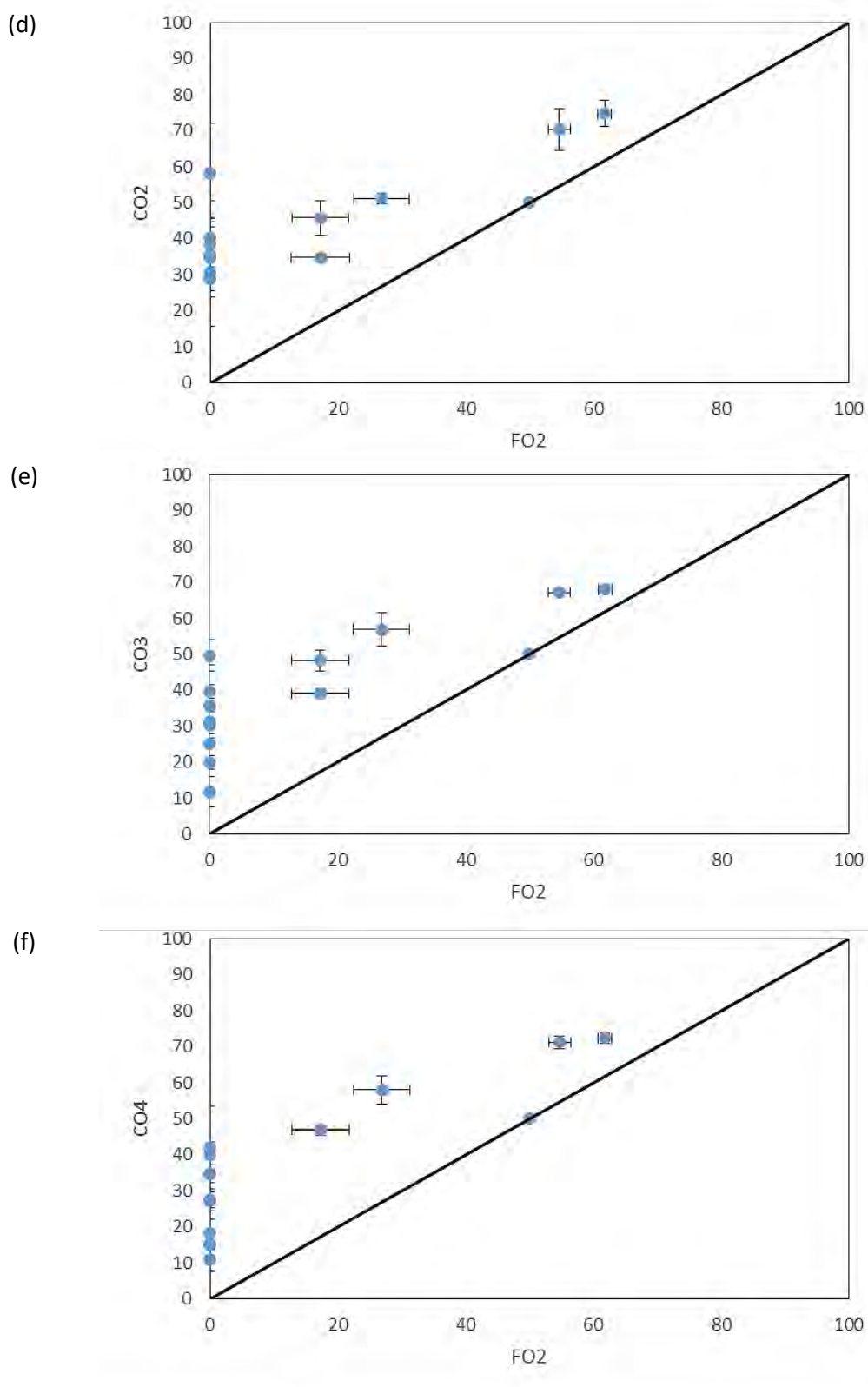
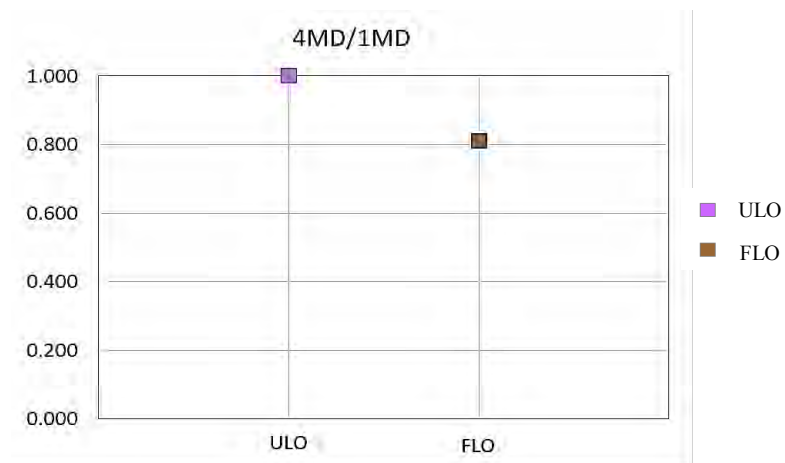
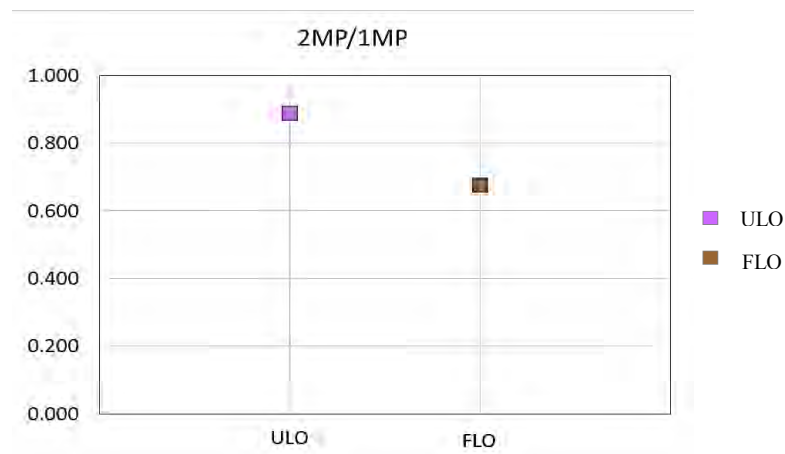


Figure 4.14 (cont.) The correlation plot of diagnostic ratios of hopane biomarkers between fuel oils (FO1 and FO2) and their crude oil feedstock using 95% confidence limit.

Table 4.8 Diagnostic ratios value in used lube oil and fresh lube oil

| Ratio | ULO | FLO |
|------------------|------|------|
| 4MD/1MD | 1.00 | 0.81 |
| 2MP/1MP | 0.89 | 0.67 |
| C2MD/C2P | 0.79 | 0.11 |
| C3MD/C3P | 0.00 | 0.88 |
| 2MA/ Σ MP | 0.00 | 0.00 |
| (3+2)MP/(9+1)MP | 0.62 | 0.54 |

**Figure 4.16** The plot of diagnostic ratio of 4-MD/1-MD of used lube oil and fresh lube oil.**Figure 4.17** The plot of diagnostic ratio of 2-MP/1-MP of used lube oil and fresh lube oil.

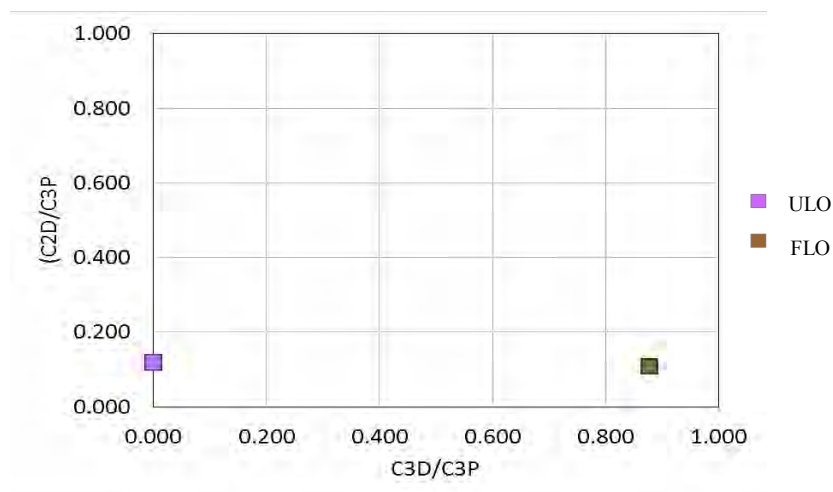


Figure 4.18 The cross plot of C2D/C2P vs C3D/C3P of used lube oil and fresh lube oil.

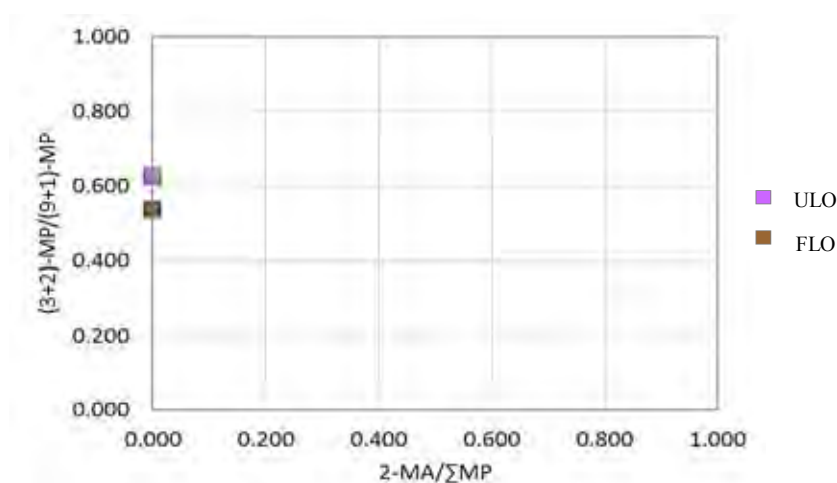


Figure 4.19 The cross plot of (3+2)-MP/(9+1)-MP vs 2-MA/ΣMP of used lube oil and fresh lube oil.

4.5.3 Biomarkers Characterization

Lube oils are produced from middle to heavy fraction of base oils which are rich in terpanes and steranes and they are remained in higher concentrations when compared to their crude oil feedstock (Yang, *et al.*, 2016). The correlation plot of diagnostic ratios of hopane biomarkers between fresh lube oil and used lube oil using 95% confidence limit is presented in Figure 4.19. The result showed that there were some hopane diagnostic keys plotted on the axis which mean some new hopanes were generated and some of hopanes were degraded in ULO. These might be happened as the heat of engine could alter and convert the structure of hopane biomarkers. From

the correlation plot, it could be concluded to be a non-match for ULO and FLO as there were several diagnostic keys not overlapping the $x=y$ line.

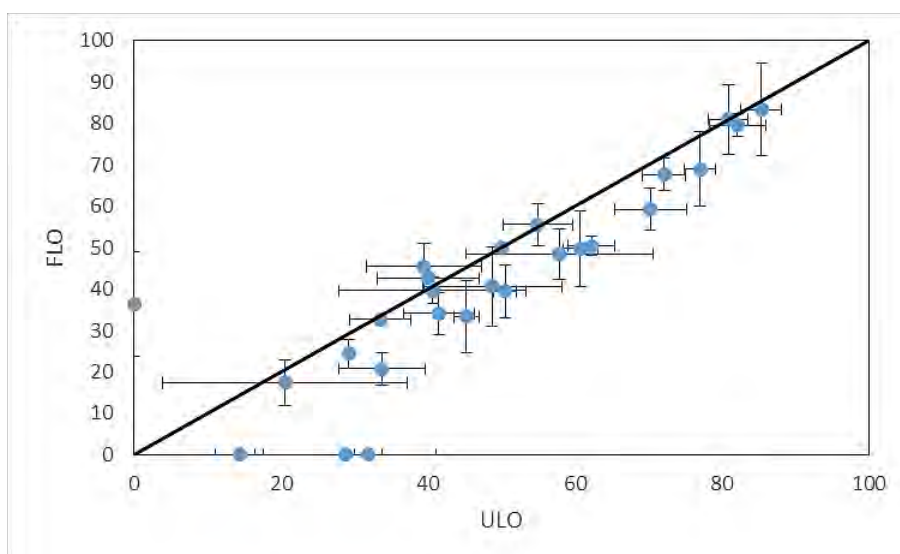


Figure 4.20 The correlation plot of hopane biomarkers between ULO and FLO using a 95% confidence limit.

4.6 The Summarized Protocol for the Differentiation of Crude Oils and Processed Oils

From the investigation in previous section, the protocol to differentiate crude oils, fuel oils and lube oils is summarized in Figure 4.21. First, the extracted samples were analyzed by GC-FID to identify basic hydrocarbon information, weathering and biodegradation degree. If GC-FID chromatogram provided a huge unresolved complex mixture (UCM), the sample probably identified to be lube oil. If only small UCM arised in the chromatogram, it probably be weathered oils which could not be identified oil types. Then, GCxGC-TOFMS was used to characterize the distribution pattern of anthracenes and phenanthrenes (m/z 178, 192, 206,220), dibenzothiophenes (m/z 184, 198, 212, 226) and hopane biomarkers (m/z 191). From the GCxGC-TOFMS surface chromatogram, the distribution pattern of methyl-anthracenes and methyl-phenanthrenes (m/z 192) were different in most of crude oils and fuel oil. The common alkyl-phenanthrenes, 3-, 2-, 9- and 1-MP were appeared in all of oil types while 4- MP and 2-MA could be detected in the fuel oil samples and some crude oils, but 2-MA

was disappeared after weathering in day 45. Moreover, the first two peak of 3-MP and 2-MP were smaller than the second double peak of 9-MP and 1-MP in most crude oils whereas, in the fuel oils, the first two peaks of 3- and 2- MP were larger than the last second peaks of 9- and 1- MP. For diagnostic ratios, the ratio of 2-MP/1-MP could be summarily distinguish crude oils and processed oils. If the ratio of 2-MP/1-MP was lower than 0.5, it was probably be crude oils. On the other hand, the ratio of 2-MP/1-MP was higher than 0.5, it was probably be processed oils. The cross plots of C2D/C3D vs C3D/C3P and (3+2)-MP/(9+1)-MP vs 2-MA/ Σ MP were the effective way to differentiate crude oils and processed oils, but the cross plot of (3+2)-MP/(9+1)-MP vs 2-MA/ Σ MP could not be used in case of heavily weathered samples. For the correlation plot of hopane biomarkers, the plots of fuel oil and crude oil feedstocks indicated a non-match as the refining processes had an effect on hopane biomarkers. Since the weathering processes had no significant effects on hopane biomarker, the correlation plots between fresh and its weathered samples indicated positive match.

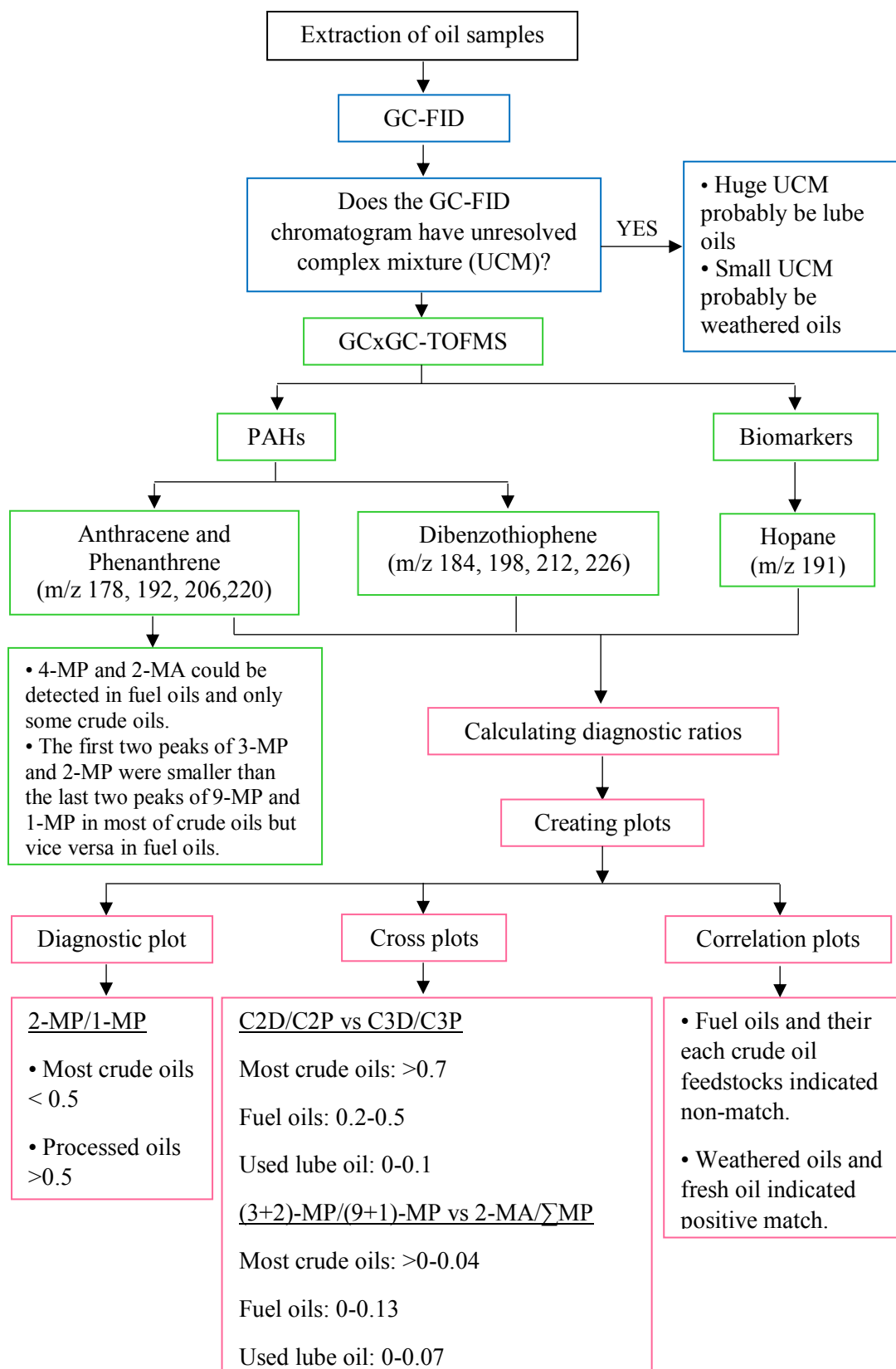


Figure 4.21 Protocol chart for differentiation of crude oil, fuel oil and used lube oil.

CHAPTER V

CONCLUSIONS AND RECOMMENDATIONS

5.1 Conclusions

This work studied the differentiation of crude oils and processed oils by focusing on the distribution patterns and several diagnostic ratios of PAHs such as anthracenes, phenanthrenes, dibenzothiophenes, and their alkylation and biomarkers in hopanes group. Five crude oils, two fuel oils and one lube oil were investigated in this study. GC-FID was used to analyze basic information of hydrocarbon and biodegradation degree. GCxGC-TOFMS was used to analyze the distribution pattern of chemical fingerprints.

Although crude oil and fuel oil had unresolved complex mixture (UCM) in their weathered samples, lube oil for both fresh and used lube oil could be identified by GC-FID chromatogram even if they were weathered due to the huge UCM. Crude oils and fuel oils could be not clearly identified by GC-FID chromatogram therefore, GCxGC-TOFMS was essential.

The distribution pattern of MA and MP in most of crude oils were different from the fuel oil. In most of crude oils, the first two peaks of 3-MP and 2-MP were smaller than the last two peaks of 9-MP and 1-MP. On the other hand, the first two peaks were larger than the last two peaks in the fuel oils and some of the crude oils. The diagnostic ratios of 4MD/1MD and 2MP/1MP, and the cross plots of C2D/C2P vs C3D/C3P, 2-MA/2-MP vs 2-MA/3-MP, 2-MA/1-MP vs 2-MA/9-MP, 2-MA/(3+2)-MP vs 2-MA/(9+1)-MP, (3+2)-MP/(9+1)-MP vs 2-MA/ Σ MP were investigated to differentiate crude oils and processed oils. The cross plot of C2D/C2P vs C3D/C3P could differentiate crude oils and refined products in the fresh and weathered samples, however the cross plot of (3+2)-MP/(9+1)-MP vs 2-MA/ Σ MP could not be used in case of heavily weathered samples.

Hopanes distribution patterns in the fuel oils and their crude oil feedstocks were different as the temperature and pressure in the refinery processes might alter the structure of hopanes. The distributions of hopanes in weathered oil samples were not

far different from the fresh oil samples therefore, hopanes were more resistant to weathering processes than PAHs.

Comparing fresh and used lube oil, there were light carbons appeared in used lube oil as it was contaminated with unburnt fuel and combustion residue. Besides, the distribution pattern of hopane biomarkers in the fresh lube oil and used lube oil were dissimilar due to generating or degrading during the combustion in the engine.

In addition, there was a high concentration peak which could be detected in every weathered samples which is believed that it was aromatic dicarboxylic acid compounds which occurred by biodegradation.

5.2 Recommendations

An important problem to characterize the chemical fingerprints is concentration of the sample. In the spill simulation, it was hard to collect the samples in last period of weathering because it might suffer from the weathering processes and spread out as a very thin film layer. However, the method to collect spilled samples might not appropriate as the spilled samples were collected in vial with small bottle nose that may make difficulty to collect spilled sample. Therefore, it could be improved by changing to the wider container. In this work, it could not identify what exactly hopanes' name are. It may be valuable to identify the hopanes in various way.

REFERENCES

- Altas, R.M. and Altas, M.C. (1991) Biodegradation of oil and bioremediation of oil spills. Current Opinion in Biotechnology, 2, 440-443.
- Baraket, A.O., Mostafa, A., EI-Gayar, M.S., and Rullkotter, J. (1997) Source-dependent biomarker properties of five crude oil from the Gulf of Suez, Egypt. Organic Geochemistry, 26(7-8), 441-450.
- Christensen, J.H., Tomasi, G., and Hansen, A.B. (2005) Chemical Fingerprinting of Petroleum Biomarkers Using Time Warping and PCA. Environmental Science and Technology, 39(1), 255-260.
- Fernandez-Varela, R., Andrade, JM., Muniategui, S., Prada, D., and Ramirez-Villalobos, F. (2009) The comparison of two heavy fuel oils in composition and weathering pattern, based on IR, GC-FID and GC-MS analyses: Application to Prestige wreckage. Water Research, 43, 1015-1026.
- Harris, D.C. (1995) Quantitative Chemical Analysis, 4th edition. New York: W.H.Freemantle and Company.
- ITOPF. (2011) Technical Information Paper: Fate of Oil Spills. Canterbury: Impact PR and design.
- Leffler, W.L. (2000) Petroleum Refining in Non-technical Language. Tulsa: Penwell Corp.
- Liv-Guri Faksness, Hermann M. Weiss., and Per S. Daling. (2002) Revision of the nordtest methodology for oil spill identification. Trondheim: SINTEF Applied Chemistry.
- Misselwitz, M., Cochran, J., English, C., and Burger, B. (2013) Fingerprinting Crude Oils and Tarballs Using Biomarkers and Comprehensive Two-Dimensional Gas Chromatography. Restek Corporation.
- Moustafa, Y.M. and Morsi, R.E. (2012) Chromatography and its Applications. In Dhanarasu, S. (Ed), Contexts for learning: Biomarkers (pp. 165-186). Croatia: Intech.
- Mulabagal, V., Yin, F., John, G.F., Hayworth, J.S., and Clement, T.P. (2013) Chemical fingerprinting of petroleum biomarkers in Deepwater Horizon oil

- spill samples collected from Alabama shoreline. Marine Pollution Bulletin, 70, 147-154.
- Pavlova, A. and Papazova, D. (2003) Oil-spill identification by gas chromatography-mass spectrometry. Journal of Chromatographic Science, 41(5), 271-273.
- Russell, C.A., Snape, C.E., Crozier, S., Kikabhai, T., Sharpe, R. (2004) Biological marker compound transformations as an extremely sensitive measure of cracking in visbreaking. Abstracts of papers of the American Chemical Society, 228.
- Speight, J.G. (2007) The Chemistry and Technology of Petroleum. Boca Raton: CRC Press.
- Stipanovic, A.J. (2003) Fuels and Lubricant Handbook. In Totten, G.E. (Ed.) Context for learning: Hydrocarbon base oil chemistry (pp. 169-184) West Conshohocken: ASTM International.
- Stout, S.A., Douglas, G.S., Uhler, A.D., McCarthy, K.J., Emsbo-Mattingly, S.D. (2005) Identifying the source of mystery waterbone oil spill: a case for quantitative chemical fingerprinting. Environmental Claims Journal, 17, 71-88.
- Sun, P., Bao, M., Li, G., Wang, X., Zhao, Y., Zhou, Q., and Cao, L. (2009) Fingerprinting and source identification of an oil spill in China Bohai Sea by gas chromatography-flame ionization detection and gas chromatography-mass spectrometry coupled with multi-statistical analyses. Journal of Chromatography A, 1216(5), 830-836.
- Uhler, A.D., Stout, S.A., Douglas, G.S., Healey, E.M., and Emsbo-Mattingly, S.D. (2016) Standard Handbook Oil Spill Environmental Forensics. In Stout, S.A. and Wang, Z. (Eds.), Context for learning: Chemical character of marine heavy oil and lubricants (pp.641-682). London: Academic Press.
- Wang, C., Chen, B., Zhang, B., He, S., and Zhao, M. (2013) Fingerprint and weathering characteristics of crude oils after Dalian oil spill, China. Marine Pollution Bulletin, 71, 64-68.
- Wang, Z., Fingas, M., Yang, C., and Hollebhone, B. (2004) Biomarker Fingerprinting: Application and Limitation for Correlation and Source Identification of Oil and Petroleum Products. Fuel Chemistry, 49(1), 331-334.

- Wang, Z., Stout, A.S., and Fingas, M. (2006) Forensic Fingerprinting of Biomarkers for Oil Spill Characterization and Source Identification. Environmental Forensics, 7, 105-106
- Wang, Z.D. and Fingas, M.F. (2003) Development of oil hydrocarbon fingerprinting and technique. Marine Pollution Bulletin, 47, 423-452.
- Winker, M.F. (2003) Fuels and lubricants Handbook: Technology, Properties, Performance and Testing. ASTM Manual Series: MNL 37WCD. In Westbrook, S.R. and Shah, R. (Eds.) Contexts for learning: Introductions to marine fuels (pp. 145-167). West Conshohocken: ASTM International.
- Yang, C., Yang, Z., Zhang, G., Hollebone, B., Landriault, M., Wang, Z., Patrick, L., and Carl, E.B. (2016) Characterization and differentiation of Chemical fingerprints of virgin and used lubricating oils identification of contamination or adulteration sources. Fuel, 163, 271-281.
- Yunker, M.B., Macdonald, R.W., Vingarzan, R., Mitchell, R.H., Goyette, D., and Sylvestre, S. (2002) PAHs in the Fraser River basin: a critical appraisal of PAH ratios as indicators of PAH source and composition. Organic Geochemistry, 33, 489-515.
- Zhang, H., Wang, C., Zhao R., Yin, X., Zhou, H., Tan, L., and Wang, J. (2016) New diagnostic ratios based on phenanthrenes and anthracenes for effective distinguishing heavy fuel oils from fuel oils from crude oils. Marine Pollution Bulletin, 106, 58-61.
- Zhang, H., Yin, X, Zhou, H., Wang, J., and Han, L. (2015) Weathering Characteristics of Crude Oils from Dalian Oil Spill Accident, China. Aquatic Procedia, 3, 238-244.
- Beans, L. "50 Tons of Crude Oil Spill in Thailand" Ecowatch. 31 Jul 2013. 7 July 2016 <<http://www.ecowatch.com/50-tons-of-crude-oil-spill-in-thailand-1881782611.html>>
- "Bunker Oil - Marine Fuel Oil: Distillate Fuels, Residual Fuels." Viscopedia: A free encyclopedia for viscosity. 28 June 2016 <<http://www.viscopedia.com/viscosity-tables/substances/bunker-oil-marine-fuel-oil/>>
- Charuvastra, T. "Week later: Authorities clueless about who caused Hua-hin oil spill." Kaosod English. 3 Nov 2015. 7 July 2016 <<http://www.khaosodenglish.com/life/2015/11/03/1446542324/>>

- Chevron. "Everything You Need to Know About Marine Fuel" ChevronMarineProduct. June 2012. 25 June 2016 <http://www.chevronmarineproducts.com/docs/Chevron_EverythingYouNeedToKnowAboutFuels_v3_1a_DESKTOP.pdf>
- Chomchuen, W. "Rayong Oil Spill Satellite." TheWallStreetJournal. 31 Jul 2013. 7 July 2016 <<http://blogs.wsj.com/indonesiarealtime/2013/07/31/thai-oil-spill-feared-to-be-spreading/>>
- Freudenrich, C. "How Oil Refining Works." HowStuffWorkScience. 14 June 2016 <<http://science.howstuffworks.com/environmental/energy/oil-refining1.htm>>
- Helmenstine, A.M. "Gas Chromatograph Diagram." AboutEducation. 5 July 2016 <<http://chemistry.about.com/od/imagesclipartstructures/ig/Lab-Equipment---Instruments/Gas-Chromatograph-Diagram.htm>>
- "History of Oil." Rix. 2014. 25 June 2016 <<http://www.rix.co.uk/history-of-oil/heating-oil-history.pdf>>
- Kopeliovich, D. "Additives in lubricating oils." SubsTech. 2 June 2012. 3 July 2016 <http://www.substech.com/dokuwiki/doku.php?id=additives_in_lubricating_oils>
- Lundegard, P.D. and Knott, J.R. "Polar Organics in Crude Oil and Their Potential Impacts on Water Quality." ResearchGate. Nov 2001. 28 June 2016 <https://www.researchgate.net/publication/260338155_Polar_Organics_in_Crude_Oil_and_Their_Potential_Impacts_on_Water_Quality>
- Mokkhasen, S. "Source of Oil Remains Unknown as Hua Hin Reopens Beach." KaosodEnglish. 30 Oct 2015. 7 July 2016 <<http://www.kaosodenglish.com/life/2015/10/30/1446206549/>>
- Nagpal, N.K. "PAHs and Their Characteristics." Feb 1993. 6 May 2016 <<http://www.env.gov.bc.ca/wat/wq/BCguidelines/pahs/pahs-01.htm>>
- "Oil Refinery Process." RefiningReport. 14 Apr 2014. 28 June 2016 <<http://refiningreport.com/wp-content/uploads/2014/04/refining-process.jpg>>
- Reusch, W. "Naphthalene Anthracene Phenanthrene." ChemistryMSU. 5 May 2013. 30 June 2016 <<https://www2.chemistry.msu.edu/faculty/reusch/virttxtjml/spectrpy/nmr/nmr2.htm>>

- Rujivanarom, P. "Recent oil spill 10 times larger than one in 2013." The Nation. 6 Nov 2015. 7 July 2016 <<http://www.nationmultimedia.com/national/Recent-oil-spill-10-times-larger-than-one-in-2013-30272382.html>>
- "Thailand's Civil Society Statement: The oil spill and the leaked pipeline." GreenPeace. 2 Aug 2013. 7 July 2016 <<http://www.greenpeace.org/seasia/Press-Centre/Press-Releases/Thailand-Civil-Society-Statement-The-oil-spill-en/>>
- Wallace, R. "Defination of EIA Distillate Categories and Fuels Contained in the Distillate Grouping." Newhealthtips.xyz. 28 June 2016 <<http://newhealthtips.xyz/definitions/definitions-of-eia-distillate-categories-and-fuels-.html>>
- Weatherford Laboratories. "Oil Biodegradation - Bacterial Alteration of Petroleum" Weatherford International. 1 May 2017 <<https://labs.weatherford.com/oil-biodegradation-bacterial-alteration-of-petroleum>>

APPENDICES

Appendix A GCxGC-TOFMS Total Ion Surface Plot Result

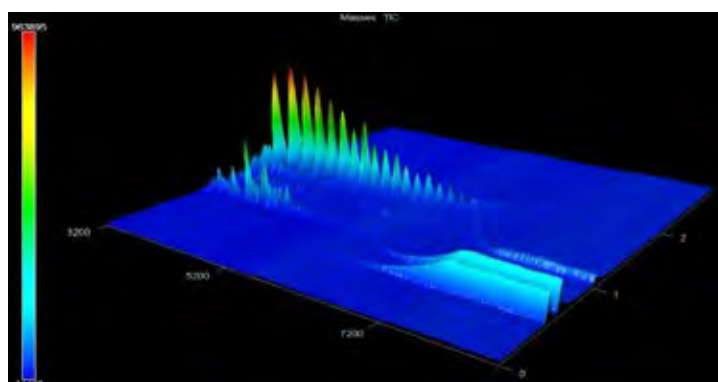


Figure A1 Total ion surface plot of CO1.

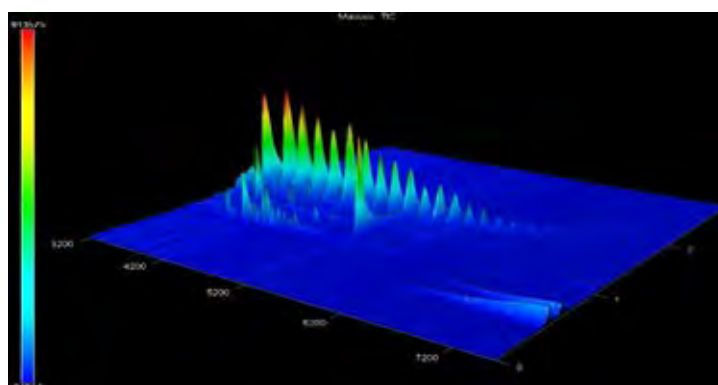


Figure A2 Total ion surface plot of WCO1-D3.

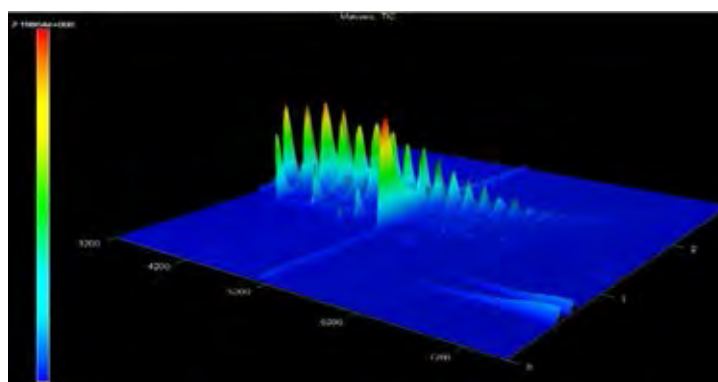


Figure A3 Total ion surface plot of WCO1-D45.

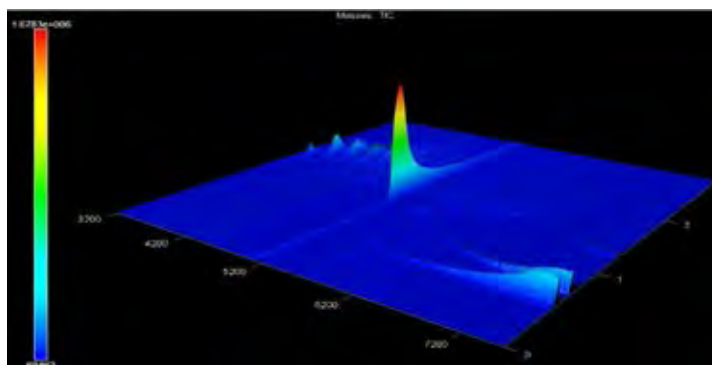


Figure A4 Total ion surface plot of WCO1-D90.

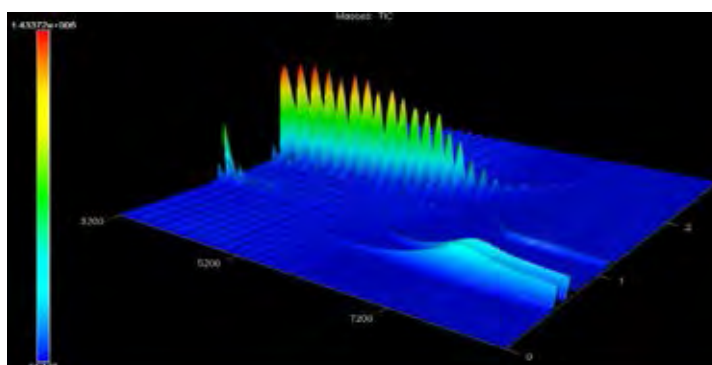


Figure A5 Total ion surface plot of CO2.

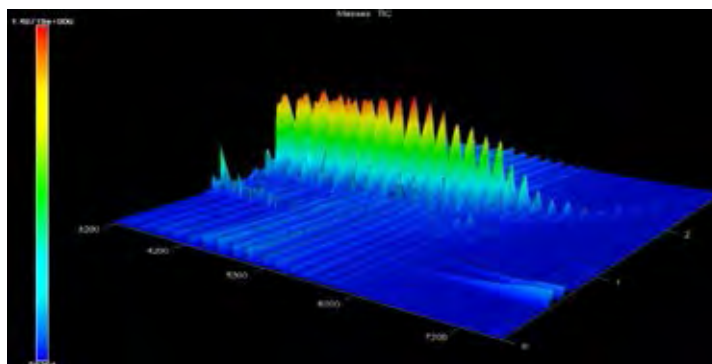


Figure A6 Total ion surface plot of WCO2-D3.

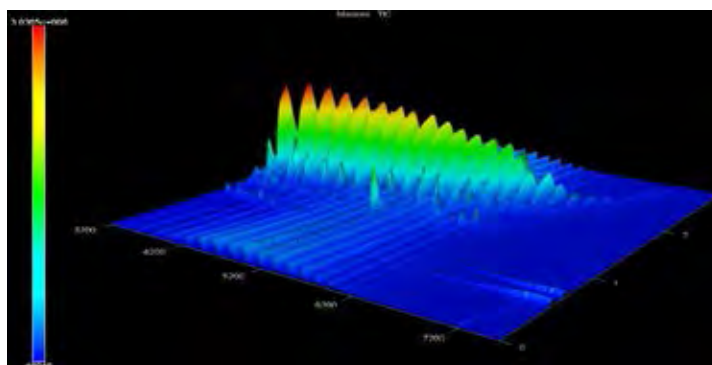


Figure A7 Total ion surface plot of WCO2-D45.

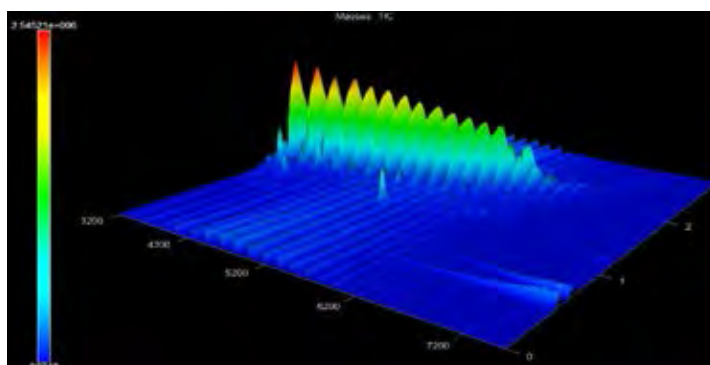


Figure A8 Total ion surface plot of WCO2-D90.

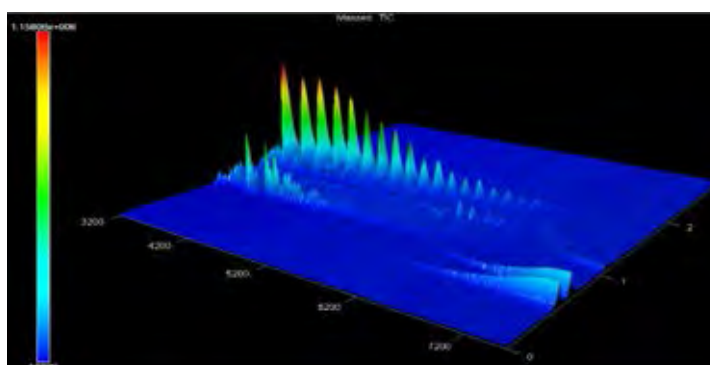


Figure A9 Total ion surface plot of CO3.

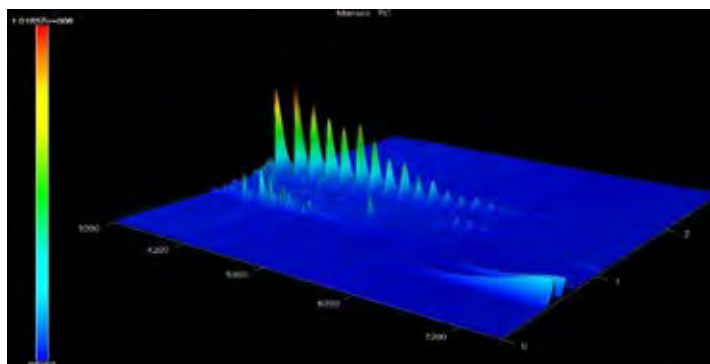


Figure A10 Total ion surface plot of WCO3-D3.

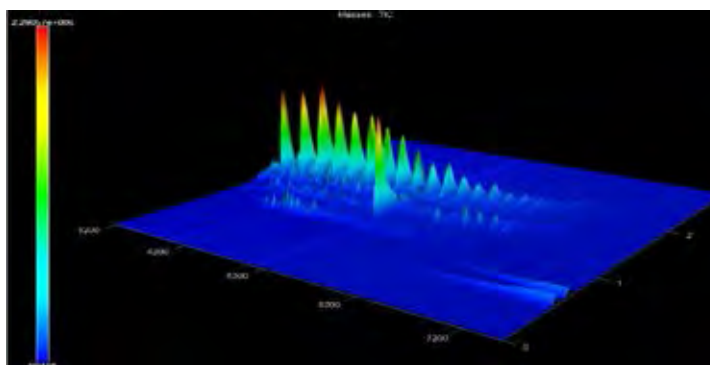


Figure A11 Total ion surface plot of WCO3-D45.

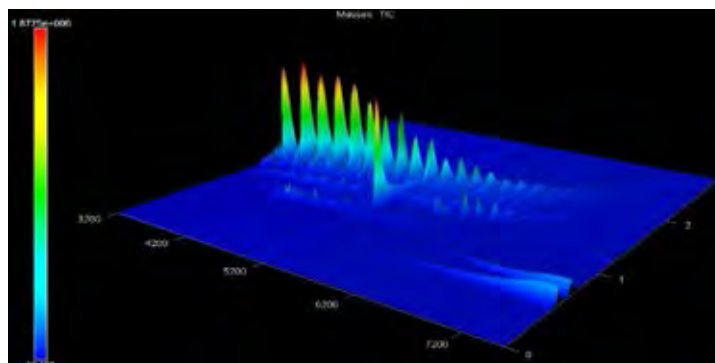


Figure A12 Total ion surface plot of WCO3-D90.

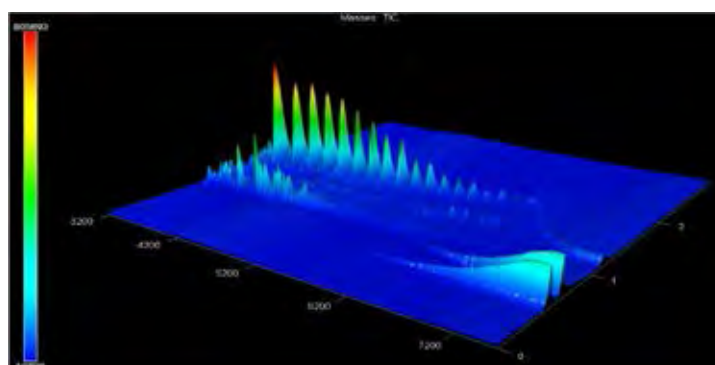


Figure A13 Total ion surface plot of CO4.

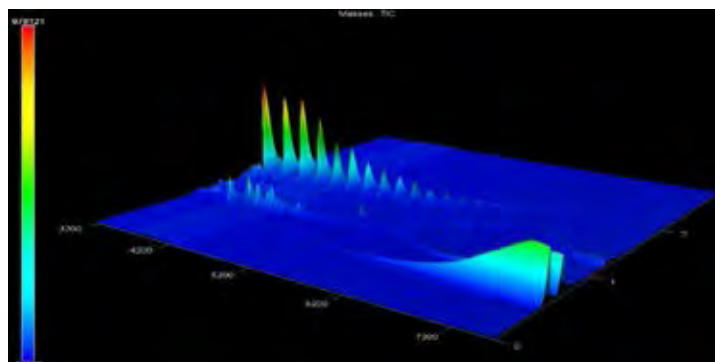


Figure A14 Total ion surface plot of WCO4-D3.

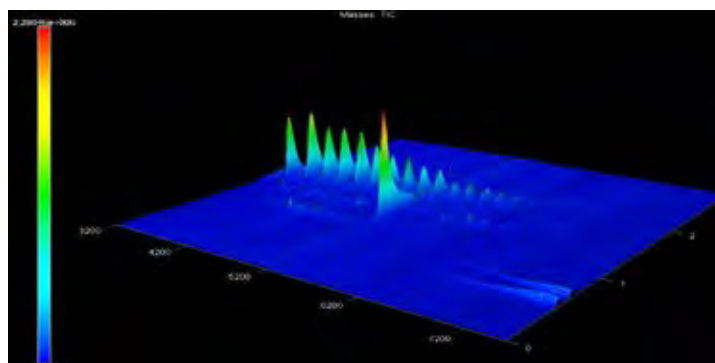


Figure A15 Total ion surface plot of WCO4-D45.

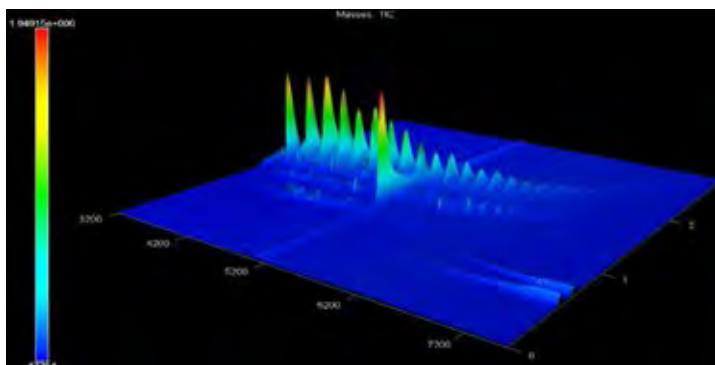


Figure A16 Total ion surface plot of WCO4-D90.

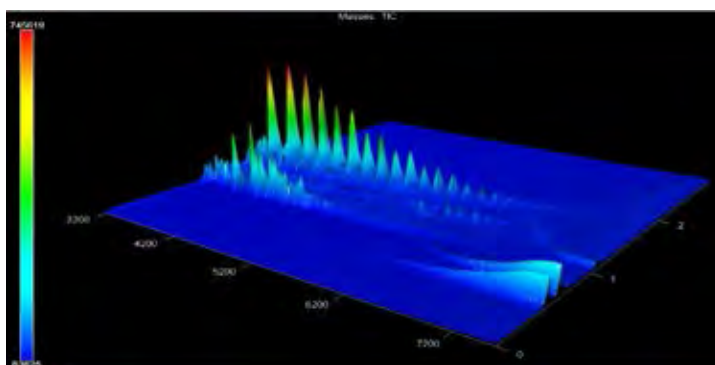


Figure A17 Total ion surface plot of CO5.

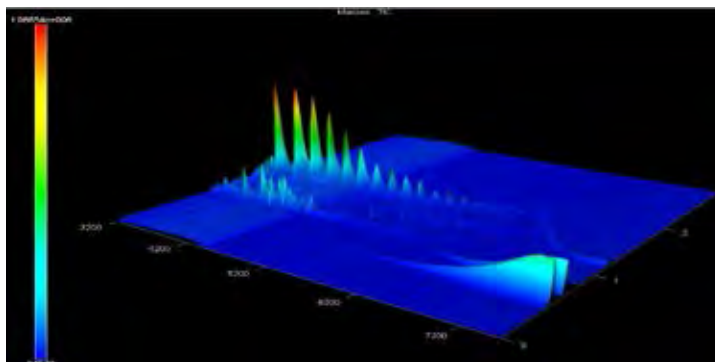


Figure A18 Total ion surface plot of WCO5-D3.

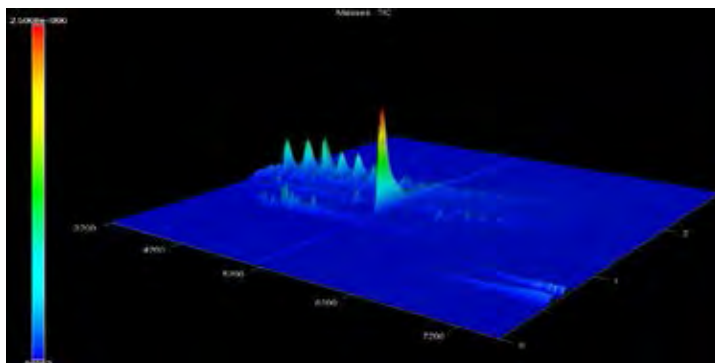


Figure A19 Total ion surface plot of WCO5-D45.

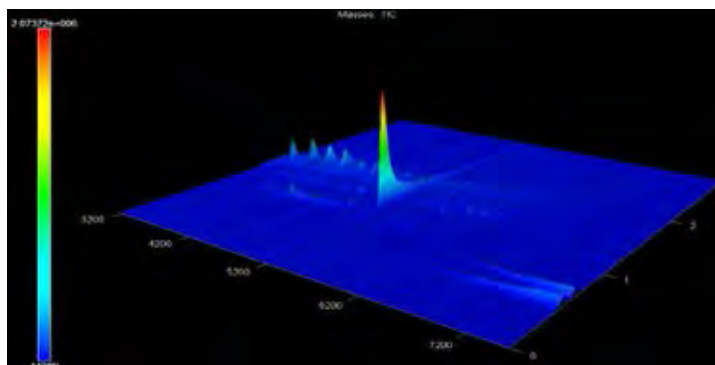


Figure A20 Total ion surface plot of WCO5-D90.

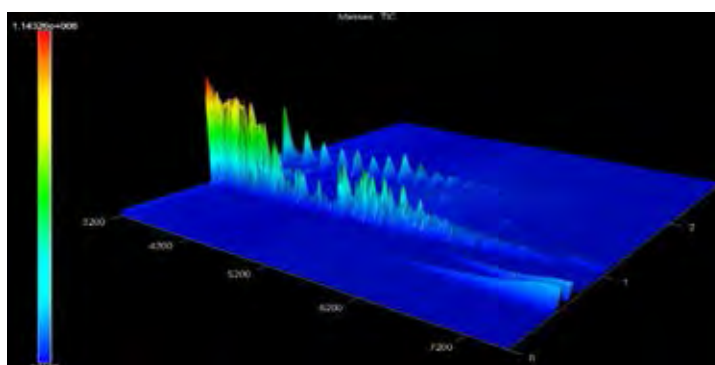


Figure A21 Total ion surface plot of FO1.

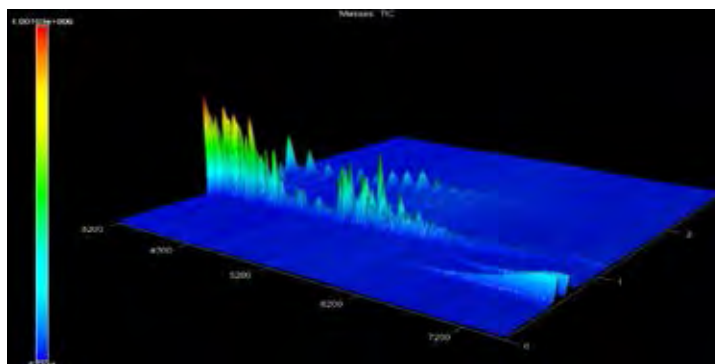


Figure A22 Total ion surface plot of WFO1-D3.

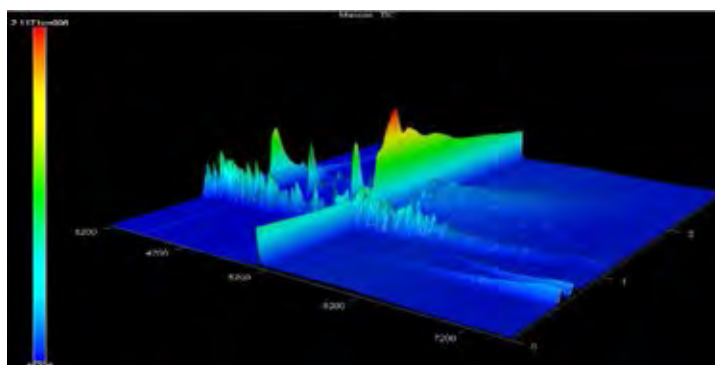


Figure A23 Total ion surface plot of WFO1-D45.

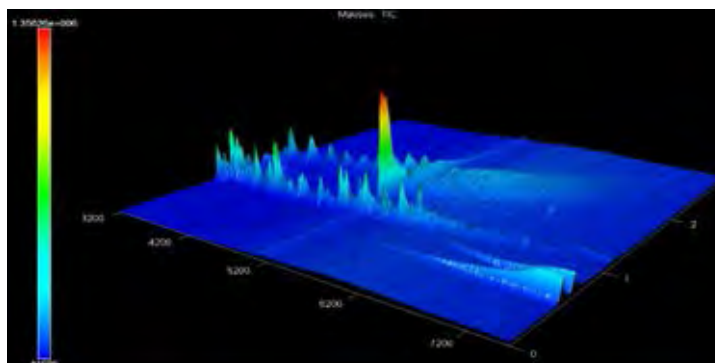


Figure A24 Total ion surface plot of WFO1-D90.

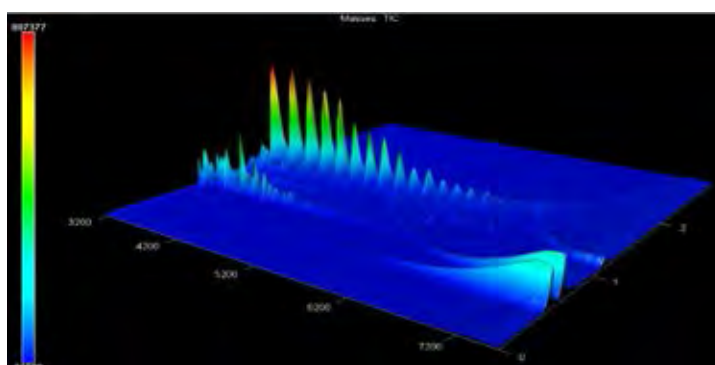


Figure A25 Total ion surface plot of FO2.

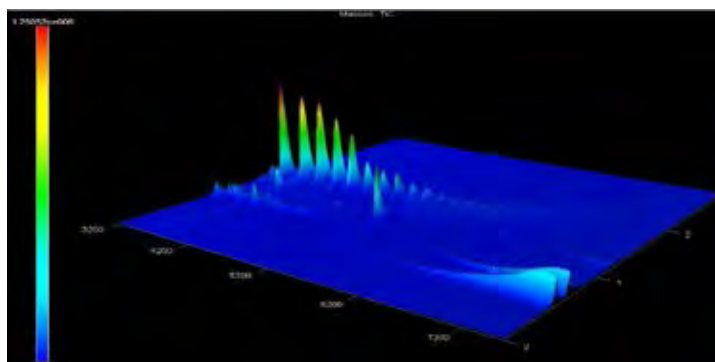


Figure A26 Total ion surface plot of WFO2-D3.

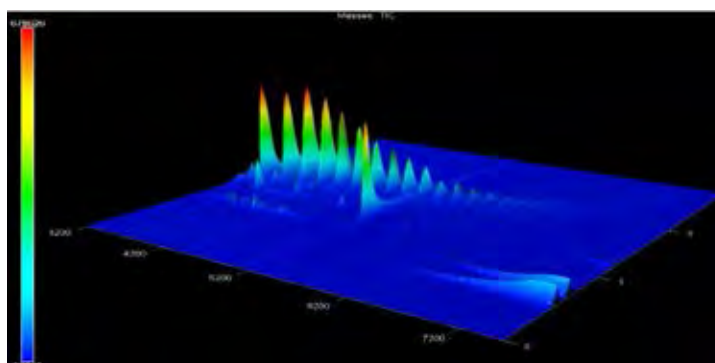


Figure A27 Total ion surface plot of WFO2-D45.

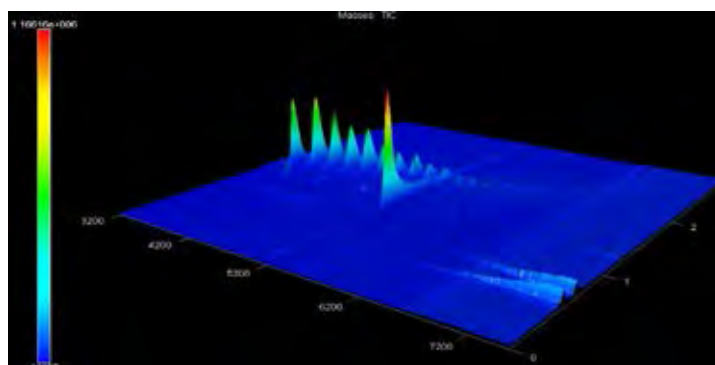


Figure A28 Total ion surface plot of WFO2-D90.

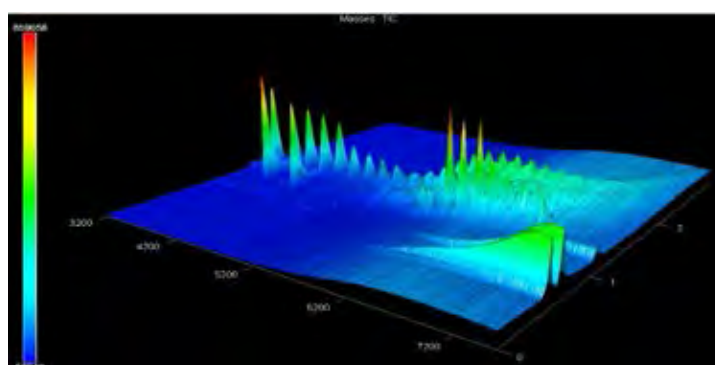


Figure A29 Total ion surface plot of ULO.

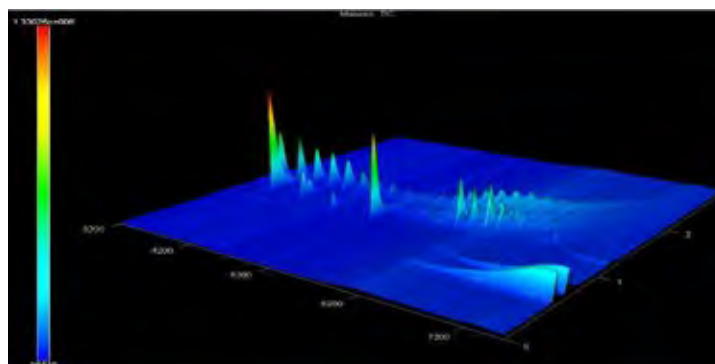


Figure A30 Total ion surface plot of WULO-D3.

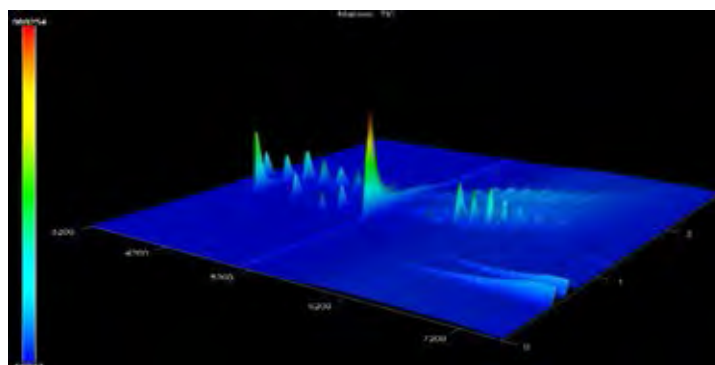


Figure A31 Total ion surface plot of WULO-D45.

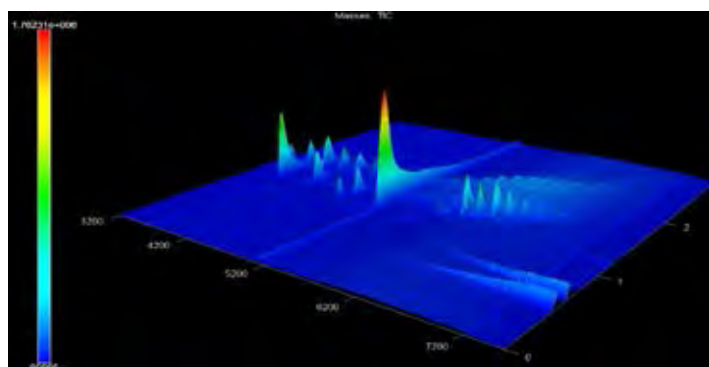


Figure A32 Total ion surface plot of WULO-D90.

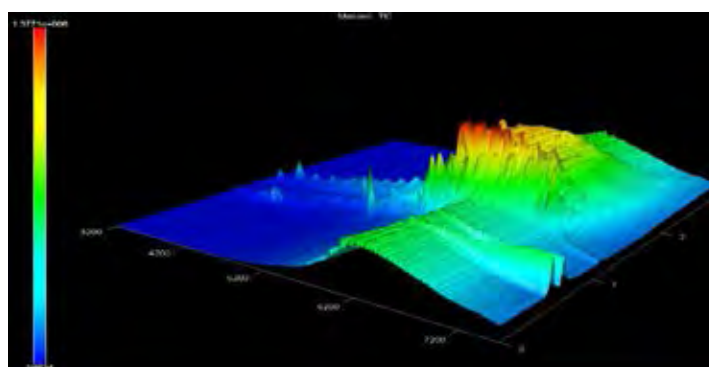
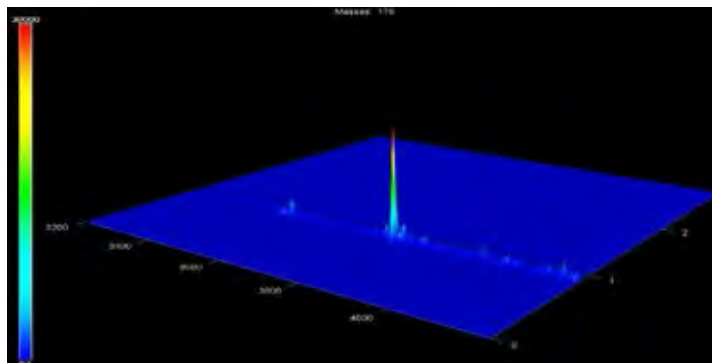
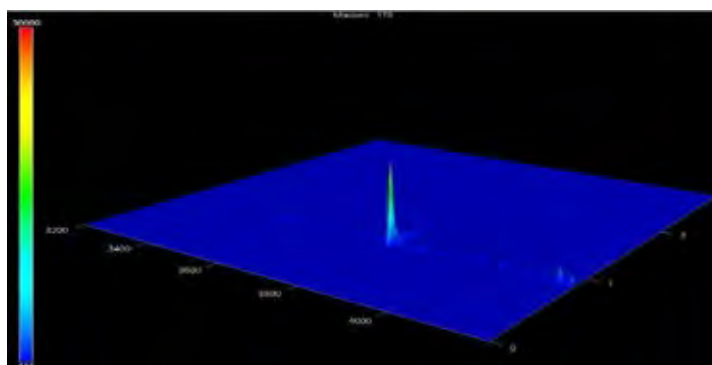
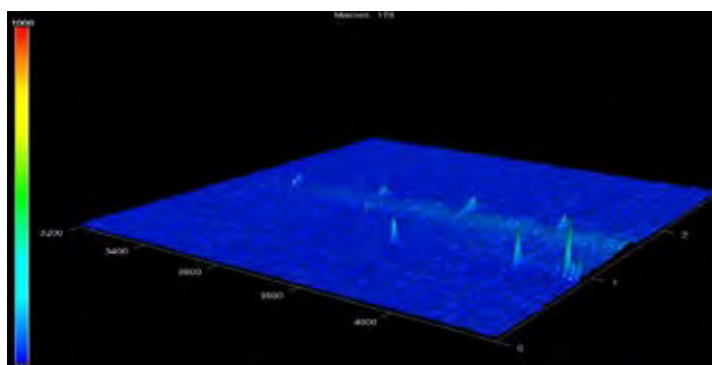


Figure A33 Total ion surface plot of FLO.

Appendix B GCxGC-TOFMS Target Ion (m/z 178) Surface Plot Result**Figure B1** Target ion (m/z 178) surface plot of CO1.**Figure B2** Target ion (m/z 178) surface plot of WCO1-D3.**Figure B3** Target ion (m/z 178) surface plot of WCO1-D45.

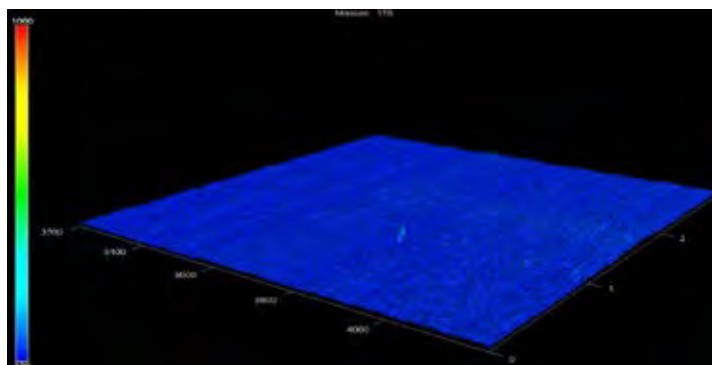


Figure B4 Target ion (m/z 178) surface plot of WCO1-D90.

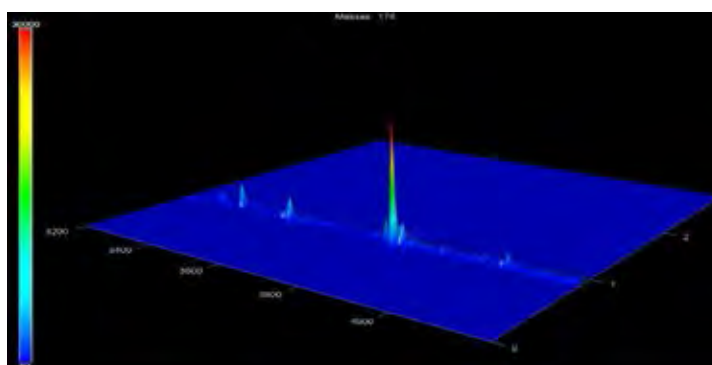


Figure B5 Target ion (m/z 178) surface plot of CO2.

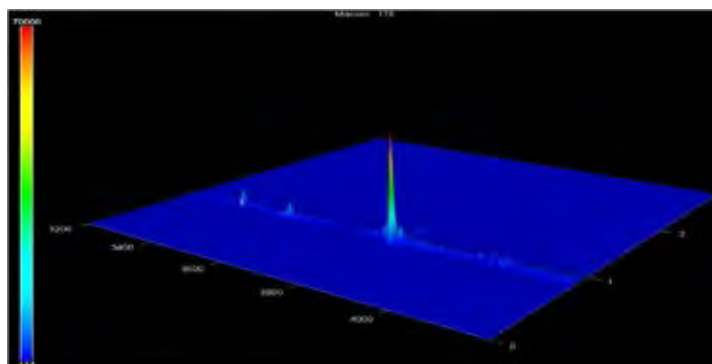


Figure B6 Target ion (m/z 178) surface plot of WCO2-D3.

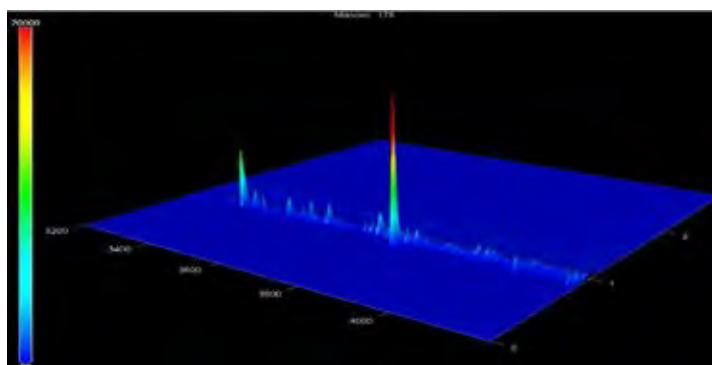


Figure B7 Target ion (m/z 178) surface plot of WCO2-D45.

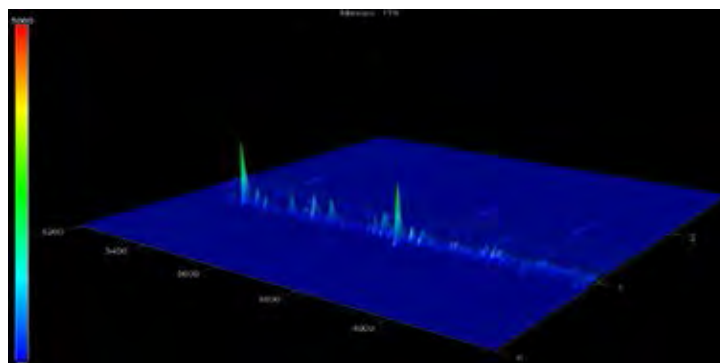


Figure B8 Target ion (m/z 178) surface plot of WCO2-D90.

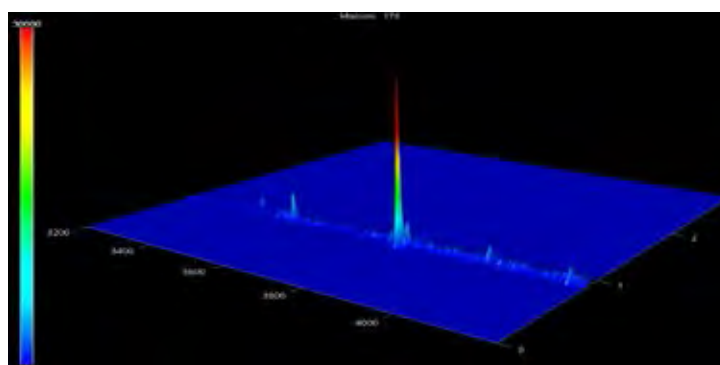


Figure B9 Target ion (m/z 178) surface plot of CO3.

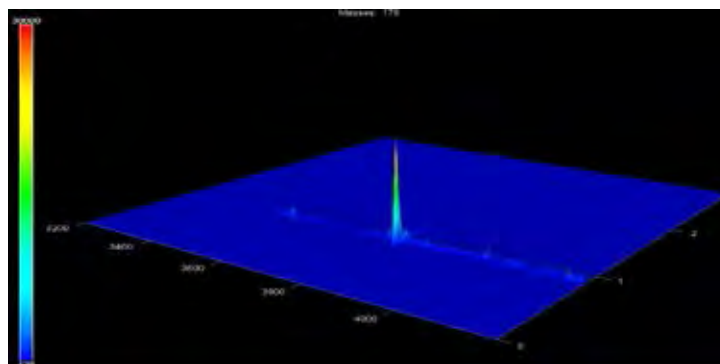


Figure B10 Target ion (m/z 178) surface plot of WCO3-D3.

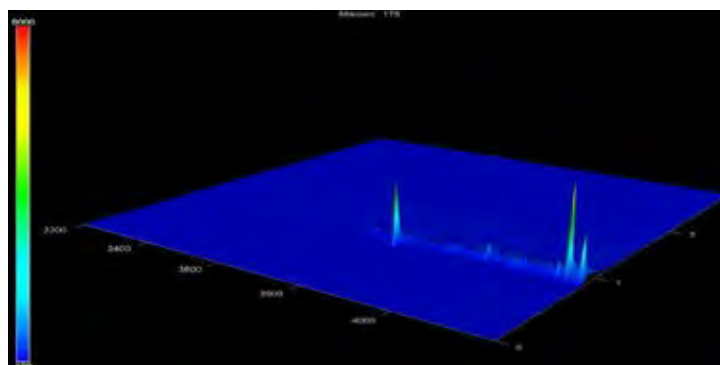


Figure B11 Target ion (m/z 178) surface plot of WCO3-D45.

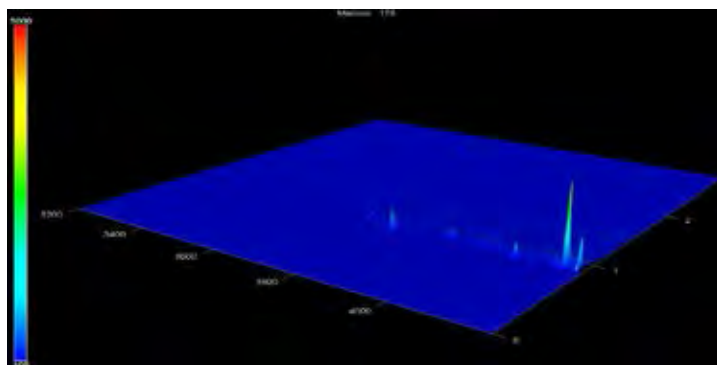


Figure B12 Target ion (m/z 178) surface plot of WCO3-D490.

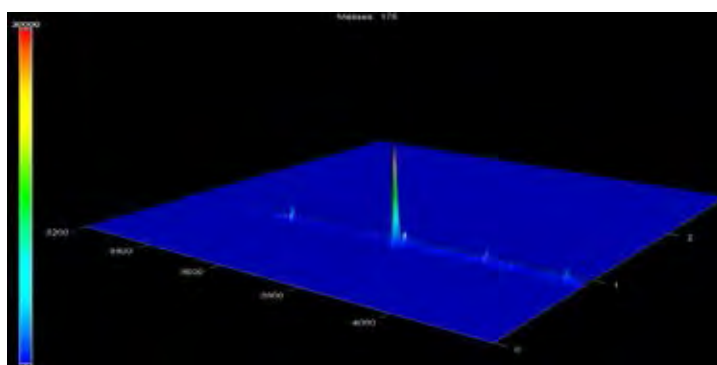


Figure B13 Target ion (m/z 178) surface plot of CO4.

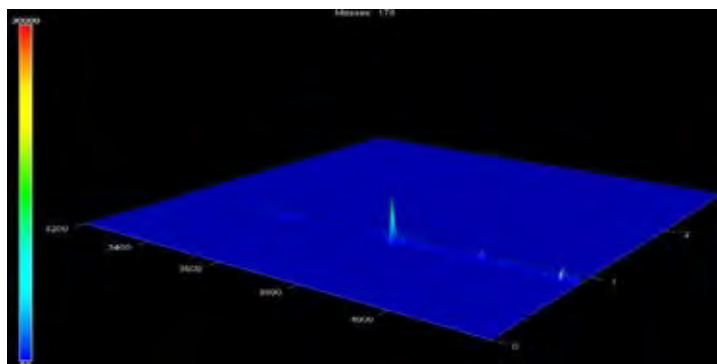


Figure B14 Target ion (m/z 178) surface plot of WCO4-D3.

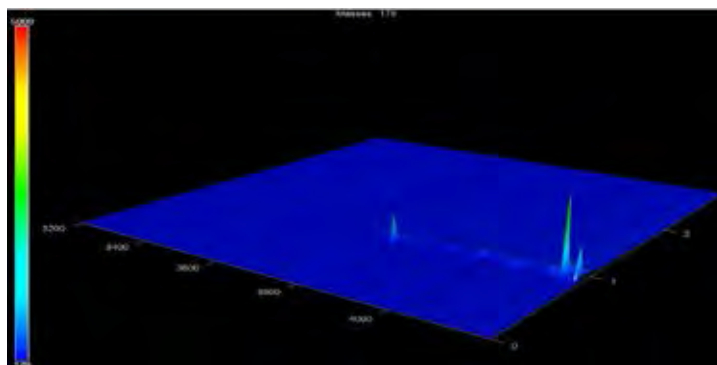


Figure B15 Target ion (m/z 178) surface plot of WCO4-D45.

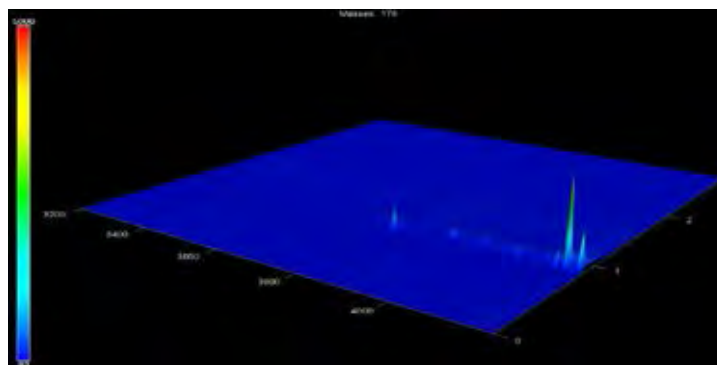


Figure B16 Target ion (m/z 178) surface plot of WCO4-D90.

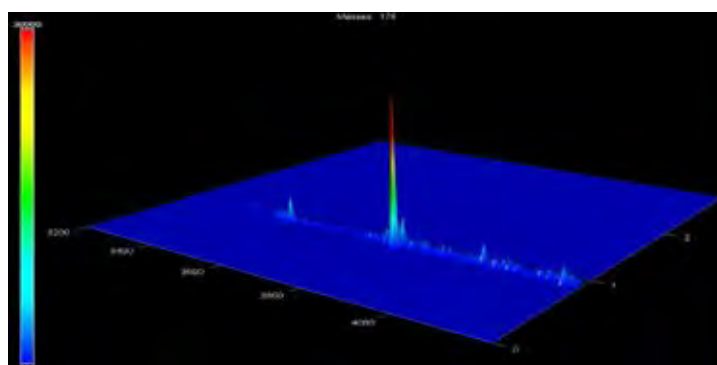


Figure B17 Target ion (m/z 178) surface plot of CO5.

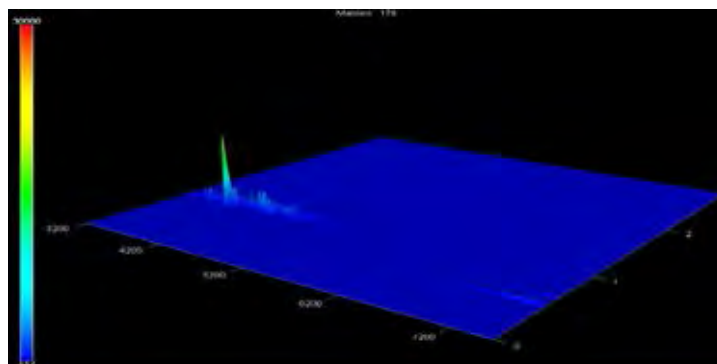


Figure B18 Target ion (m/z 178) surface plot of WCO5-D3.

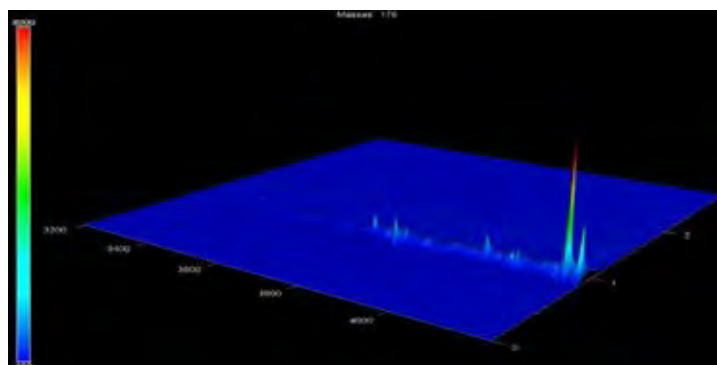


Figure B19 Target ion (m/z 178) surface plot of WCO5-D45.

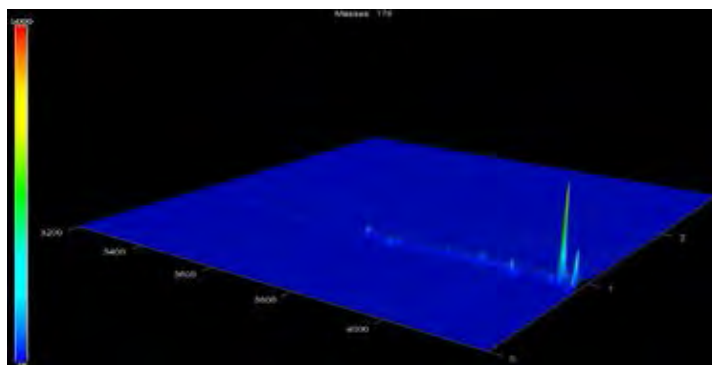


Figure B20 Target ion (m/z 178) surface plot of WCO5-D90.

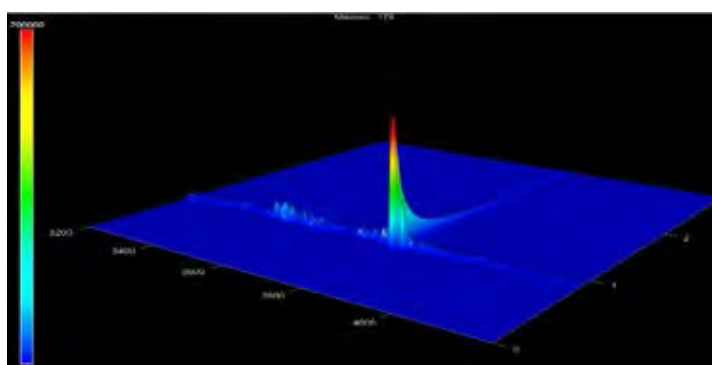


Figure B21 Target ion (m/z 178) surface plot of FO1.

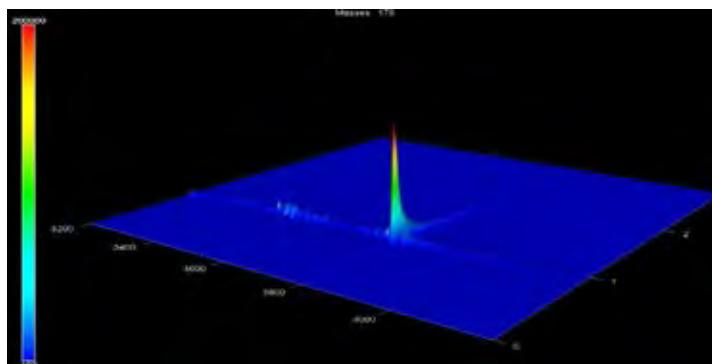


Figure B22 Target ion (m/z 178) surface plot of WFO1-D3.

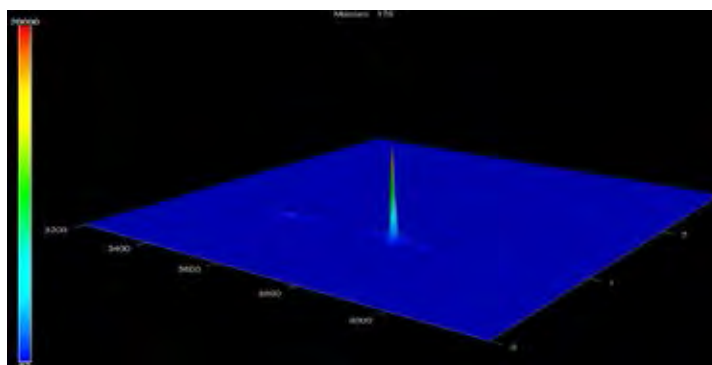


Figure B23 Target ion (m/z 178) surface plot of WFO1-D45.

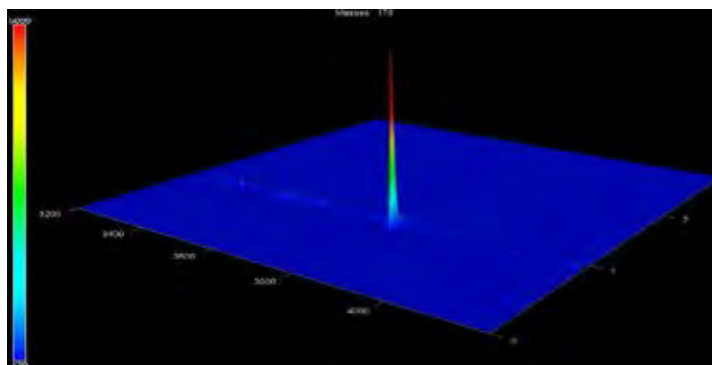


Figure B24 Target ion (m/z 178) surface plot of WFO1-D90.

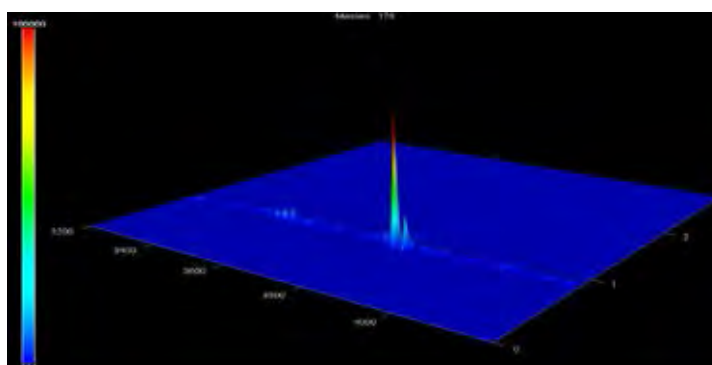


Figure B25 Target ion (m/z 178) surface plot of FO2.

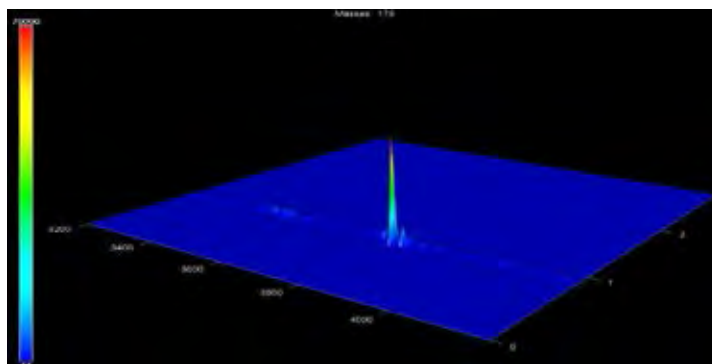


Figure B26 Target ion (m/z 178) surface plot of WFO2-D3.

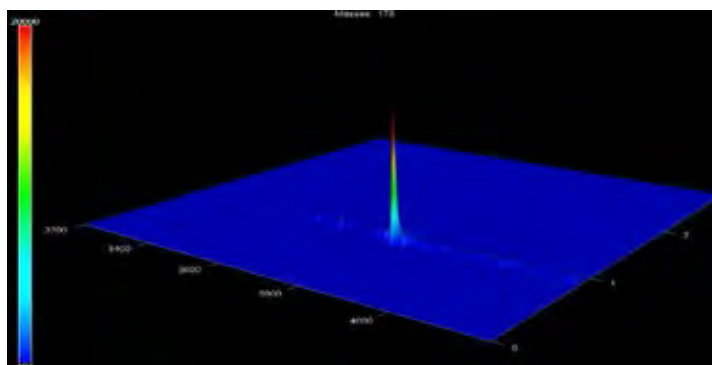


Figure B27 Target ion (m/z 178) surface plot of WFO2-D45.

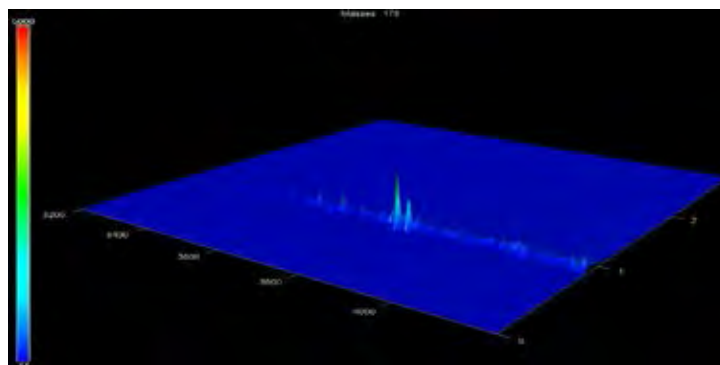


Figure B28 Target ion (m/z 178) surface plot of WFO2-D90.

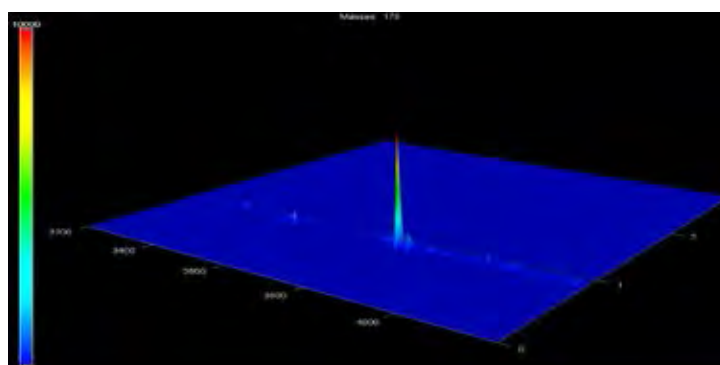


Figure B29 Target ion (m/z 178) surface plot of ULO.

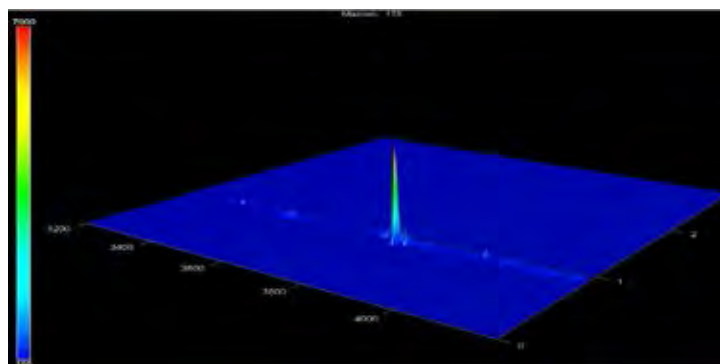


Figure B30 Target ion (m/z 178) surface plot of WULO-D3.

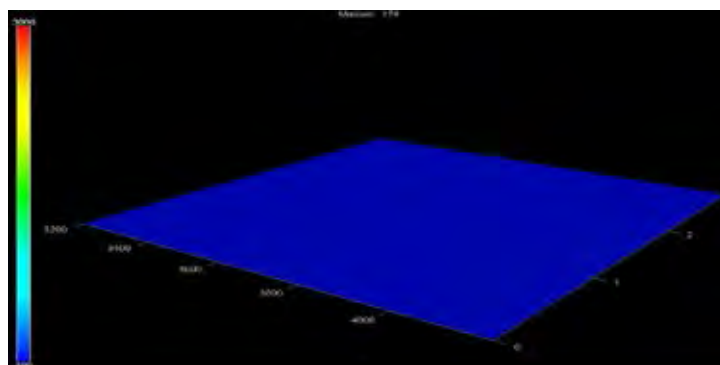


Figure B31 Target ion (m/z 178) surface plot of WULO-D45.

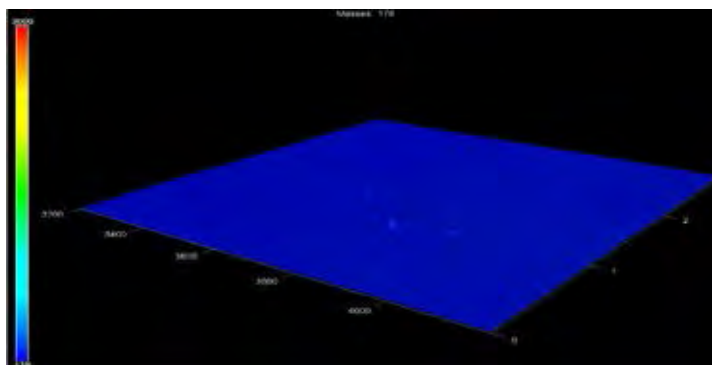


Figure B32 Target ion (m/z 178) surface plot of WULO-D90.

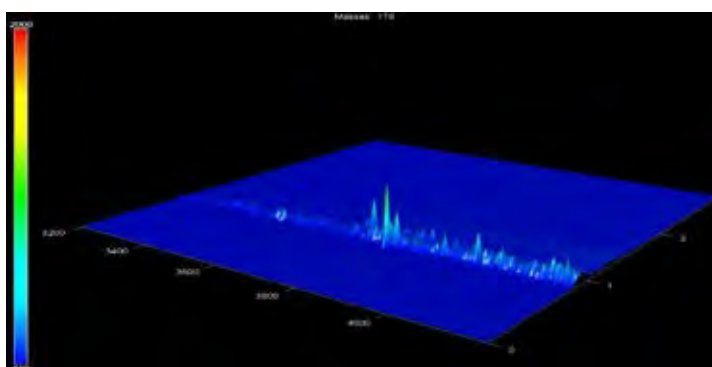
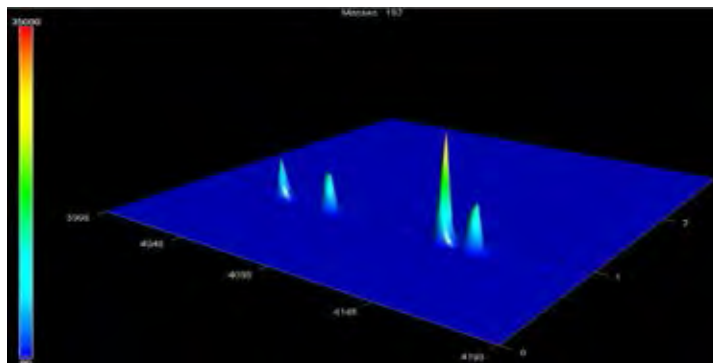
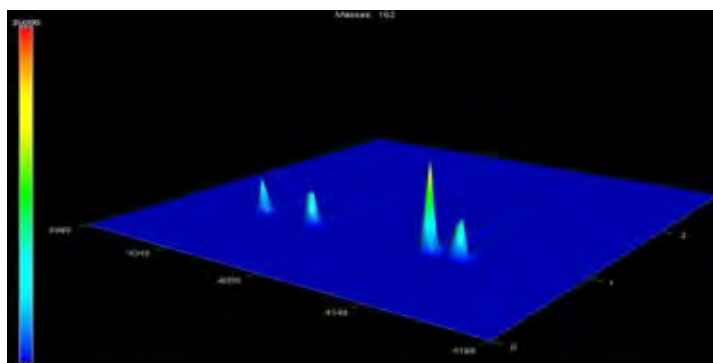
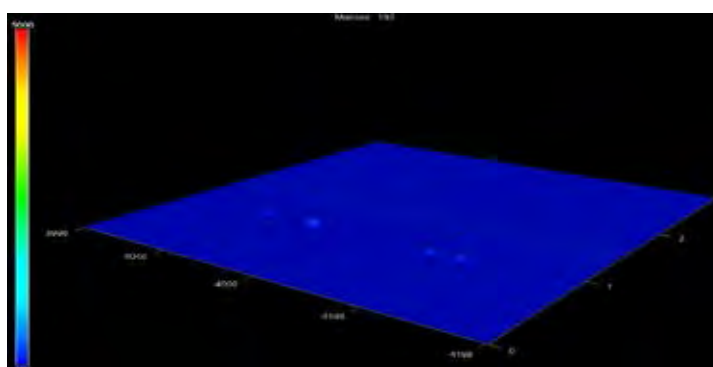


Figure B33 Target ion (m/z 178) surface plot of FLO.

Appendix C GCxGC-TOFMS Target Ion (m/z 192) Surface Plot Result**Figure C1** Target ion (m/z 192) surface plot of CO1.**Figure C2** Target ion (m/z 192) surface plot of WCO1-D3.**Figure C3** Target ion (m/z 192) surface plot of WCO1-D45.

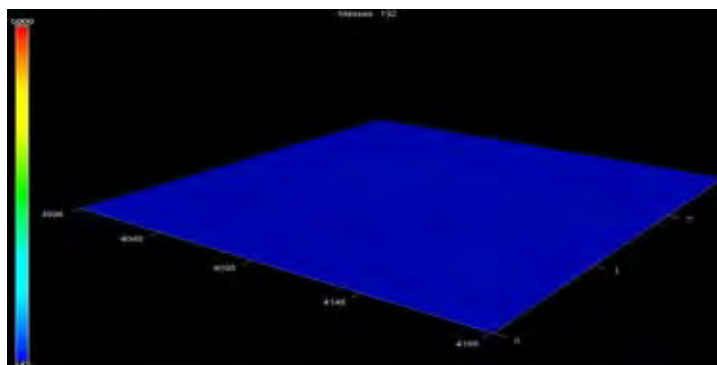


Figure C4 Target ion (m/z 192) surface plot of WCO1-D90.

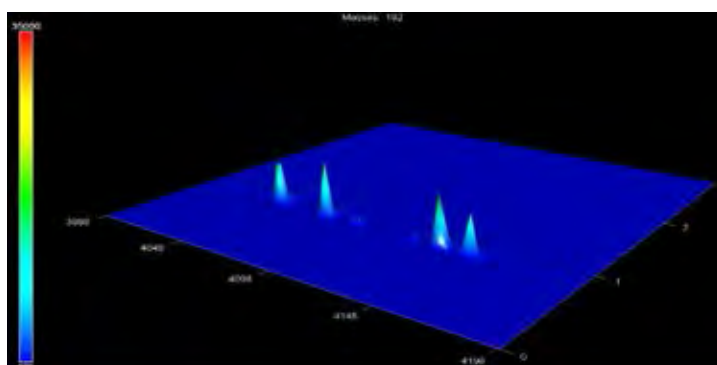


Figure C5 Target ion (m/z 192) surface plot of CO2.

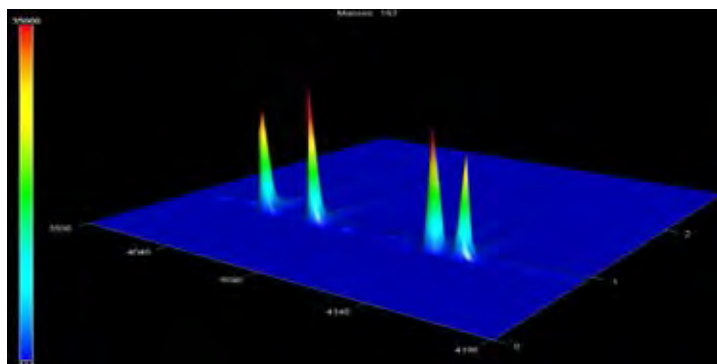


Figure C6 Target ion (m/z 192) surface plot of WCO2-D3.

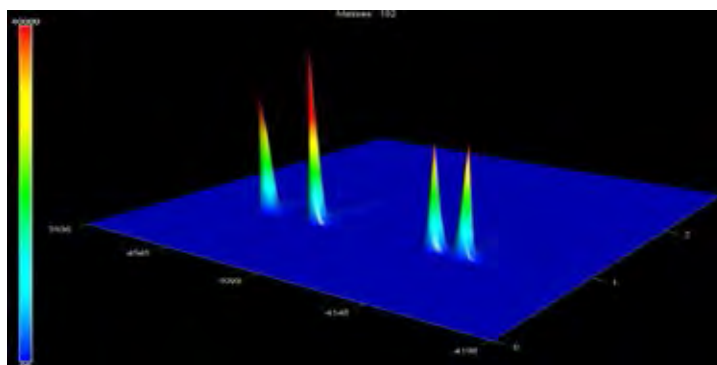


Figure C7 Target ion (m/z 192) surface plot of WCO2-D45.

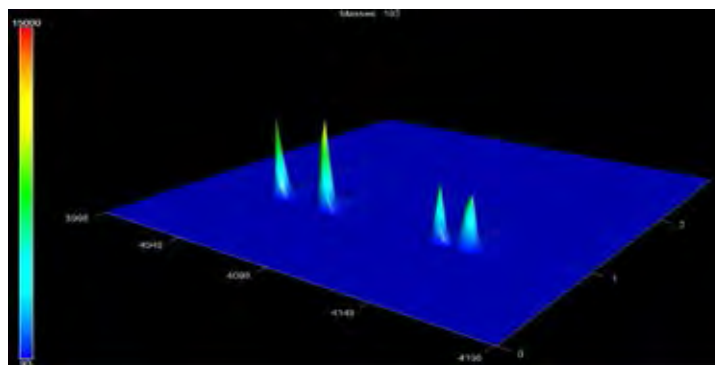


Figure C8 Target ion (m/z 192) surface plot of WCO2-D90.

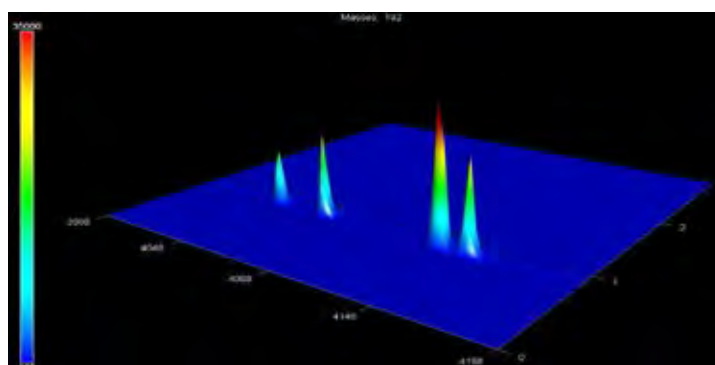


Figure C9 Target ion (m/z 192) surface plot of CO3.

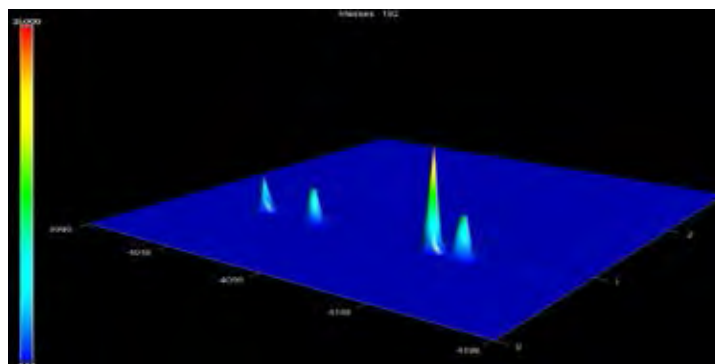


Figure C10 Target ion (m/z 192) surface plot of WCO3-D3.

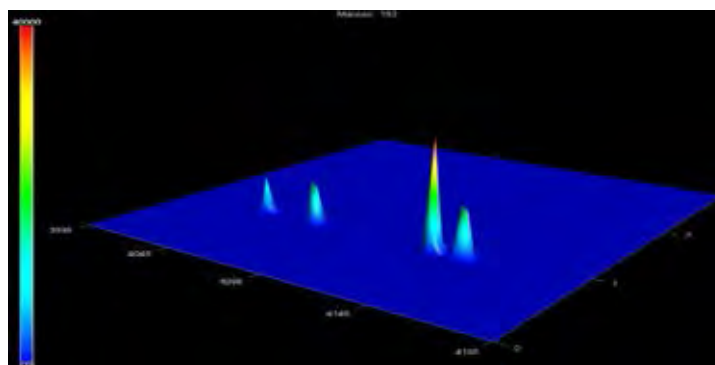


Figure C11 Target ion (m/z 192) surface plot of WCO3-D45.

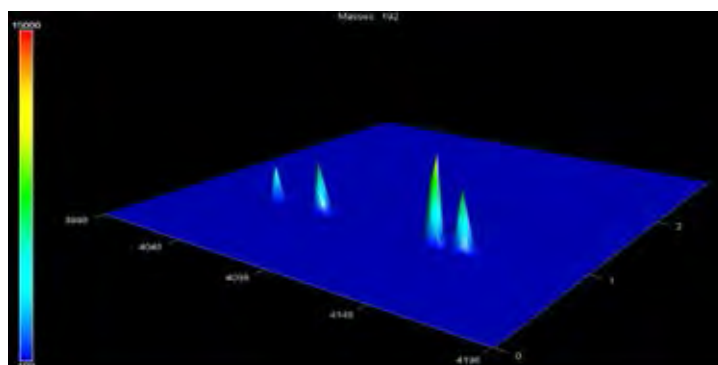


Figure C12 Target ion (m/z 192) surface plot of WCO3-D90.

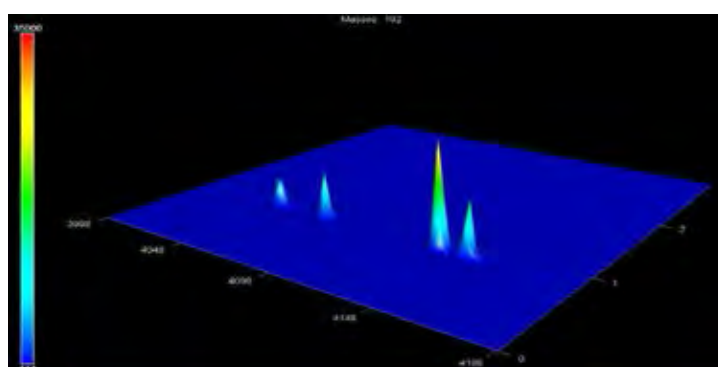


Figure C13 Target ion (m/z 192) surface plot of CO4.

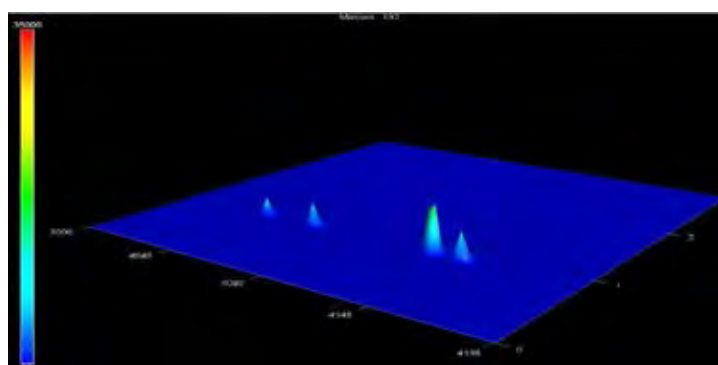


Figure C14 Target ion (m/z 192) surface plot of WCO4-D3.

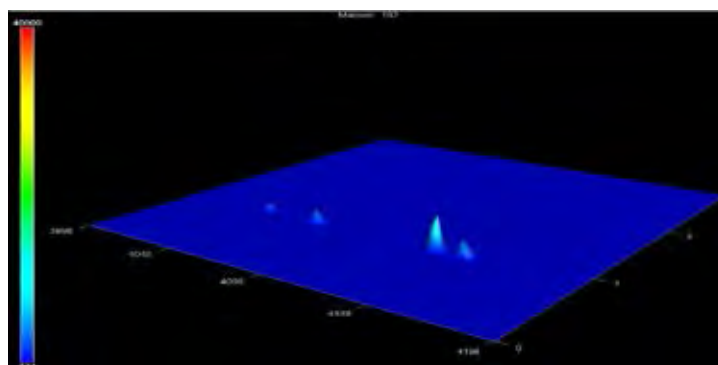


Figure C15 Target ion (m/z 192) surface plot of WCO4-D45.

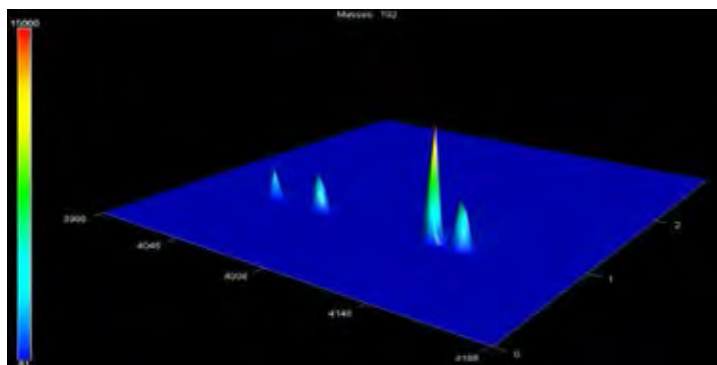


Figure C16 Target ion (m/z 192) surface plot of WCO4-D90.

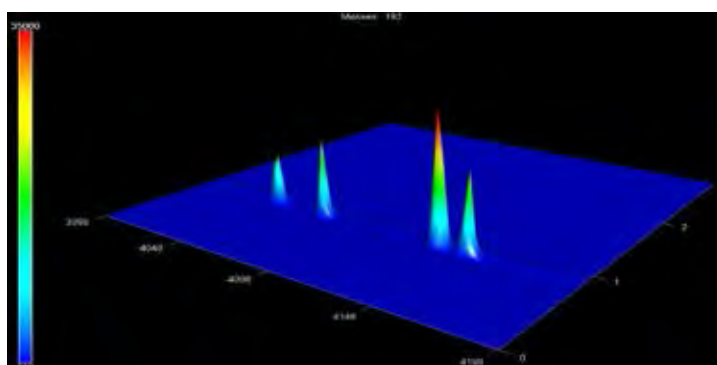


Figure C17 Target ion (m/z 192) surface plot of CO5.

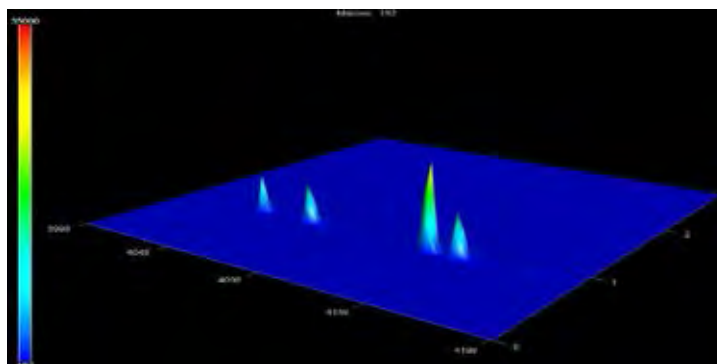


Figure C18 Target ion (m/z 192) surface plot of WCO5-D3.

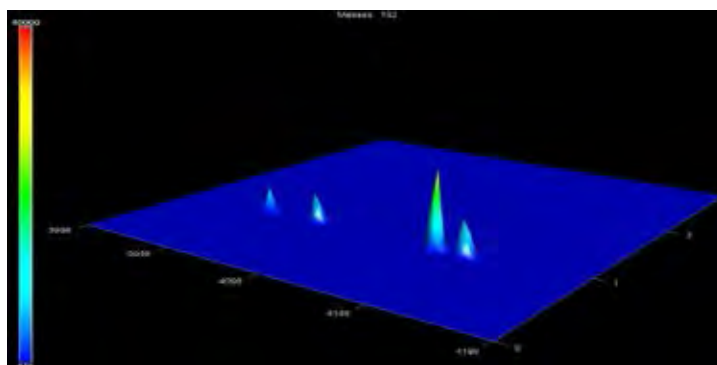


Figure C19 Target ion (m/z 192) surface plot of WCO5-D45.

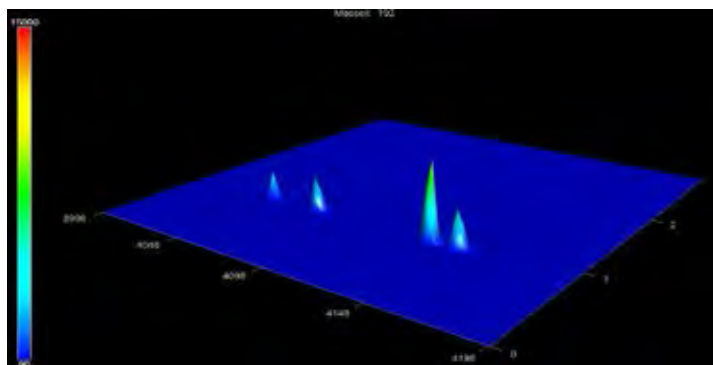


Figure C20 Target ion (m/z 192) surface plot of WCO5-D90.

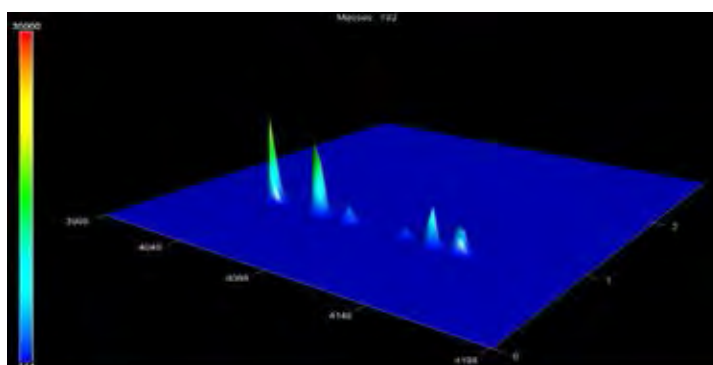


Figure C21 Target ion (m/z 192) surface plot of FO1.

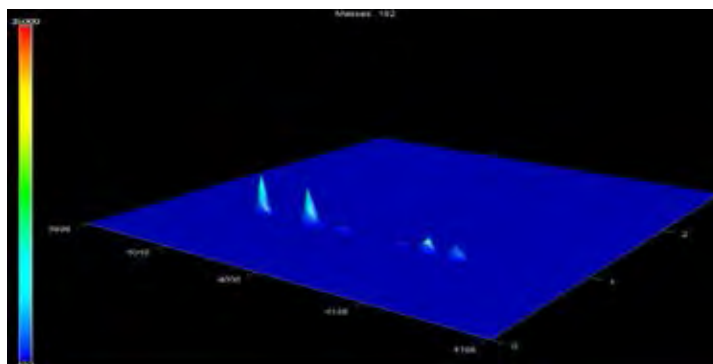


Figure C22 Target ion (m/z 192) surface plot of WFO1-D3.

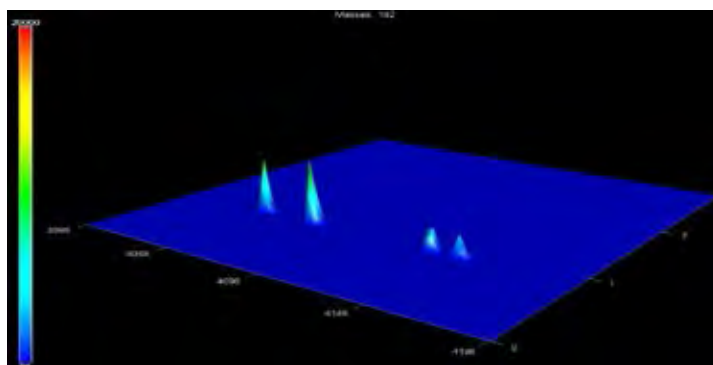


Figure C23 Target ion (m/z 192) surface plot of WFO1-D45.

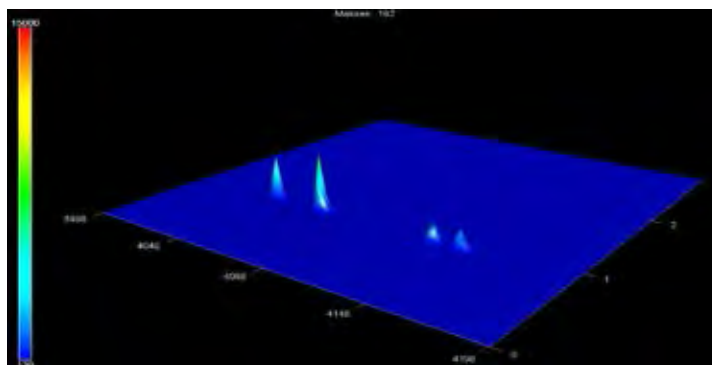


Figure C24 Target ion (m/z 192) surface plot of WFO1-D90.

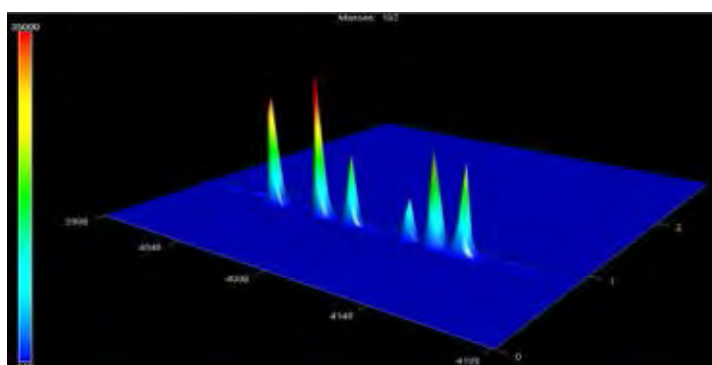


Figure C25 Target ion (m/z 192) surface plot of FO2.

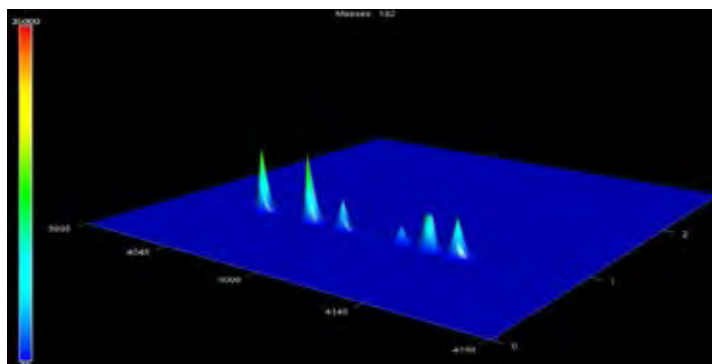


Figure C26 Target ion (m/z 192) surface plot of WFO2-D3.

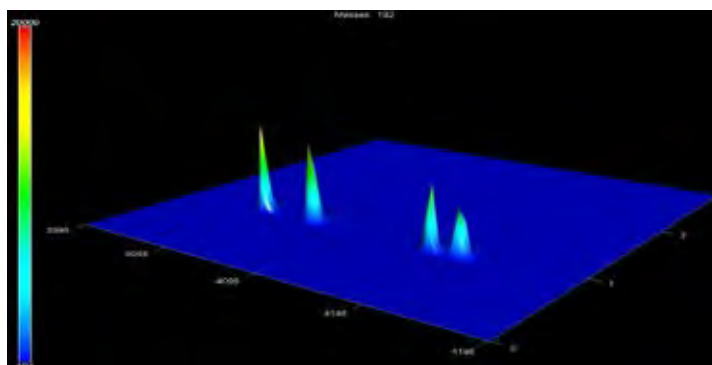


Figure C27 Target ion (m/z 192) surface plot of WFO2-D45.

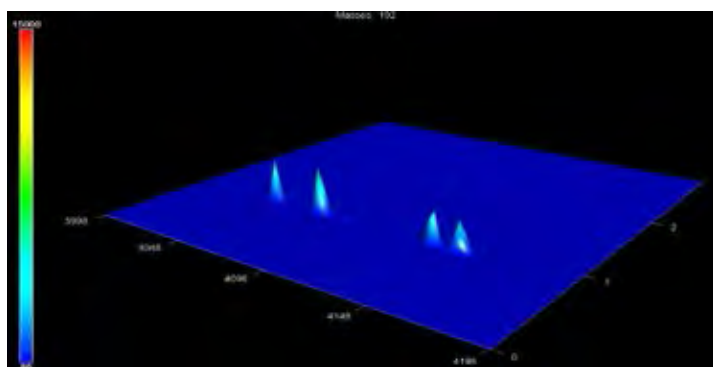


Figure C28 Target ion (m/z 192) surface plot of WFO2-D90.

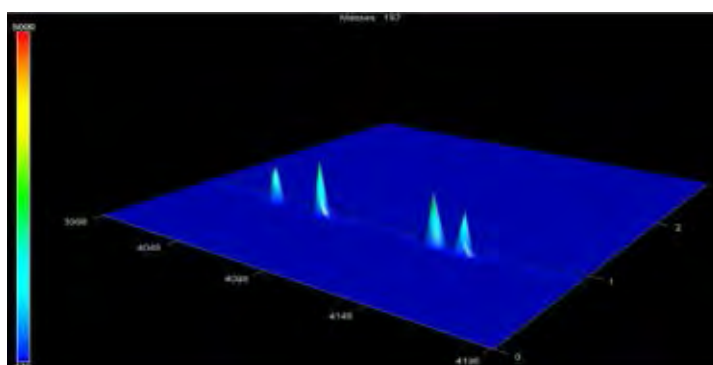


Figure C29 Target ion (m/z 192) surface plot of ULO.

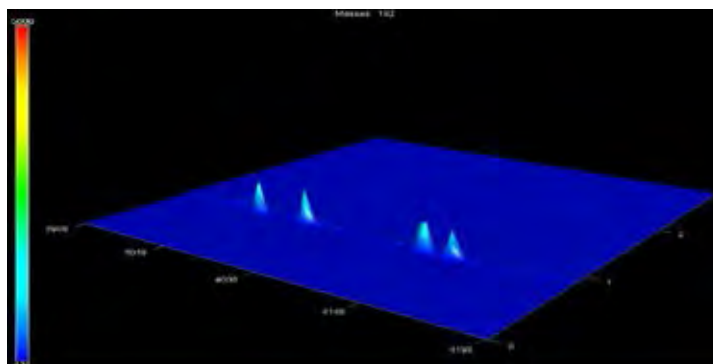


Figure C30 Target ion (m/z 192) surface plot of WULO-D3.

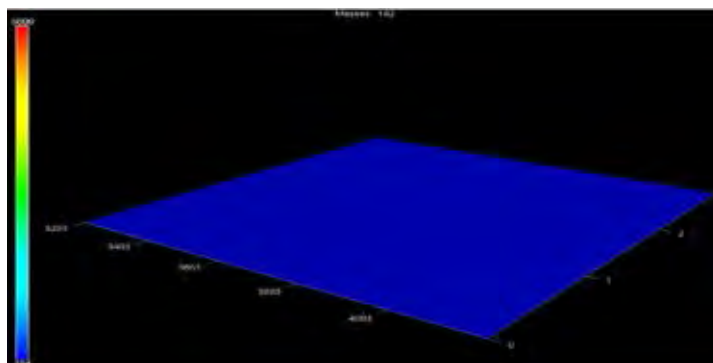


Figure C31 Target ion (m/z 192) surface plot of WULO-D45.

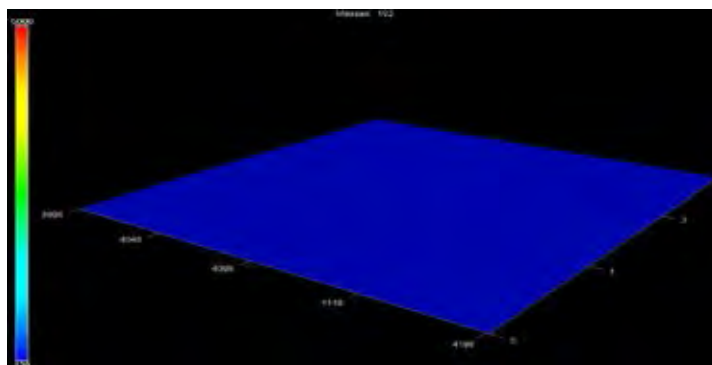


Figure C32 Target ion (m/z 192) surface plot of WULO-D90.

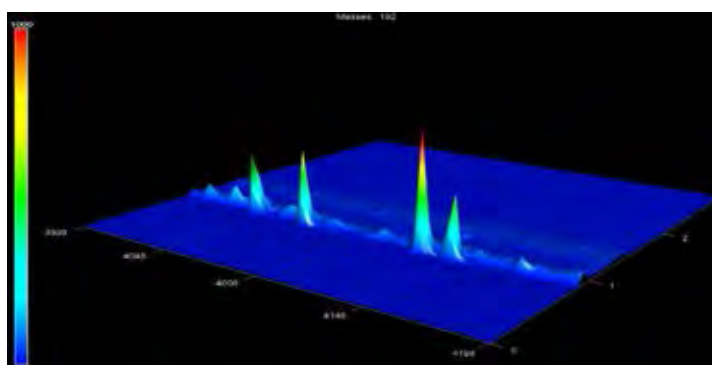
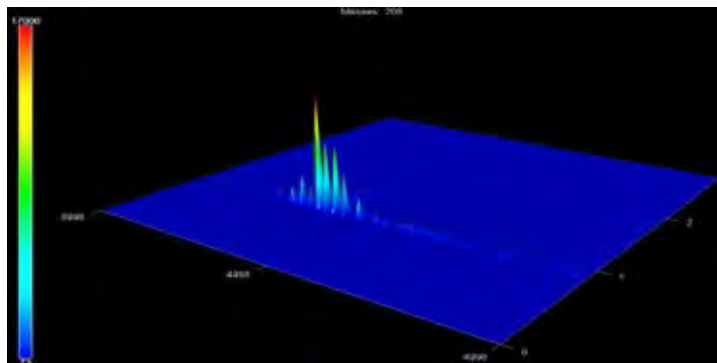
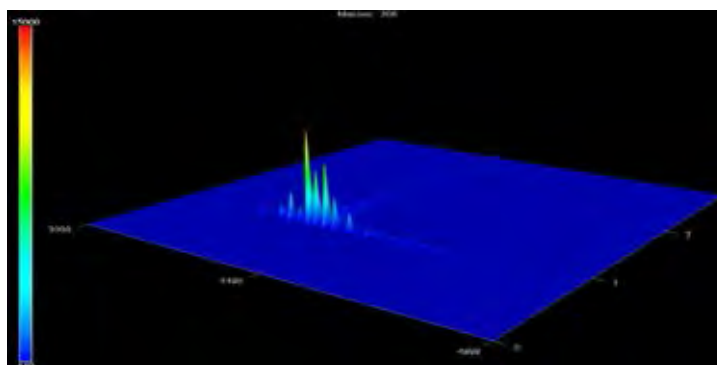
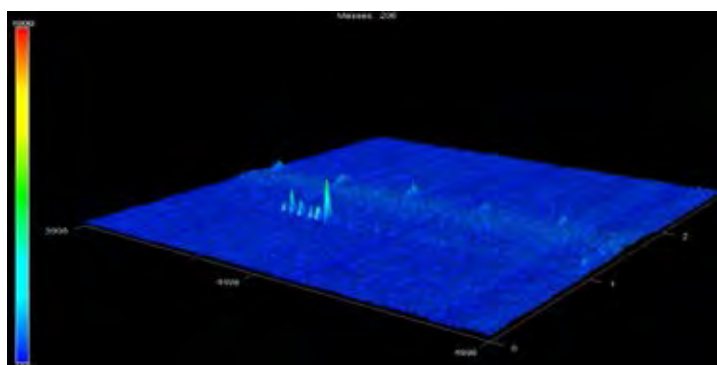


Figure C33 Target ion (m/z 192) surface plot of FLO.

Appendix D GCxGC-TOFMS Target Ion (m/z 206) Surface Plot Result**Figure D1** Target ion (m/z 206) surface plot of CO1.**Figure D2** Target ion (m/z 206) surface plot of WCO1-D3.**Figure D3** Target ion (m/z 206) surface plot of WCO1-D45.

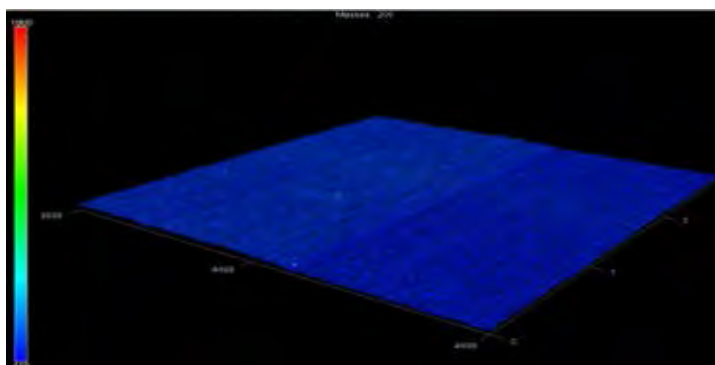


Figure D4 Target ion (m/z 206) surface plot of WCO1-D90.

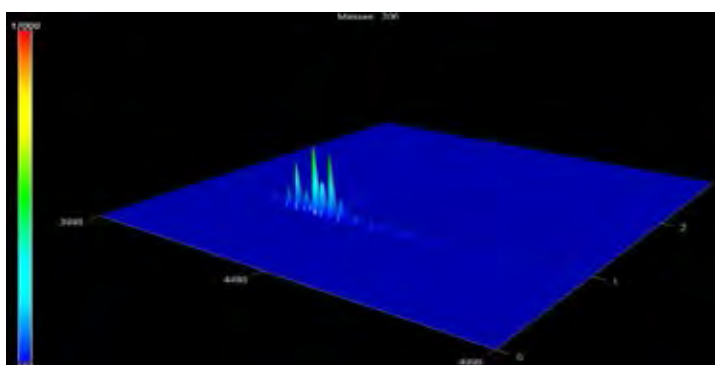


Figure D5 Target ion (m/z 206) surface plot of CO2.

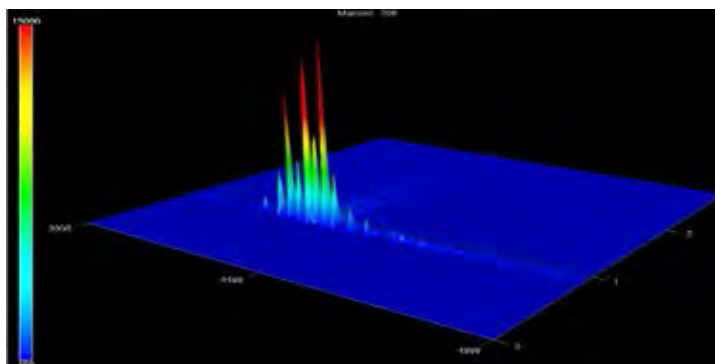


Figure D6 Target ion (m/z 206) surface plot of WCO2-D3.

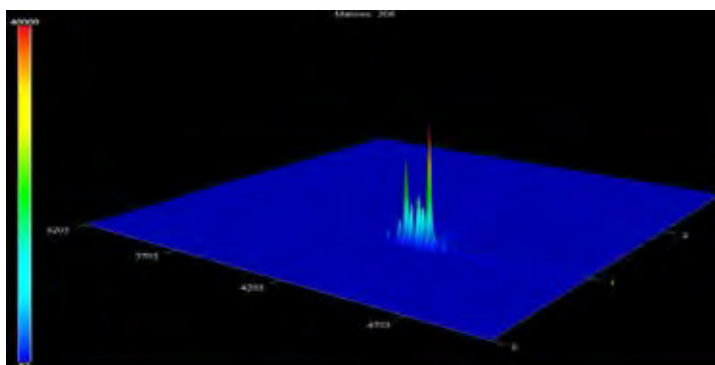


Figure D7 Target ion (m/z 206) surface plot of WCO2-D45.

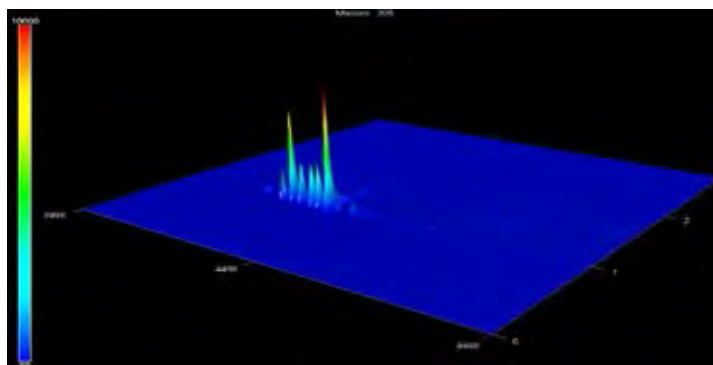


Figure D8 Target ion (m/z 206) surface plot of WCO2-D90.

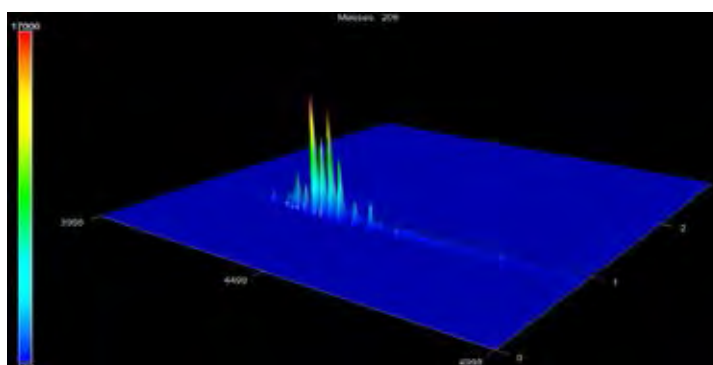


Figure D9 Target ion (m/z 206) surface plot of CO3.

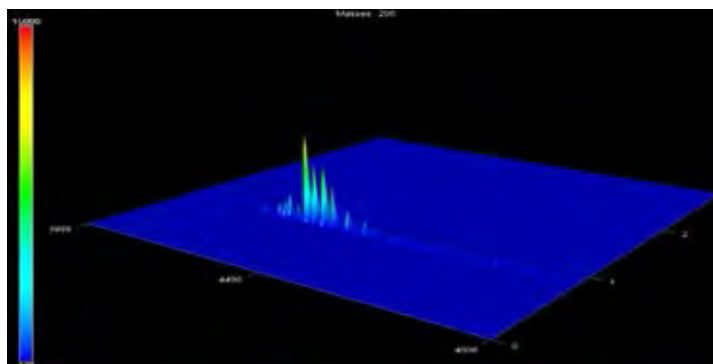


Figure D10 Target ion (m/z 206) surface plot of WCO3-D3.

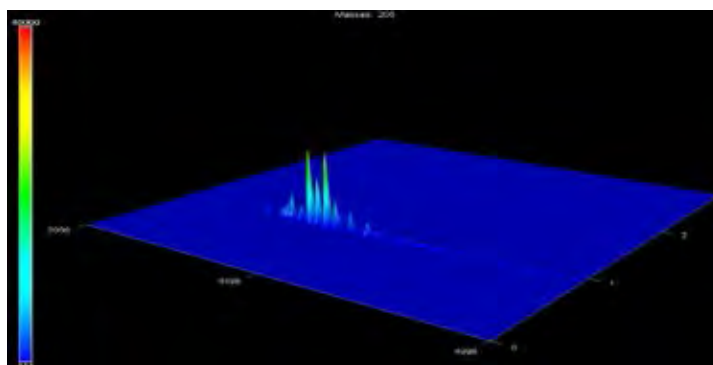


Figure D11 Target ion (m/z 206) surface plot of WCO3-D45.

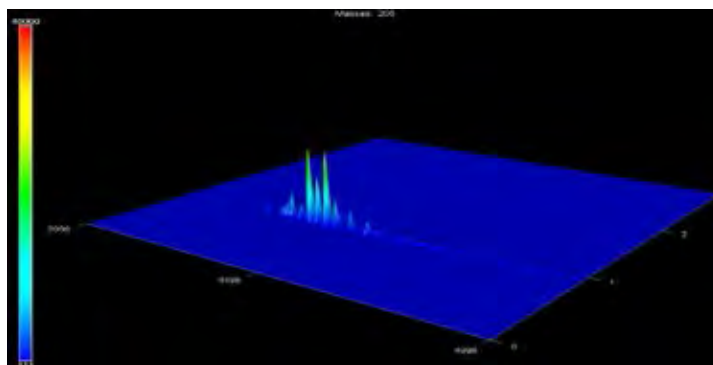


Figure D12 Target ion (m/z 206) surface plot of WCO3-D90.

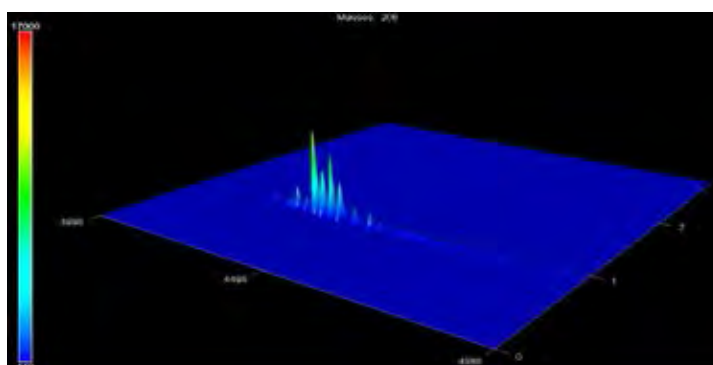


Figure D13 Target ion (m/z 206) surface plot of CO4.

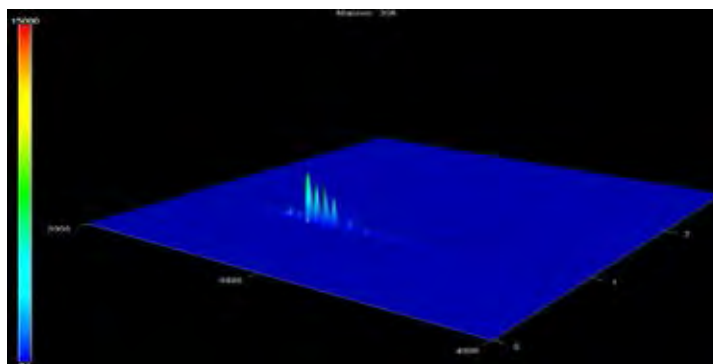


Figure D14 Target ion (m/z 206) surface plot of WCO4-D3.

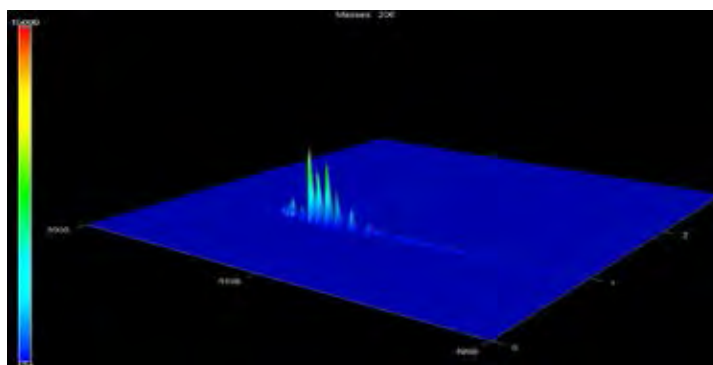


Figure D15 Target ion (m/z 206) surface plot of WCO4-D45.

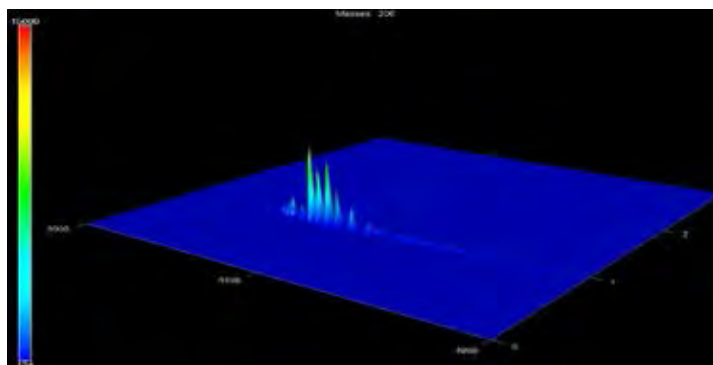


Figure D16 Target ion (m/z 206) surface plot of WCO4-D90.

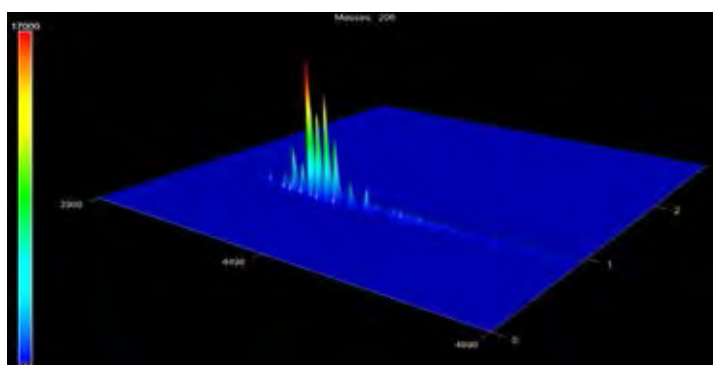


Figure D17 Target ion (m/z 206) surface plot of CO5.

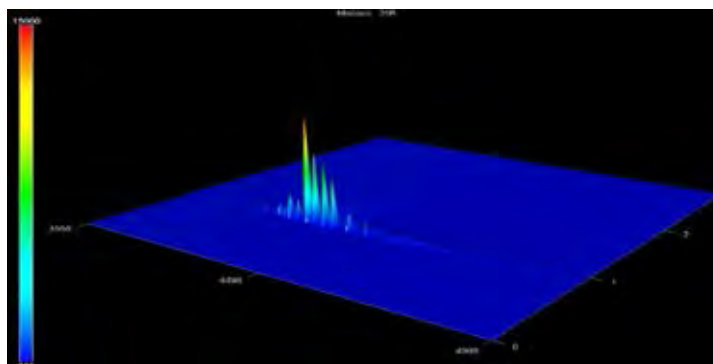


Figure D18 Target ion (m/z 206) surface plot of WCO5-D3.

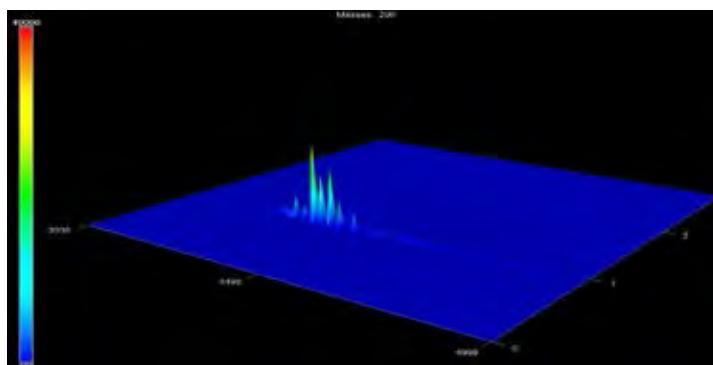


Figure D19 Target ion (m/z 206) surface plot of WCO5-D45.

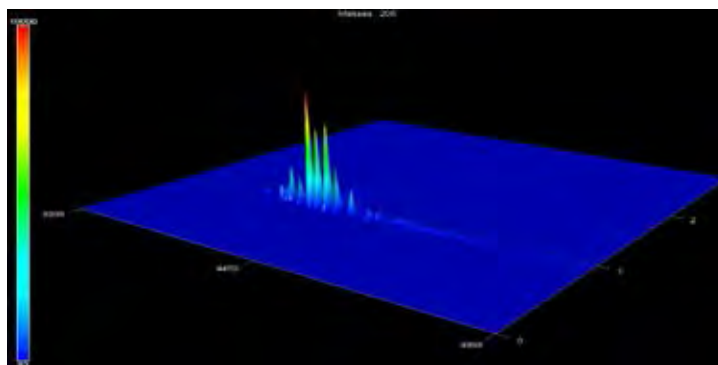


Figure D20 Target ion (m/z 206) surface plot of WCO5-D90.

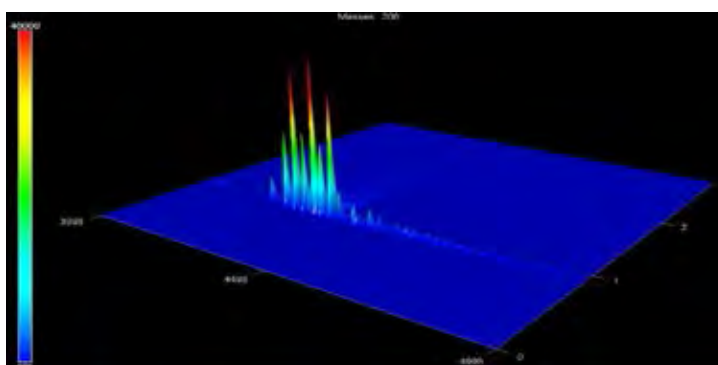


Figure D21 Target ion (m/z 206) surface plot of FO1.

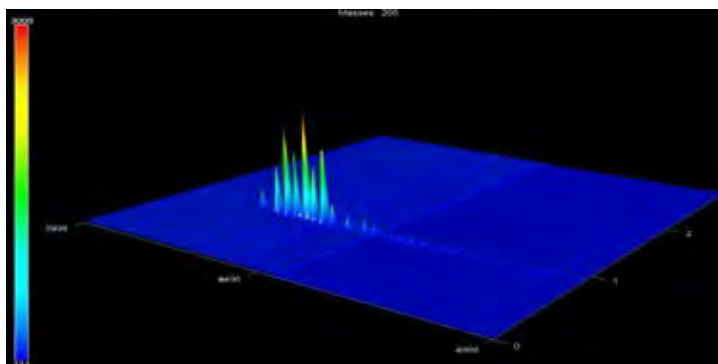


Figure D22 Target ion (m/z 206) surface plot of WFO1-D3.

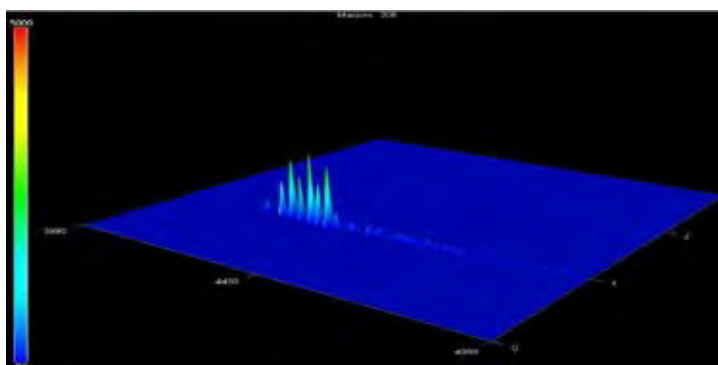


Figure D23 Target ion (m/z 206) surface plot of WFO1-D45.

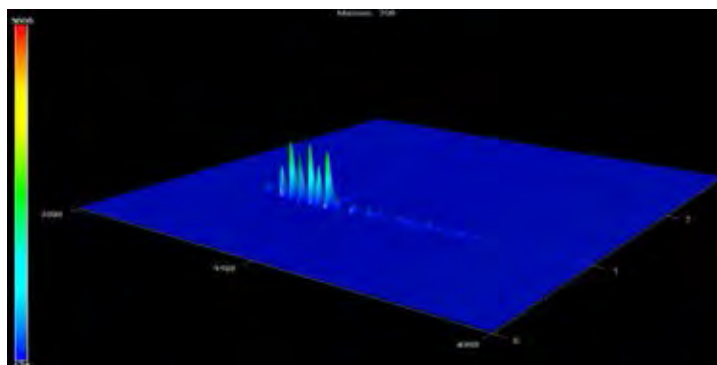


Figure D24 Target ion (m/z 206) surface plot of WFO1-D90.

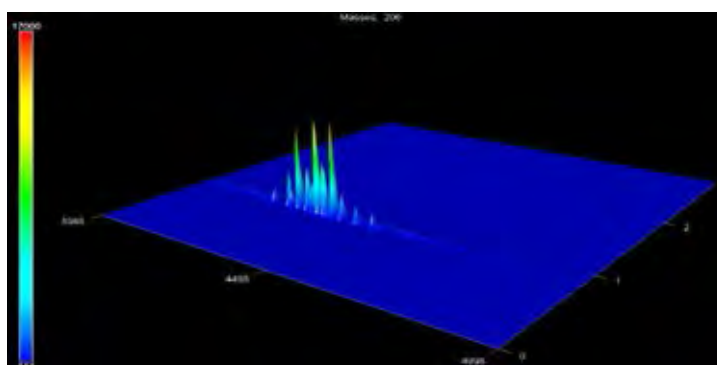


Figure D25 Target ion (m/z 206) surface plot of FO2.

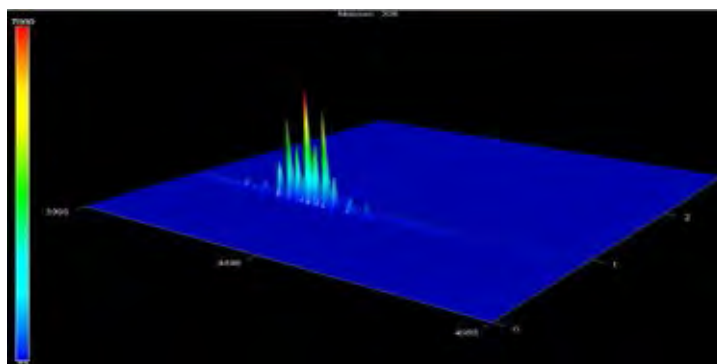


Figure D26 Target ion (m/z 206) surface plot of WFO2-D3.

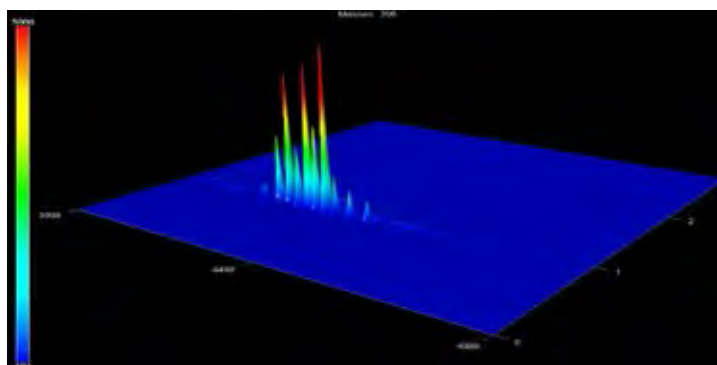


Figure D27 Target ion (m/z 206) surface plot of WFO2-D45.

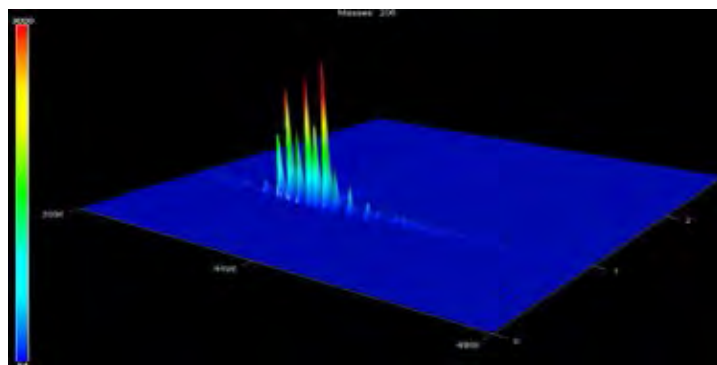


Figure D28 Target ion (m/z 206) surface plot of WFO2-D90.

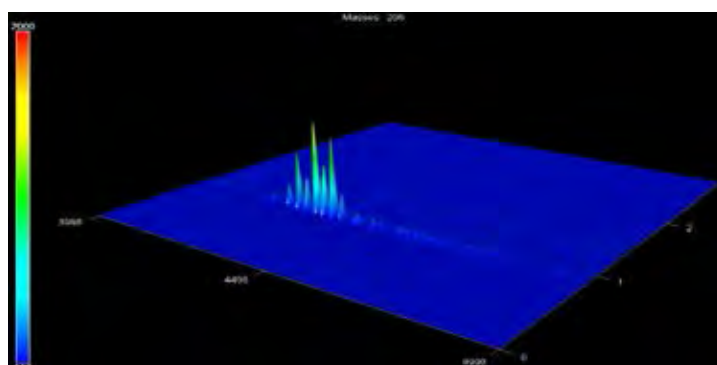


Figure D29 Target ion (m/z 206) surface plot of ULO.

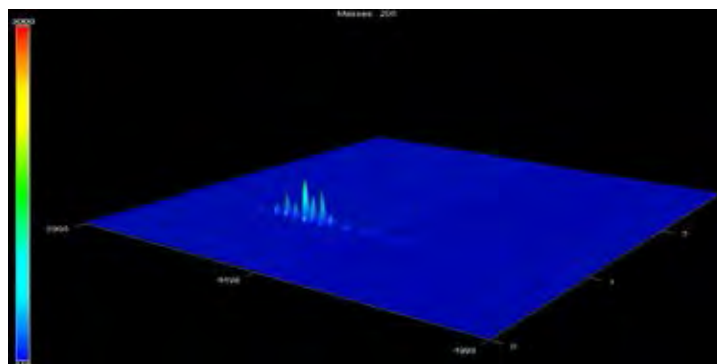


Figure D30 Target ion (m/z 206) surface plot of WULO-D3.

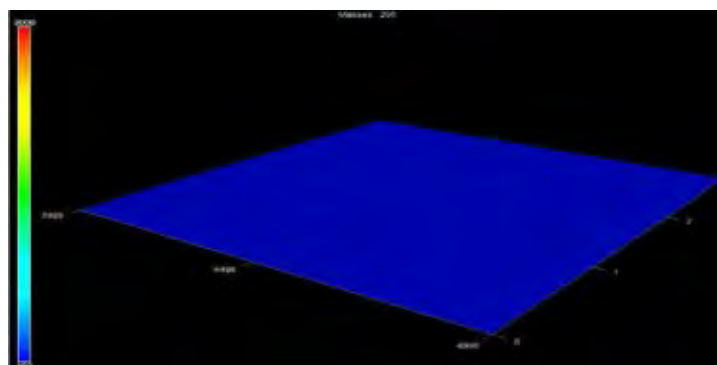


Figure D31 Target ion (m/z 206) surface plot of WULO-D45.

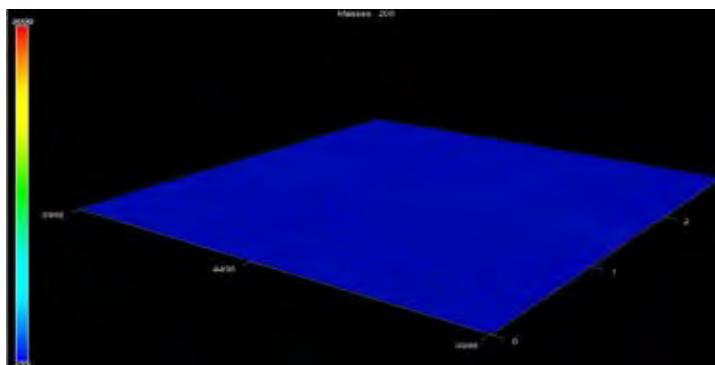


Figure D32 Target ion (m/z 206) surface plot of WULO-90.

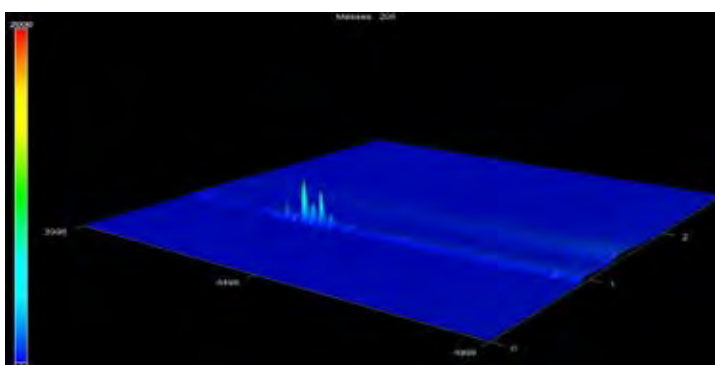
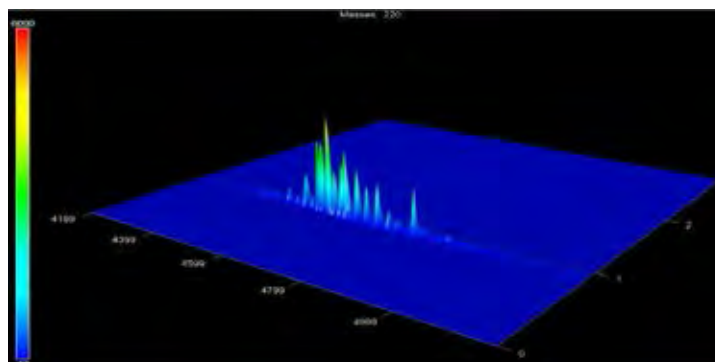
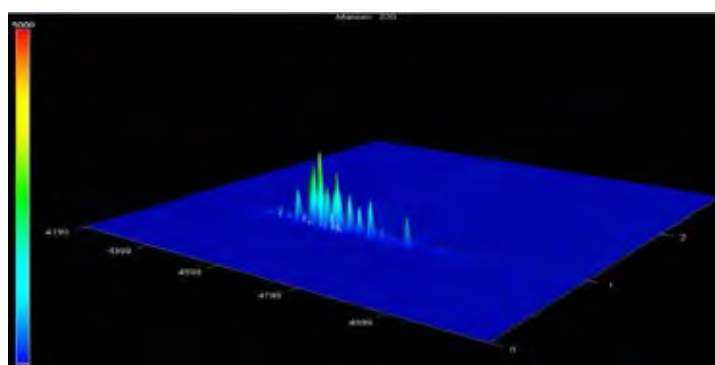
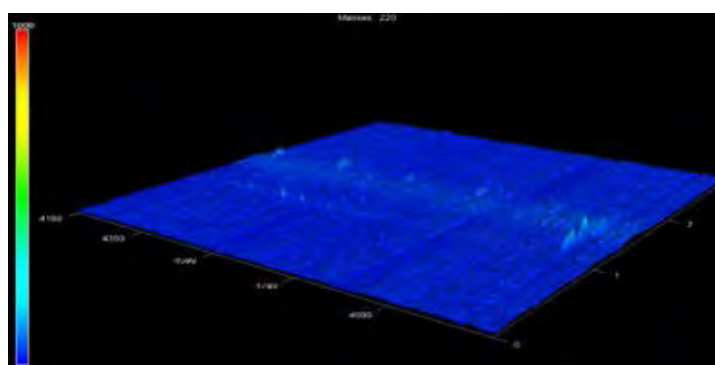


Figure D33 Target ion (m/z 206) surface plot of FLO.

Appendix E GCxGC-TOFMS Target Ion (m/z 220) Surface Plot Result**Figure E1** Target ion (m/z 220) surface plot of CO1.**Figure E2** Target ion (m/z 220) surface plot of WCO1-D3.**Figure E3** Target ion (m/z 220) surface plot of WCO1-D45.

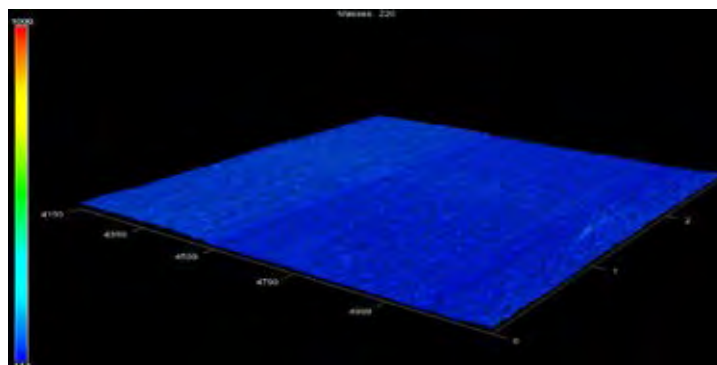


Figure E4 Target ion (m/z 220) surface plot of WCO1-D90.

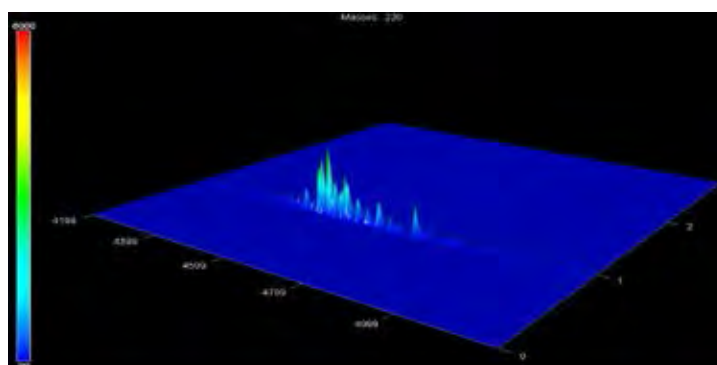


Figure E5 Target ion (m/z 220) surface plot of CO2.

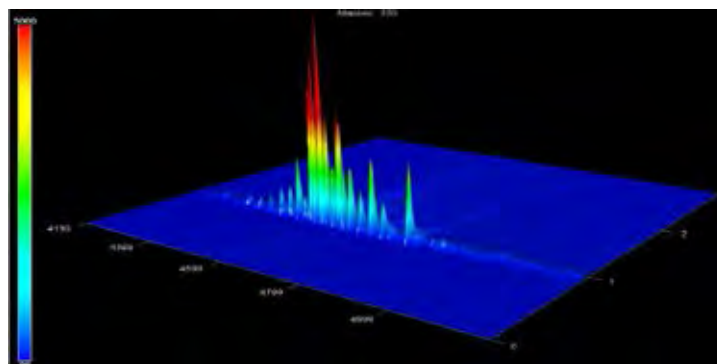


Figure E6 Target ion (m/z 220) surface plot of WCO2-D3.

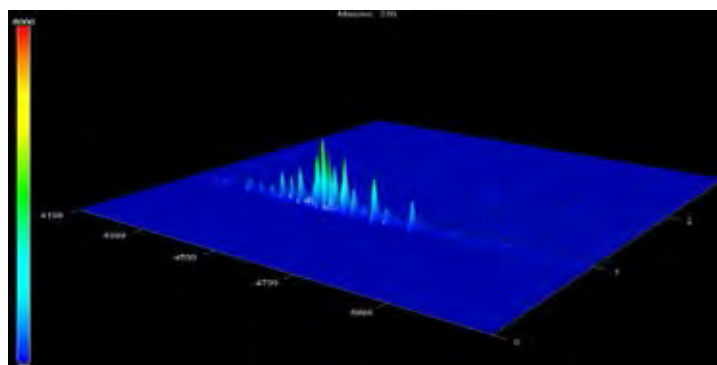


Figure E7 Target ion (m/z 220) surface plot of WCO2-D45.

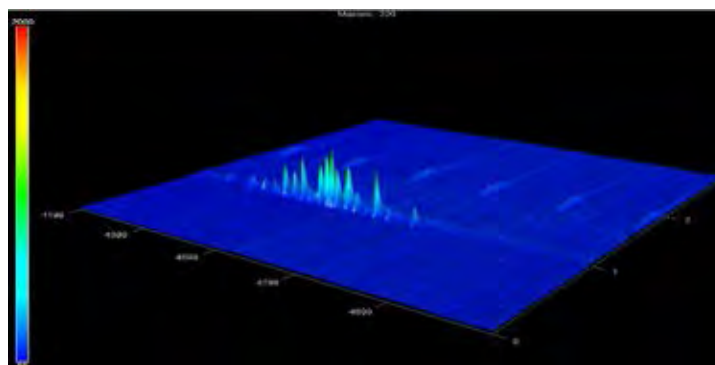


Figure E8 Target ion (m/z 220) surface plot of WCO2-D90.

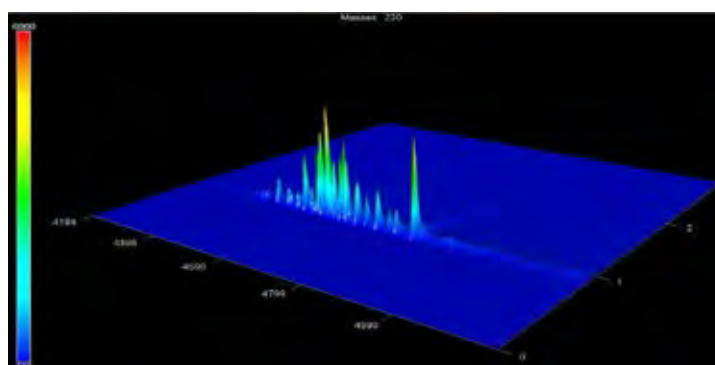


Figure E9 Target ion (m/z 220) surface plot of CO3.

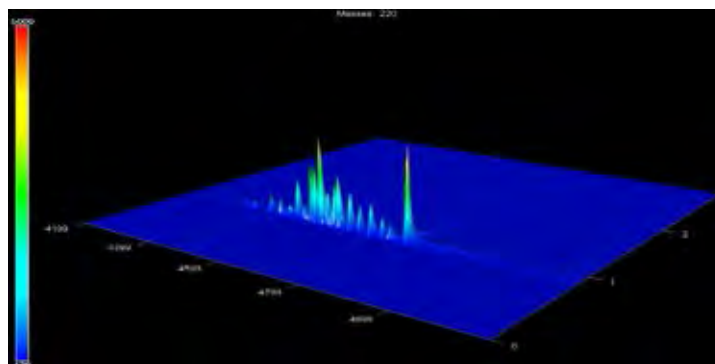


Figure E10 Target ion (m/z 220) surface plot of WCO3-D3.

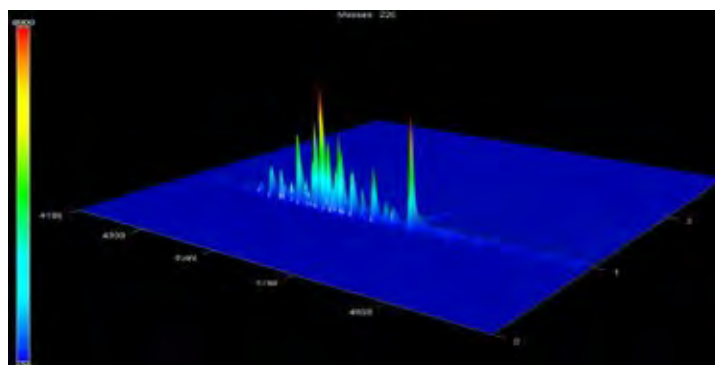


Figure E11 Target ion (m/z 220) surface plot of WCO3-D45.

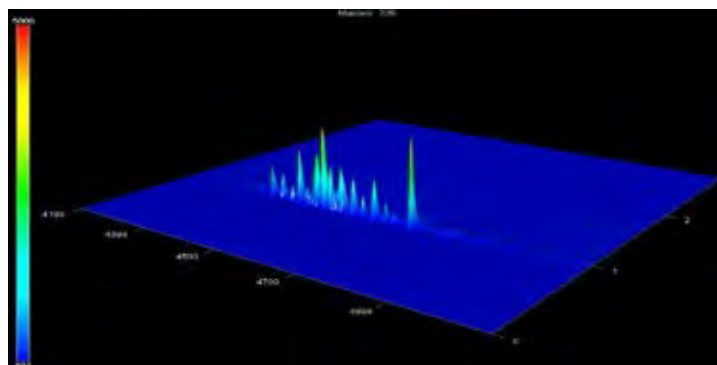


Figure E12 Target ion (m/z 220) surface plot of WCO3-D90.

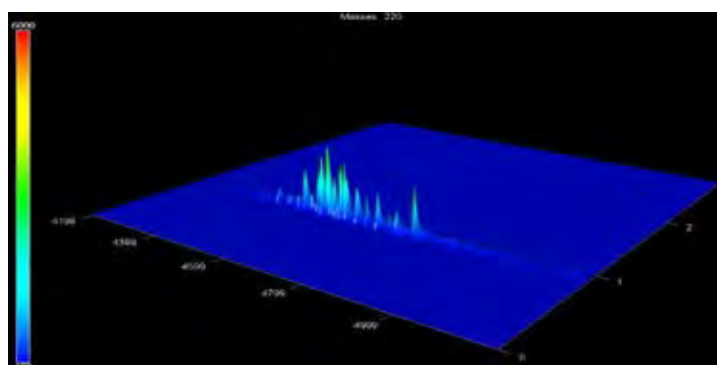


Figure E13 Target ion (m/z 220) surface plot of CO4.

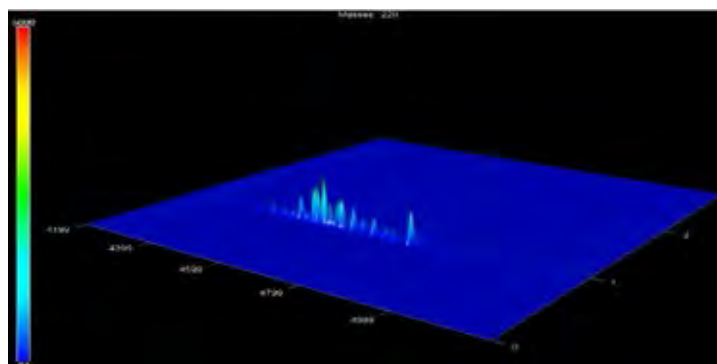


Figure E14 Target ion (m/z 220) surface plot of WCO4-D3.

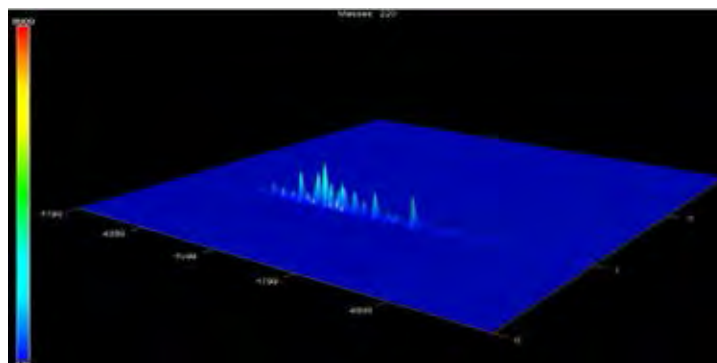


Figure E15 Target ion (m/z 220) surface plot of WCO4-D45.

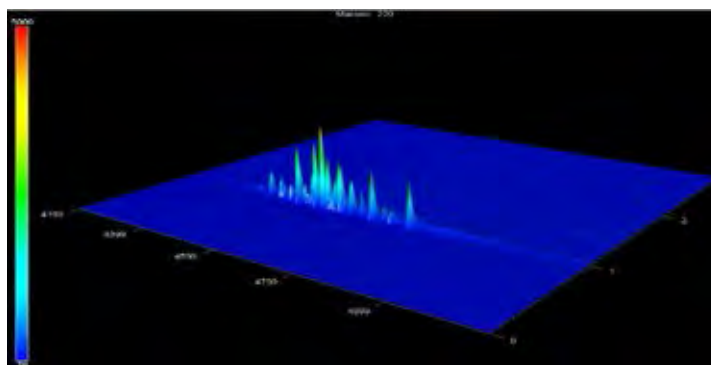


Figure E16 Target ion (m/z 220) surface plot of WCO4-D90.

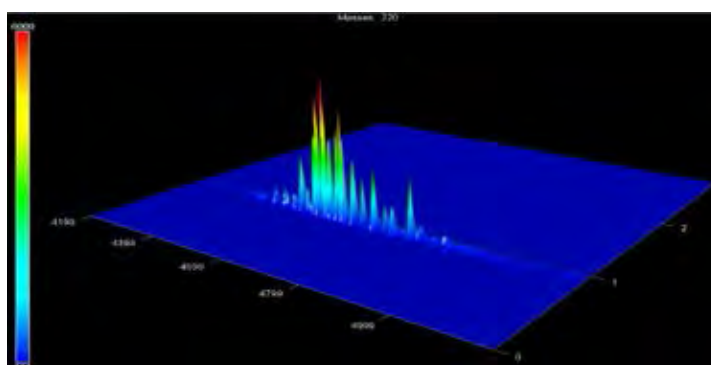


Figure E17 Target ion (m/z 220) surface plot of CO5.

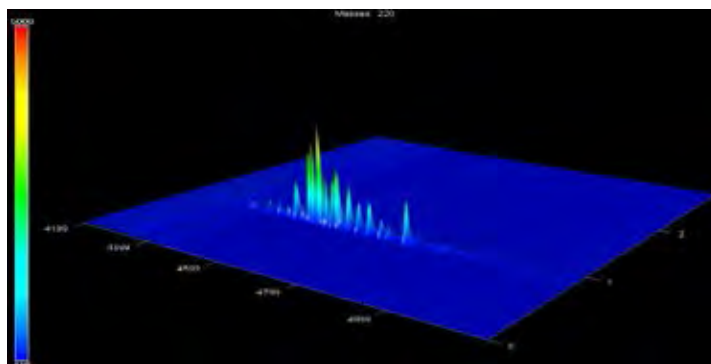


Figure E18 Target ion (m/z 220) surface plot of WCO5-D3.

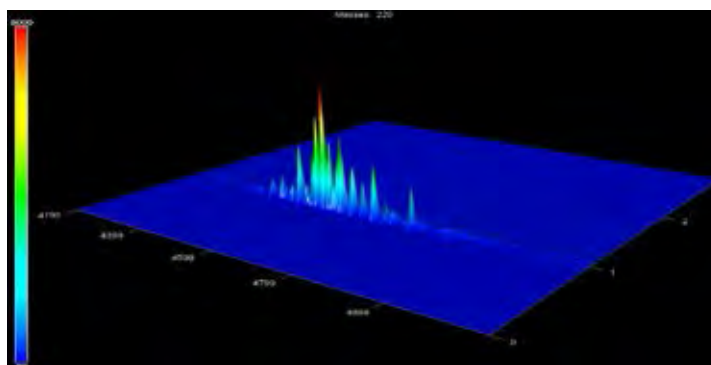


Figure E19 Target ion (m/z 220) surface plot of WCO5-D45.

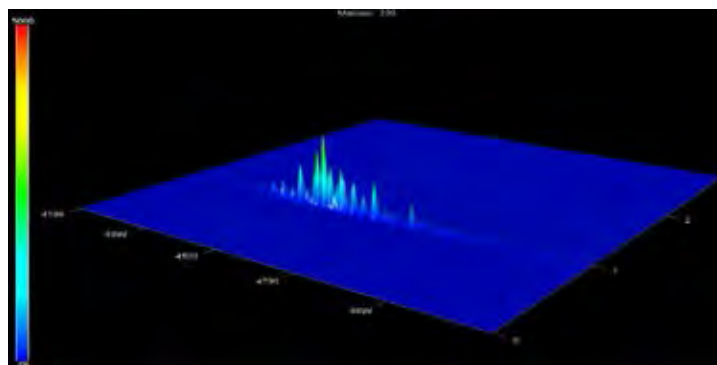


Figure E20 Target ion (m/z 220) surface plot of WCO5-D90.

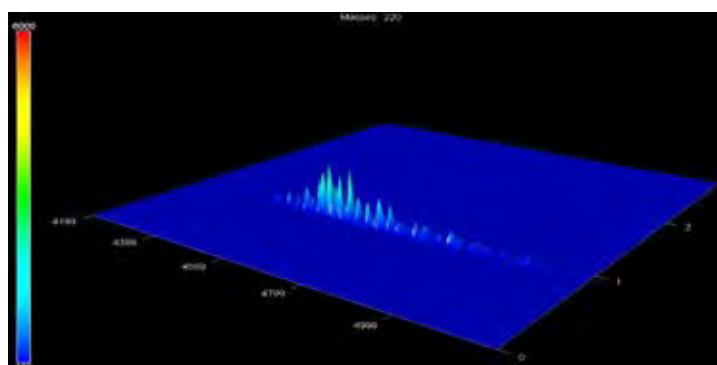


Figure E21 Target ion (m/z 220) surface plot of FO1.

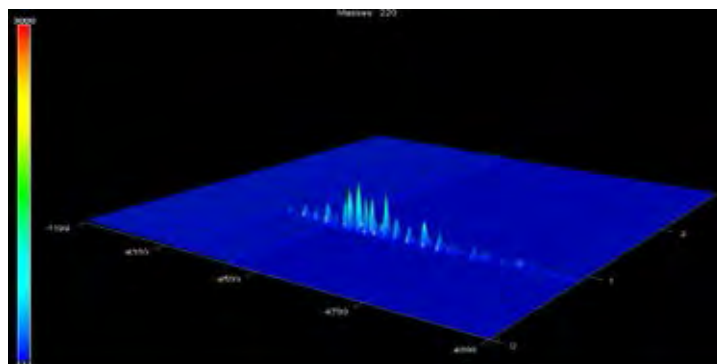


Figure E22 Target ion (m/z 220) surface plot of WFO1-D3.

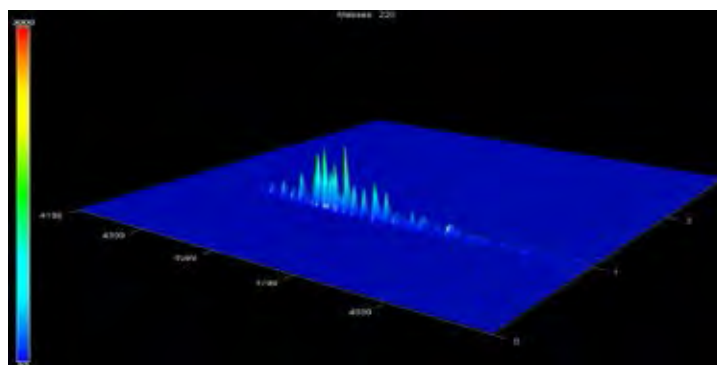


Figure E23 Target ion (m/z 220) surface plot of WFO1-D45.

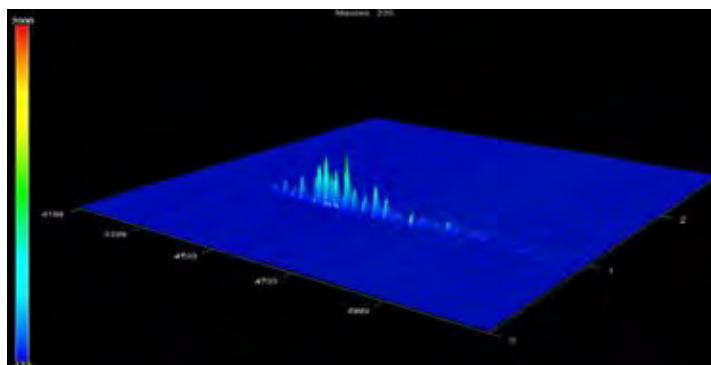


Figure E24 Target ion (m/z 220) surface plot of WFO1-D90.

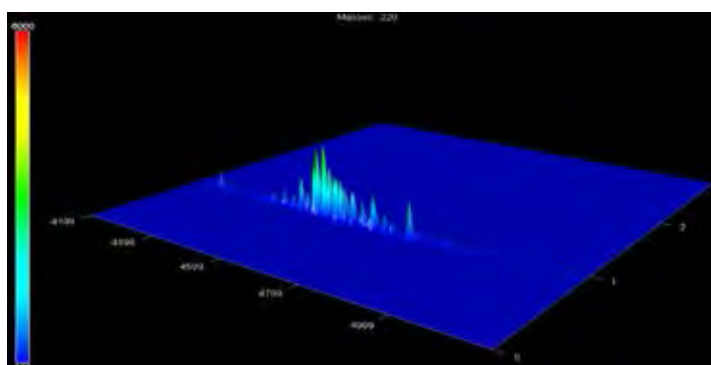


Figure E25 Target ion (m/z 220) surface plot of FO2.

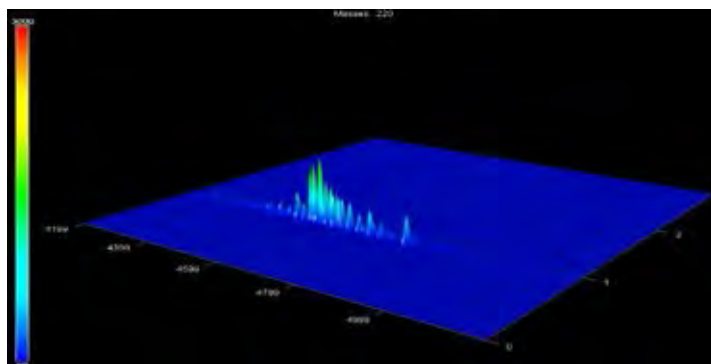


Figure E26 Target ion (m/z 220) surface plot of WFO2-D3.

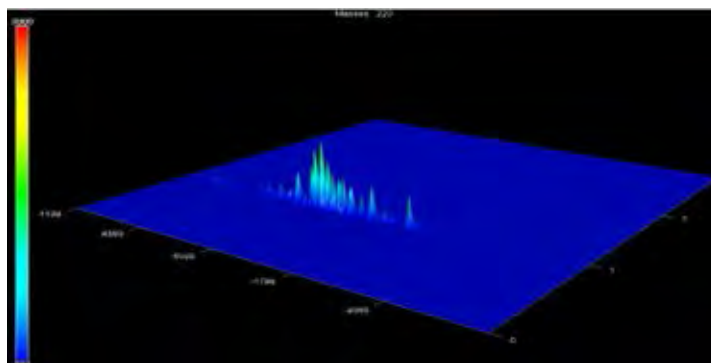


Figure E27 Target ion (m/z 220) surface plot of WFO2-D45.

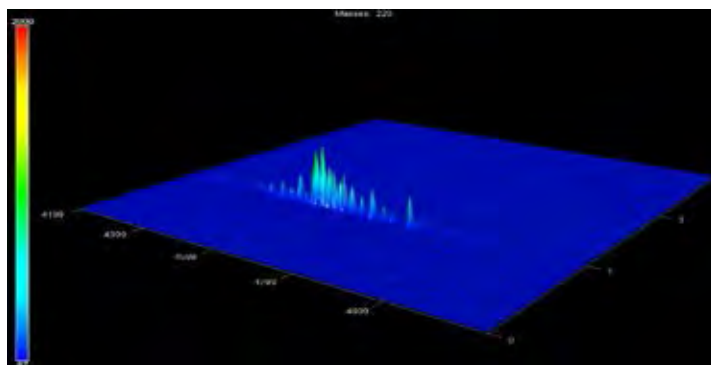


Figure E28 Target ion (m/z 220) surface plot of WFO2-D90.

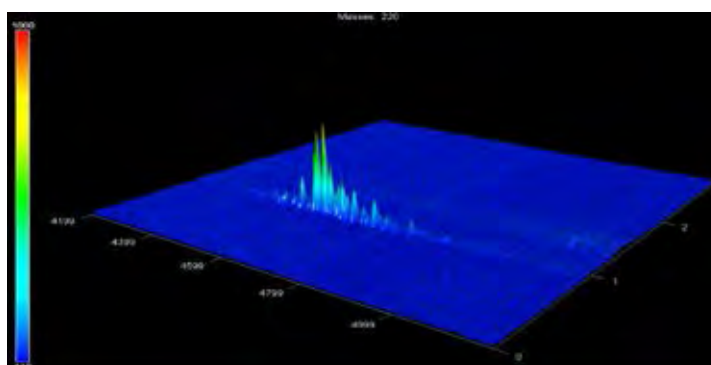


Figure E29 Target ion (m/z 220) surface plot of ULO.

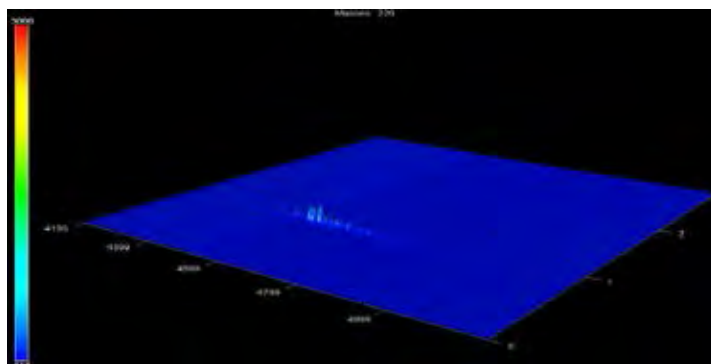


Figure E30 Target ion (m/z 220) surface plot of ULO-D3.

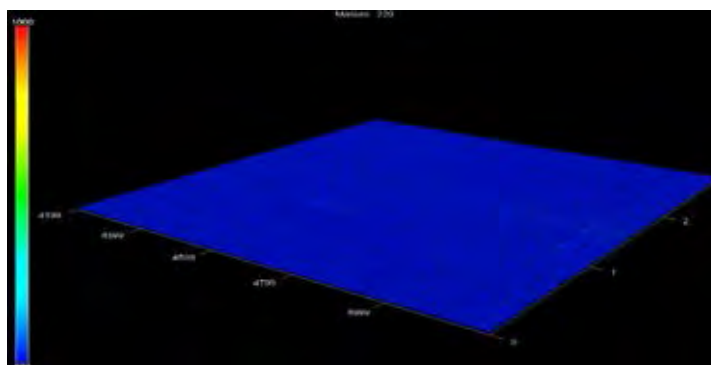


Figure E31 Target ion (m/z 220) surface plot of ULO-D45.

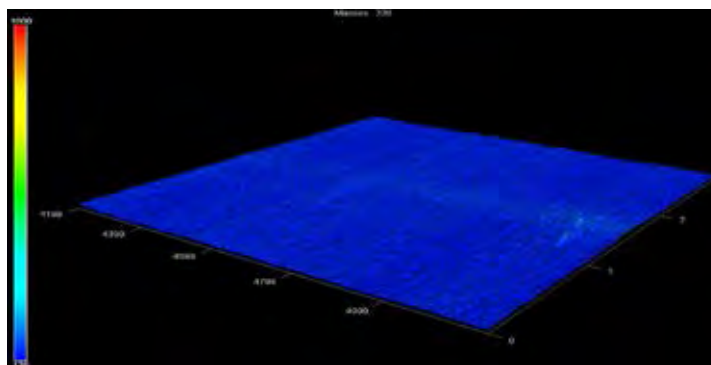


Figure E32 Target ion (m/z 220) surface plot of ULO-D90.

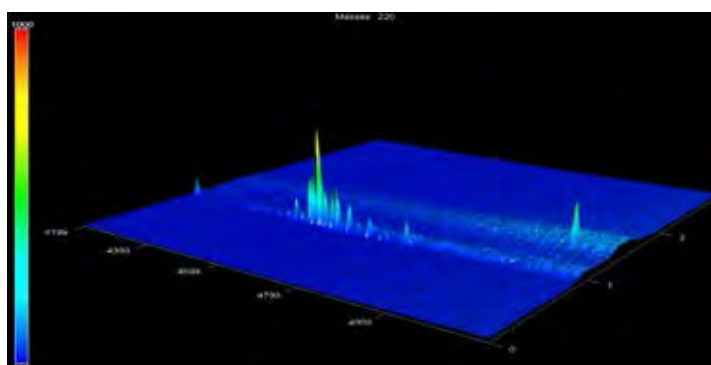
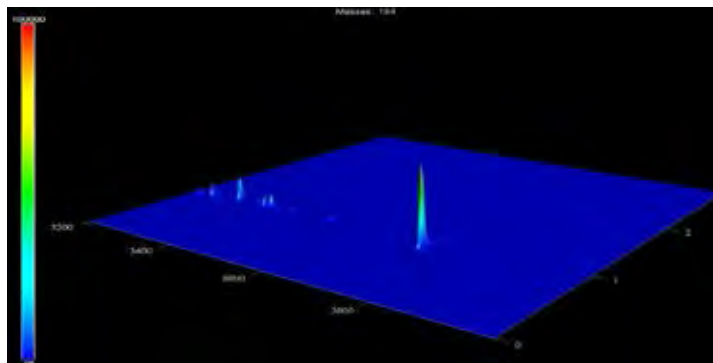
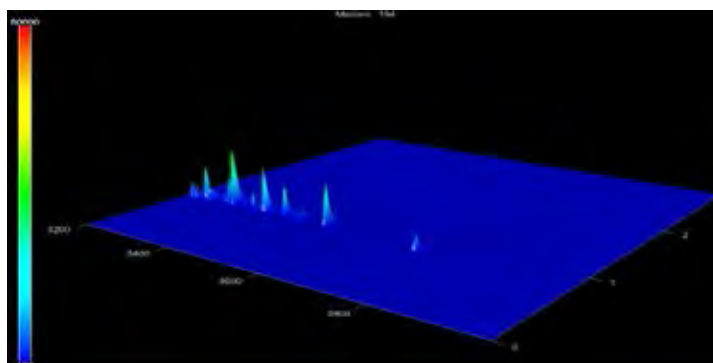
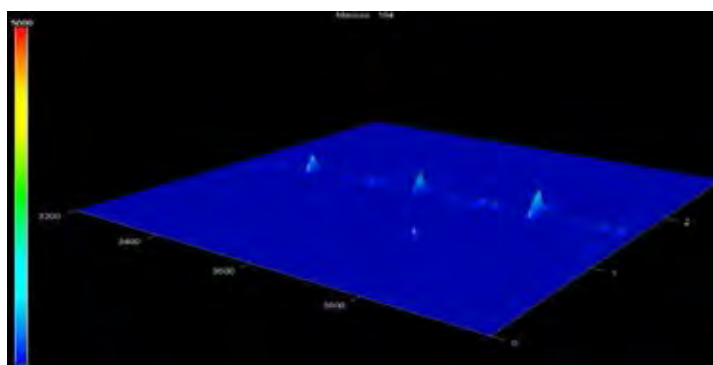


Figure E33 Target ion (m/z 220) surface plot of FLO.

Appendix F GCxGC-TOFMS Target Ion (m/z 184) Surface Plot Result**Figure F1** Target ion (m/z 184) surface plot of CO1.**Figure F2** Target ion (m/z 184) surface plot of WCO1-D3.**Figure F3** Target ion (m/z 184) surface plot of WCO1-D45.

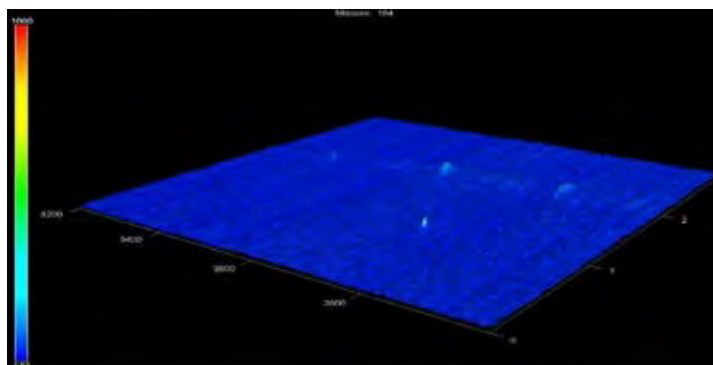


Figure F4 Target ion (m/z 184) surface plot of WCO1-90.

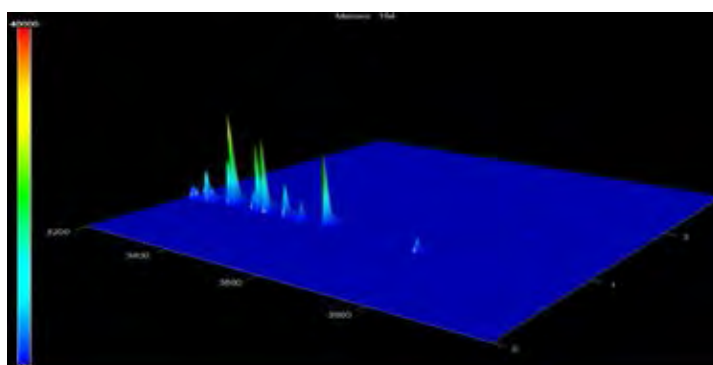


Figure F5 Target ion (m/z 184) surface plot of CO2.

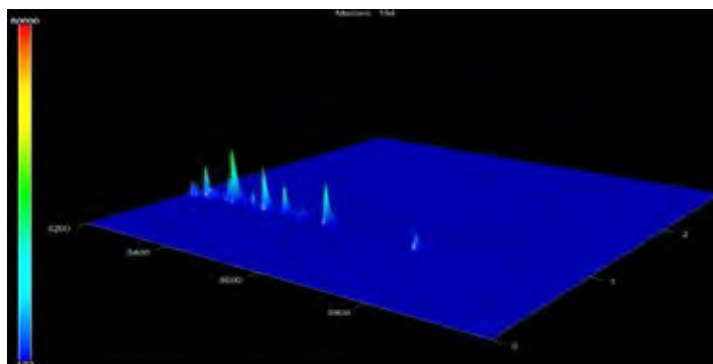


Figure F6 Target ion (m/z 184) surface plot of WCO2-D3.

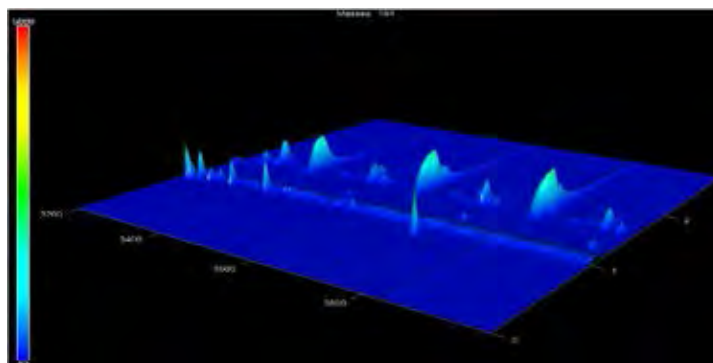


Figure F7 Target ion (m/z 184) surface plot of WCO2-D45.

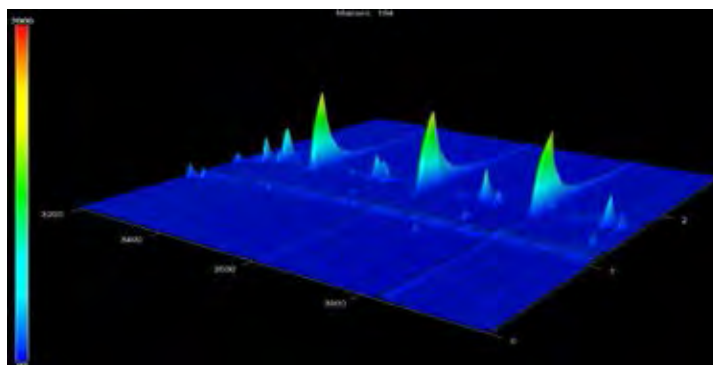


Figure F8 Target ion (m/z 184) surface plot of WCO2-90.

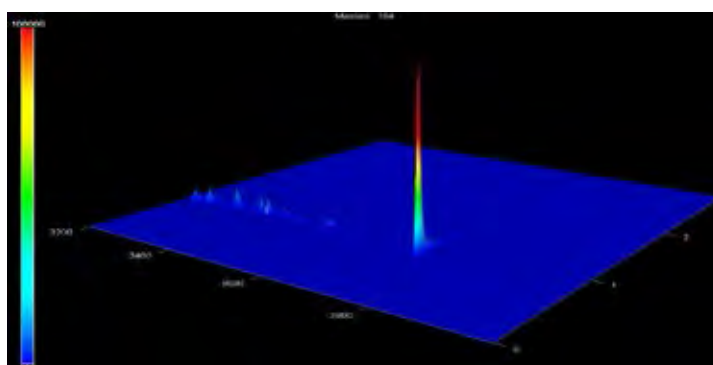


Figure F9 Target ion (m/z 184) surface plot of CO3.

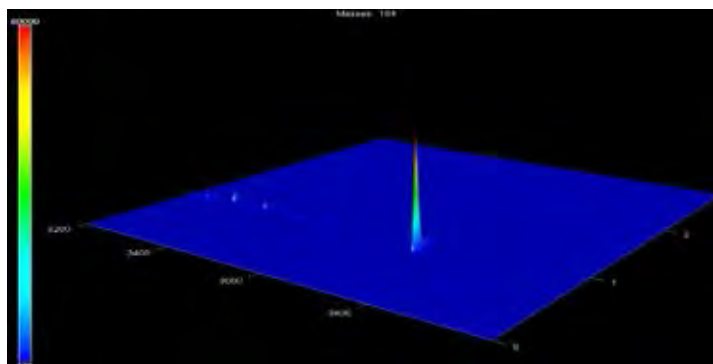


Figure F10 Target ion (m/z 184) surface plot of WCO3-D3.

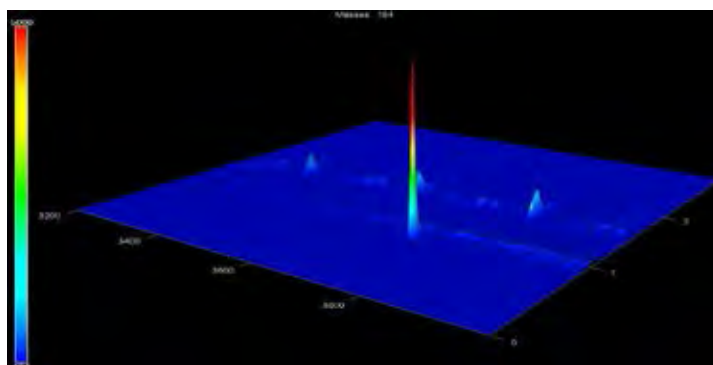


Figure F11 Target ion (m/z 184) surface plot of WCO3-D45.

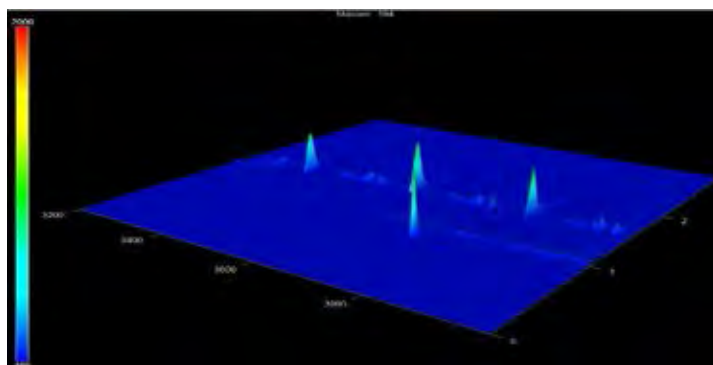


Figure F12 Target ion (m/z 184) surface plot of WCO3-90.

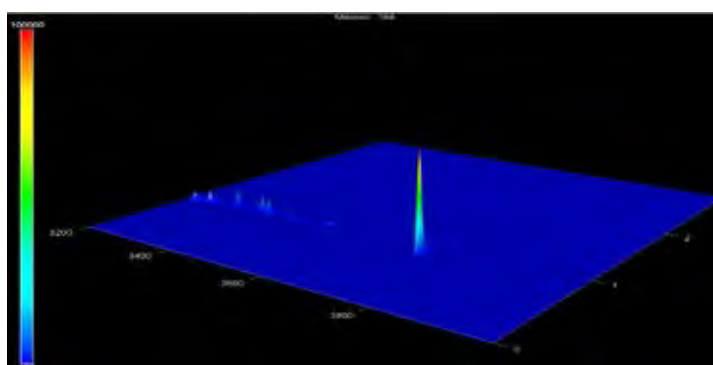


Figure F13 Target ion (m/z 184) surface plot of CO4.

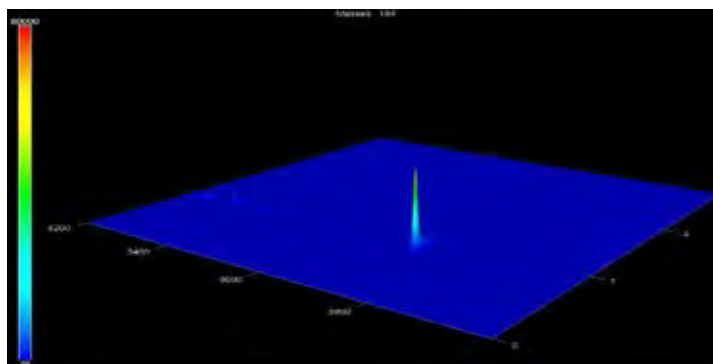


Figure F14 Target ion (m/z 184) surface plot of WCO4-D3.

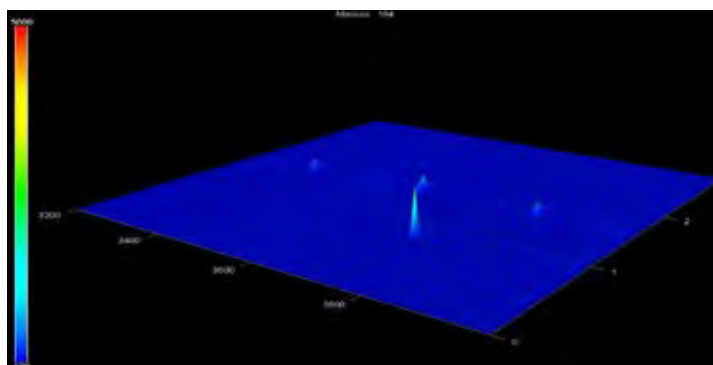


Figure F15 Target ion (m/z 184) surface plot of WCO4-D45.

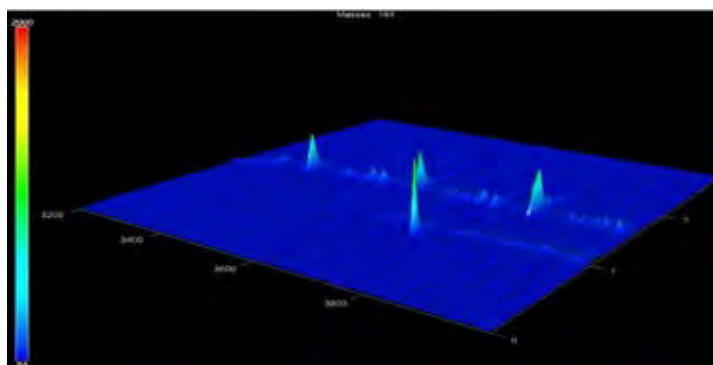


Figure F16 Target ion (m/z 184) surface plot of WCO4-90.

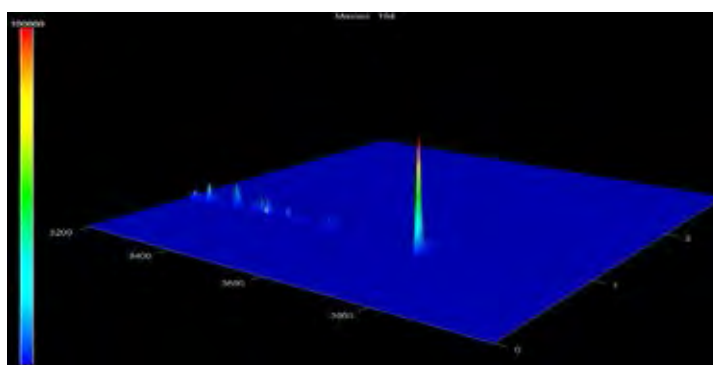


Figure F17 Target ion (m/z 184) surface plot of CO5.

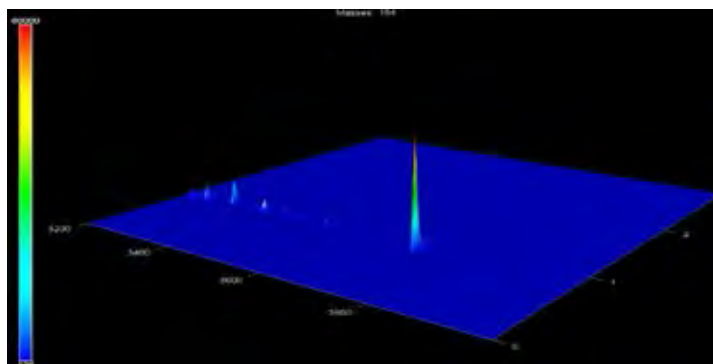


Figure F18 Target ion (m/z 184) surface plot of WCO5-D3.

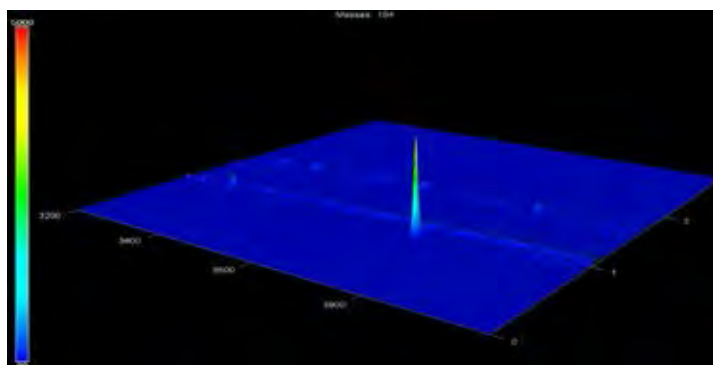


Figure F19 Target ion (m/z 184) surface plot of WCO5-D45.

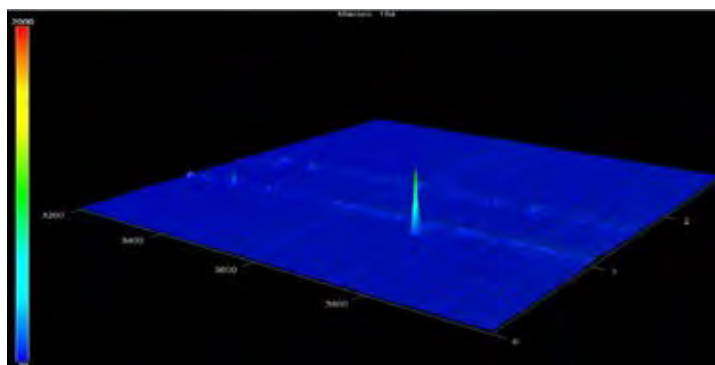


Figure F20 Target ion (m/z 184) surface plot of WCO5-90.

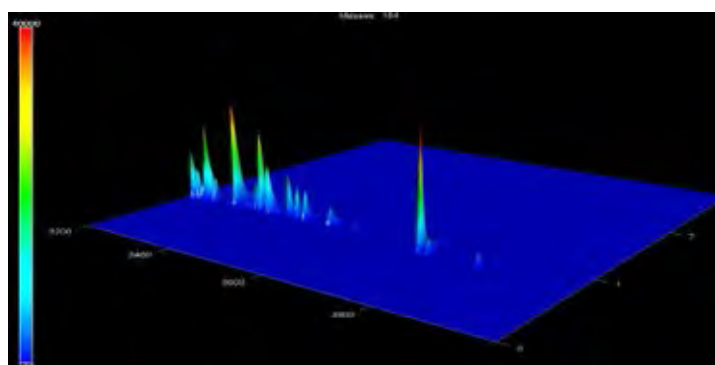


Figure F21 Target ion (m/z 184) surface plot of FO1.

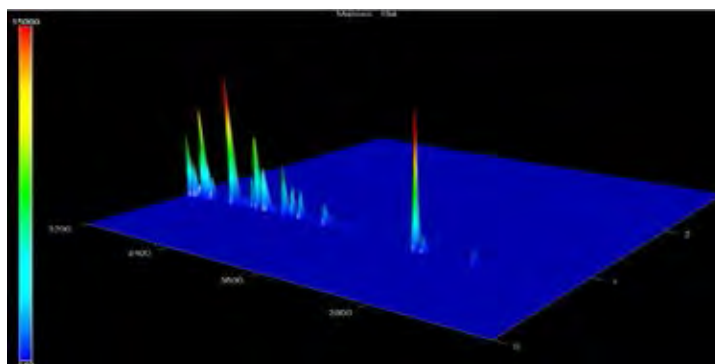


Figure F22 Target ion (m/z 184) surface plot of WFO1-D3.

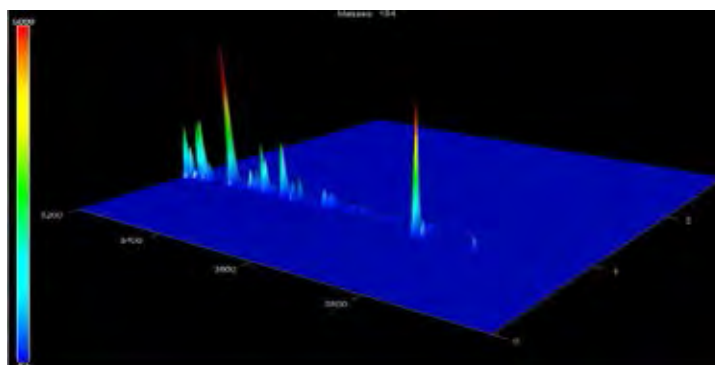


Figure F23 Target ion (m/z 184) surface plot of WFO1-D45.

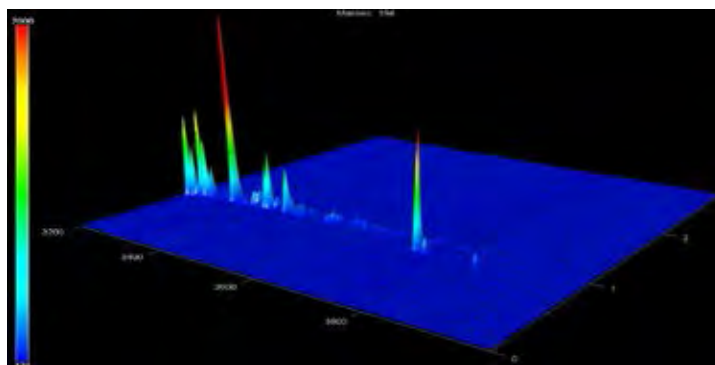


Figure F24 Target ion (m/z 184) surface plot of WFO1-90.

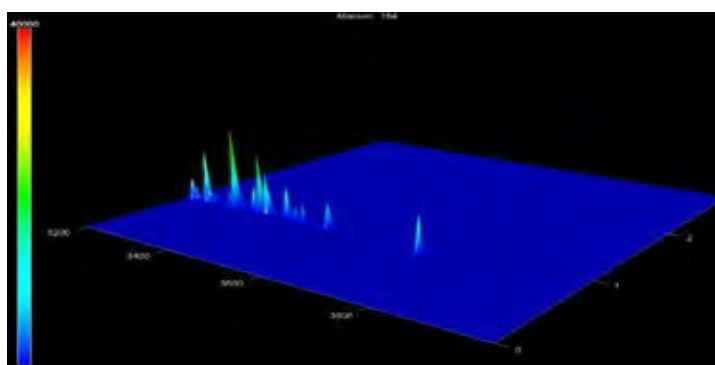


Figure F25 Target ion (m/z 184) surface plot of FO2.

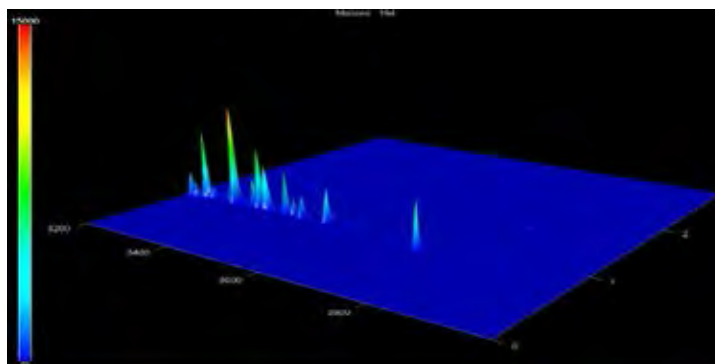


Figure F26 Target ion (m/z 184) surface plot of WFO2-D3.

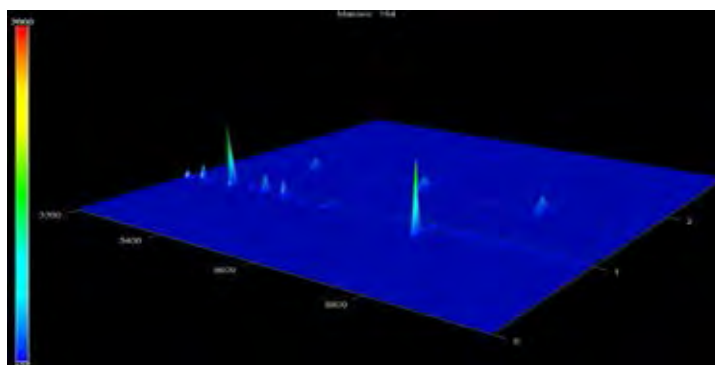


Figure F27 Target ion (m/z 184) surface plot of WFO2-D45.

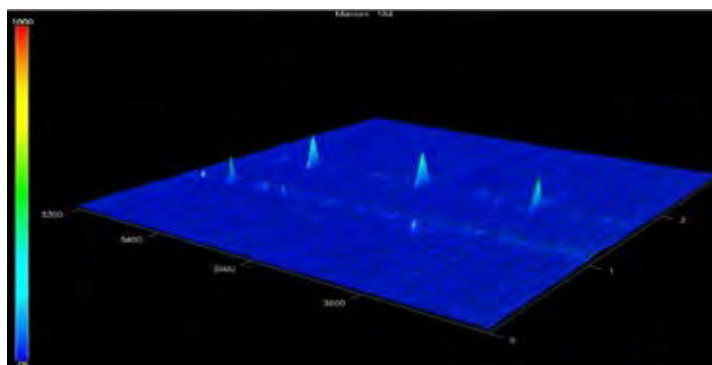


Figure F28 Target ion (m/z 184) surface plot of WFO2-90.

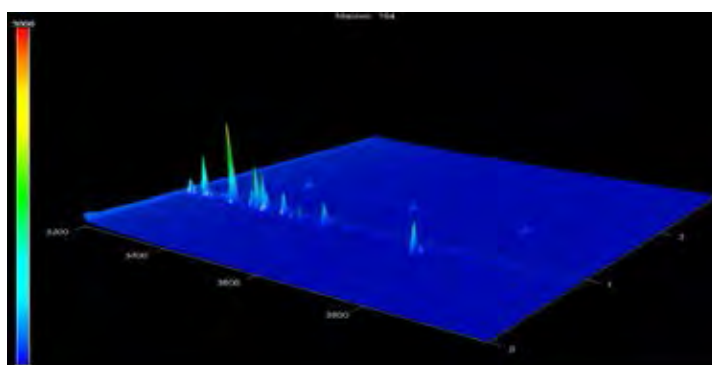


Figure F29 Target ion (m/z 184) surface plot of ULO.

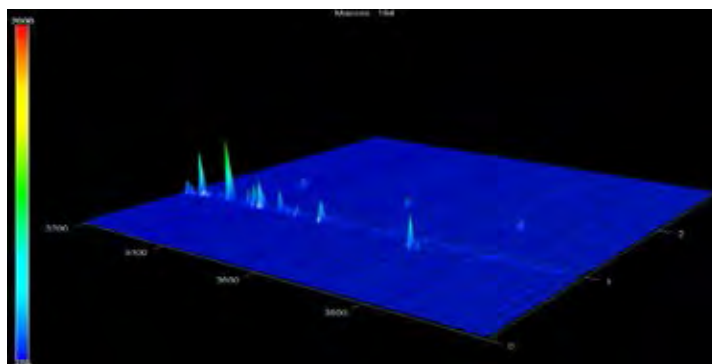


Figure F30 Target ion (m/z 184) surface plot of WULO-D3.

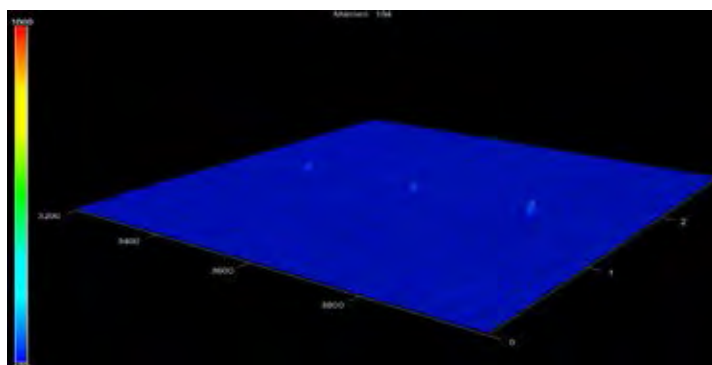


Figure F31 Target ion (m/z 184) surface plot of WULO-D45.

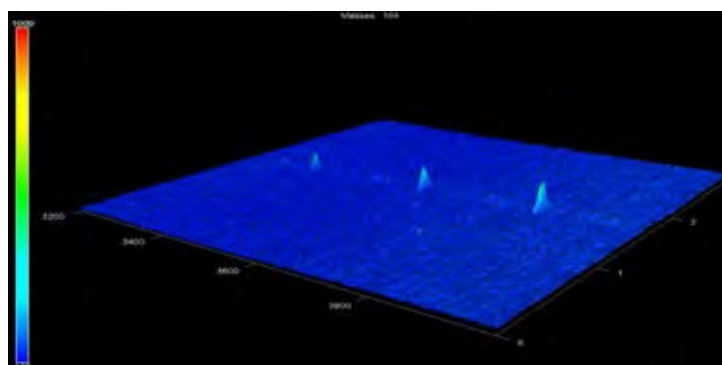


Figure F32 Target ion (m/z 184) surface plot of WULO-D90.

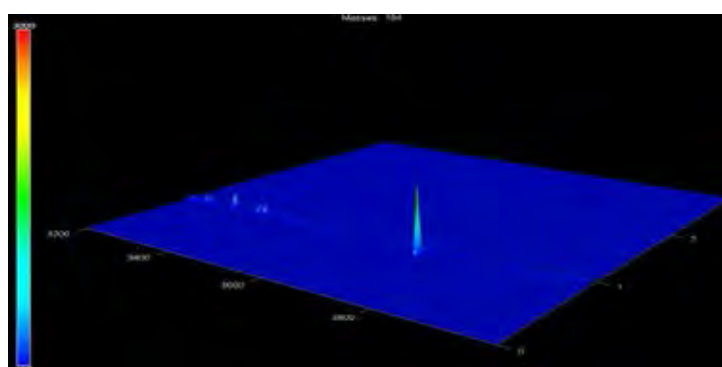
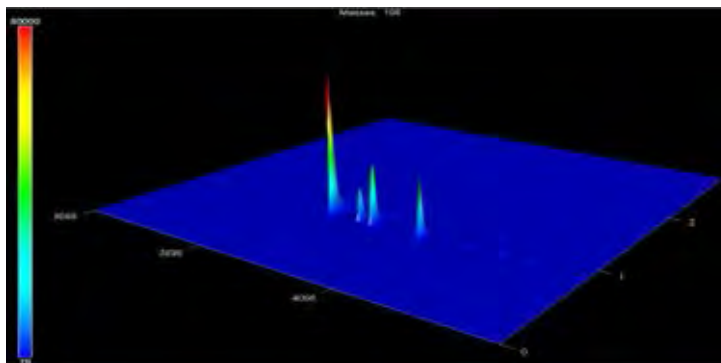
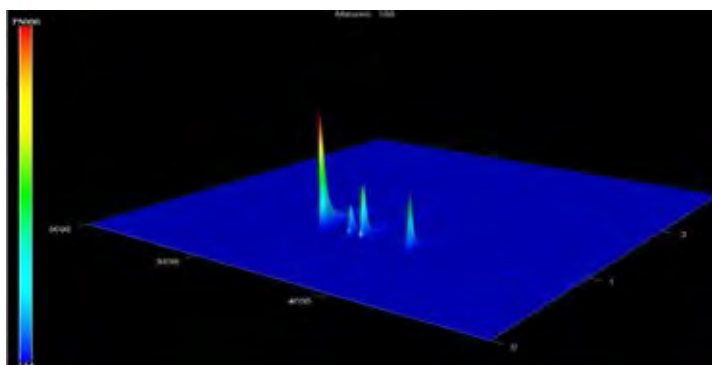
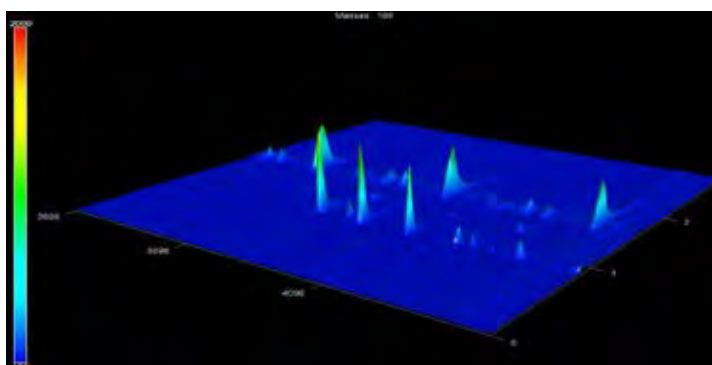


Figure F33 Target ion (m/z 184) surface plot of FLO.

Appendix G GCxGC-TOFMS Target Ion (m/z 198) Surface Plot Result**Figure G1** Target ion (m/z 198) surface plot of CO1.**Figure G2** Target ion (m/z 198) surface plot of WCO1-D3.**Figure G3** Target ion (m/z 198) surface plot of WCO1-D45.

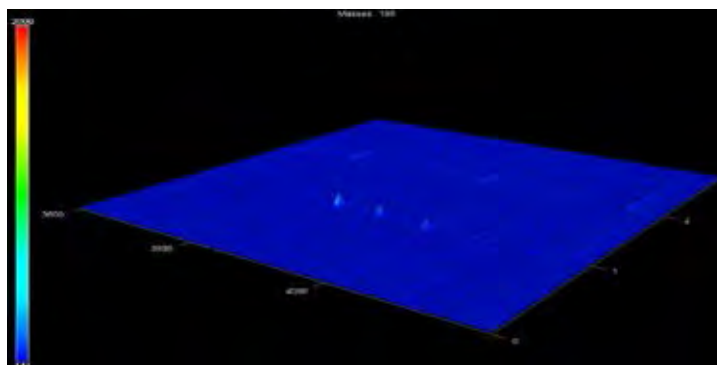


Figure G4 Target ion (m/z 198) surface plot of WCO1-D90.

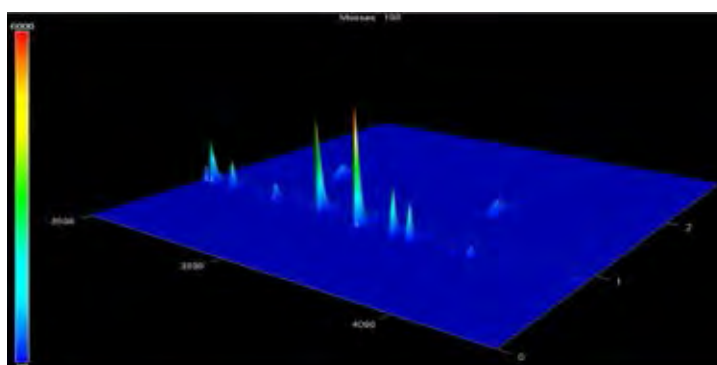


Figure G5 Target ion (m/z 198) surface plot of CO2.

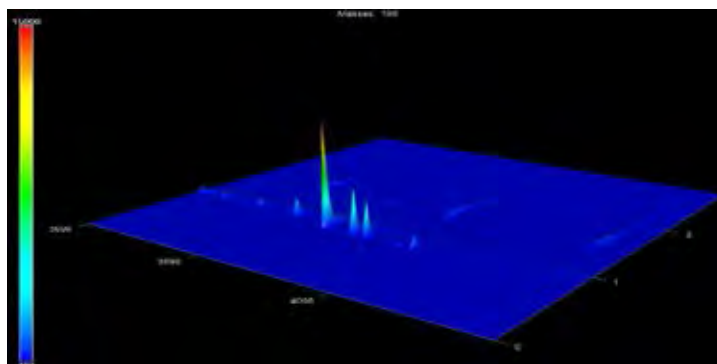


Figure G6 Target ion (m/z 198) surface plot of WCO2-D3.

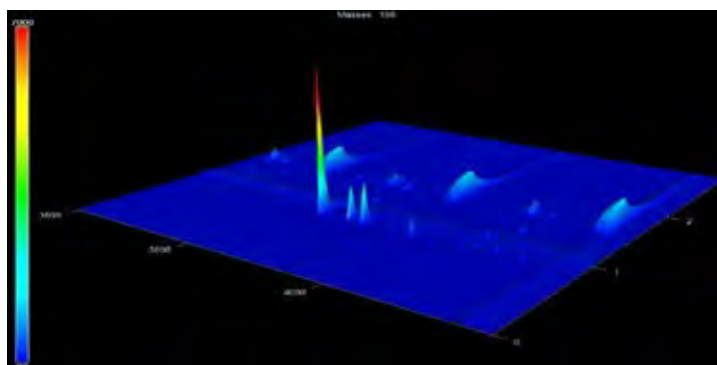


Figure G7 Target ion (m/z 198) surface plot of WCO2-D45.

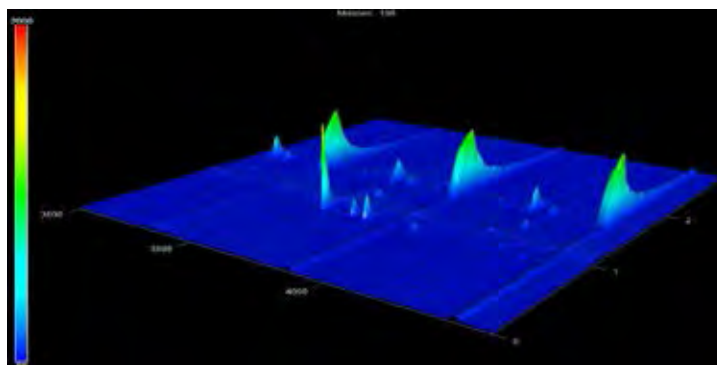


Figure G8 Target ion (m/z 198) surface plot of WCO2-D90.

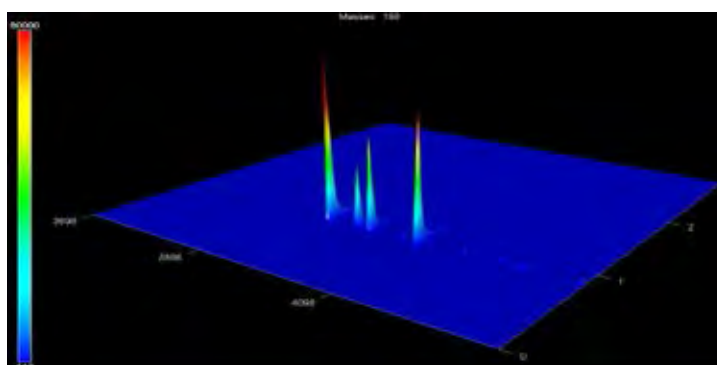


Figure G9 Target ion (m/z 198) surface plot of CO3.

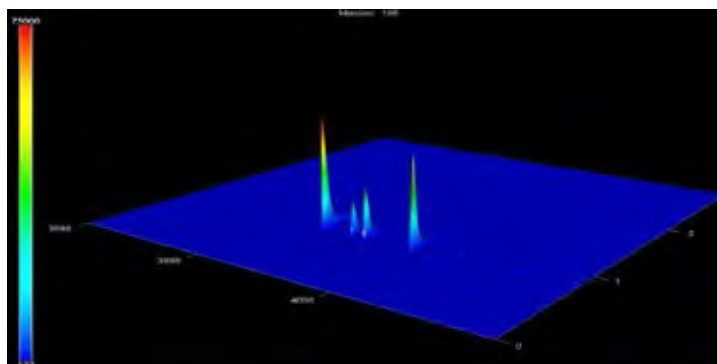


Figure G10 Target ion (m/z 198) surface plot of WCO3-D3.

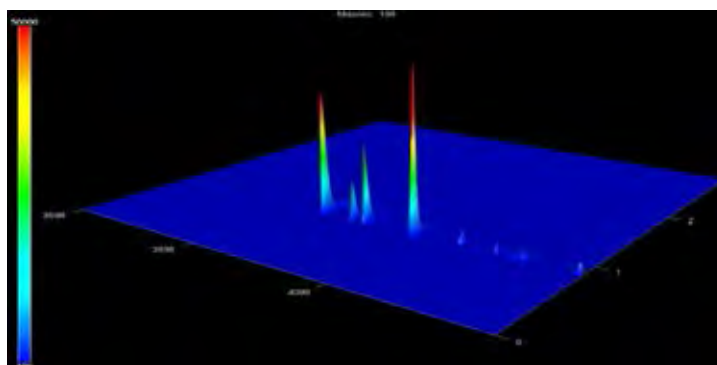


Figure G11 Target ion (m/z 198) surface plot of WCO3-D45.

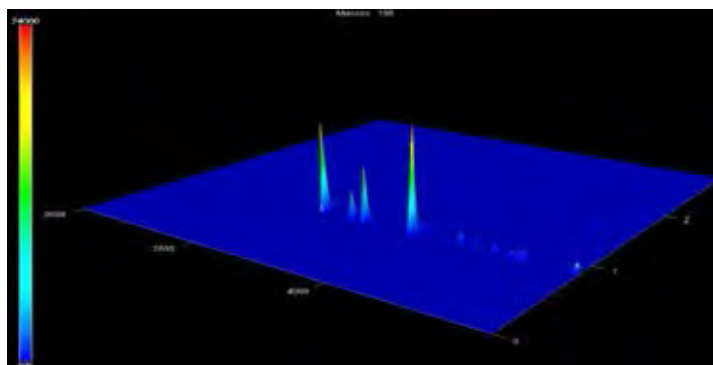


Figure G12 Target ion (m/z 198) surface plot of WCO3-D90.

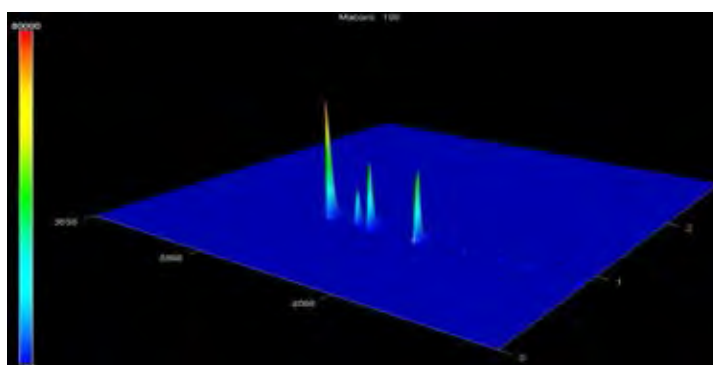


Figure G13 Target ion (m/z 198) surface plot of CO4.

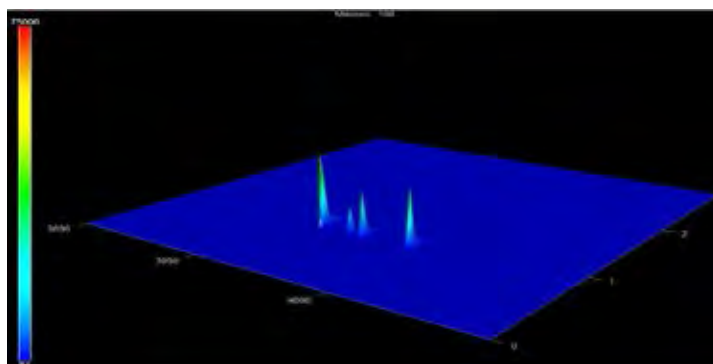


Figure G14 Target ion (m/z 198) surface plot of WCO4-D3.

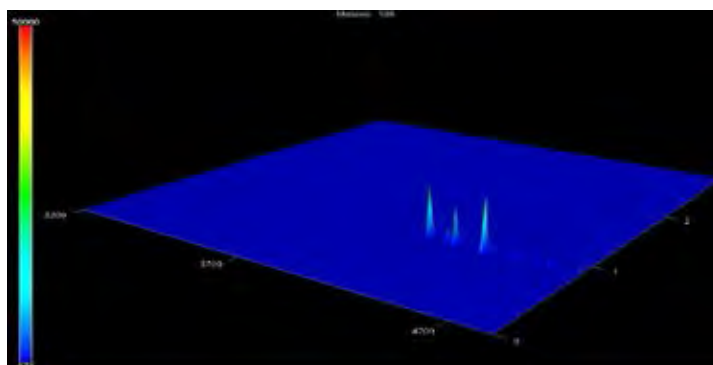


Figure G15 Target ion (m/z 198) surface plot of WCO4-D45.

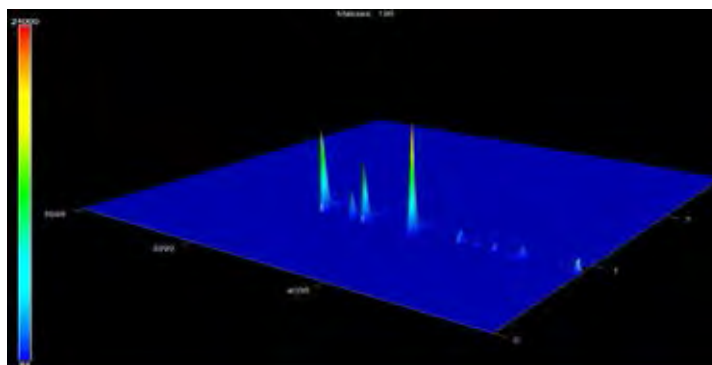


Figure G16 Target ion (m/z 198) surface plot of WCO4-D90.

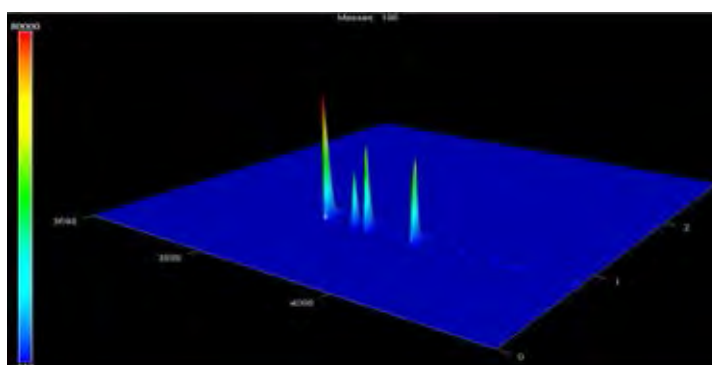


Figure G17 Target ion (m/z 198) surface plot of CO5.

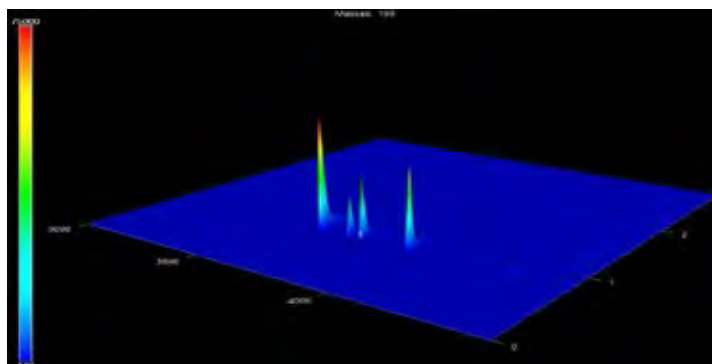


Figure G18 Target ion (m/z 198) surface plot of WCO5-D3.

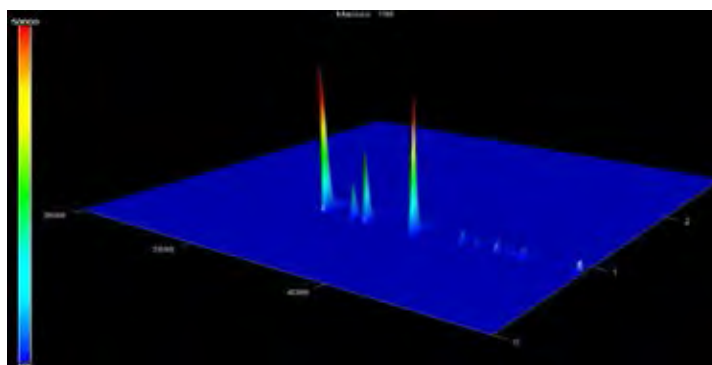


Figure G19 Target ion (m/z 198) surface plot of WCO5-D45.

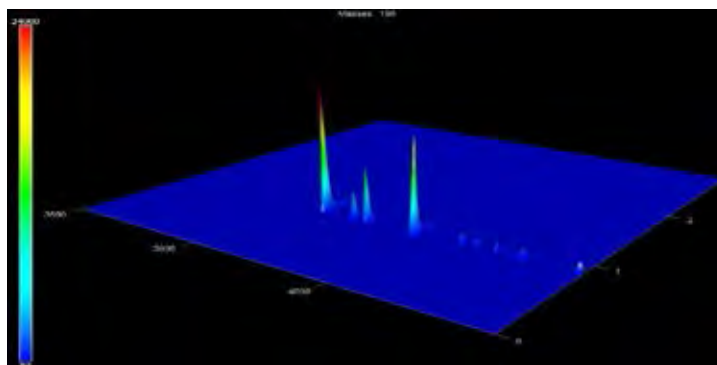


Figure G20 Target ion (m/z 198) surface plot of WCO5-D90.

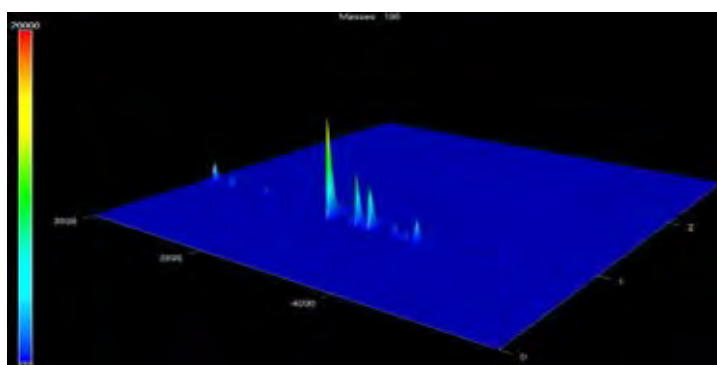


Figure G21 Target ion (m/z 198) surface plot of FO1.

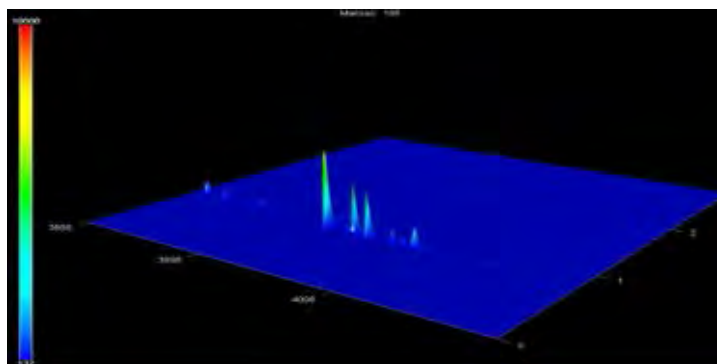


Figure G22 Target ion (m/z 198) surface plot of WFO1-D3.

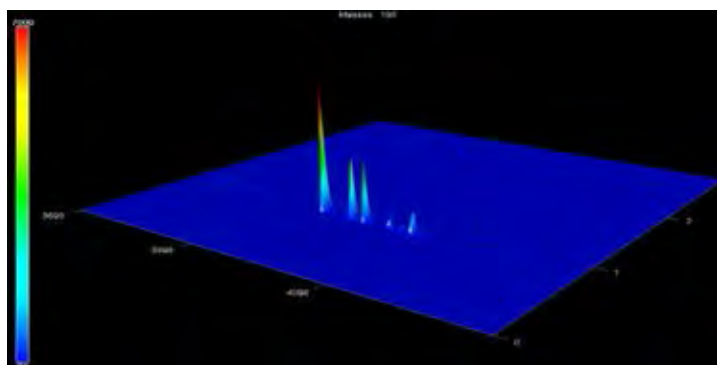


Figure G23 Target ion (m/z 198) surface plot of WFO1-D45.

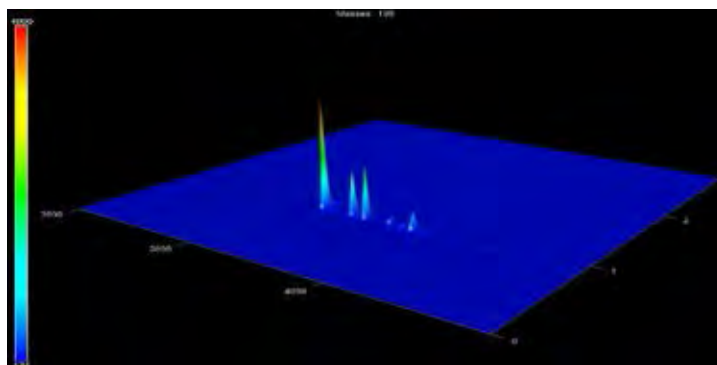


Figure G24 Target ion (m/z 198) surface plot of WFO1-D90.

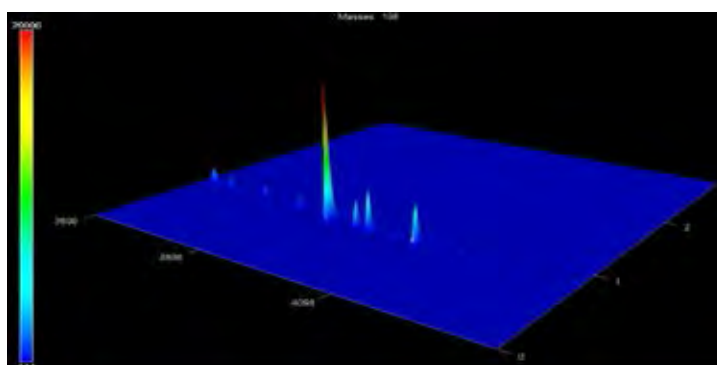


Figure G25 Target ion (m/z 198) surface plot of FO2.

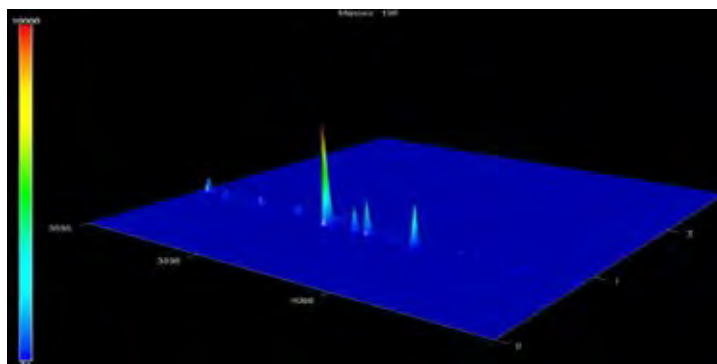


Figure G26 Target ion (m/z 198) surface plot of WFO2-D3.

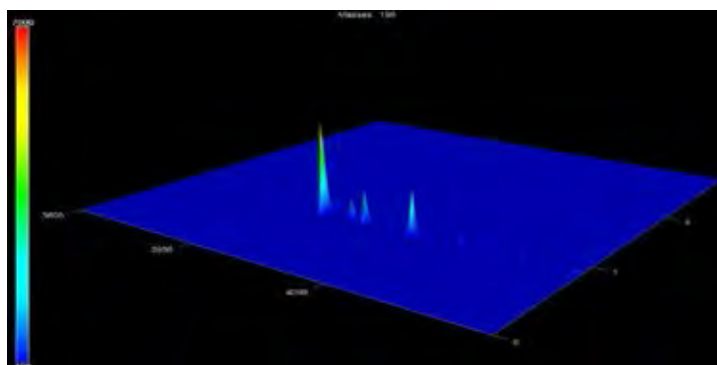


Figure G27 Target ion (m/z 198) surface plot of WFO2-D45.

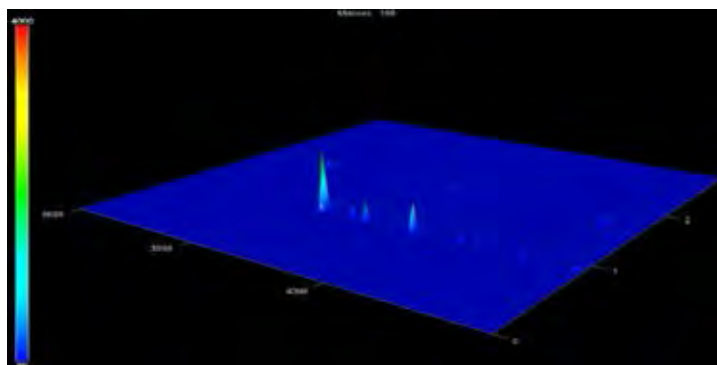


Figure G28 Target ion (m/z 198) surface plot of WFO2-D90.

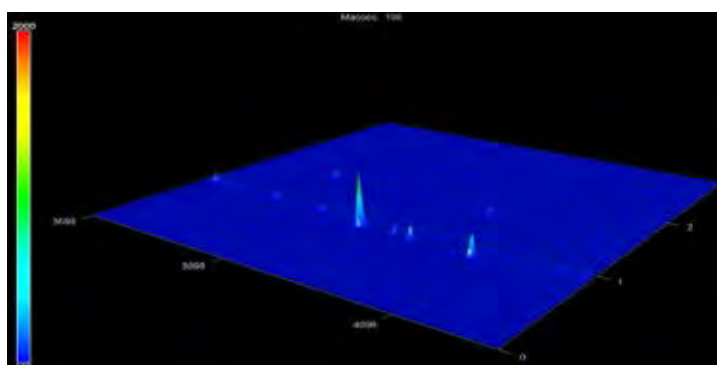


Figure G29 Target ion (m/z 198) surface plot of ULO.

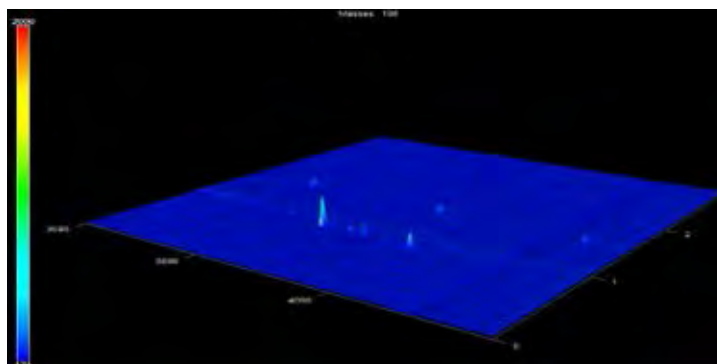


Figure G30 Target ion (m/z 198) surface plot of WULO-D3.

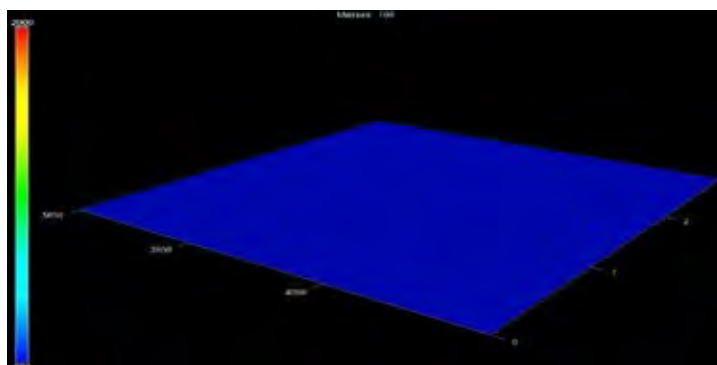


Figure G31 Target ion (m/z 198) surface plot of WULO-D45.

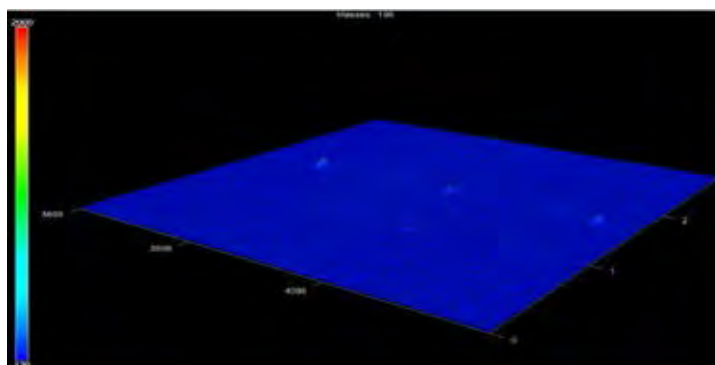


Figure G32 Target ion (m/z 198) surface plot of WULO-D90.

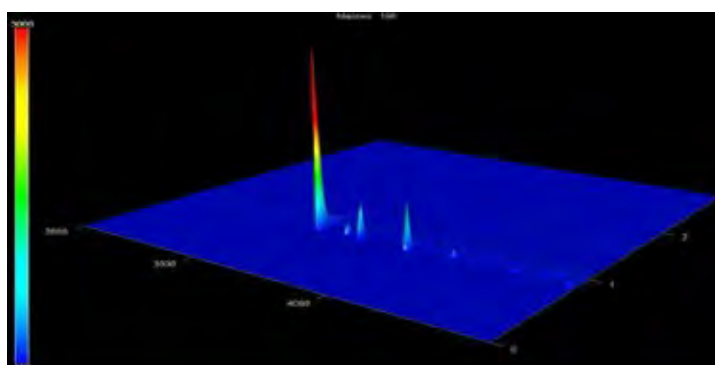
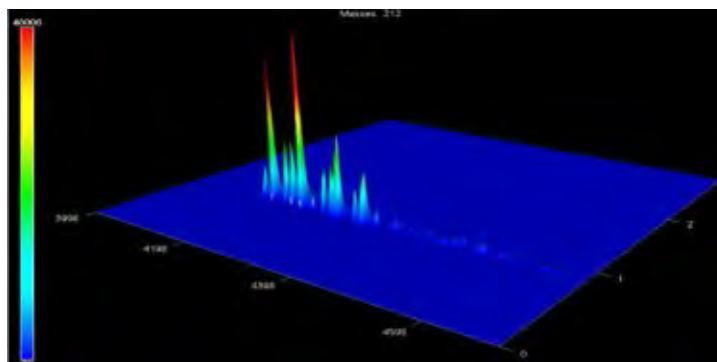
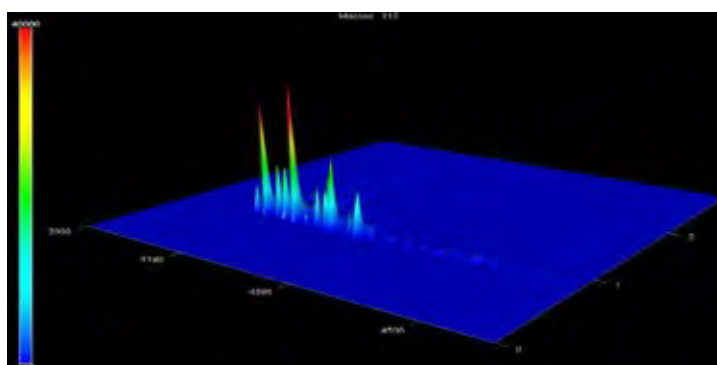
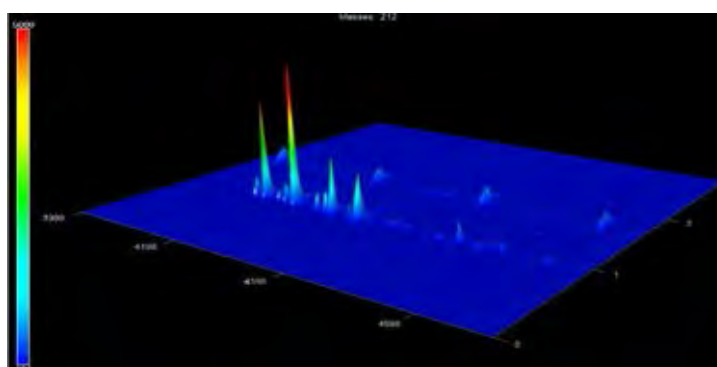


Figure G33 Target ion (m/z 198) surface plot of FLO.

Appendix H GCxGC-TOFMS Target Ion (m/z 212) Surface Plot Result**Figure H1** Target ion (m/z 212) surface plot of CO1.**Figure H2** Target ion (m/z 212) surface plot of WCO1-D3.**Figure H3** Target ion (m/z 212) surface plot of WCO1-D45.

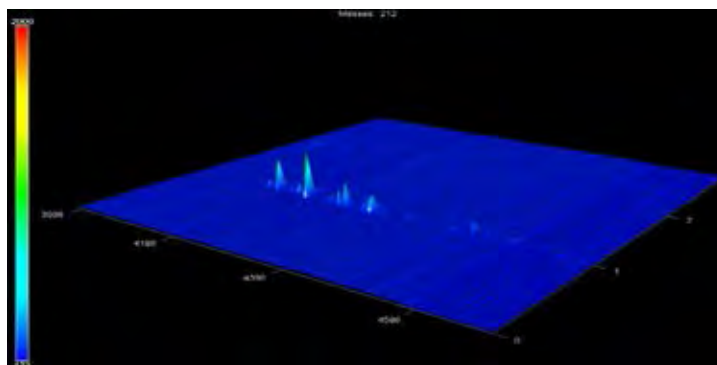


Figure H4 Target ion (m/z 212) surface plot of WCO1-D90.

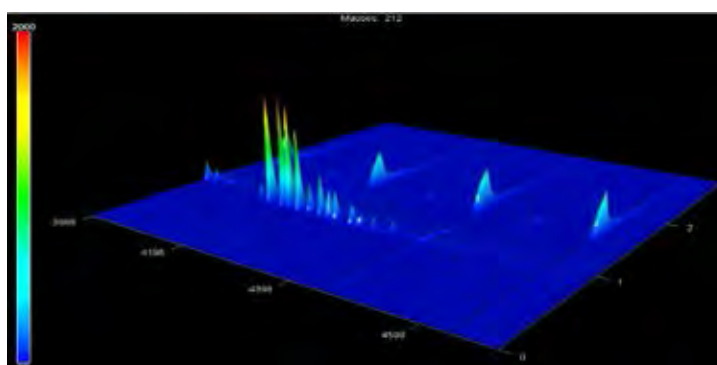


Figure H5 Target ion (m/z 212) surface plot of CO2.

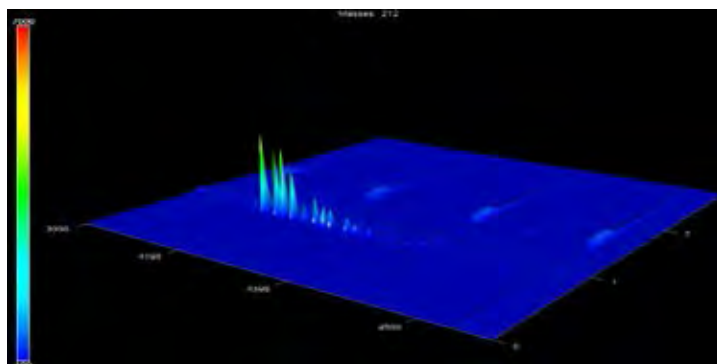


Figure H6 Target ion (m/z 212) surface plot of WCO2-D3.

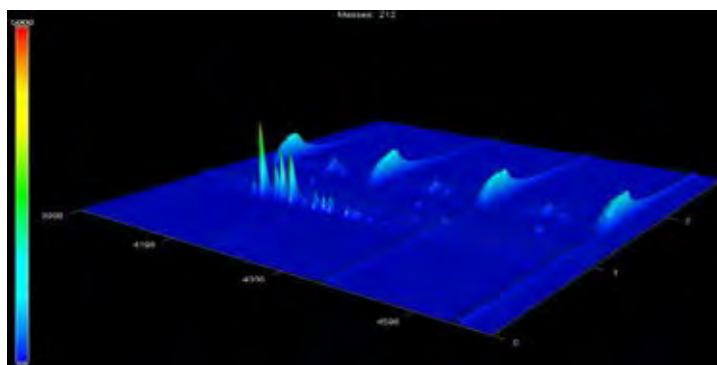


Figure H7 Target ion (m/z 212) surface plot of WCO2-D45.

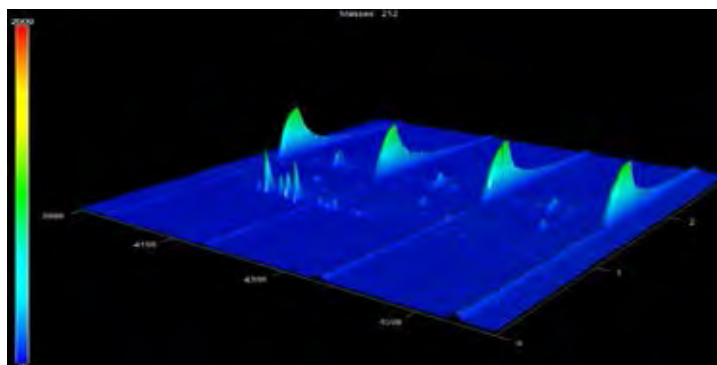


Figure H8 Target ion (m/z 212) surface plot of WCO2-D90.

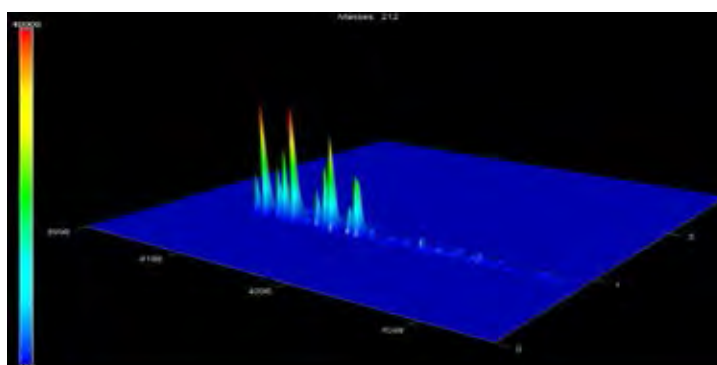


Figure H9 Target ion (m/z 212) surface plot of CO3.

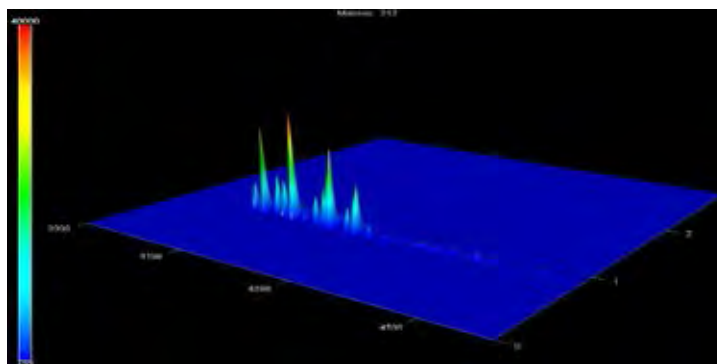


Figure H10 Target ion (m/z 212) surface plot of WCO3-D3.

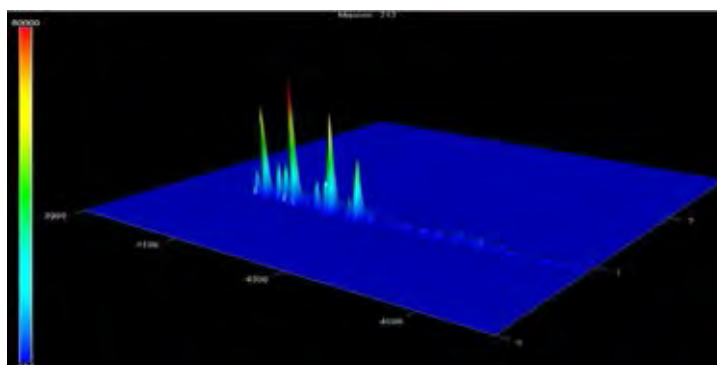


Figure H11 Target ion (m/z 212) surface plot of WCO3-D45.

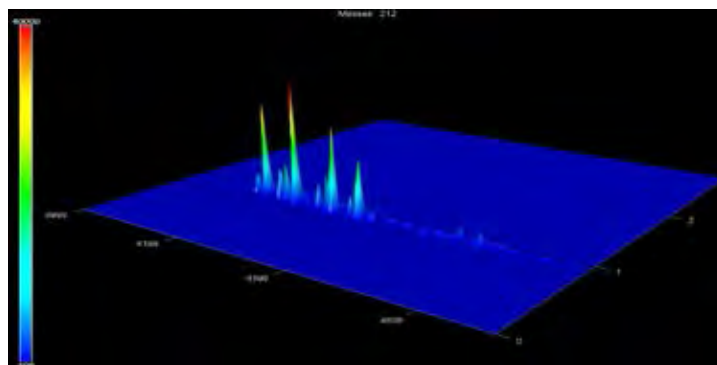


Figure H12 Target ion (m/z 212) surface plot of WCO3-D90.

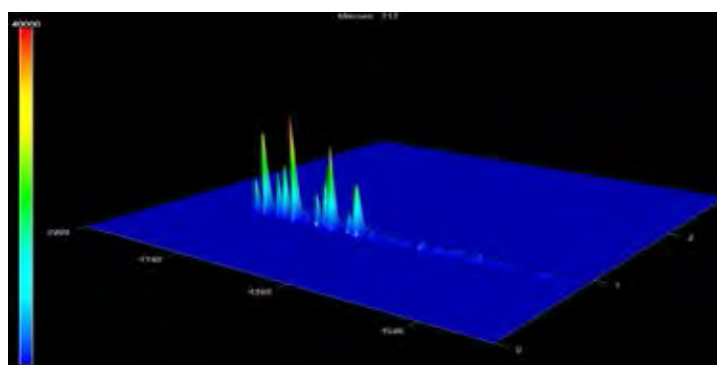


Figure H13 Target ion (m/z 212) surface plot of CO4.

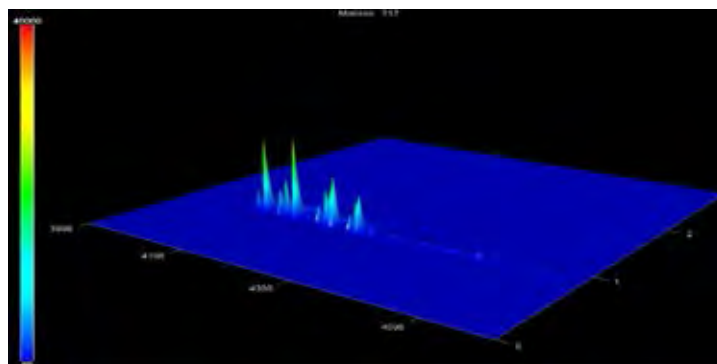


Figure H14 Target ion (m/z 212) surface plot of WCO4-D3.

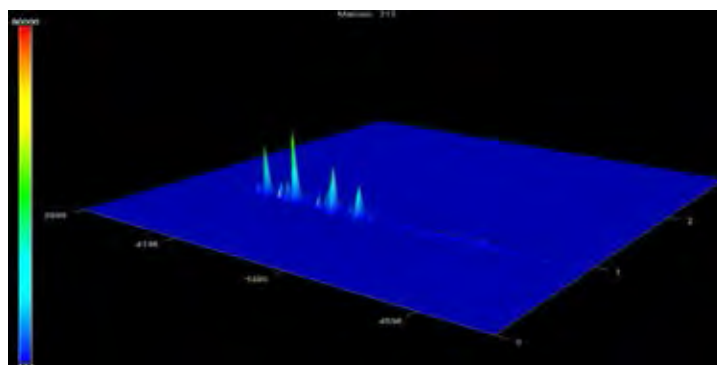


Figure H15 Target ion (m/z 212) surface plot of WCO4-D45.

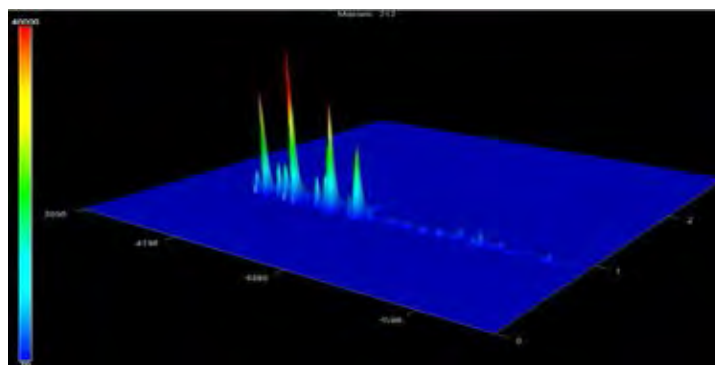


Figure H16 Target ion (m/z 212) surface plot of WCO4-D90.

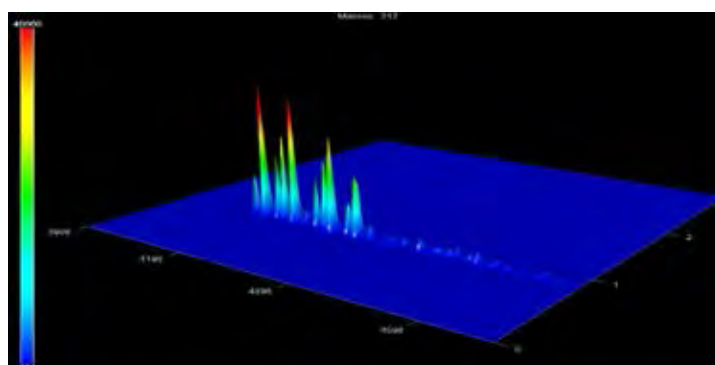


Figure H17 Target ion (m/z 212) surface plot of CO5.

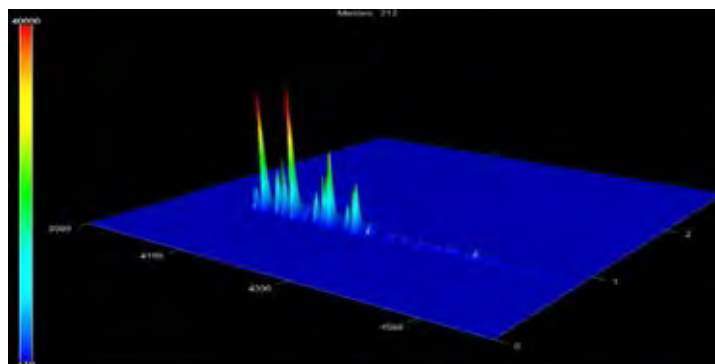


Figure H18 Target ion (m/z 212) surface plot of WCO5-D3.

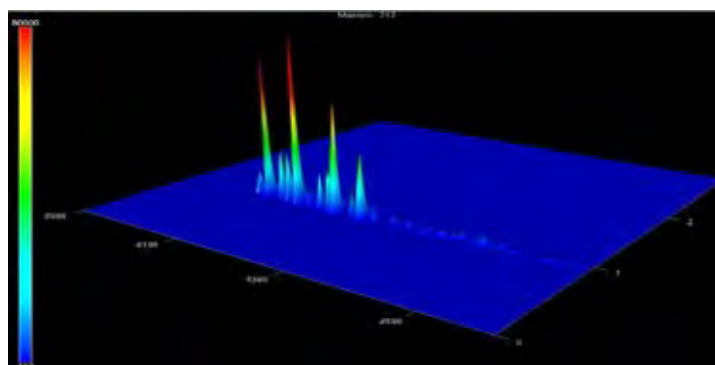


Figure H19 Target ion (m/z 212) surface plot of WCO5-D45.

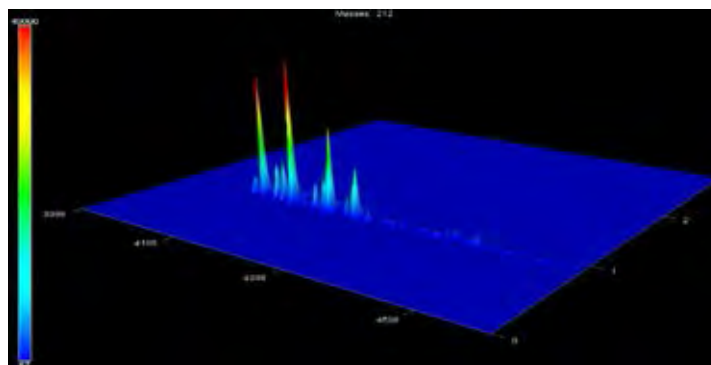


Figure H20 Target ion (m/z 212) surface plot of WCO5-D90.

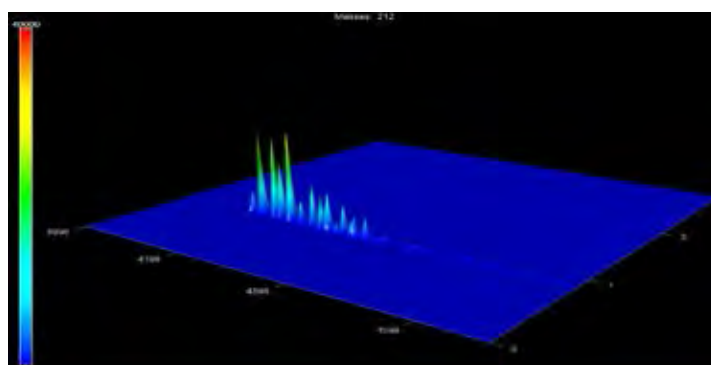


Figure H21 Target ion (m/z 212) surface plot of FO1.

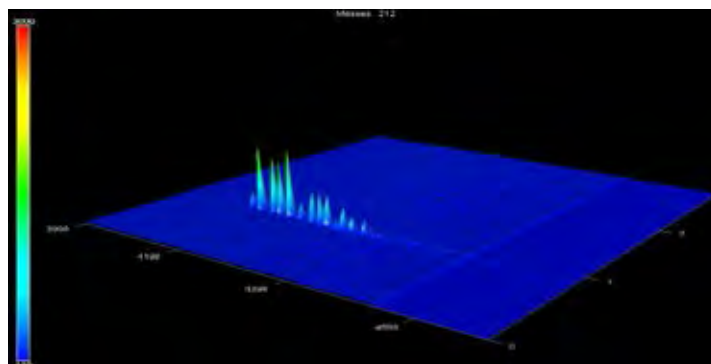


Figure H22 Target ion (m/z 212) surface plot of WFO1-D3.

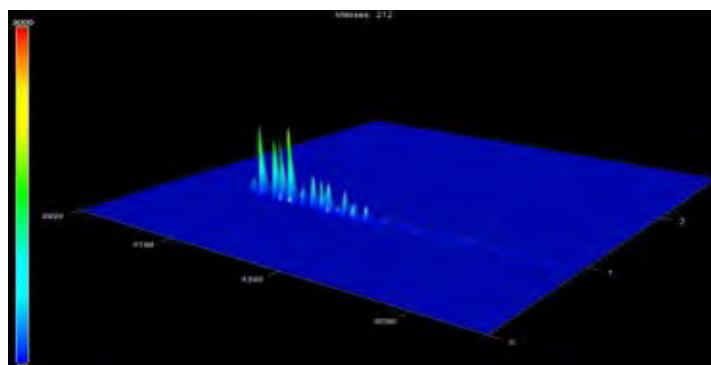


Figure H23 Target ion (m/z 212) surface plot of WFO1-D45.

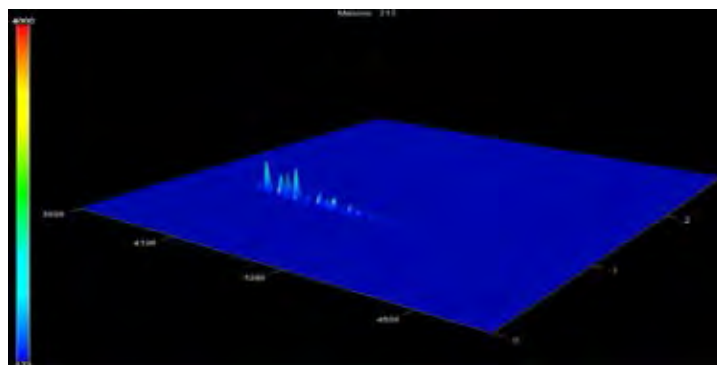


Figure H24 Target ion (m/z 212) surface plot of WFO1-D90.

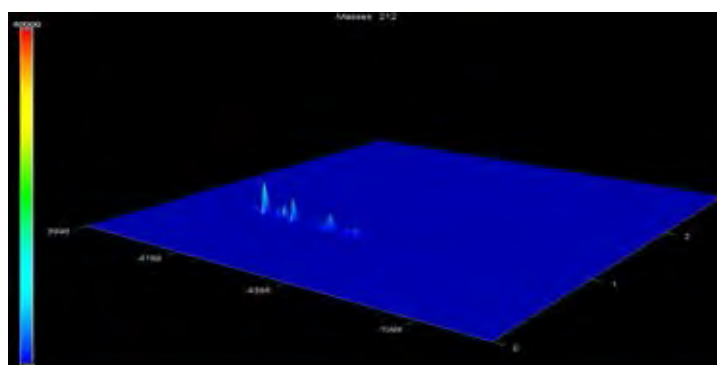


Figure H25 Target ion (m/z 212) surface plot of FO2.

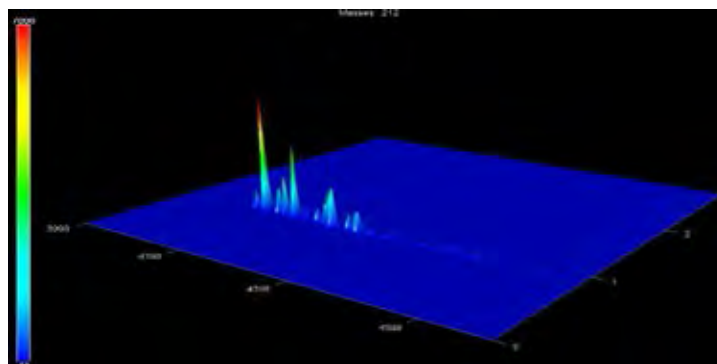


Figure H26 Target ion (m/z 212) surface plot of WFO2-D3.

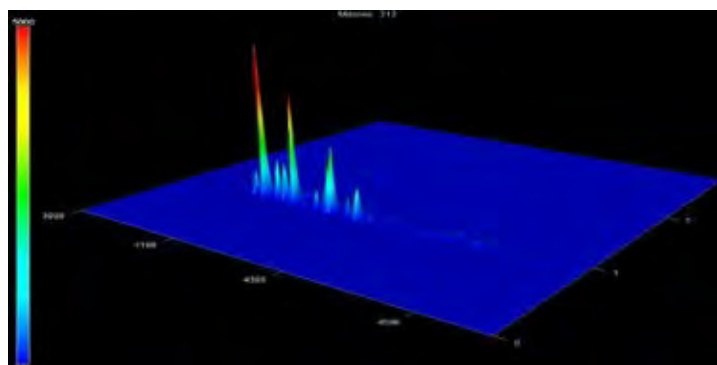


Figure H27 Target ion (m/z 212) surface plot of WFO2-D45.

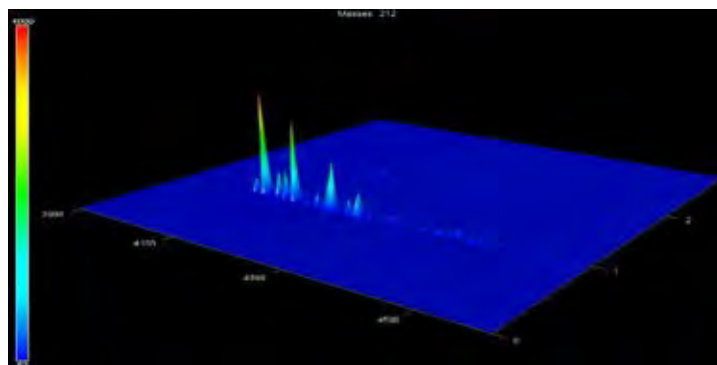


Figure H28 Target ion (m/z 212) surface plot of WFO2-D90.

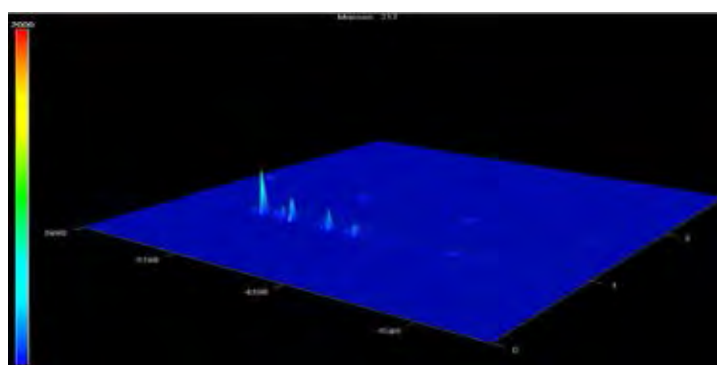


Figure H29 Target ion (m/z 212) surface plot of ULO.

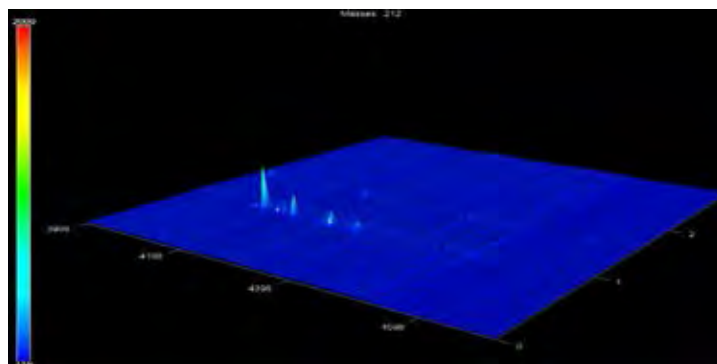


Figure H30 Target ion (m/z 212) surface plot of WULO-D3.

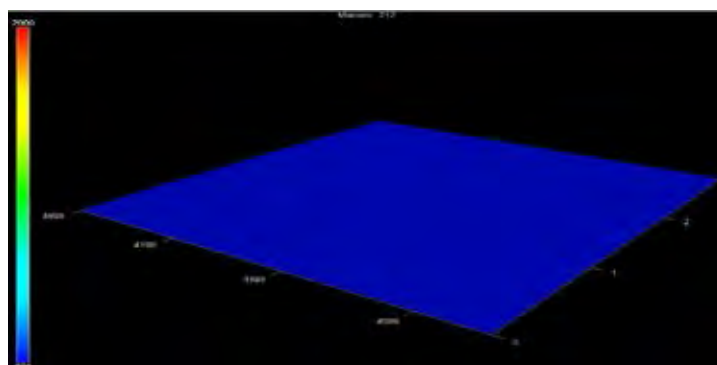


Figure H31 Target ion (m/z 212) surface plot of WULO-D45.

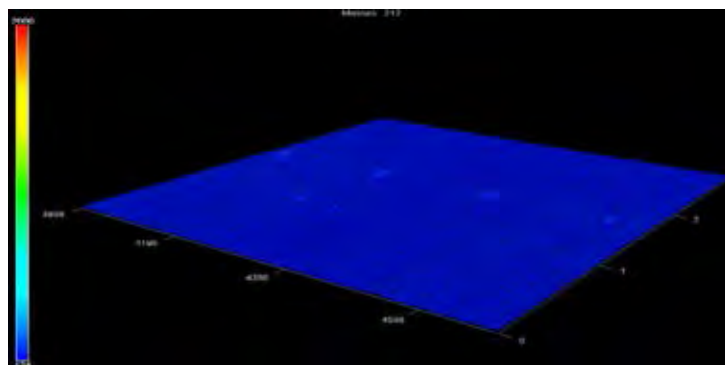


Figure H32 Target ion (m/z 212) surface plot of WULO-D90.

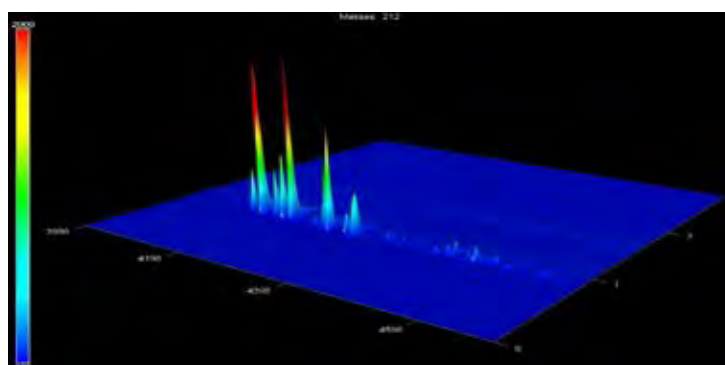
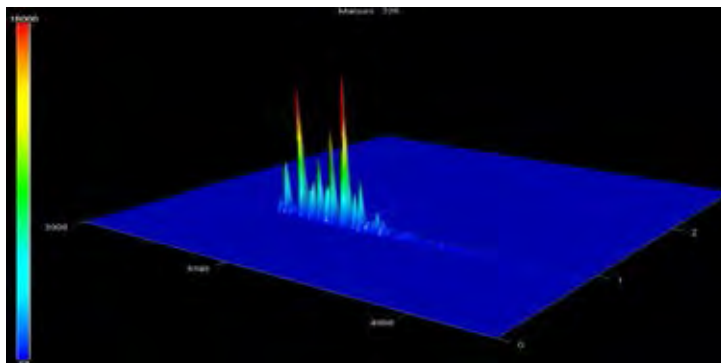
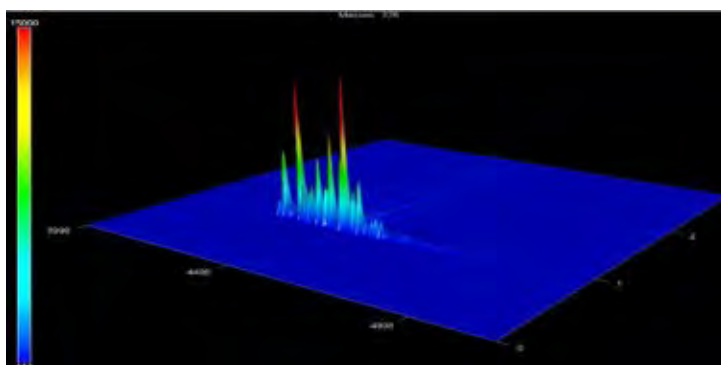
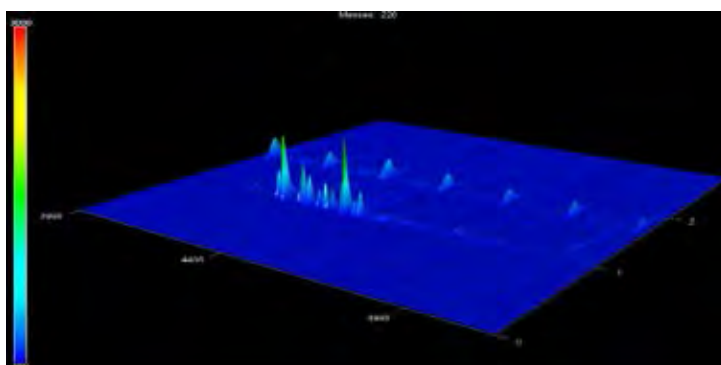


Figure H33 Target ion (m/z 212) surface plot of FLO.

Appendix I GCxGC-TOFMS Target Ion (m/z 226) Surface Plot Result**Figure I1** Target ion (m/z 226) surface plot of CO1.**Figure I2** Target ion (m/z 226) surface plot of WCO1-D3.**Figure I3** Target ion (m/z 226) surface plot of WCO1-D45.

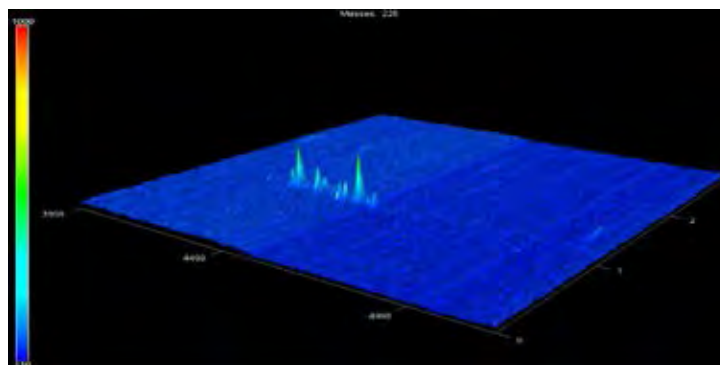


Figure I4 Target ion (m/z 226) surface plot of WCO1-D90.

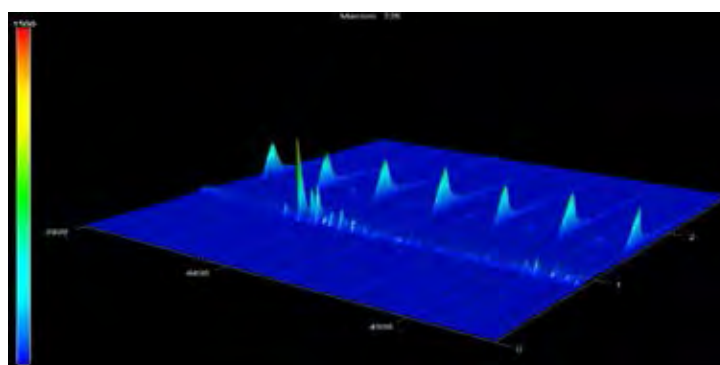


Figure I5 Target ion (m/z 226) surface plot of CO2.

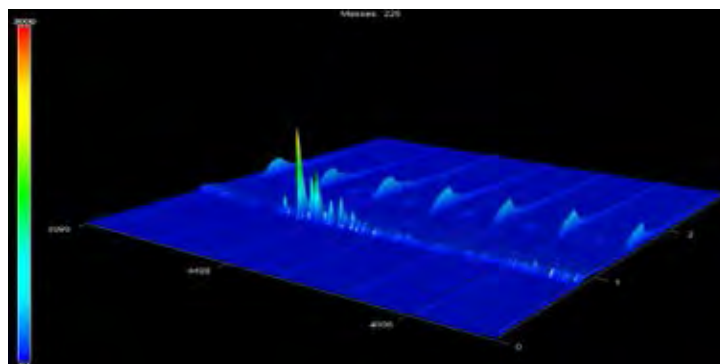


Figure I6 Target ion (m/z 226) surface plot of WCO2-D3.

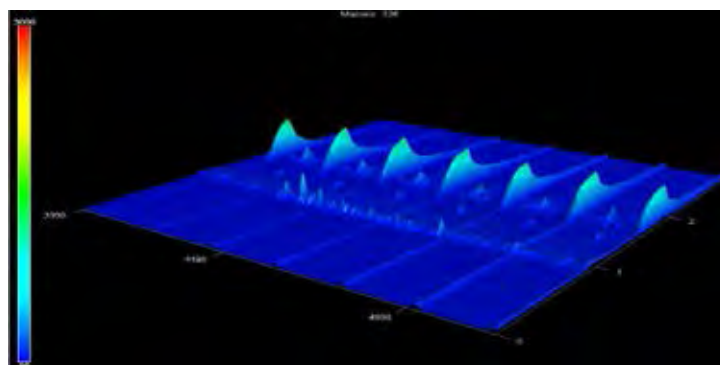


Figure I7 Target ion (m/z 226) surface plot of WCO2-D45.

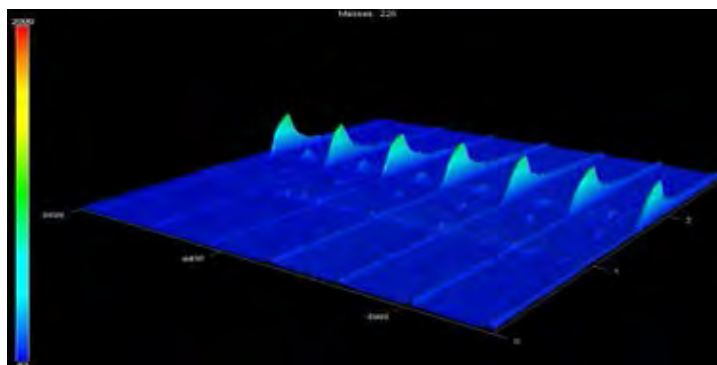


Figure I8 Target ion (m/z 226) surface plot of WCO2-D90.

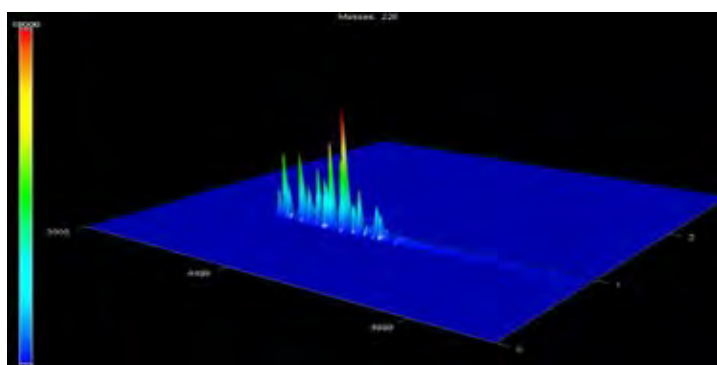


Figure I9 Target ion (m/z 226) surface plot of CO3.

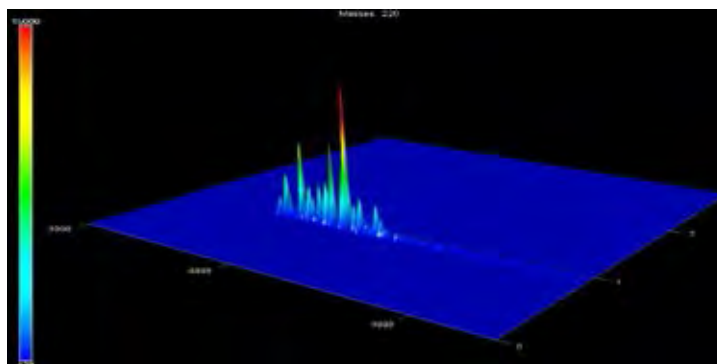


Figure I10 Target ion (m/z 226) surface plot of WCO3-D3.

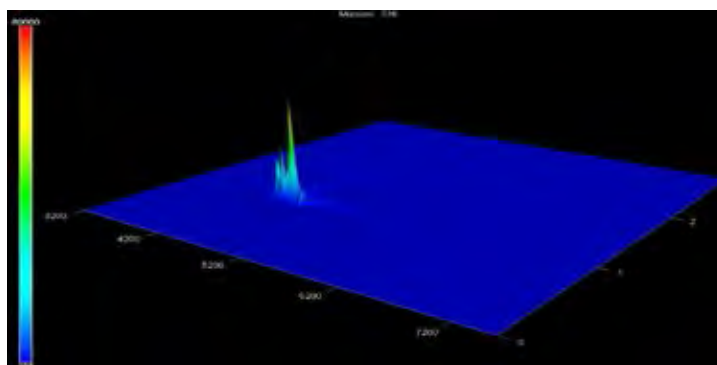


Figure I11 Target ion (m/z 226) surface plot of WCO3-D45.

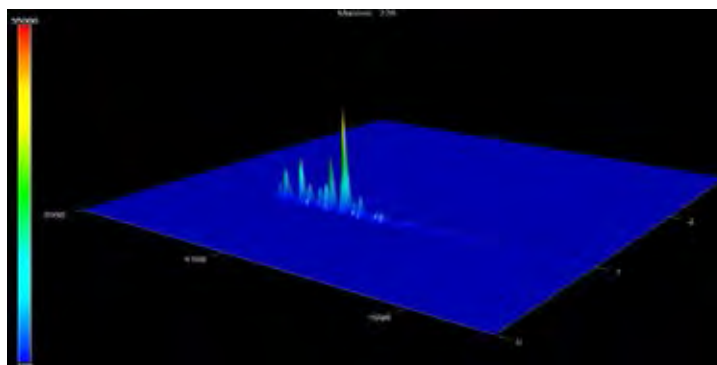


Figure I12 Target ion (m/z 226) surface plot of WCO3-D90.

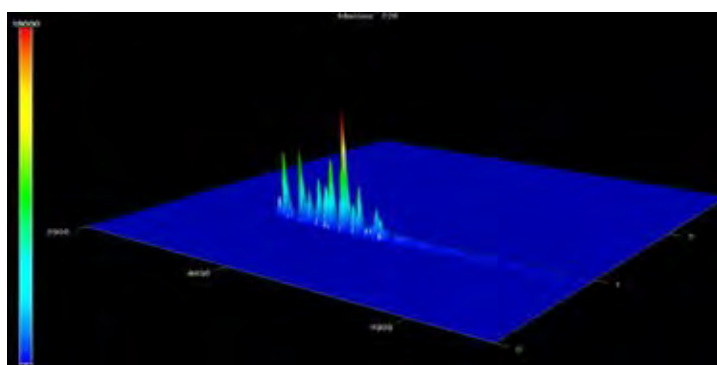


Figure I13 Target ion (m/z 226) surface plot of CO4.

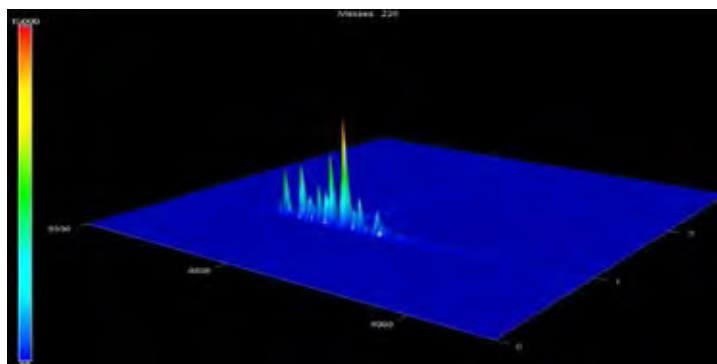


Figure I14 Target ion (m/z 226) surface plot of WCO4-D3.

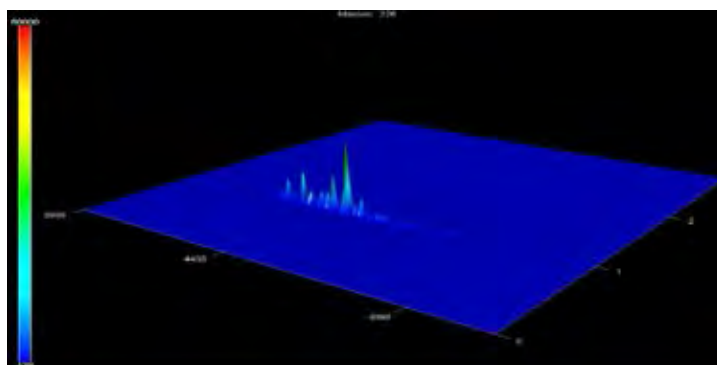


Figure I15 Target ion (m/z 226) surface plot of WCO4-D45.

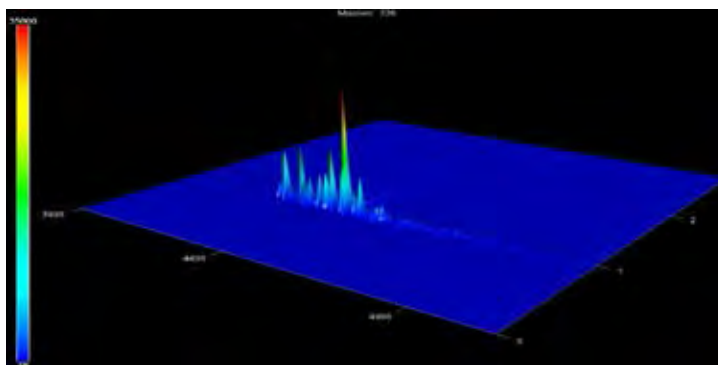


Figure I16 Target ion (m/z 226) surface plot of WCO4-D90.

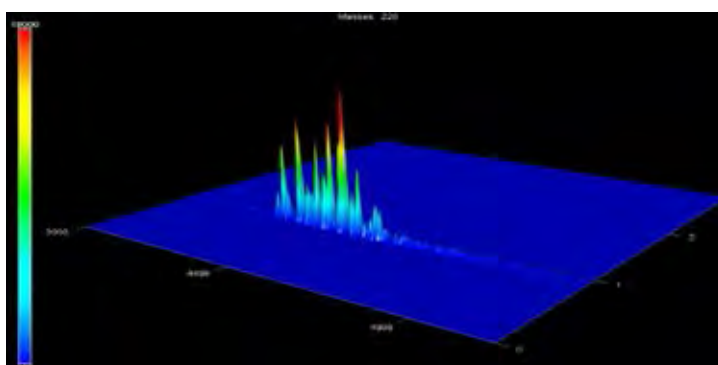


Figure I17 Target ion (m/z 226) surface plot of CO5.

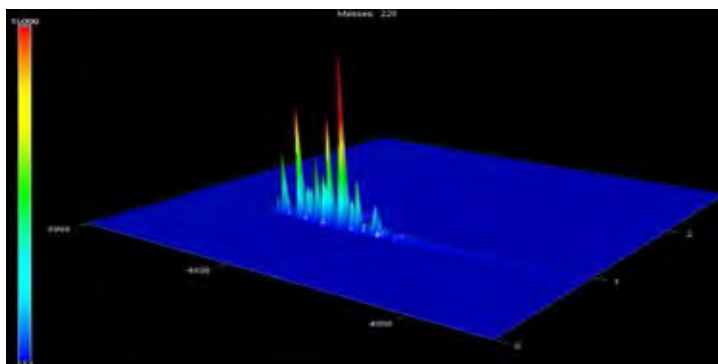


Figure I18 Target ion (m/z 226) surface plot of WCO5-D3.

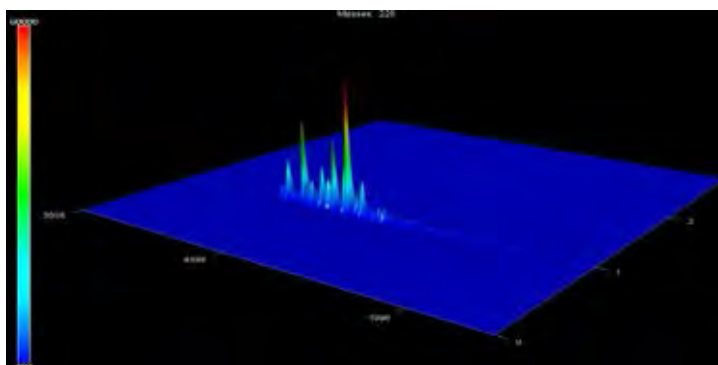


Figure I19 Target ion (m/z 226) surface plot of WCO5-D45.

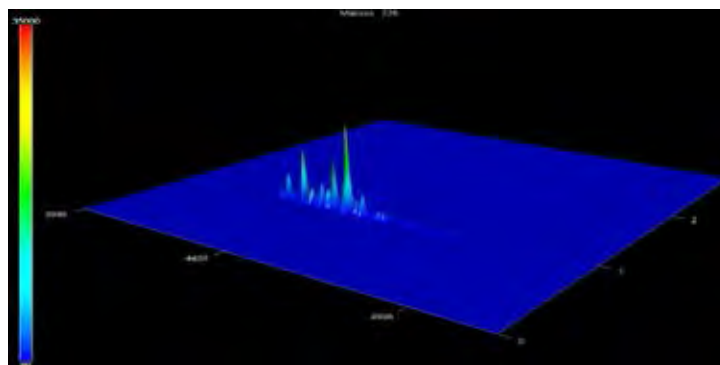


Figure I20 Target ion (m/z 226) surface plot of WCO5-D90.

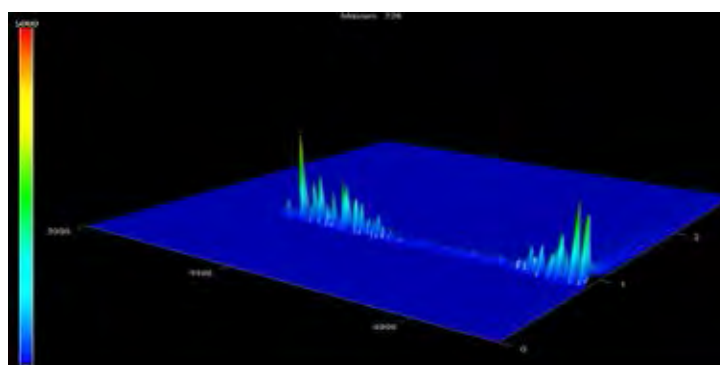


Figure I21 Target ion (m/z 226) surface plot of FO1.

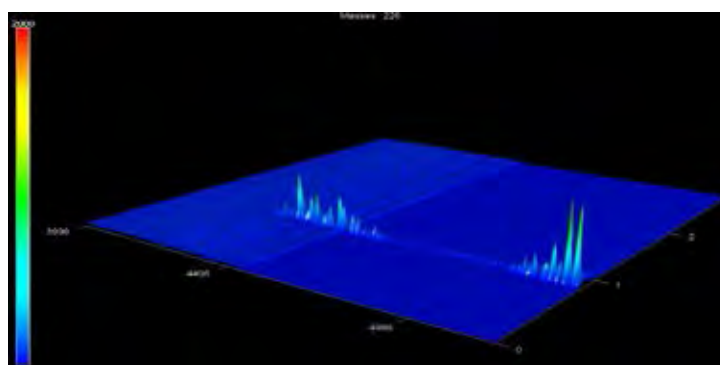


Figure I22 Target ion (m/z 226) surface plot of WFO1-D3.

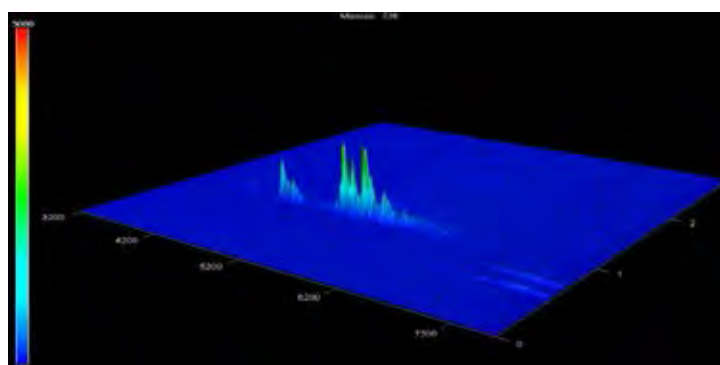


Figure I23 Target ion (m/z 226) surface plot of WFO1-D45.

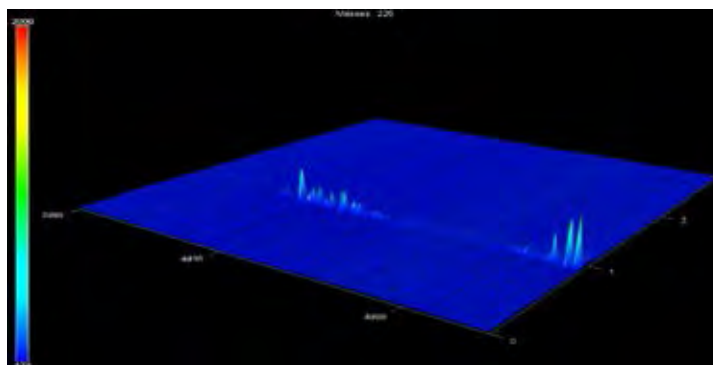


Figure I24 Target ion (m/z 226) surface plot of WFO1-D90.

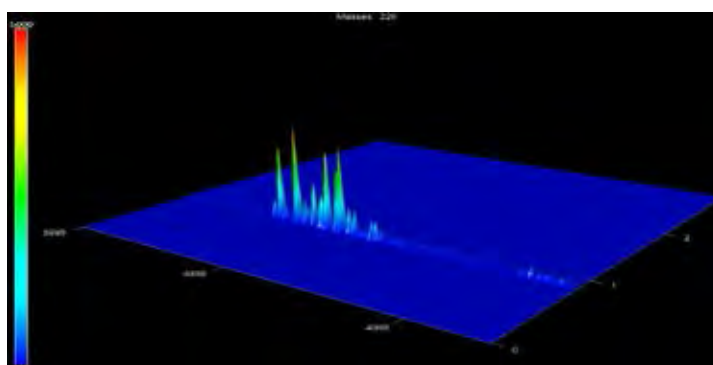


Figure I25 Target ion (m/z 226) surface plot of FO2.

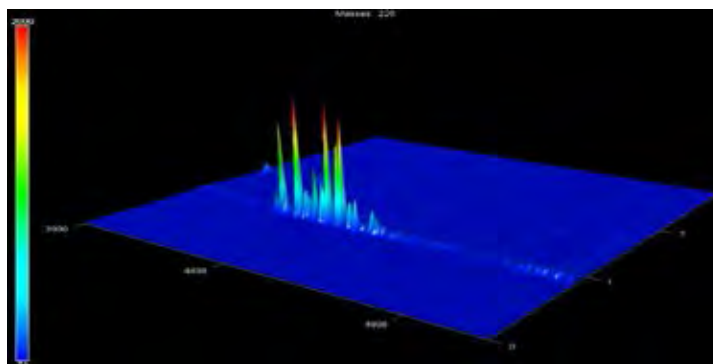


Figure I26 Target ion (m/z 226) surface plot of WFO2-D3.

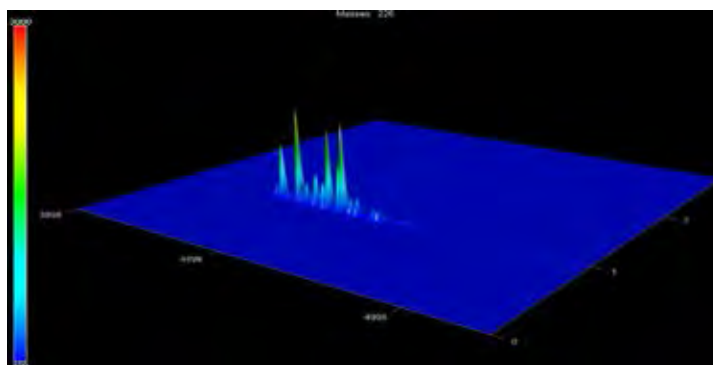


Figure I27 Target ion (m/z 226) surface plot of WFO2-D45.

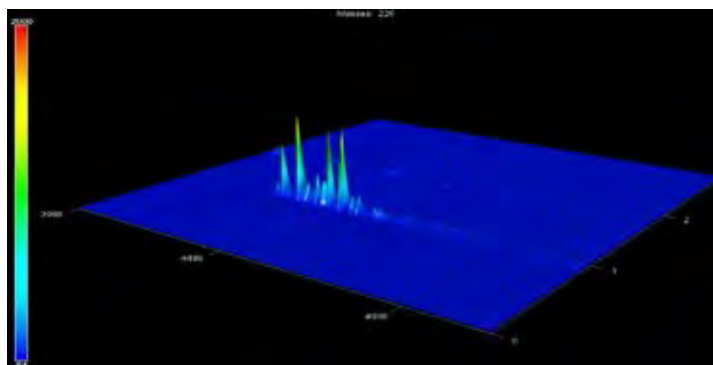


Figure I28 Target ion (m/z 226) surface plot of WFO2-D90.

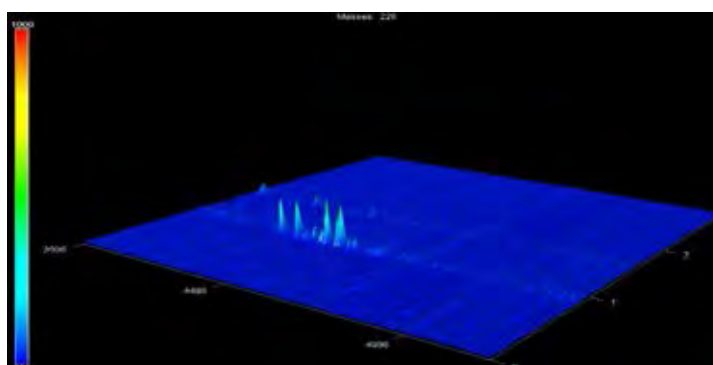


Figure I29 Target ion (m/z 226) surface plot of ULO.

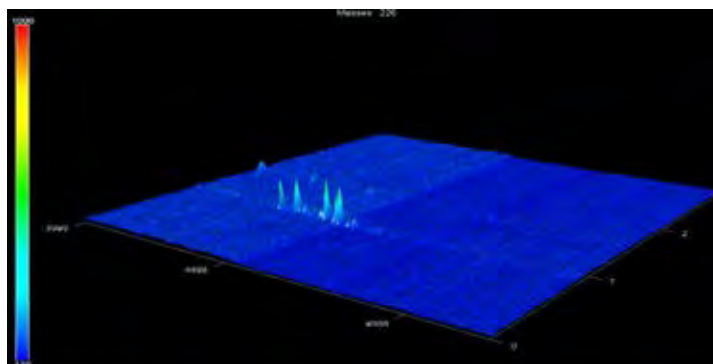


Figure I30 Target ion (m/z 226) surface plot of WULO-D3.

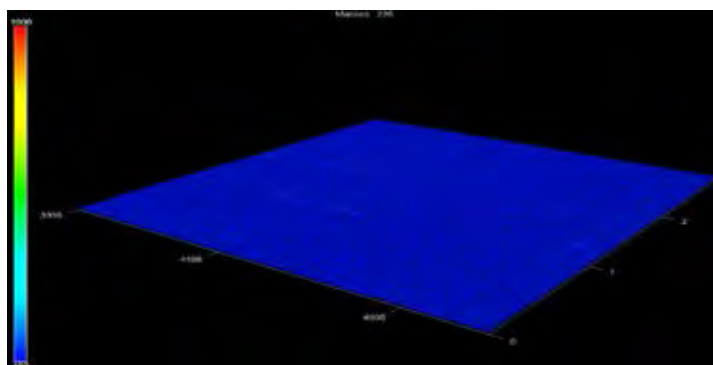


Figure I31 Target ion (m/z 226) surface plot of WULO-D45.

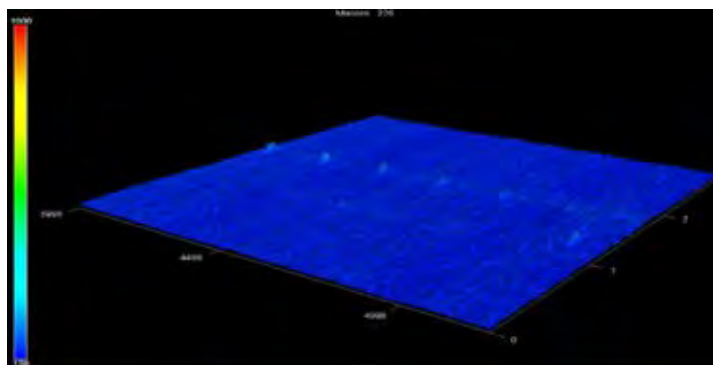


Figure I32 Target ion (m/z 226) surface plot of WULO-D90.

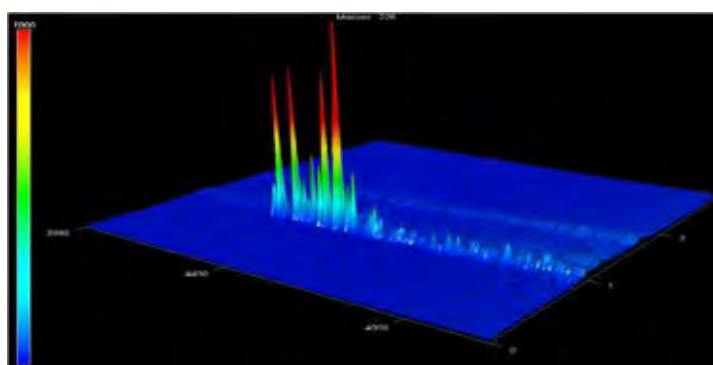
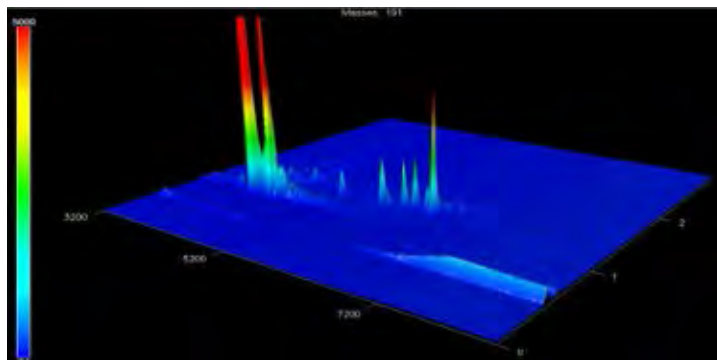
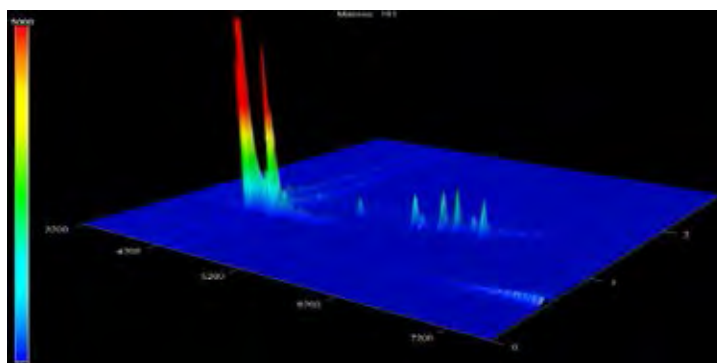
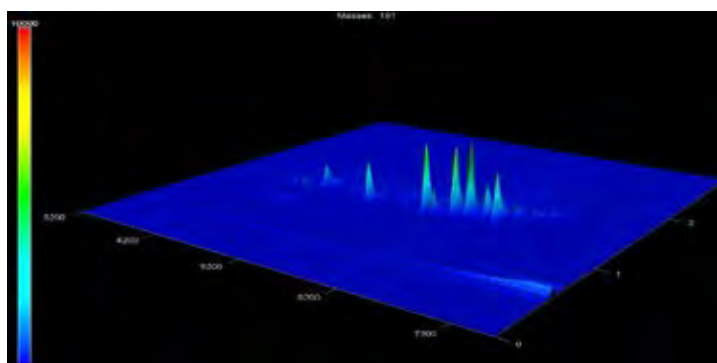


Figure I33 Target ion (m/z 226) surface plot of FLO.

Appendix J GCxGC-TOFMS Target Ion (m/z 191) Surface Plot Result**Figure J1** Target ion (m/z 191) surface plot of CO1.**Figure J2** Target ion (m/z 191) surface plot of WCO1-D3.**Figure J3** Target ion (m/z 191) surface plot of WCO1-D45.

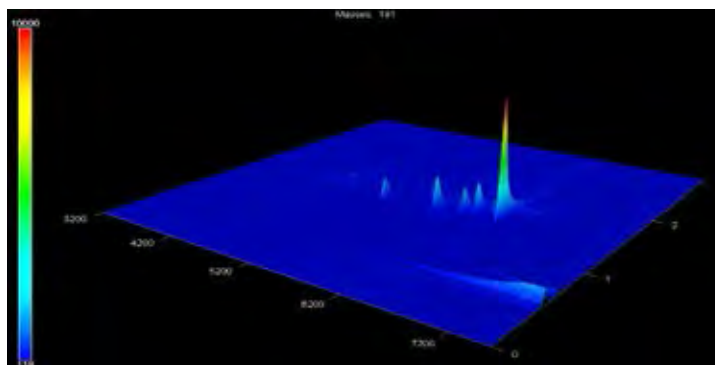


Figure J4 Target ion (m/z 191) surface plot of WCO1-D90.

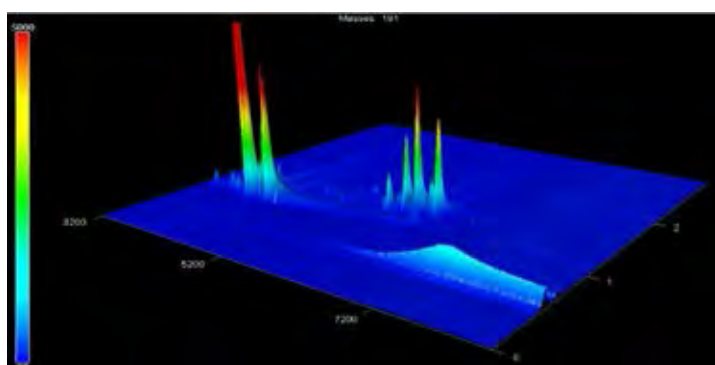


Figure J5 Target ion (m/z 191) surface plot of CO2.

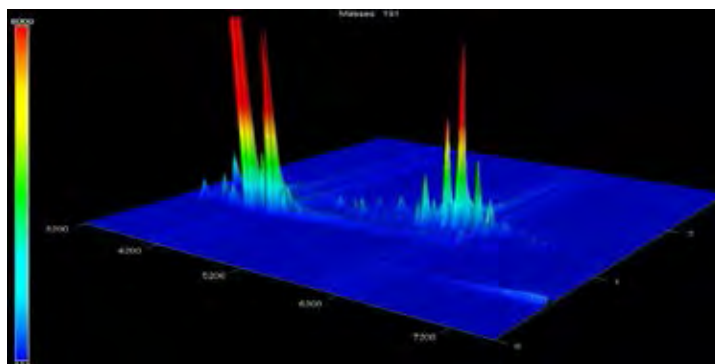


Figure J6 Target ion (m/z 191) surface plot of WCO2-D3.

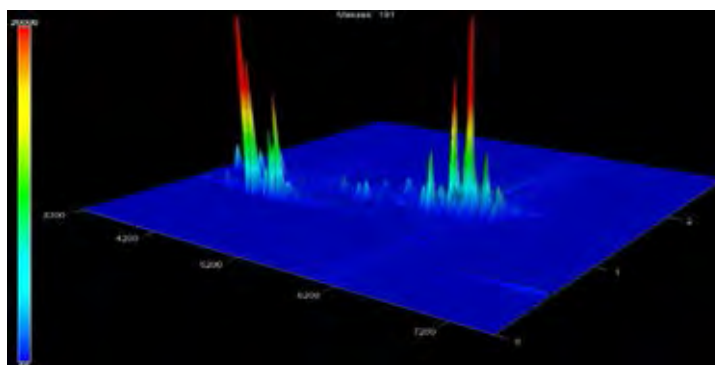


Figure J7 Target ion (m/z 191) surface plot of WCO2-D45.

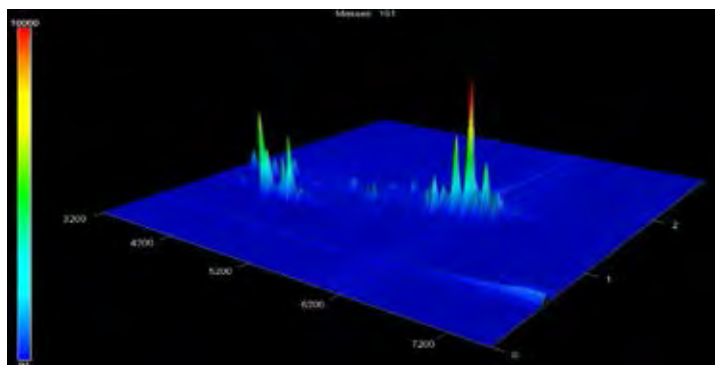


Figure J8 Target ion (m/z 191) surface plot of WCO2-D90.

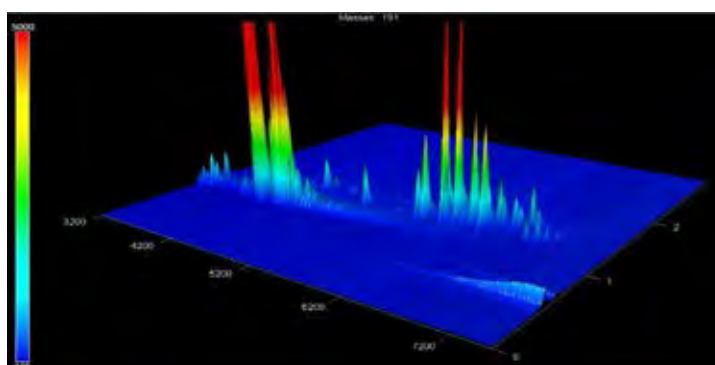


Figure J9 Target ion (m/z 191) surface plot of CO3.

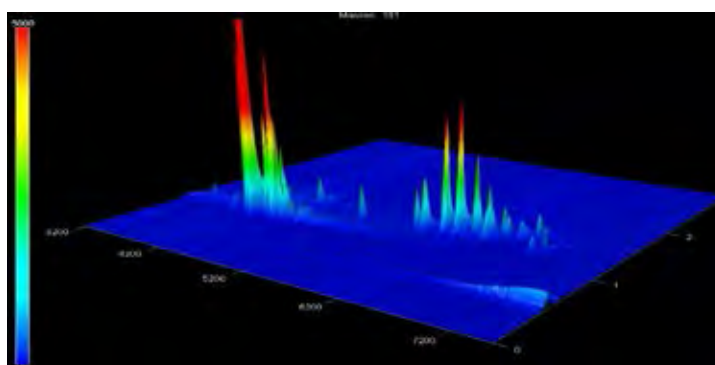


Figure J10 Target ion (m/z 191) surface plot of WCO3-D3.

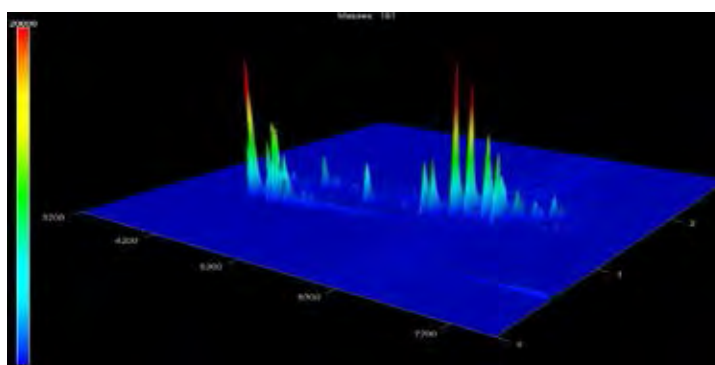


Figure J11 Target ion (m/z 191) surface plot of WCO3-D45.

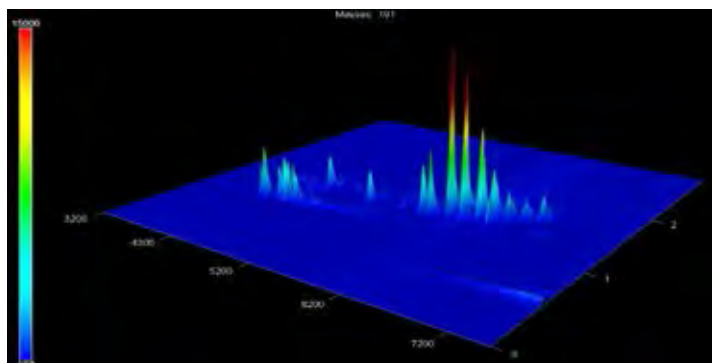


Figure J12 Target ion (m/z 191) surface plot of WCO3-D90.

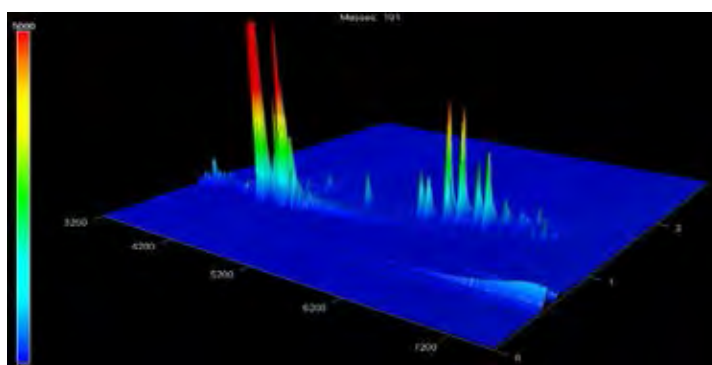


Figure J13 Target ion (m/z 191) surface plot of CO4.

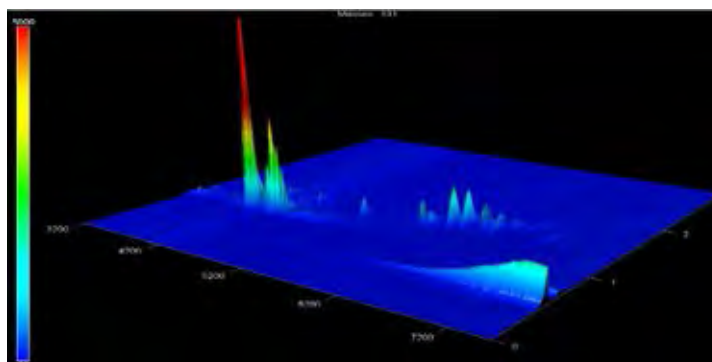


Figure J14 Target ion (m/z 191) surface plot of WCO4-D3.

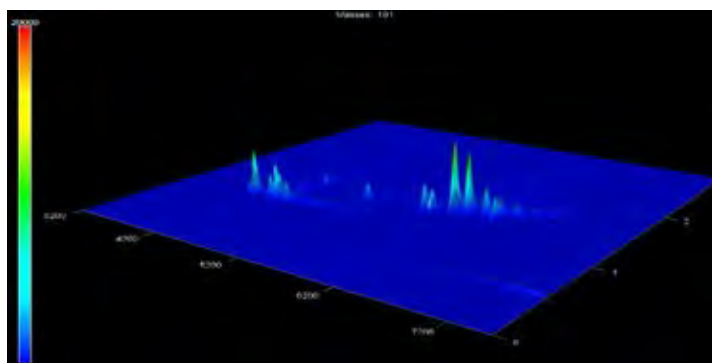


Figure J15 Target ion (m/z 191) surface plot of WCO4-D45.

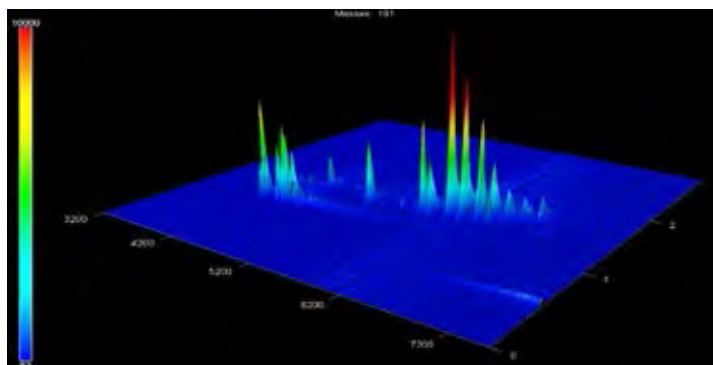


Figure J16 Target ion (m/z 191) surface plot of WCO4-D90.

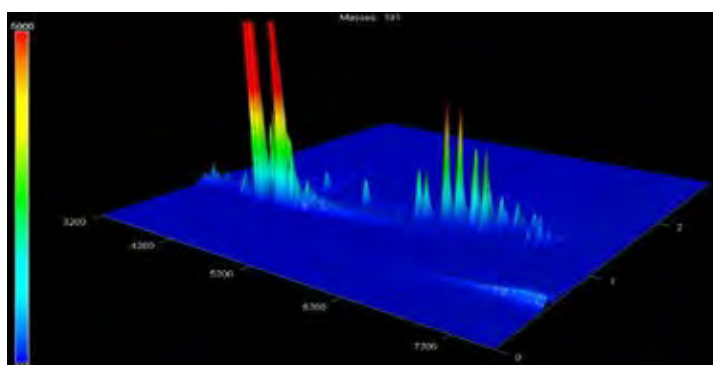


Figure J17 Target ion (m/z 191) surface plot of CO5.

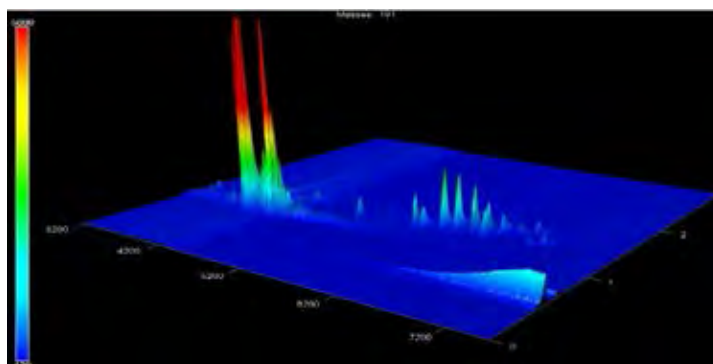


Figure J18 Target ion (m/z 191) surface plot of WCO5-D3.

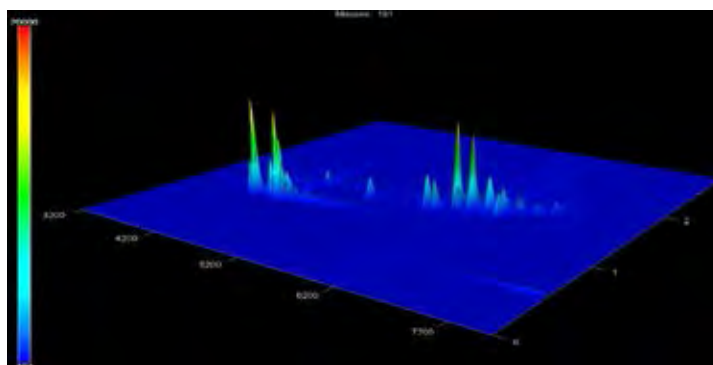


Figure J19 Target ion (m/z 191) surface plot of WCO5-D45.

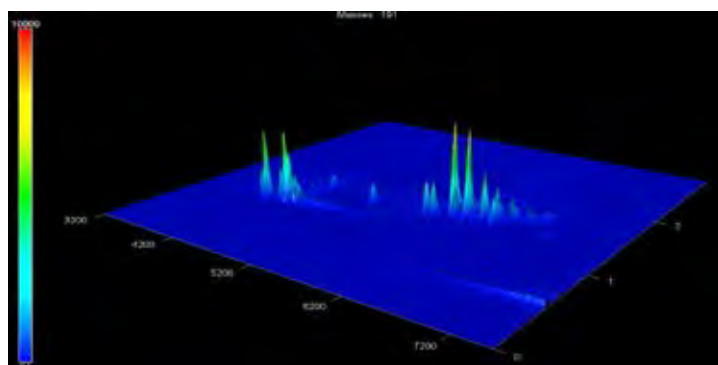


Figure J20 Target ion (m/z 191) surface plot of WCO5-D90.

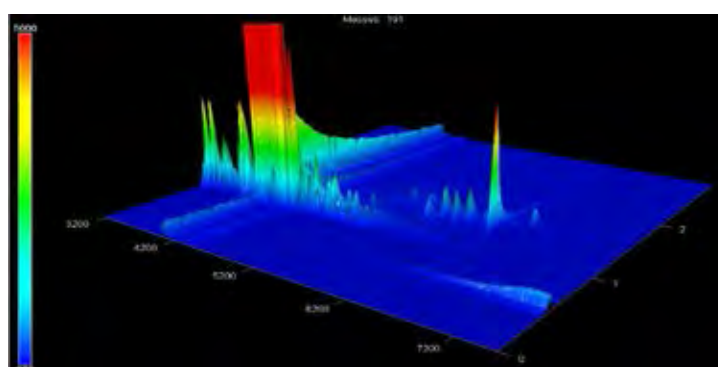


Figure J21 Target ion (m/z 191) surface plot of FO1.

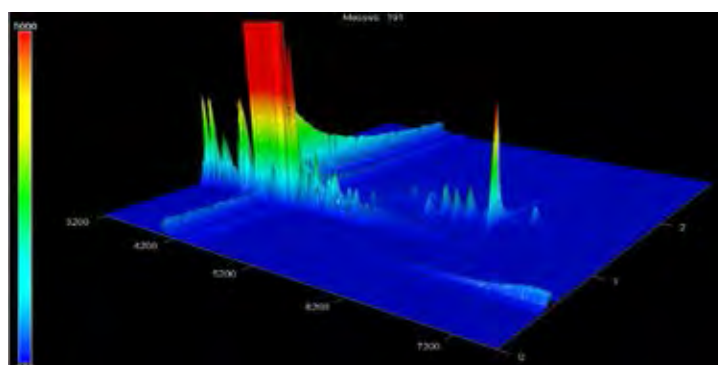


Figure J22 Target ion (m/z 191) surface plot of WFO1-D3.

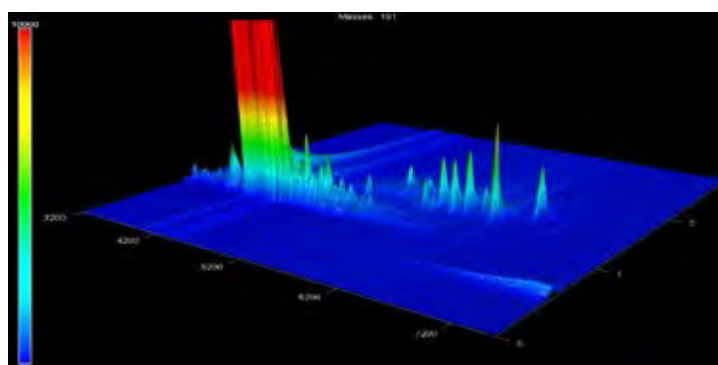


Figure J23 Target ion (m/z 191) surface plot of WFO1-D45.

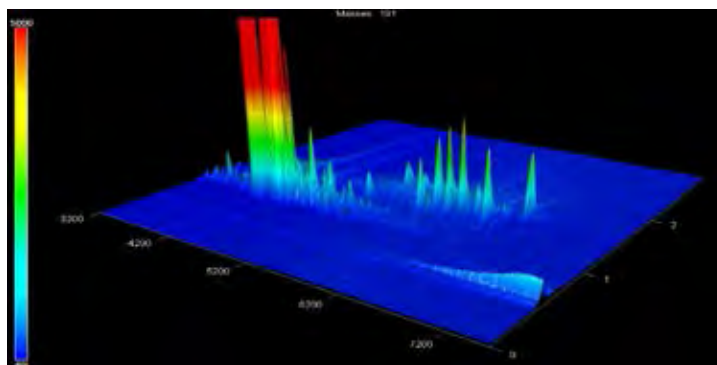


Figure J24 Target ion (m/z 191) surface plot of WFO1-D90.

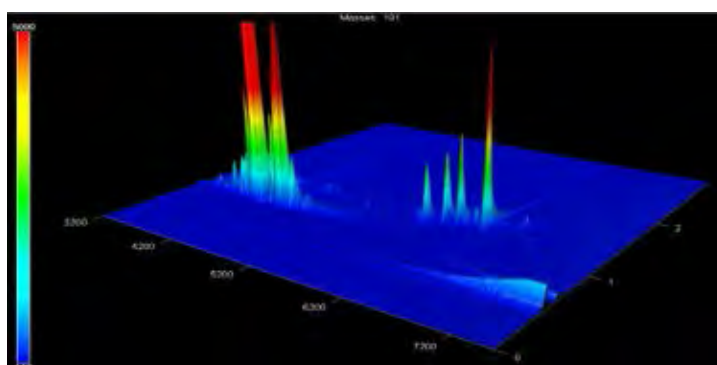


Figure J25 Target ion (m/z 191) surface plot of FO2.

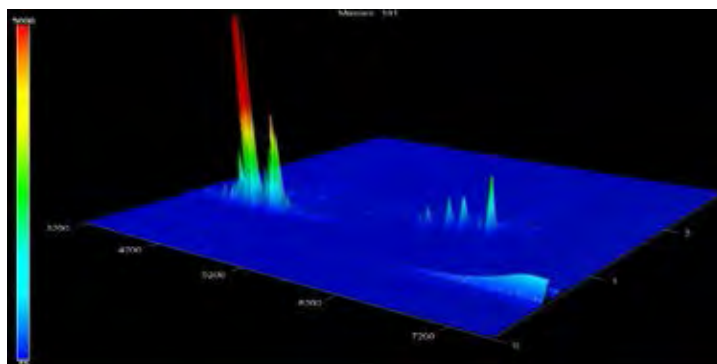


Figure J26 Target ion (m/z 191) surface plot of WFO2-D3.

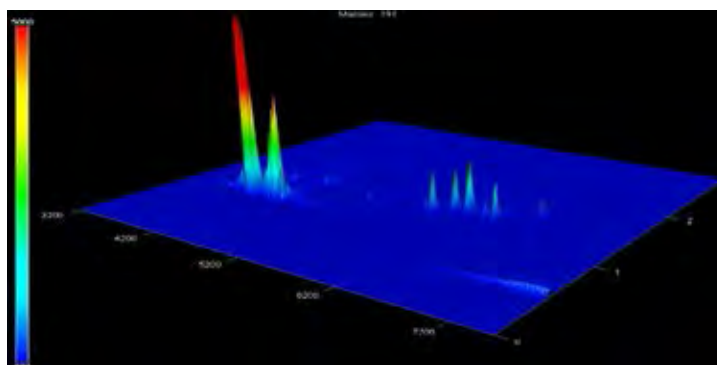


Figure J27 Target ion (m/z 191) surface plot of WFO2-D45.

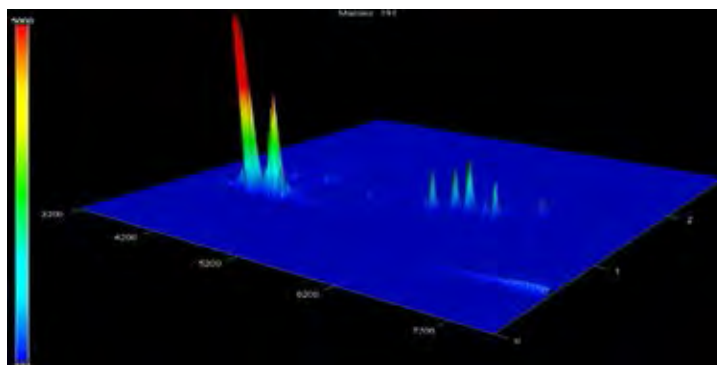


Figure J28 Target ion (m/z 191) surface plot of WFO2-D90.

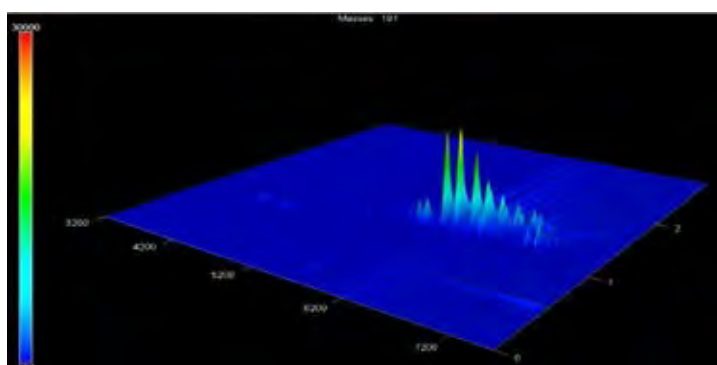


Figure J29 Target ion (m/z 191) surface plot of ULO.

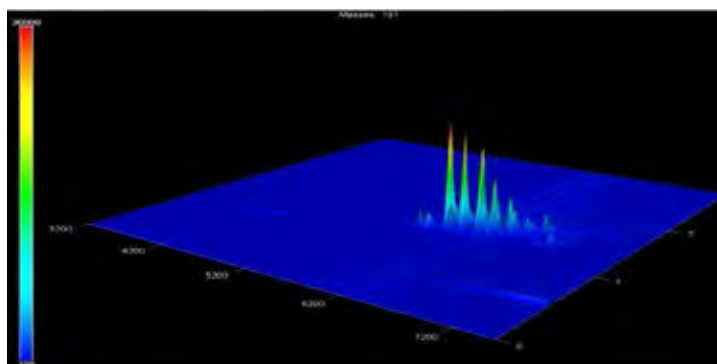


Figure J30 Target ion (m/z 191) surface plot of WULO-D3.

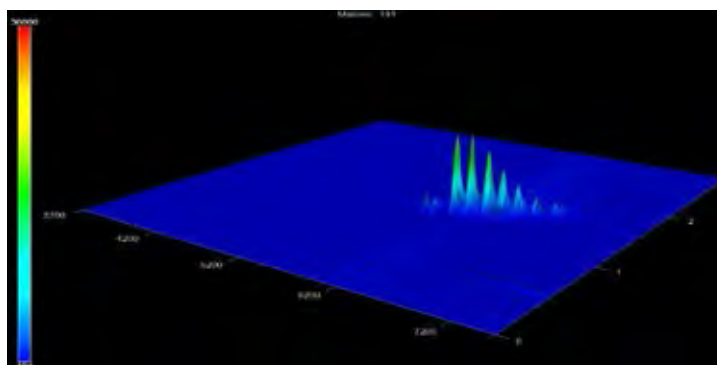


Figure J31 Target ion (m/z 191) surface plot of WULO-D45.

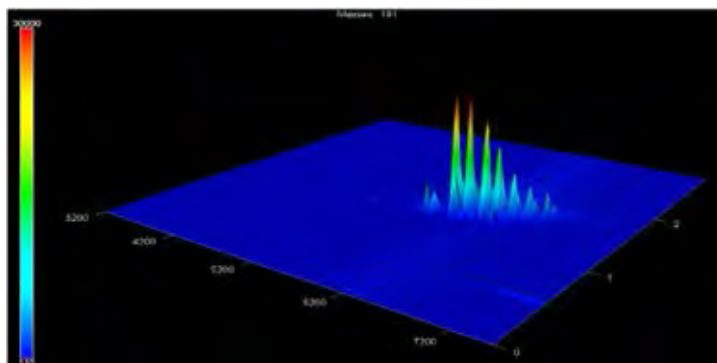


Figure J32 Target ion (m/z 191) surface plot of WULO-D90.

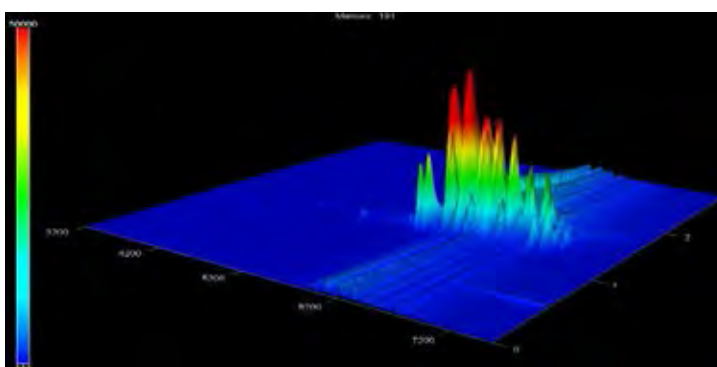


Figure J33 Target ion (m/z 191) surface plot of FLO.

CURRICULUM VITAE

Name: Ms. Pornpetch Hattakijvilai

Date of Birth: January 28, 1993

Nationality: Thai

University Education:

2011-2014 Bachelor Degree of Science, Faculty of Science, Chulalongkorn University, Bangkok, Thailand

Work Experience:

2013 Position: Trainee

Company name: PTT Tank Terminal Co., Ltd.

Proceedings:

1. Hattakijvilai, P. and Jongpatiwut, S. (2017, May 23) Differentiation of crude oils, fuel oils, and used lubricating oil using diagnostic ratios. Proceedings of the 23rd PPC Symposium on Petroleum and Petrochemicals and Polymers and the 8th Research Symposium on Petrochemical and Materials Technology, Bangkok, Thailand.

Presentation:

1. Hattakijvilai, P., Jongpatiwut, S. (2017, May 28-31) Analysis of Biomarkers in crude oils, processed oils, and spilled oils. Poster presented at 13th International Conference on Chemical and Process Engineering, Milan, Italy.